Molecular mechanisms implicated in bone resorption

Dan Georgess

THÈSE

en vue de l'obtention du grade de

Docteur de l'Université de Lyon, délivré par l'École Normale Supérieure de Lyon

Discipline : Sciences de la vie

Laboratoire de biologie cellulaire et physiopathologie osseuse

École Doctorale de Biologie Moléculaire Intégrative et Cellulaire

présentée et soutenue publiquement le 01/10/2013

par Monsieur Dan GEORGESS

Mécanismes moléculaires impliqués dans la résorption osseuse

Directeur de thèse : Dr. Pierre JURDIC

Après l'avis de :

Pr. Stefan LINDER

Dr. Isabelle MARIDONNEAU-PARINI

Devant la commission d'examen formée de :

Dr. Elisabeth GENOT	**Directeur de recherche, INSERM**	**Membre**
Dr. Pierre JURDIC	**Directeur de recherche, INSERM**	**Directeur**
Pr. Vincent LAUDET	**Professeur, ENS de Lyon**	**Président**
Pr. Stefan LINDER	**Professeur, UKE**	**Rapporteur**
Dr. Isabelle MARIDONNEAU-PARINI	**Directeur de recherche, INSERM**	**Rapporteur**

Acknowledgments

Achievement is impossible without opportunity. First and foremost, I would like to express my gratitude to my mentor, Dr. Pierre Jurdic, for opening the gates of research when many would not and for his openness, patience and advice over the past years. Pierre, you have been a formidable boss and an exemplary role model. Thank you for all the discussions, stories and collaboration opportunities.

The undeniable cornerstone of my doctoral training and accomplishments was my co-mentor, Dr. Irma Machuca-Gayet. Irma, thank you for your relentless support, constant honesty, thoughtful mentoring and continuously reliable solutions.

To Pierre and Irma, I will be forever grateful for sculpting the scientist and person I am today.

I would like to extend my thanks to Dr. Marlène Mazzorana for laying down the foundations of my thesis project, sharing her valuable knowledge and taking time to discuss and enlighten. Thanks are also enjoyably due to Mrs. Chantal Domenget for sharing her indispensable expertise and for listening to a student with open ears and, more importantly, an open heart. Over the years, I have greatly appreciated the healthy, friendly and supportive environment created by the members of the Jurdic lab: Dr. Marlène Gallet and the "Marlenettes" Pauline & Margot, Dr. Subramanya Pandruvada, Dr. Romain Daquin, Dr. Justine Bacchetta, Dr. Fabienne Coury, Dr. Kelig Pernelle, Mr. Jean Wach, Mrs. Lise Allard and Ms. Nathalie Demoncheaux. You have all been magnificent colleagues. I have also much enjoyed the dynamic environment of the IGFL which is first owed to our director, Pr. Vincent Laudet, and to young and friendly colleagues. I give my sincere thanks to Ms. Julie Carnesechi, Ms. Juliana Guttierez, Dr. Juliette Sailland, Dr. Cyrielle Billon, Ms. Alexa Sadier and Mr. Damien Curton.

If being apart of a superb lab wasn't in itself a wonderful experience, being apart of a community was beyond amazing. The T3-Net was more than a network of exceptional experts; it was the extended scientific family every student wishes for.
I would like to particularly acknowledge Pr. Stefan Linder for his never-ending guidance and encouragement. I would also like to thank Dr. Elisabeth Genot for trusting me as a collaborator, for hosting me in Bordeaux and for her constant support.

The T3-Net experience was extremely pleasant also thanks to young peers that have become friends. Thank you Mr. Pascuale Cervero, Mr. Karima Azouzi, Mr. Franco Klingberg, Mr. Nilesh Talele, Dr. Filipa Curado, Ms. Isabel Egana, Dr. Vineetha Vijayakumar, Mr. Paolo Ciufici and Dr. Vinoth Khandelwal.

Together with Dr. Linder, I would like to specially acknowledge Dr. Isabelle Maridonneau-Parini, whom I admire for seminal work in the podosome field, for critical revision leading to significant enhancement of this manuscript.

I would like to specially acknowledge Pr. Georg Schett, Dr. Jose Terrado-Vicente and Dr. Jean-Christophe Geminard for trusting me with wonderful collaborations. These experiences have not only been pleasant and fruitful, but also giant leaps in my scientific career.

Before this thesis, I would only dream of applying for a doctoral position. These dreams became reality thanks to Dr. Andrei Popov who has taught me the essentials in

experimental biology along with the proactive perseverance necessary for a professional life. I would also like to thank Pr. Stefan Nonchev for seeing potential in me and for defending it.

On a personal level, I would like to thank my parents Hossam and Penka Georgess. I owe everything I am to you. Thank you for your unconditional love and limitless belief in me. Thank you for teaching me hope and installing in me the means to realize my dreams.

Samar, thank you for hope, love, support, motivation and inspiration. You are my sunshine in the storm.

Aunt Salam, uncle Daher and Heba, thank you for all your support, encouragement and love.

The Mediterranean-Far East connection – Olimpia, Imtiaz and Esber – thank you for being my home-away-from-home.

The Welcome Committee co-founders – François and Florent – with its star artist Emilien and big sister Delphine, your friendship has brought much needed balance to my life.

L'ancien and Super G – Laurent and Audrey – thank you for continuous support, heartfelt friendship and smiles.

Contents

Abstract

Bone remodeling is a physiological process by which old bone is replaced by new bone. Osteoclasts are multinucleated giant cells of the monocytic lineage. Their function is bone resorption, the first step of bone remodeling. The work of this thesis is in continuity with a theme long developed in our laboratory, that of the actin cytoskeleton organization in bone-resorbing osteoclasts. Our first study investigated the role of the podosome organization in osteoclast spreading, adhesion and migration. Our results showed that podosome patterning into rings exerted outward tension upon the substrate and thereby triggered cell migration. Through cycles of assembly, growth and alternating disassembly, rings promote a saltatory mode of migration universal to all osteoclasts.
The main objective of this thesis, however, was dedicated to finding new genes that govern podosome patterning in resorption-related processes such as osteoclast migration and sealing zone formation. To find such new genes, we employed a differential transcriptomic analysis of osteoclasts and osteoclast-like cells that exhibit podosomes but are unable to resorb bone. Among a list of six genes highly and exclusively expressed in osteoclasts, we chose to investigate RhoE, a constitutively active GTP-binding protein known for its regulation of actin structures. We provided evidence, using primary RhoE-deficient osteoclasts, that RhoE activity is essential to bone resorption. We unveiled a new role for RhoE in the control of actin turnover in podosomes through a Rock-antagonistic function. Finally, we demonstrated that the role of RhoE in osteoclasts is essential to their migration and sealing zone formation.

Résumé

Le remodelage osseux est un processus physiologique de renouvellement de l'os ancien par de l'os nouveau. Les ostéoclastes sont des cellules multinucléées géantes dont la fonction principale est de dégrader la matrice osseuse, première étape de ce remodelage. Le travail réalisé s'inscrit dans une thématique d'expertise de notre laboratoire, celle de l'organisation du cytosquelette d'actine dans les ostéoclastes résorbants. Nous avons pu élucider le rôle de la formation des podosomes et de leur organisation collective sur l'adhérence et la migration ostéoclastique. Nos résultats ont démontré que l'assemblage de podosomes sous forme de structures circulaires dites « anneaux » exerce une force centripète sur le substrat et ainsi déclenche la migration de l'ostéoclaste. L'alternance entre apparition et disparition de ces anneaux au sein de la cellule résulte en une migration saltatoire universelle pour tous les ostéoclastes.
L'objectif principal de cette thèse était de trouver de nouveaux gènes impliqués dans l'organisation des podosomes. Nous avons mis en place une analyse transcriptomique comparant les ostéoclastes avec d'autres cellules multinucléées géantes qui présentent des podosomes mais sont incapables de résorber l'os. Parmi la liste de six gènes établie par cette méthode, nous avons étudié RhoE. En exploitant la culture d'ostéoclastes primaires déplétés de RhoE, nous avons démontré que ce gène est essentiel pour la migration ostéoclastique et la résorption osseuse. Nous avons ensuite établi que RhoE agit comme antagoniste de la voie de Rock pour assurer le renouvellement d'actine au sein des podosomes, ce qui entretien la fonction ostéoclastique.

Abbreviations

2D: 2-demensional
3D: 3-dimensional
ACPA: anti-citrullinated protein autoantibodies
Ap-1: activator protein 1
BCG: bacillus Calmette-Guérin
BLNK: B-cell linker protein
BL: Basolaterak domain
BRU: bone remodeling unit
csf1r (c-fms): colony stimulating factor 1 receptor
CLP: common lymphoid progenitor
CMP: common myeloid progenitor
CTR: calcitonin receptor
DC-17ϒ-MGC: multinucleated giant cell derived from dendritic cells by stimulation with IL-17 and IFN-γ
DC-MGC: multinucleated giant cell derived from dendritic cells, not including OCs
DC-OC: dendritic-cell derived osteoclast
DC-STAMP: dendritic cell-specific transmembrane protein
DC: dendritic cell
DMP1: dentin matrix protein 1
ECM: extracellular matrix
ERK: extracellular signal-regulated kinases
FcRγ: Fc (Fragment, crystallizable region) receptor γ
FLS: fibroblast-like synoviocytes
FRAP: Fluorescence recovery after photobleaching
FSD: functional secrectory domain
GM-CSF: granulocyte-macrophage colony-stimulating factor
GMP: granulocyte/macrophage progenitor
gt: gene trap
HSC: hematopoietic stem cell
IFN-γ: interferon-γ
IL-1 : interleukin-1
IL-17: interleukin-17
ITAM the Immunoreceptor Tyrosine-based Activation Motif
JNK: Jun N-terminal kinase
LRC: Leukocyte Receptor Complex
LRF: Leukemia Related Factor
M-CSF, macrophage colony-stimulating factor
MGC: multinucleated giant cell
MITF: microphthalmia-associated transcription factor
MMP: Matrix Metalloprotease member
Mo-OC: monocyte-derived osteoclast
Mo: monocyte
MTs: microtubules
MV: Measles virus
NFAT(c): Nuclear factor of activated T cells NFAT (cytoplasmic)
OB: osteoblast
OC: osteoclast
OcMDC: osteoclast/macrophage/DC precursor

ODF: osteoclast Differentiation Factor
OPG: osteoprotegerin
Osteoprotegerin(OPG)-Ligand. OPG
OY: osteocyte
PAX5: paired box protein 5
PI3K: phosphoinositide 3-kinase
PLC-γ: Phospholipase C γ
RA: rheumatoid arthritis
RANK: receptor activator of nuclear factor κB
RANKL: receptor activator of nuclear factor κB ligand
RB: ruffled border
RF: rheumatoid factor
RGD: Arginyl-glycyl-aspartic acid motif
SLP76: lymphocyte cytosolic protein 2 (SH2 domain containing leukocyte protein of 76kDa)
SZ: sealing zone
SZL: sealing-zone like structure
TACE : TNF-α convertase
TLR: Toll-like receptor
TNF-α: tumor necrosis factor α
TRAF: tumor necrosis factor receptor-associated factor
TRANCE: TNF-Related Activation-Induced Cytokine
TRAP: tartrate-resistant acid phosphatase

List of introductory figures

Chapter 1: Introduction

I. BONE REMODELING

I.1. The skeleton: cells and matrix

Bone is a living tissue comprised of a stiff extracellular matrix, bone cells, blood vessels and nerves. The extracellular matrix is itself mineralized and composed of Type I Collagen mostly as well as glycoproteins and proteoglycans. Besides its obvious role in mechanical support for movement, bone also provides protection of vital tissues and organs as well as regulation of the immune, endocrine and nervous systems and mineral homeostasis.

The growth of this tissue during development, its renewal during adulthood and its repair are coordinated processes ensured by the three bone cells: osteoblasts (OBs), osteoclasts (OCs) and osteocytes (OYs).

I.1.1. Osteoblasts

OBs are derived from mesenchymal stem cells. Their main function is the deposition and arrangement of the organic matrix of bone mainly composed at 90% of of Type I collagen. OBs also secrete fibronectin, osteopontin, osteocalcin and sialoprotein which allow the mineralization of bone after crystallization of hydroxyapatite from deposited calcium and phosphate (Khurana, 2009). OBs are also able to regulate OC differentiation and function through a variety of cytokines such as RANKL, OPG, MCSF and interleukins IL-6 and IL-11 and growth factors such as TGF-β and BMPs. In addition, OBs can respond to two hormones that are central to mineral homeostasis and bone metabolism namely parathyroid hormone (PTH) and 1,25-dihydroxyvitamin D. With the aging of bone, OBs are thought to transform into “bone lining cells”, quiescent cells present at sites of bone where active bone formation is absent (Bartl, 2009).

I.1.2. Osteoclasts

OCs are multinucleated giant cells deriving from hematopoietic precursors. They are responsible for bone degradation, also known as bone resorption. To degrade the most compact and stiff matrix of the organism, OCs actively secrete protons and proteases thereby allowing the dissolution of its mineral phase and the breakdown of its protein scaffold, respectively (Coxon and Taylor, 2008b). This process ensures the release of minerals (Calcium, Phosphate, Magnesium,…), peptides (from degraded matrix proteins) and signaling molecules (TGF-β,…) formerly embedded in bone into the blood stream (Mulari *et al.*, 2003a; Yadav *et al.*, 2011). Both osteoclastogenesis and bone resorption are regulated by OBs

through RANKL and OPG expression, by OYs through RANKL and by immune cells though several cytokines such as MCSF, RANKL, TNF-α, interleukins, etc ... (Nakashima and Takayanagi, 2011a; O'Brien *et al.*, 2013). Conversely, OC are themselves able to regulate OB chemotaxis through PDGF expression (Sanchez-Fernandez *et al.*, 2008).

I.1.3. Osteocytes

In contrast to bone surface cells, i.e. OBs and OCs, OYs are embedded in the bone matrix. They comprise more than 90% of all bone cells and are derived from OBs that became trapped by the bone matrix that they themselves secreted and organized. OYs are mechanosensory cells able to translate loading stress into facilitation of macromolecule diffusion. OYs are not only able to communicate with each other through gap junctions but are also implicated in signaling to other bone cells (Khurana, 2009). For example, they can modulate OB-mediated bone formation through the expression of OB-specific factor 1 (OSF-1), dentin matrix protein 1 (DMP1) and sclerostin (Tezuka *et al.*, 1990; O'Brien *et al.*, 2013). OYs can control OCs as well by being the major source of RANKL, an indispensable cytokine for OC differentiation and function (Xiong *et al.*, 2011).

Bone modeling during the development and bone remodeling during adulthood occur in discrete foci or packets approximately 2-3mm long and with a diameter of 200-300µm (Gruber *et al.*, 2008). These were termed "Bone remodeling units" (BRU) when first described by Frost in 1964 (Figure 1,2). Whether during bone modeling or remodeling, the first step during the lifetime of a BRU is always bone resorption by osteoclasts, followed by a reversal phase where OC-like macrophages, probably differentiating from circulating monocytes (Kotani *et al.*, 2013), resorb the remainder of the fragmented collagen and finally a bone formation phase by OBs (Figure 1,2) (Bartl, 2009). BRUs have a lifespan of 3-9 months and are present in an estimated number of 10^6 at any time in the adult human organism (Bartl, 2009). These BRUs are responsible for the entire renewal of the human bone matrix every 10 years. Human BRUs outlast the lifespans of OCs (3 weeks) and OBs (3 months). Both these cell types are therefore constantly differentiating from new precursors that are thought to be delivered by blood vessels and chemically attracted or docked using matrix components (Gruber *et al.*, 2008)

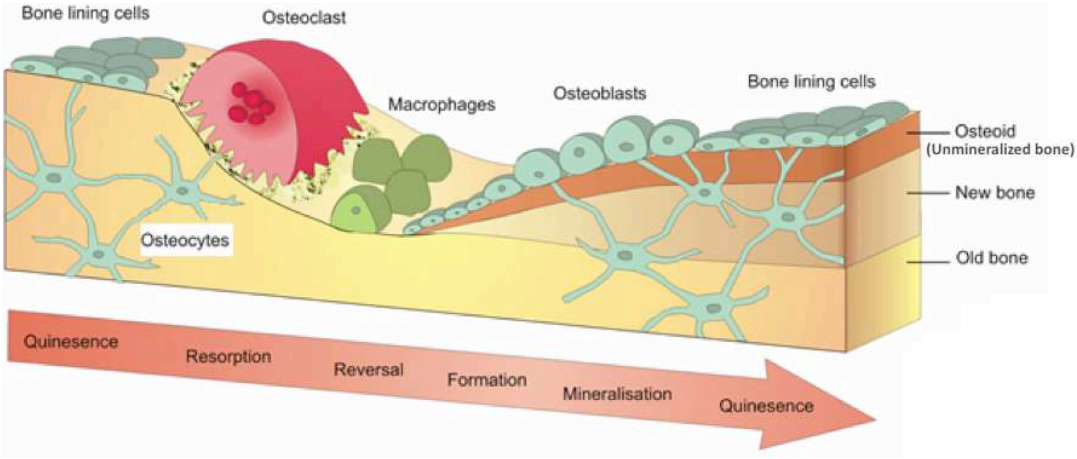

Figure 1. Chronological order of phases in a bone remodeling cycle. The first step is resorption of old bone by OCs. Secondly, OC-like macrophages thought to be differentiated from circulating monocytes (Kotani *et al.*, 2013) remove matrix debris during the reversal phase. Third, osteoblasts secrete proteins that form the osteoid layer (unmineralized bone), which is later mineralized by the same cells to become the new bone. Osteoblasts either remain on the surface of bone and become lining cells or are embeded within the bone matrix that they secreted to become osteocytes. Osteocytes contact both osteoclasts and osteoblasts and can regulate their activities. (http://imueos.wordpress.com/2010/09/29/bone-physiology/)

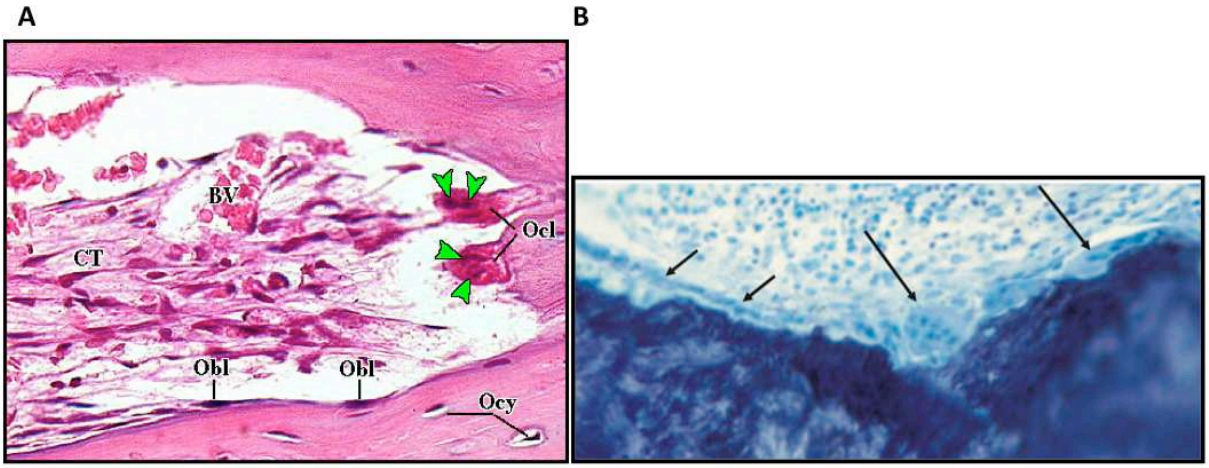

Figure 2. Histological sections of human bone remodeling units (BRUs). (A) Hematoxylin and eosin stained section. BV: blood vessel; CT: connective tissue; Obl: osteoblasts; Ocl: osteoclasts; Ocy: osteocytes; Green arrowheads: nuclei of osteoclasts (From http://courses.md.huji.ac.il/histology/cartilage&bone/I-9L.html). (B) Toluidine blue-stained section. Osteoclasts (long arrows) advancing from left to right, have formed a resorption lacuna. Osteoblasts (short arrows) are laying down unmineralized osteoid matrix in the resorption lacuna (Boyce *et al.*, 2012).

I.2. Bone pathologies: the prevalence of osteoporosis

An imbalance in the dynamic equilibrium between bone formation and resorption can result in rare cases in an increase of bone mass and density called osteopetrosis, or, more often, in a decrease in those parameters called osteoporosis.

Osteopetrosis is due to hereditary genetic disorders that rarely occur in humans (Balemans *et al.*, 2005). However, it is a common bone phenotype in transgenic animals that are engineered for use in bone biology research. Examples of such animals will be mentioned in the course of this manuscript.

Osteoporosis is one of the 10 most common diseases that affect humans with a prevalence of one in every three women and one in every eight men worldwide (Bartl and Frisch, 2004). Osteoporosis is the cause of bone fractures in 70% of US individuals (Khurana, 2009). Besides the obvious burden of these fractures on the quality of life, they pose an increased risk of mortality (Bartl and Frisch, 2004).

The cause of osteoporosis in women, and in most cases in men, is the decrease in steroid hormones with age, which always leads first to an increase in osteoclastic resorption. Steroid hormones are also important for OB formation because they promote the differentiation of HSCs into OB while blocking differentiation into adipocytes (Gruber *et al.*, 2008). Most of the clinical treatments so far used to reduce pathological decrease in bone mass have aimed at blocking OC-mediated bone resorption, although emerging treatments rather stimulate OB-mediated bone formation (Marie and Kassem, 2011).

I.3. Osteoimmunology

Evidence of the regulation of bone cells by the immune system started emerging in the 1970s when several studies described OC-stimulating soluble factors secreted by leucocytes and myeloma cells. (Horton *et al.*, 1972; Mundy *et al.*, 1974). The first of soluble factor to be identified was IL-1 (Dewhirst *et al.*, 1985) secreted by peripheral blood mononuclear cells. Since then, bone and immune cells have been found to share several pathways regulating common transcription factors, cytokines, signaling factors, receptors,… In addition to these molecular findings, the immediate vicinity of bone cells with hematopoietic precursors and immune cells within the bone marrow has raised questions about the physiological cross-regulation between the bone and immune systems, especially on the effect of the pathology of one system on the other. The study of functional links between these two systems has given

rise to a new scientific field dubbed “Osteoimmunology” by Arron and Choi (Arron and Choi, 2000).

Advancements in this field have so far established a major axis of osteoimmune crosstalk: T-lymphocyte and macrophage regulation of OC (Takayanagi, 2009; Okamoto and Takayanagi, 2011b). It has been shown that different sub-populations of T cells, namely helper T cells, can promote OC differentiation and activity directly through RANKL, TNF expression and indirectly by IL-17-mediated stimulation of synovial fibroblasts and macrophages (Okamoto and Takayanagi, 2011a). T cells can also directly inhibit these OC processes through IL-4 and IFN-γ secretion. More recently, a second axis has emerged depicting OB regulation of hematopoietic stem cell (HSC) (Yoon *et al.*, 2012).

I.4. Autoimmunity in bone diseases: the case of Rheumatoid Arthritis

A large area of osteoimmunology deals with the implication of autoimmune diseases in pathological bone remodeling. A major example of such an implication is the case of Rheumatoid arthritis (RA). RA is a systemic autoimmune disease characterized by acute inflammation of the joints with severe articular bone and cartilage erosion, often accompanied, in its late stages, by systemic inflammation-induced osteoporosis (Schett and Gravallese, 2012).

RA affects about 1% of the worldwide population but its origin is still unknown McInnes, 2011 #8386}. Current knowledge has allowed the drafting of a model of development of RA, although the exact molecular and physiological links remain elusive. At the preclinical stage, years before the actual onset of RA, the interaction of environmental factors (smoking, gut microbiome,..) with genetic and epigenetic regulation would result in post-translational modifications of certain self antigens (McInnes and Schett, 2011). The immune system would then loose tolerance to these “neoantigens” and lymphocytes would release autoantibodies in secondary lymphoid tissues or in the bone marrow. These autoantibodies include the “Rheumatoid factor” (RF) and anti-citrullinated protein autoantibodies (ACPA) (Aigner *et al.*, 2007; Kuna, 2012). RF recognizes the Fc portion of IgGs. ACPA recognizes the post-translationally citrullinated proteins such as α-enolase, keratin, fibrinogen, fibronectin, collagen, and vimentin (McInnes and Schett, 2011). These antibodies are currently used as early clinical markers of RA, although their suspected contributions to the onset of the disease are unknown. In a recent collaboration with Pr. Georg Schett’s laboratory, we have demonstrated that ACPA, by recognizing citrullinated vimentin at the surface of OCs, markedly stimulates their differentiation by promoting an autocrine TNF-α effect in these

cells (see Annex section of this manuscript: Harre*, Georgess* *et al*). Increased osteoclast numbers therefore result in severe bone loss in joints (Figure 3). This study provided the first proof that autoantibody response to citrullinated vimentin can induce bone loss ((Harre *et al.*, 2012) commented in (Leah, 2012)).The maturation of RF and ACPA antibody response could be triggered by infectious agents, neuroimmune factors, biomechanical stimuli and/or microvasculature anomalies. This maturation coincides with onset of synovitis, the local inflammation of the synovial membrane at the joints, thus starting the clinical/symptomatic phase of arthritis (Figure 3) (McInnes and Schett, 2011; Komatsu and Takayanagi, 2012a). Lymphocytes, macrophages, neutrophiles and mast cells are then recruited to synovial compartment and induce the formation of pannus, an abnormal layer of fibroblast-like synoviocytes (FLSs) and neoangiogenesis (Pap *et al.*, 2003; Okamoto and Takayanagi, 2011b; Komatsu and Takayanagi, 2012b). All these cell types intricately coordinate bone and cartilage erosion by secreting inflammatory cytokines, namely TNF-α. The latter is therefore the most relevant cytokine in RA because it directly promotes OC-mediated bone resorption. In addition to this local bone and cartilage erosion, the chronic and systemic inflammation is correlated in a longer term with osteoporosis (Schett, 2012).

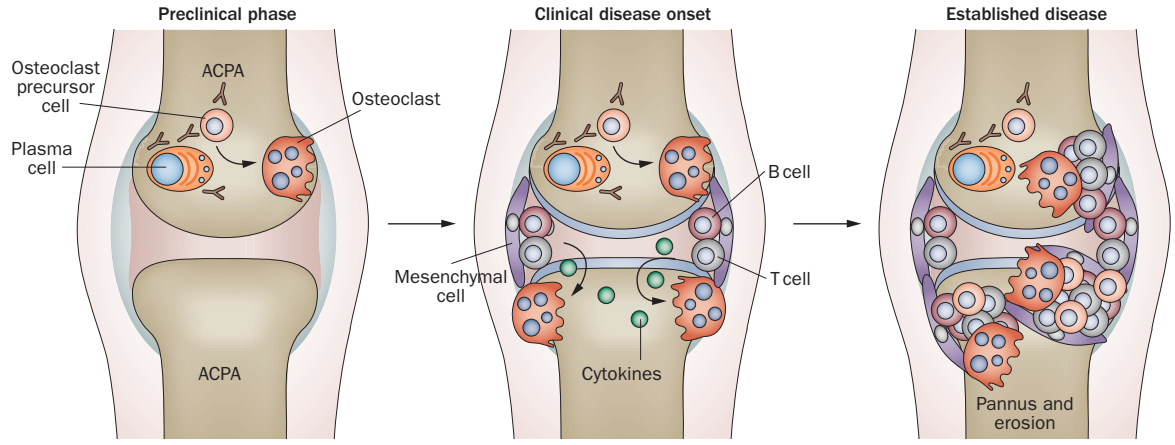

Figure 3. Evolution of periarticular bone erosion in the course of rheumatoid arthritis (RA). During the preclinical phase of RA, autoantibodies that target citrullinated proteins, namely vimentin, are produced early on by plasma cells. Citrullination is posttranslational modification consisting of the replacement of an Arginine by a Citrulline. The anti-citrullinated protein autoantibodies (ACPA) can stimulate the differentiation of osteoclasts and therefore lead to initial bone loss. These early changes may initiate in the bone marrow adjacent to the joint. Synovitis at the onset of clinical disease leads to production of cytokines

which stimulate osteoclastogenesis. The established phase of RA is characterized by the presence of large bone erosions filled with inflamed, synovially derived pannus tissue (Schett, 2012).

II. OSTEOCLAST DIFFERENTIATION

OCs are giant multinucleated cells that derive from the differentiation and fusion of mononucleated precursors. This part of the manuscript will summarize current standing on the identity of these precursors, the key signaling pathways involved in osteoclastogenesis and the link between adhesion and differentiation.

II.1. Identification of osteoclast precursors data from human and murine models

The first documented micrograph of an OC was published by Pr. A.C. Geddes in 1913 (Figure 4) (Geddes, 1913). "*In the course of the search for the origin of the osteoblast*, stated Dr. Geddes, *the origin of the osteoclast was observed*." The OC, found in the second metatarsal of an 8-9 week-old human embryo, was then defined as "*composed of the fused bodies of one or more cartilage cells, with numerous osteoblasts living within the protoplasmic mass as cell inclusions (multiple nuclei)*".

The hematopoietic origin of the OC, however, was not described before several studies in the 1970s (Steven, 1961; Kahn and Simmons, 1975; Walker, 1975; Mundy *et al.*, 1977; Jotereau and Le Douarin, 1978; Kahn *et al.*, 1978; Ash *et al.*, 1980).
In general, hematopoietic stem cells (HSCs) can give rise to two types of multipotent lineage progenitors: common lymphoid progenitors (CLPs) and common myeloid progenitors (CMPs) (Akashi *et al.*, 2000; Xing *et al.*, 2005a). CLPs can give rise to B and T lymphocytes and to natural killer cells, but not to OCs. There is one documented exception to this rule observed in $Pax5^{-/-}$ mice where pro-B cells can differentiate into OCs (Nutt *et al.*, 1999). On the other hand, CMPs can give rise to megakaryocytes, erythrocytes, and **granulocyte/macrophage progenitors (GMPs)** which themselves can differentiate either into monocytes (Mo), dendritic cells (DCs), macrophages and osteoclasts under stimulation with M-CSF or into ganulocytes under stimulation with GF-MSF (Geissmann, 2007).

FIG. 12 — × 666. To illustrate the origin of the osteoclast. Stain: Sabin's modification of Mallory's. An osteoclast is seen near the centre of the oval. The main part of its mass lies in a large cartilage cell capsule; from this a process of the cell extends to the right into a neighbouring cartilage cell capsule. It is especially to be noted that two of the nuclei of the osteoclast which are in the focal plane agree in staining reaction with an osteoblast present in the upper part of the space in which the osteoclast lies, whereas the body of the osteoclast agrees in stain reaction with the undoubted debris of a cartilage cell seen low down on the right of the oval. Beside this is an osteoblast which looks dark, but, on close examination, its darkness is seen to be due to the presence of lumps of dark matter within it. These agree in stain reaction with the debris of the cartilage cell which the osteoblast is touching. (Evidence of ingestion of the debris of cartilage cells by osteoblasts. Compare also fig. 3.)

This specimen is from the second metatarsal of a fœtus of the 8th–9th week. At this stage of development there is no piece of bone in, or in connection with, the metatarsals so large as this osteoclast. This is of some importance as negativing the recent suggestion that osteoclasts are merely pieces of bone from which the lime salts have been removed through the action of some enzyme.

Figure 4. The first documented micrograph of an osteoclast in a histological section by Pr. Geddes. The figure is explained by its legend from the original publication in 1913 (Geddes, 1913).

The identification of the two main osteoclastogenic cytokines, M-CSF in 1993 (Tanaka *et al.*, 1993) and, more importantly, RANKL in 1998 (Fuller *et al.*, 1998; Matsuzaki *et al.*, 1998; Yasuda *et al.*, 1998), accompanied by technological advancements, mainly Fluorescence-Activated Cell Sorting (FACS), have allowed to specifically isolate human and murine monoclonal GMP-derived populations and test their osteoclastogenic potential *ex vivo*. It is noteworthy to mention that mice deficient of c-Fms (the M-CSF receptor), RANKL or its receptor, RANK, do not have OCs (Dougall *et al.*, 1999; Pettit *et al.*, 2001). Strikingly, all the data so far obtained have described wide osteoclastogenic plasticity within the myeloid lineage where very early myeloid precursors as well as committed monocytes, macrophages and dendritic cells can differentiate into OCs.

When isolated from murine bone marrow, blood or spleen, GMPs that are expanded *ex vivo* under stimulation by M-CSF and GM-CSF are called Colony Forming Units-Macrophage/Ganulocyte (CFU-GMs); these can give rise to $CD11b^{+}$ OC precursors

(Roodman, 1999). Similarly, bone marrow-derived $Flt3^+$ cells that are expanded ex vivo in the presence of Flt3-ligand give rise to $CD11b^+$ $CD11c^-$ OC precursor colonies (Servet-Delprat *et al.*, 2002). Cells from both $CD11b^+$ expanded colonies can be directly differentiated not only into OCs, but also into macrophages and dendritic cells.

GMPs can also differentiate into osteoclast/macrophage/DC precursors (OcMDCs) characterized by $CD11b^+$ $Gr\text{-}1^{-/lo}$ $c\text{-}Fms^{-/+}$ expression (Arai *et al.*, 1999; Xing *et al.*, 2005b). M-CSF, through its receptor c-Fms, induces proliferation and differentiation of these $C\text{-}Fms^{-/+}$ precursors. These OcDMCs can be subsequently differentiated into OCs in the presence of RANKL. Further dissection of OC precursor clonality in mice has allowed a surface marker-based distinction between bone marrow-residing OcDMCs which had the following phenotype $B220^-$ $CD3^-$ $CD11b^{/low}$ $C\text{-}Fms^+$ $CD117^{hi/intermediate/low}$ and peripheral OcDMCs, residing in the blood or in the spleen, which conversely had high CD11b surface expression (Jacome-Galarza *et al.*, 2013). Again, similarly to the two colony-derived precursors described above, the $CD117^{hi}$ subpopulation of OcDMCs can also differentiate into DCs and macrophages.

These studies have cumulatively demonstrated that OCs cannot differentiate directly neither from the original hematopoietic stem cells (HSCs), nor from myeloid-committed GMPs, but that they derive from more committed cells: OcMDCs. Within OcMDCs pool, however, several different sub-populations exist depending on their initial hematopoietic organs (CD11b-positive or -negative) or on c-fms expression (positive or negative).

The osteoclastogenic potential of terminally differentiated myeloid cells, i.e. macrophages, monocytes and DC has also been studied, adding more complexity to the scheme. In fact, human and murine Mo ($CD14^+$ $CD16^{low}$ $CD3^-$ $CD19^-$ $CD56^-$), human osteoarthritic macrophages and the murine monocytic/macrophage cell-line RAW 264.7 can all directly give rise into OCs in the presence of M-CSF and RANKL (Sabokbar *et al.*, 2000; Gallois *et al.*, 2010). More strikingly, Mo-derived immature DCs ($CD1a^+$ $CD14^-$ HLA a,b,ci^{nt}, HLA DR^{int}, and $CD80l^{ow}$, $CD83^{low}$, and $CD86^{low}$) can also directly differentiate into OCs, even more efficiently so than Mo. Indeed, a transcriptome-wide study showed that OCs are transcriptionally closer to DC than to Mo (Rivollier *et al.*, 2004; Speziani *et al.*, 2007; Gallois *et al.*, 2010).

In conclusion, the origin of the OCs does not seem to be unique. However diverse and complex, information about the origin of OC precursors remains physiologically relevant because it may assist in answering three other questions: (1) Where does osteoclastogenesis

take place in the body? (2) Does it occur before or after recruitment on the site of resorption? (3) Are OCs a unique population or do OC subtypes exist?

II.2. The site of osteoclast differentiation

It is unclear, *in vivo*, whether or when OCs are derived from circulating precursors or bone-tissue-resident precursors. One hypothesis claims that precursors in bone marrow or near bone can differentiate into OCs on adjacent sites where resorption is needed. Resorption activity, unlike hematopoiesis which is widespread in the marrow, occurs focally i.e. heterogeneously across the bone matrix. This hypothesis would then suggest the presence of a mechanism that spatially directs the initiation of differentiation to where resorption activity is needed. Although mature OCs are themselves capable of migration through cell layers (Saltel *et al.*, 2006), data supporting the stated hypothesis *per se* has not yet been published. A second hypothesis claims that OC precursors leave hematopoietic tissues, invade the systemic circulation and are homed to site of bone requiring resorption (Muto *et al.*, 2011). This hypothesis implies that OC precursors have a significant migration capacity. Indeed, OC precursors are capable of migrating and the genetic depletion of the Hck gene, that promotes their migration, results in impaired homing to bone sites *in vivo* and, consequently, to reduced differentiation (Verollet *et al.*, 2013). In addition to the studies mentioned in the previous paragraph depicting the high *ex vivo* osteoclastogenic potential of circulating myeloid cells, more recent work using *in vivo* two-photon microscopy in mice has showed that OC precursors originating from the spleen can transmigrate into the systemic circulation, enter the bone spaces and differentiate into OCs (Kotani *et al.*, 2013). Lipid mediators and some chemokines such as sphingosine-1-phosphate (S1P), SDF-1/CXCL12 and RANKL have been shown to regulate this homing process (Ishii *et al.*, 2009). In addition, in RA murine models, CD11b+ precursors have been shown to be mobilized by inflammatory cytokines, mainly TNF-α and RANKL, towards sites of increased OC bone erosion in the joint where the presence of mature OC was significantly increased (Ritchlin *et al.*, 2003; Li *et al.*, 2004). Interestingly, in RA patients, DC numbers are severely increased in the synovium. The differentiation of these DCs into OCs *ex vivo* has been highly induced by RA synovial fluid extracted from patients (Rivollier *et al.*, 2004).

Given the accumulation of evidence albeit not absolutely demonstrative, the second hypothesis on the whereabouts of osteoclastogenesis seems more plausible. Finally, one common fact, regardless of the originating location of OC precursors, is that the terminal

phase of differentiation of already committed OC precursors cannot occur away from the bone tissue because of the main sources of RANKL, essentially OYs and OBs, are bone-residing.

II.3. Relevant cytokines involved in osteoclast differentiation

Several cytokines and their respective receptors are essential for OC precursor differentiation and fusion. Their sources, downstream signaling pathways and spatio-temporal roles are distinct.

II.3.1. M-CSF

M-CSF is a key cytokine for the determination of precursors commitment into the macrophage/OC lineage (MacDonald *et al.*, 1986)(Figures 5,7). Its osteoclastogenic function was identified in the early 1990s. In fact, investigators searching for the genetic factor behind the absence of OC and consequent osteopetrosis in *op/op* mice found that it was the alteration of the M-CSF gene expression (Wiktor-Jedrzejczak *et al.*, 1990; Kodama *et al.*, 1991). M-CSF is produced constitutively in the bone microenvironment by a range of cells, including stromal cells/OB and T-lymphocytes in response to high PTH levels and inflammatory molecules such as TNF-α and IL-1 (Weir *et al.*, 1996; Yavropoulou and Yovos, 2008). By binding to its sole receptor, c-fms (also known as CSF1-R, at the cell membrane, M-CSF promotes the proliferation, survival, and early commitment of OcMDCs (Figures 5,7). When recognized by its ligand, the receptor dimerizes and its tyrosine kinase is activated leading to auto-phosphorylation of specific tyrosine residues. This launches a downstream signaling cascade that includes PI3K, ERK1/2, PLC-γ and the proto-oncogene c-CBL (Ross, 2006). M-CSF can induce the expression of its own receptor, c-fms, by an autocrine loop that amplifies M-CSF-mediated signals, while it has also been reported to stimulate PU.1, an essential transcription factor in osteoclastogenesis (see below section II.4.1. PU-1). M-CSF can also induce the expression of RANK, the receptor of RANKL which is another indispensible cytokine in OC differentiation (Figure 7). The mutation of the M-CSF gene in *op/op* mice or in *tl/tl* rats causes a marked decrease of tissue macrophages and a lack of OCs resulting in an osteopetrotic bone phenotype (Wiktor-Jedrzejczak *et al.*, 1990; Yoshida *et al.*, 1990; Dobbins *et al.*, 2002a; Dobbins *et al.*, 2002b)). Accordingly, the genetic knockout of c-fms also leads to osteopetrosis in mice (Dai *et al.*, 2002).

II.3.2. RANKL/RANK/OPG triad:

A "giant leap" for OC research was the characterization of the indispensable role of RANKL in osteoclastogenesis (Figures 5-7). RANKL, a member of the TNF family, has been first identified on the surface of activated T-lymphocytes where it participates in the survival and activation of DCs (Anderson *et al.*, 1997; Wong *et al.*, 1997). RANKL had several other names prior to the specific identification of its importance for OCs. Some of these names were related to its general functions like "TNF-Related Activation-Induced Cytokine" (TRANCE) for example. Other names, however, were more specific of its OC-targeting function as its identification became more imminent, such as Osteoclast Differentiation Factor (ODF), and more importantly, Osteoprotegerin(OPG)-Ligand. OPG, a molecule also belonging to the TNF family, was identified as a secreted inhibitor of OC differentiation in vivo and in vitro (Simonet *et al.*, 1997) (Figures 6,7). It was not before several studies in 1998 that the antagonist of OPG was found to be the immune cytokine RANKL (Fuller *et al.*, 1998; Lacey *et al.*, 1998; Yasuda *et al.*, 1998). RANKL and its receptor RANK were therefore established as important for the development of the immune system (e.g. lymph nodes) and the bone tissue (Dougall *et al.*, 1999). In bone, secreted OPG acts as a decoy receptor for RANKL thus blocking its binding to RANK (Simonet *et al.*, 1997; Yasuda *et al.*, 1998) (Figures 6,7). RANKL is synthesized by OBs, stromal cells, hypertrophic chondrocytes, B- and T-lymphocytes, osteocytes and even OCs themselves. Upon its synthesis, RANKL is relocated at the membrane of the cell and can be cleaved by proteases such as TNF-α convertase (TACE), Matrix Metalloprotease-14 (MMP-14) and A Disintegrin And Metalloprotease family member 10 (ADAM-10) (Hikita *et al.*, 2006). Its most functionally dominant role is when it remains at the surface of source cells and acts through cell-cell contact. Although OBs had been considered for many years as the primary physiological source of RANKL to OCs, two distinct studies using mouse genetic models recently described OYs as the major source of RANKL needed for OC differentiation (Nakashima and Takayanagi, 2011b; Xiong *et al.*, 2011). It is currently claimed that OYs are the major source of OPG as well (O'Brien *et al.*, 2013). The ratio of RANKL/OPG is therefore crucial for bone resorption. An interesting challenge in the future of bone research would be to understand why and how the same cells, OYs, induce and inhibit OC differentiation and activity.

Because RANK lacks intrinsic enzymatic activity in its intracellular domain, after it is bound by RANKL, it recruits adaptor molecules such as TRAF family proteins, namely TRAF6 which transduces NF-κB and mitogen-activated kinases (MAPKs) pathways that include Jun p38 and N-terminal kinase (JNK), respectively (Matsumoto *et al.*, 2004; Vernejoul and Marie,

2008) (Figures 5,6). RANK thereby activates several key transcription factors including AP-1 through its component c-fos and NFATc1 through NF-κB and c-fos signaling (Figure 6). Genetic depletions is these key signaling molecules in osteoclastogenesis such as RANKL$^{-/-}$, RANK$^{-/-}$, TRAF6$^{-/-}$ and c-fos$^{-/-}$ lead to osteopetrosis in mice due to the absence of differentiated OCs (Grigoriadis *et al.*, 1994; Dougall *et al.*, 1999; Kong *et al.*, 1999; Lomaga *et al.*, 1999). Conversely, OPG$^{-/-}$ mice are osteoporotic due to lack of OC activity (Bucay *et al.*, 1998; Mizuno *et al.*, 1998). Given the central role of RANKL, a monoclonal antibody targeting it, Denosumab, is now clinically administered for the treatment of several bone pathologies such as rheumatoid arthritis, giant cell tumor of bone, … (Dempster *et al.*, 2012).

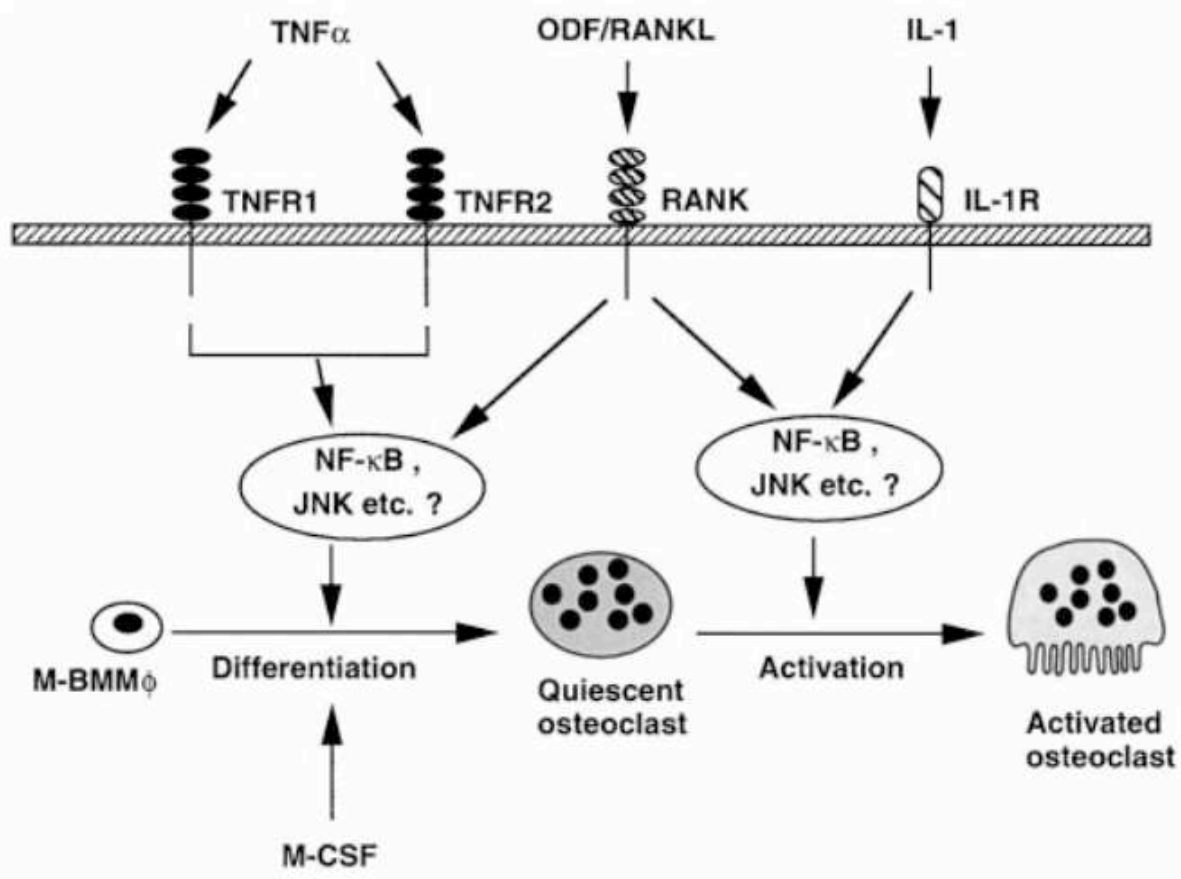

Figure 5. Schematic representation of major ligand-receptor systems in OC differentiation and function regulated by TNF-α, ODF/RANKL, and IL-1α. TNF-α and RANKL (also known as Osteoclast Differentiation Factor, ODF) independently stimulate osteoclast differentiation. OC differentiation induced by TNF-α occurs via TNFR1 and TNFR2 expressed by osteoclast precursors (here abbreviated as M-BMMϕ for Monocytes-

Bone Marrow Macrophaghes). ODF/RANKL induces osteoclast differentiation through RANK-mediated signals. M-CSF is a common factor required for both TNF-α– and ODF/RANKL-induced osteoclast differentiation. Activation of osteoclasts is induced by ODF/RANKL and IL-1α through RANK and type 1 IL-1 receptor, respectively. Common signaling cascades such as NF-κB and JNK activation may be involved in the differentiation and activation of osteoclasts induced by TNF-α, ODF/RANKL, and IL-1α (Kobayashi *et al.*, 2000).

II.3.3. TNF-α/IL-1

TNF-α is the predominant inflammatory cytokine in immuno-mediated pathological bone resorption. It can be secreted along with RANKL by activated lymphocytes, synovial fibroblasts and macrophages in the vicinity of OCs. This cytokine can induce osteoclastogenesis in two manners i.e. directly, by acting on OCs, or, indirectly by stimulating proximal cells to express RANKL, IL-1 and IL-1R (Wei *et al.*, 2005). Once secreted, both TNF-α and IL-1 are potent inducers of OC differentiation through their respective receptors on the surface of OC precursors. TNF-α has two cell surface receptors, TNFR-I and TNFR-II, which are expressed in various cell types including HSCs (Kobayashi *et al.*, 2000) (Figure 5). When TNFR-I is bound, it activates the TRADD/TRAF pathway leading to a regulation of caspase-mediated apoptosis. When TNFR II is bound, it interacts with TRAFs 2, 5 and 6 resulting in the activations of NF-κB and JNK pathways (Figure 5). Due to its ability to overlap RANKL/RANK signaling, TNF-α potently induces osteoclastogenesis (Kobayashi *et al.*, 2000).

Like TNF-α, IL-1 is also secreted by macrophages and stromal cells and present at bone erosion sites linked with inflammation, e.g. rheumatoid arthritis. Since IL-1 and its receptor, IL-1R, expression by stromal cells and macrophages in the vicinity of OCs is promoted by TNF-α, IL-1 is considered downstream of TNF-α in this signaling interplay. When IL-1 binds to its receptor IL-1R, its leads to the activation of the TRAF6-dependent NF-κB and JNK pathways via MyD88 and IRAK recruitment (Kwan Tat *et al.*, 2004) (Figure 5). Due to the overlapping of their signaling with that of RANKL, TNF-α and/or IL-1R have osteoclastogenic effects that are synergetic with RANKL (Thomson *et al.*, 1987; Konig *et al.*, 1988) (Figure 5) but a minimal level of RANKL is still required for osteoclastogenesis *in vivo* and *in vitro* (Kwan Tat *et al.*, 2004).

It is now clear that the signals induced by the pro- and anti-osteoclastogenic cytokines modulate a variety of complex intracellular processes that will determine the fate of the precursors. Once vital process that is controlled by these cytokines is the expression and activity of certain transcription factors during OC differentiation.

II.4. Transcription factors involved in OC differentiation and function

The differentiation of HSCs all the way to OCs is comprised of sequential stages that are tightly regulated by several transcription factors. For example, PU.1 and PAX5 are "early" factors responsible for steering HSCs either into CMPs or CLPs, respectively. Other factors such as MITF, NF-κB and NFATc1 control later stages of osteoclastogenesis and lymphopoiesis.

II.4.1. PU.1

PU.1 is a member of the ETS transcription factor family characterized by its DNA-binding domain ETS. PU.1$^{-/-}$ mice, in addition to suffering from a lethal immune deficiency linked to the absence of B-lymphocytes and macrophages, are also osteopetrotic and devoid of OCs (Tondravi *et al.*, 1997). PUI.1 regulates therefore both the lymphoid and myeloid lineages, mainly through its expression levels (Figure 7). In other words, low levels of this transcription factor in HSCs lead to their differentiation into CLPs and high levels leads to macrophages, that can differentiate into OCs in theory, all the while inhibiting B-cell transition (DeKoter and Singh, 2000).

II.4.2. PAX5

PAX5 is a member of a large family of transcription factors that are highly conserved during evolution and responsible for development and morphogenesis. PAX5$^{-/-}$ mice do not have mature B-lymphocytes and therefore die a few days post-birth. Additionally, these mice exhibit a sever increase in OCs numbers and are osteopenic (i.e. with low bone mass but still higher than in osteoporosis) (Horowitz *et al.*, 2004). Interestingly, the PAX5 gene encodes the protein B-cell-lineage-specific activator protein (BSAP) that is expressed only in B-lymphopoietic lineage, downstream of PU.1; it is undetected in OBs and OCs. The ablation of PAX5 in mice results in the expansion of spleen-derived c-fms^{+} Mac-1^{+} FcRγ^{+} B220^{-} macrophage precursors that are highly osteoclastogenic. This population would be otherwise repressed by PAX5 expression (Horowitz *et al.*, 2004; Horowitz and Lorenzo, 2007a, b). PAX5 has also been shown to repress other lineage-specific genes such as Flt3 (required for

multipotent B-cell progenitors), c-fms (OcMDCs) and Notch 1 (T-cells) (Nutt *et al.*, 1999; Souabni *et al.*, 2002; Holmes *et al.*, 2006). Given these properties, PAX5 is now considered to be an "early" repressor of osteoclastogenesis.

II.4.3. MITF

Microphtalmia-associated transcription factor (MITF) is the most characterized member of the MIT family of transcription factors. An important functional aspect of MITF activity during osteoclastogenesis lies in its cooperation with other transcription factors to promote the expression of proteinase, essential molecules for bone degradation (Luchin *et al.*, 2000). By interacting with PU.1, MITF can promote the expression of the TRAP gene, a protease that is critical for bone resorption (Luchin *et al.*, 2000) (Figure 7. MITF also associates with TFE3 to drive Cathepsin K expression (Motyckova *et al.*, 2001). The spontaneous ophthalmic mutation "mi" in the DNA-binding domain of MITF1 results in the blockade of expression of its target genes (Mansky *et al.*, 2002a; Mansky *et al.*, 2002b). Consequently, *mi/mi* mice are osteopetrotic and do not form OCs. Interestingly, RANKL is overexpressed in the bone marrow of these mice suggesting that MITF participates in the negative autoregulation of RANKL (Tagaya *et al.*, 2000). B-lymphopoiesis in these mice is affected *in vivo* but not *in vitro* and it has been suggested that osteopetrosis could be responsible for this *in vivo* phenotype by reducing the available space within the bone medulla (Franzoso *et al.*, 1997) (Tagaya *et al.*, 2000).

II.4.4. NF-κB

Transcription factors of the NF-κB/Rel family are ubiquitously expressed and include 5 members in mammals: p65 (RelA), c-Rel, Rel-B, NF-κB1 (p50/p105) and NF-κB2 (p52/p100). To be functional, these members form homo- or heterodimers translocate from the cytoplasm to the nucleus where they regulate transcription on chromatin sites. Many murine knockout models have shown the importance of NF-κB family in OC differentiation (Franzoso *et al.*, 1997). For example, the expression of p50 and p52 is required in OC but not macrophages, indicating that NF-κB acts on precursors that are already specifically committed to osteoclastogenesis, i.e. downstream of PU.1 (Yamashita *et al.*, 2007b) (Figures 5-7).

II.4.5. c-Fos and AP-1 complex

Along with Fra1, Fra2 and FosB, c-Fos is part of the Fos family genes. Its viral homologue, v-Fos, induces osteosarcoma in mice (Matsuo and Ray, 2004). Fos family members each

carry the highly conserved "basic leucine zipper" structure responsible for DNA-binding and for heterodimerization, typically with Jun proteins. This dimerization results in the transcription complex called Activator Protein 1 (AP-1) (Figure 6). The only component of AP-1 so far demonstrated as indispensable for OC formation is c-Fos. Mice lacking c-Fos have all suffered from impaired osteoclastogenesis coupled with osteopetrosis (Johnson *et al.*, 1992; Wang *et al.*, 1992; Grigoriadis *et al.*, 1994), thus revealing the importance of this gene in the myeloid lineage. Although c-Fos depletion can be rescued *in vivo* and *in vitro* by exogenous expression of its family member Fra1, the endogenous expression of the latter is c-Fos-dependent. Furthermore, c-fos induced the expression of another OC-differentiating transcription factors, NFATc1 (see below, section II.4.6. NFATc1). RANKL and Ca^{2+}-signaling are both known to activate c-fos (Figure 6) while IFN-γ is known for its inhibition (Takayanagi *et al.*, 2000). In addition, but both c-fos and NFAT can interact at the protein level and cooperatively bind to DNA to launch transcription at promoter sites (Matsuo and Ray, 2004).

II.4.6. NFATc1

Transcription factors of the Nuclear factor of activated T cells (NFAT) family have been shown to regulate a diverse set of functions in several tissues and the immune system. This family is comprised of five members: NFAT1 (NFATc2), NFAT2 (NFATc1), NFAT3 (NFATc4), NFAT4 (NFATc3) and NFAT5. NFAT1, 2, 3 and 4 are regulated by calcineurine/calcium signaling (Takayanagi, 2007). They are activated when engaged by receptor adaptors linked with calcium signaling such as FcRγ and KARAP/DAP12 of the Immunoreceptor Tyrosine-based Activation Motif (ITAM) family. The engagement of these receptors leads to the activation of phospholipase C-γ (PLC-γ) which in turn liberates calcium from the endoplasmic reticulum and thus allows its binding to calmodulin. Ca^{2+}-bound calmodulin thus activates calcineurin, a serine-threonine phosphatase, which relocates NFAT to the nucleus (Figure 7) (Vernejoul and Marie, 2008). The importance of NFATc1 to osteoclastogenesis was first highlighted by Takayanagi and colleagues in the course of a highthroughput study of RANKL-induced genes in OCs (Takayanagi *et al.*, 2002a). They found that this gene was the most highly induced 24 to 72 hours post-induction with RANKL. Additionally, $NFATc1^{-/-}$ myeloid progenitors could not differentiate into OCs. RANKL acts on NFATc1 in two distinct mechanisms during this process. First, RANKL induces its expression via c-fos and TRAF6 (Figures 6,7) (Takayanagi *et al.*, 2002b). Indeed, in $c\text{-}fos^{-/-}$ and $TRAF6^{-/-}$ OCs, NFATc1 is barely induced. Second, RANKL produces calcium oscillation

thus resulting in calcineurin-dependent NFATc1 sequestering in the nucleus (Takayanagi, 2007; Negishi-Koga and Takayanagi, 2009). The chemical inhibition of calcineurin in murine bone marrow OCMDCs not only blocks this nuclear translocation but also inhibits NFATc1 mRNA transcription, indicating that NFATc1 is responsible for its auto-amplification (Takayanagi, 2007).

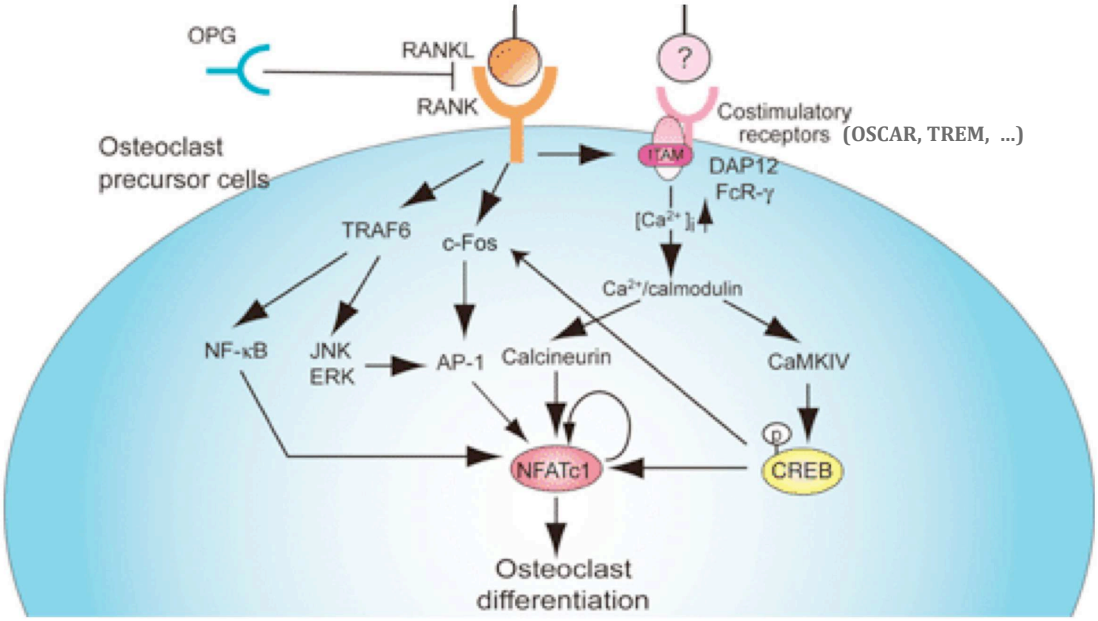

Figure 6. Schematic of signaling cascades in osteoclast differentiation. Osteoclastogenesis is supported by osteoblasts or bone marrow stromal cells, which provide RANKL, M-CSF, and poorly characterized ligands for costimulatory receptors. RANKL binding to RANK results in the recruitment of TRAF6, which activates NF-κB and MAPKs. The induction of NFATc1, a key transcription factor for osteoclastogenesis, is dependent on the transcription factors AP-1 (containing c-Fos) and NF-κB. Costimulatory signals for RANK: immunoreceptors associated with ITAM-harboring adaptors stimulate Ca^{2+} signaling. NFATc1 is translocated to the nucleus after the dephosphorylation by calcineurin that is activated by calcium (Ca^{2+}) signaling. Ca^{2+}/calmodulin kinases IV is a main kinase that activates cAMP response element-binding protein (CREB), which is also important for osteoclast differentiation. Induction of c-Fos is partly mediated by CREB. In the nucleus, NFATc1 works together with other transcription factors, such as AP-1, PU.1, MITF, and CREB, to induce various osteoclast-specific genes (Takayanagi, 2007).

NFATc1 is the master regulator of osteoclastogenesis. Its central role is supported by the fact that its overexpression in c-Fos$^{-/-}$ mice rescues the defect in osteoclastogenesis (Matsuo K 2004 JBC). In OCs, the calcium flux needed for NFATc1 activation is mediated by the phosphorylation of the ITAM adaptors DAP12 and FcRγ (Takayanagi *et al.*, 2002a; Koga *et al.*, 2004; Despars *et al.*, 2013). This pathway is synergetic with RANKL/RANK signaling and the two converge in a signaling complex that contains phosphorylated adaptors (BLNK and SLP76) and Tec family kinases, downstream of FcRγ and RANK, respectively. This complex is responsible for the induction and activation of NFATc1 (Ikeda *et al.*, 2004; Koga *et al.*, 2004; Matsuo *et al.*, 2004). However, NFATc1 expression has to be tightly tuned to avoid excessive osteoclastogenesis. Indeed, during the early stages of differentiation, strong repression is exerted on the promoter of NFATc1 by negative regulators of osteoclastogenesis such as IRF8, MafB and Bcl6. But as differentiation develops, these negative regulators are blocked by Blimp-1 thus allowing NFATc1 expression (Nishikawa *et al.*, 2010). Additionally, Leukemia Related Factor (LRF) negatively regulates NFATc1 in the early phase of differentiation but, as differentiation proceeds, its expression level increases and it becomes a positive co-factor of NFATc1 (Tsuji-Takechi *et al.*, 2012).

Once activated, NFATc1 directly regulates a number of OC-specific genes. Using promoter analyses and chromatin immunoprecipitation techniques, it has been shown that TRAP, calcitonin receptor (Takayanagi *et al.*, 2002a), cathepsin K (Matsumoto *et al.*, 2004), β3 integrin (Crotti *et al.*, 2006) and OSCAR (Kim *et al.*, 2005a) expression are NFATc1-dependent in OCs (Figure 6). The AP-1 complex (previously described in the c-Fos paragraph) has been shown in some cases to be the DNA-binding partner of NFATc1. Indeed, AP-1 and NFATc1 co-binding is required for transcription of TRAP and calcitonin receptor genes as well as the autoamplification of NFATc1 (Yamashita *et al.*, 2007a). NFATc1 can also cooperate with PU.1 and MITF in the effect on the cathepsin K and OSCAR promoters (Matsumoto *et al.*, 2004). Both PU.1 and MITF, which had been previously suspected as only relevant to the survival of early OC precursors, are therefore also important in the induction of late-stage differentiation of OCs. Together with NFATc1, these transcription factors make an OC-specific gene induction complex. This cooperation between NFATc1 and either PU.1 or MITF is however not always observed (Figure 7), such as in the case of the calcitonin receptor promoter (Kim *et al.*, 2005a), suggesting that the component variability of this complex can contribute to gene-specific spatiotemporal regulation of transcription (Takayanagi, 2007). Finally, it is worth noting that despite its unambiguous importance during osteoclastogenesis, NFATc1 is not the only member of the NFAT family to intervene

during this process. NFATc2 has also been shown to be important in this context (Ikeda *et al.*, 2004).

In conclusion of sections II.1 and II.2, it is worth noting that, although a full "molecular map" of the elements regulating OC differentiation is not yet available, serious advancements have allowed the establishment of a working model that depicts how the most essential cytokines, transcription factors and OC markers intervene during osteoclastogenesis (Figure 7).

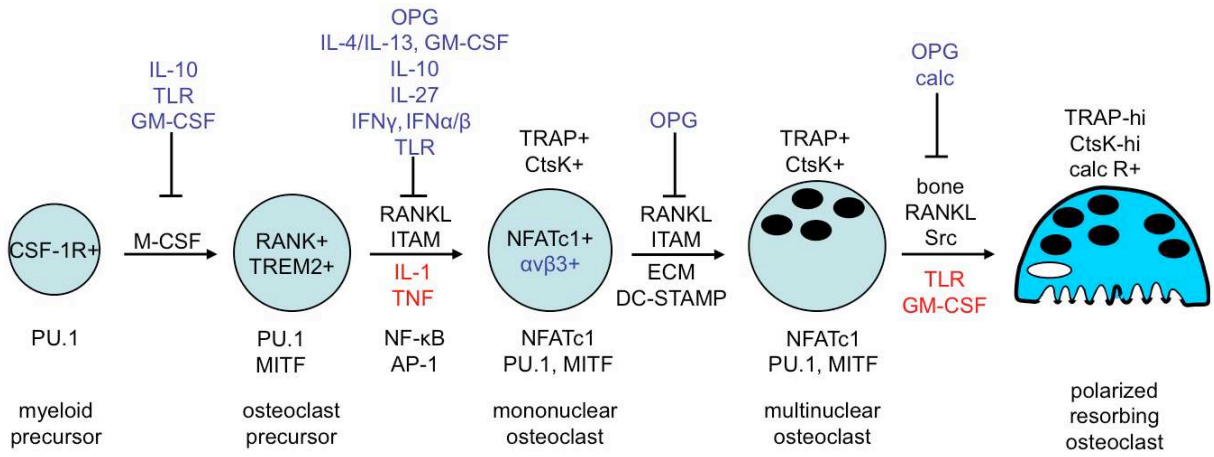

Figure 7. Regulation of OC differentiation. OCs are derived from myeloid precursors. Macrophage colony-stimulating factor (M-CSF) induces myeloid precursors to differentiate to osteoclast precursors that express RANK (Receptor activator of NF-κB) and TREM2 (Triggering receptor expressed by myeloid cells-2) receptors. Upon RANK ligand (RANKL) stimulation and ITAM (Immunoreceptor tyrosine-based activation motif) activation, osteoclast precursors undergo further differentiation to mononuclear osteoclasts with NFATc1 (Nuclear factor of activated T cells, cytoplasmic 1) induction and express osteoclast-related genes such as those encoding Tartrate-resitant acidic phosphatase (TRAP), cathepsin K (CtsK) and αvβ3. Mononuclear osteoclasts then fuse to multinuclear osteoclasts and function as polarized bone resorbing cells. This process of osteoclast differentiation is regulated by various transcription factors and exogenous factors at different stages. Inflammatory factors that promote osteoclastogenesis are shown in red. Inhibitors of osteoclastogenesis are shown in blue. Calc, calcitonin; Calc R, calcitonin receptor; CSF-1R, colony stimulating factor 1 receptor; DC-STAMP, dendritic cell-specific transmembrane protein; ECM, extracellular

matrix; GM-CSF, granulocyte-macrophage colony-stimulating factor; M-CSF, macrophage colony-stimulating factor; MITF, microphthalmia-associated transcription factor; OPG, osteoprotegerin; TLR, Toll-like receptor (Zhao and Ivashkiv, 2011).

II.5. OC precursor fusion

As a result of stimulation by RANKL, $RANK^+$ OC monocytic precursors undergo cell-cell fusion to form giant multinucleated bone-resorbing cells. Why functional OCs need be multinucleated to efficiently degrade bone is not understood. It is widely hypothesized that mononucleated $RANK^+$ $TRAP^+$ cells are not efficient in bone resorption but there is no evidence neither supporting nor disproving this hypothesis in mammals. In teleost fish, for example, the majority of resorbing OCs is mononucleated. However, several drastic differences in the bone and immune systems exist between of mammals and fishes, including the absence of haematopoietic bone marrow and of OYs (Witten and Huysseune, 2009).

Usually, bone tissue sections in mammals as well as ex vivo differentiated OCs simply show that OCs cells resorb bone in their multinucleated state. As for the precursor fusion process, extensive videomicroscopy of OCs differentiating in culture performed in our lab over the past 10 years has made it quite clear that fusion is not a random process. Prior to fusion, cells seem to select their fusing partner and to repulse other cells after a cell-cell contacts that is maintained for a certain period of time (minutes to hours) before a decision is made.

Whilst M-CSF is responsible for the proliferation, survival and early steering of myeloid precursors into the osteoclast pathway, RANKL is the main cytokine controlling cell-cell fusion and terminal osteoclastogenesis. RANKL signaling initiates a cascade of gene expression that includes the production of chemokines such as RANTES as well as MCP-1 and its two receptors CCR2 and CCR4. These are chemotactic molecules able to signal to monocytes (Kim *et al.*, 2005b). Chemokine-mediated fusion is thought to transduce $RANK^-$ quiescent precursors to fuse with $RANK^+$ ones. In the absence of RANKL signaling, MCP-1 has been shown to stimulate TRAP and CTR by inducing NFATc1 in rheumatoid arthritis, but the resulting multinucleated cells did not resorb bone efficiently (Kim *et al.*, 2006). This proves the presence of a more important RANKL-mediated mechanism of fusion: activating NFATc1 to bind to promoter region and activated the expression of DC-STAMP and ATP6V0D2 (Lee *et al.*, 2006). DC-STAMP-expression at the surface of OC precursors is sufficient to make them fuse with $DC\text{-}STAMP^-$ precursors. In that manner DC-STAMP expression is passed on from a single cell to a binucleated cell which in turn can recruit

another DC-STAMP^{-} mononucleated precursor, etc… (Vignery, 2005). DC-STAMP$^{-/-}$ and ATP6V0D2$^{-/-}$ mice are osteopetrotic as a result of perturbed OC fusion leading to absence of OCs (Lee *et al.*, 2006). The genetic depletion of these fusion genes highlights the importance of fusion to bone resorption activity.

When differentiated *ex vivo* in culture-treated dishes, fully differentiated murine marrow- or spleen-derived OCs in the presence of M-CSF and RANKL can contain up to 100 nuclei per cell. However, a much lower number of nuclei is seen in murine OCs in vivo (histological section of bone tissue) or when these murine precursors are differentiated on bone (Jurdic lab, unpublished data). This puts forth the possibility of a matrix-dependent control as well as other possible physiological limitations of fusion. This discrepancy of nuclei numbers between *in vivo* and *in vitro* is not observed in human osteoclasts.

II.5. Matrix-cytokine converging pathways in osteoclastogenesis

The priming of myeloid precursors, their fusion and their homing in the bone microenvironment is accompanied by costimulatory signals from the bone matrix. Indeed, matrix proteins are recognized by activated surface receptors of differentiating OCs and contribute to (1) the differentiation process and (2) to the launching of degradation-related functions once OCs are fully differentiated. The second step is also known as OC maturation.

II.5.1. OSCAR-RANKL axis:

RANKL induces for the expression of an OC-specific member of the Leukocyte Receptor Complex (LRC) protein family: OSCAR (Kim *et al.*, 2002). This immunoglobulin-like receptor is expressed in OC precursors and mature OCs in humans in mice and recognizes collagens I, II and III (Barrow *et al.*, 2011). Although collagen I is the predominant collagen in bone, collagen III is, along with collagen I, expressed by OBs and by RANKL^{+} endothelial cells of the microvasculature (Barrow *et al.*, 2011). The matrix-independent role of OSCAR is to co-stimulate RANKL signaling through FcRγ, a member of the ITAM adaptor family (Figure 5). Another role of OSCAR has also exists. By binding to specific helical motifs in these collagens, OSCAR can potently induce osteoclastogenesis independently ITAM adaptor family members such as FcRγ and DAP12 (Kim *et al.*, 2002). In fact, OSCAR overexpression was shown to recue the osteoclastogenesis defect in DAP12$^{-/-}$ mice and OC differentiation *ex*

vivo from humans suffering from DAP12 mutations (Barrow *et al.*, 2011). In conclusion, given the ability of OSCAR to recognize collagen and its high osteoclastogenic potential in synergy with activate RANK, it is hypothesized that $OSCAR^+$ $RANK^+$ OC precursors can therefore be properly directed along $RANKL^+$ vessels ending in the bone microenvironment, then docked on collagen I/III^+ bone surface cells and naked collagen I^+ bone sites to reach degradation-requiring destinations (Barrow *et al.*, 2011). The complete molecular mechanism corresponding to matrix-dependent OSCAR signaling is not yet revealed.

II.5.2. Integrin-RANK and Integrin- MCSF axes:

The αV family of integrins recognizes the Arg-Gly-Asp (RGD) amino-acid motif that is present in several bone matrix proteins such as bone sialoproteins and osteopontin. Integrins are transmembrane receptors have a long extracellular domain and a shorter intracellular domain (Hynes, 2002). This allows them not only to bind and transmit signals from the extracellular matrix into the cell, therefore accomplishing what is called "outside-in" signaling, but also to be modulated by signals within the cell, a process called "inside-out signaling" (Hynes, 2002). Integrins are differentially expressed by OCs along their differentiation: αVβ5 is initially expressed in M-CSF-stimulated bone marrow macrophages but its expression is lost in favor of αVβ3 after exposure to RANKL (Lakkakorpi and Rajaniemi, 1991; Inoue *et al.*, 1998; Lane *et al.*, 2005; Teitelbaum, 2007). OCs also express α2β1, αVβ1 and α9β1 but αVβ3 is the most abundant and therefore the principal integrin in OCs (Rao *et al.*, 2006). It is currently admitted that αVβ3 has 2 distinct functions during OC differentiation and maturation: (1) c-fms-dependent stimulation of osteoclastogenesis and (2) RANK-dependent cytoskeletal organization (Teitelbaum, 2007).

In mice lacking the β3 subunit, the resorptive capacity is abolished due to defects in OC cytoskeleton and cell spreading (McHugh *et al.*, 2000). The cytoskeleton-specific interplay between αVβ3 and RANK is, in fact, mediated by another relevant molecule to actin arrangement: c-Src. In RANKL-stimulated OCs, αVβ3 and activated RANK coprecipitate *in vitro* uniquely in the presence of c-Src. The latter binds ligand-linked RANK via its SH2 domain and αVβ3 via SH3 domain, thus providing a possible link between these two receptors (Teitelbaum, 2007). More detailed descriptions of the role of integrins and Src in OC cytoskeletal arrangement are available in section

Molecular studies, however, have shown that the importance of αVβ3 during OC differentiation is actually mediated by M-CSF and its receptor c-Fms. In $\beta3^{-/-}$ mice, OC numbers are increased *in vivo* although osteoclastogenesis is attenuated *ex vivo.*

Physiologically, mice have low circulating Ca^{2+} and they suffer from osteosclerosis (i.e. increased bone density) with age (McHugh *et al.*, 2000). Having hypothesized that differential cytokine conditions between the two environments, i.e. between real bone marrow and experimental tissue culture, could be responsible for this paradox, Faccio and colleagues have demonstrated that high doses of M-CSF, but not RANKL, recues $\beta3^{-/-}$ osteoclastogenesis in *ex vivo* bone marrow cultures (Faccio *et al.*, 2003b). The authors have proposed a molecular mechanism through which c-Fms occupancy and subsequent phosphorylation on Y697 are responsible for ERK and c-fos upregulation and, ultimately, stimulation of differentiation (Faccio *et al.*, 2003b).

II.5.3. Is adhesion required for differentiation?

Osteoclastogenesis seems to integrate signals from specific cytokines and from the matrix via integrins and other receptors. These have an unequivocal role during the bone resorption process in mature OCs, but the extent of their contribution to OC differentiation is still controversial. A study by Mochizuki and colleagues has shown that the culture of OC precursors in the presence of M-CSF and RANKL on a 2D non-adherent substrate markedly reduces RANK expression and OC differentiation efficiency (Mochizuki *et al.*, 2012). These precursors adopt macrophage instead of OC characteristics, thus suggesting that the adhesion of precursors to the substratum in required for osteoclastogenesis. Even more, the chemical inhibition of integrins with an RGD-containing disintegrin in OC precursors also reduces RANK expression and OC differentiation (Mochizuki *et al.*, 2012). The importance of adhesion, but not integrin-mediated signaling *per se*, in osteoclastogenesis has been confirmed by a more recent study (Touaitahuata *et al.*, 2013). The role of CD44, a non-integrin OC receptor, in OC differentiation (Chabadel *et al.*, 2007) has not yet been addressed. Starting from the earliest stages of their differentiation, OCs precursors exhibit at their ventral surface integrin-based, actin-rich adhesive puncta called “podosomes” that are thought to maintain adhesion, cell spreading and migration in a wide range of cells (Linder *et al.*, 2011a) (Jurdic *et al.*, 2006). Whether podosomes are required for OC precursor fusion and differentiation *in vitro* is controversial. Touaitahuata and colleagues have argued that integrin signaling, assayed by podosome formation, is needed neither for fusion nor differentiation (Touaitahuata *et al.*, 2013). Additionally, these same authors also concluded that podosomes are dispensable for OCs migration and, ultimately, differentiation (Touaitahuata *et al.*, 2013). These findings are in contradiction with detailed molecular and imaging data provided by Oikawa and colleagues depicting a central role of podosomes in OC precursor fusion (Oikawa

et al., 2012). The data showed that podosome organization at the circumference of OC precursors maintains cell spreading and thus sustains the contact of plasma membranes of apposed cells during fusion. Oikawa and colleagues provided a molecular mechanism in which the scaffold protein Tks5, known for its role in podosome formation, is activated by phosphoinositide 3-kinase and Src kinase and thus promotes podosome-mediated cell-cell contact and fusion (Oikawa *et al.*, 2012)

In order to give rise to mature multinucleated cells *in vivo*, OC precursors need to migrate before making cell-cell contacts and finally fusing together. There is strong evidence pointing towards mononucleated precursor recruitment to the bone and formation of mature multinucleated OCs on the bone surface. What is unknown is whether *in vivo* the fusion occurs within the bone marrow (i.e. in a 3D context, before reaching the bone matrix) or after reaching the bone matrix (i.e. in a 2D context). If the first case is true, it would then be possible that OC precursors can dispense of podosomes even though, macrophages, which derive from the same OC precursors and also form podosomes, are capable of exhibiting podosome-like structures in a 3D matrix (Van Goethem *et al.*, 2011). If the second case is true, podosome are likely to be important for migration and fusion because OCs precursors spontaneously make podosomes on bone and podosomes are the principal cytoskeletal structures that drive OC migration (Jurdic *et al.*, 2006; Saltel *et al.*, 2008).

Finally, matrix receptors such as integrins are, in some cases, directly involved in cell-cell interaction (Ojakian *et al.*, 2001). Hence, cell-cell contact is a factor that should be considered alongside adhesion and migration in order to better understand OC differentiation and fusion (Oikawa *et al.*, 2012). In *in vitro* osteoclastogenesis assays, while low seeding densities of mononucleated precursors can challenge their migration by reducing the probability of passive cell-cell contacts, a relatively high density can trigger cell aggregation and, consequently, both surface expression of αVβ3 in these precursors (Boissy *et al.*, 1998) as well as podosome-maintained membrane contacts (Oikawa *et al.*, 2012). It would therefore be interesting to investigate the balance between matrix-dependent adhesion, cell-cell adhesion and migration on different substrates: adherent and non-adherent, 2D and 3D.

As a result all the available stimuli and activated pathways that are required for their differentiation, OCs become giant multinucleated cells and acquire the proper molecular

arsenal allowing them to reach and degrade bone. How they use their arsenal to fulfill their destined function will the topic of the following section III.

III. PODOSOME ORGANIZATION IN OSTEOCLASTS

At very early stages of their differentiation *in vitro*, OCs form integrin-based and actin-rich microscopic adhesive structures called podosomes. Although the existence of podosomes has not yet been demonstrated *in vivo* due to technological limitations of imaging methods, their formation in OCs seeded on their natural substrate, i.e. bone, has been documented by electronic microscopy and fluorescence microscopy (Luxenburg *et al.*, 2007). Hence, their formation *in vivo* is highly plausible. Podosomes are circular structures that are around 1µm-wide and that rise from the plasma membrane into the cytoplasm reaching a height of around 0.6 µm (Destaing *et al.*, 2003; Labernadie *et al.*, 2010; Linder *et al.*, 2011b) (Figures 9,10). They are essential for OC adhesion, spreading, migration and bone degradation. In fact, genetic depletions of their components or regulatory proteins in mice have serious consequences on the bone phenotype through disruption of OC structures.

III.1. General principles of integrin activation

Under cytokine stimulation, specific transcription factors activated in differentiating OCs stimulate the expression of proteins required for mature OC functions. Then, signals from cytokines and substrate simultaneously orchestrate the adhesive and cytoskeletal proteins into functional structures such as podosomes.

Integrins undergo large-scale conformational changes in order to attain a high-affinity configuration during the process of integrin activation (Paradise *et al.*, 2011). These receptors are currently understood to exist in equilibrium among three main conformational states (Figure 8). In the low-affinity state, the extracellular leg domains are bent and the headpiece is closed, with an acute angle between the I-like and hybrid domains. This conformation generally exhibits little to no binding to biological ligands but can bind to small RGD peptides in solution. In the high-affinity conformation, the leg domains are extended and separated, and the headpiece is open (Paradise *et al.*, 2011). The third conformation, with extended legs and a closed headpiece, is expected to be of intermediate affinity (Xiong *et al.*, 2001; Takagi *et al.*, 2002; Xiong *et al.*, 2002; Paradise *et al.*, 2011) (Figure 8). Although the "bent" state has a low binding affinity to RGD motifs in biological ligands, it is the physiologically dominant form, in particular in the presence of

Ca^{2+} and Mg^{2+} (Takagi *et al.*, 2002; Paradise *et al.*, 2011) and is sufficient for podosome formation (Faccio *et al.*, 2002). However, both outside-in and inside-out signaling have been demonstrated capable of activation of the heterodimer (Takagi *et al.*, 2002) (Figure 8). Indeed, the presence of MCSF, responsible for the inside-out activation of αVβ3 through the cytoplasmic tail of β3, can induce active αVβ3 enrichment at podosome sites (Faccio *et al.*, 2003a).

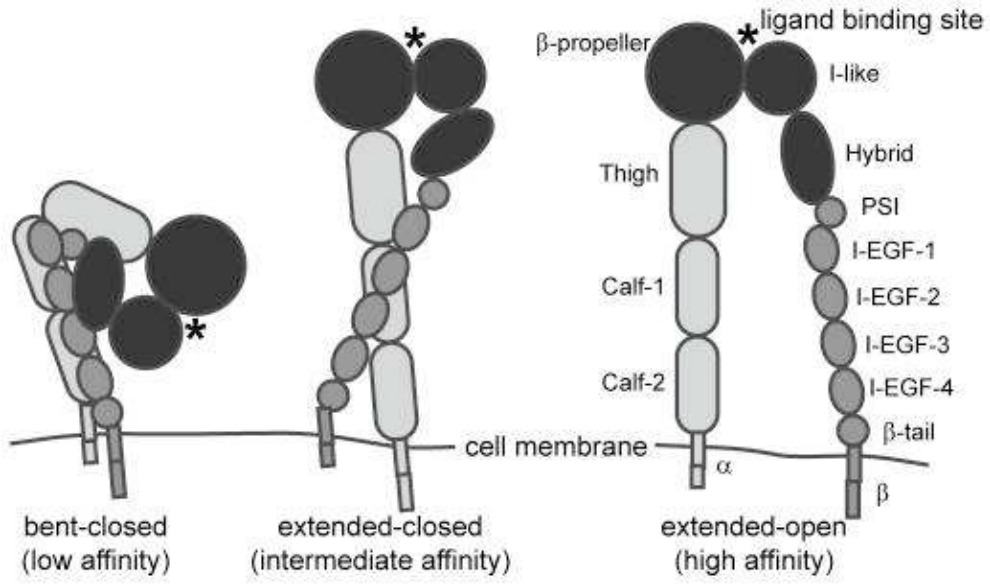

Figure 8. Integrins exhibit three distinct conformations correlated with binding affinity. Headpiece domains are depicted in black. In the low affinity conformation, the integrin leg domains are bent and the headpiece is closed. In the intermediate affinity conformation, the leg domains are extended and the headpiece is closed. In the high affinity conformation the leg domains are extended, and the headpiece is open (Paradise *et al.*, 2011).

Importance of integrins in OCs has been realized through the extensive studies of αvβ3 integrin and the matrix-degradation defects observed in Glanzmann patients or mice carrying null mutations in the β3 integrin gene (Gluckman *et al.*, 1989; Hodivala-Dilke *et al.*, 1999; McHugh *et al.*, 2000). The reduced resorptive activity of β3-/- osteoclasts was thought to be caused by loss of αvb3-mediated signaling that regulates cell polarity and cytoskeletal reorganization (Faccio *et al.*, 2003) (Brunner *et al.*, 2013). Likely, other integrin and specifically β1 integrins are also involved in osteoclast function. Indeed, a recent report using β1-deficient osteoclast point to an important role for this integrin family in the formation of

podosomes or invadopodia (Destaing *et al*., 2010; Schmidt *et al*., 2011). Some studies of integrin expression on osteoclasts show that αv, α2, β1, and β3 subunits are found in osteoclasts from human bone tissue (Nesbitt *et al.*, 1993; Brunner *et al.*, 2013). Deletion in mice of kindlin-3, an intracellular activator of integrins, leads to a severe osteoclast defect. This mimicks osteopetrosis observed in several patients with mutations in the Kindlin-3 gene, due to a block into their resorptive capacities (Schmidt *et al*., 2011). It has shown that loss of αv, β1, and β3 subunits, through kindlin-3 inactivation, ends up in a more severe osteopetrotic phenotype than β3 mutants alone. Most of the role of integrins in osteoclasts is seen through their implication in adhesion and resorption through podosome organization (Schmidt *et al.*, 2011).

III.2. Recruitment of adhesion plaque molecules

Besides integrins, other structural proteins are recruited to build the podosome. These proteins are described as cytoskeletal adaptors that organize F-actin. They are called collectively "plaque proteins". One of these proteins is talin, which binds the cytodomain of β3 integtin subunit and also contributes to its inside-out activation (Calderwood, 2004; Paradise *et al.*, 2011; Zou *et al.*, 2013). Talin is an elongated antiparallel flexible dimer (Winkler *et al.*, 1997) capable of also binding F-actin and vinculin (Papagrigoriou *et al.*, 2004). In turn, vinculin is able to bind F-actin, α-actinin and paxillin (Turner *et al.*, 1990; Jockusch and Rudiger, 1996). The sequestration of these F-actin anchoring/docking proteins to several concentric integrin sites at the immediate vicinity of the plasma membrane, an interface usually called the "adhesion plaque", indicates that podosome assembly/growth occurs in a bottom-up direction. Furthermore, the actin filaments anchored by these integrin-associated proteins are crosslinked by myosin II and α-actinin and organize into co-axial/radial segments linking concentric integrin sites (Luxenburg *et al.*, 2007). This peripheral region of the podosome is collectively called the cloud. At the centre of the podosome, the F-actin network is characterized by a higher order of density called the "podosome core" (Figures 9,10).

This high F-actin density in the podosome core is largely due to oriented and highly dynamic actin nucleation and branching machinery composed of cortactin (Wu and Parsons, 1993), the Arp2/3 complex, (Neuronal-)Wiskott Alrdich Syndrome Protein ((N-)WASP), WASP-associated Protein (WIP) (Calle *et al.*, 2004; Monypenny *et al.*, 2011). The latter is necessary to the formation of the actin core for several reasons. First, WIP interacts and activates actin-

organizing molecules (N)WASP, Nck and myosin (Krzewski *et al.*, 2006; Anton *et al.*, 2007; Monypenny *et al.*, 2011). WIP also protects WASP from proteasomal degradation (de la Fuente *et al.*, 2007). Second, by binding both to cortactin and actin monomers (G-actin), WIP recruits G-actin to cortactin-activated Arp2/3 nucleation sites proximal to the cytoplasmic membrane (Kinley *et al.*, 2003) . The importance of WIP is visible through the cytoskeletal phenotype of $WIP^{-/-}$ murine OCs which produce podosomes that lack the core domain (Chabadel *et al.*, 2007). Because WIP colocalizes with the podosome core, this phenotype provides experimental proof that the podosome cloud forms independently of the podosome core.

III.3. The podosome subdomains

III.3.1. The podosome core defined by CD44

The study of WIP in OCs has underlined the importance of an unexpected podosome component: CD44. CD44 is a cell-surface transmembrane proteoglycan that binds to hyaluronic acid, collagen, osteopontin and laminin (Goodison *et al.*, 1999). The matrix-dependent activation of CD44 can rescue podosome core formation in $WIP^{-/-}$ OCs and increases overall adhesion of these cells to their substrate. The need for outside-in activation of CD44 was additionally demonstrated by addition of activating antibodies and testing its podosome-rescuing capacity on different substrates (Chabadel *et al.*, 2007). Surprisingly, inside-out activation of this receptor has not been investigated so far and the detailed mechanism used by CD44 to support podosome core formation remains unclear. The non-overlapping localizations and functions of αVβ3 and CD44 served as decisive proof for the distinction between the two podosome domains: the cloud and the core.

III.3.2. The podosome cloud defined by Src

In parallel to the core-specific function of CD44, the tyrosine kinase Src has podosome-cloud specific function. In fact, the $Src^{-/-}$ OCs exhibit podosomes with cores but without clouds (Destaing *et al.*, 2008). The SH2 or SH3 domains of Src are necessary for the docking of Src to the podosome cloud. This localization of Src can therefore allow it to exert its tyrosine kinase activity on podosomal proteins. Both the localization of Src and its enzymatic activity are essential for full podosome assembly (Destaing *et al.*, 2008).

III.3.3. The podosome cap

Finally, a novel podosomal subdomain has been reported: the podosome "cap". The existence of this domain has been concluded from the localization of the formin FRL1 on top of the podosome core (Mersich *et al.*, 2010; Linder *et al.*, 2011a). Its potential role, however, is still to be elucidated.

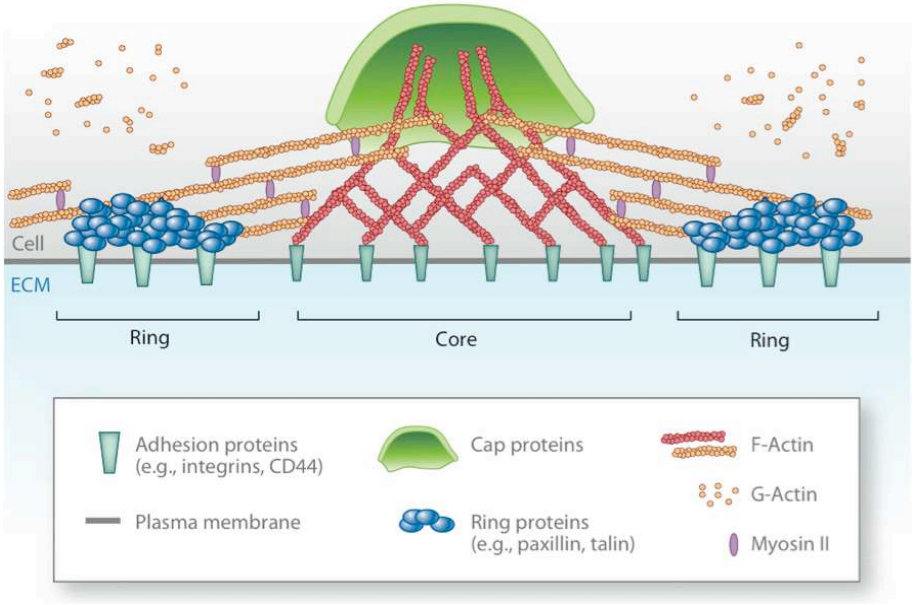

Figure 9. General schema of podosome architecture. The cloud subdomain of the podosome links the cell to the extracellular matrix (ECM) by integrins, and is contains F-actin (yellow) that is organized by adaptor (or plaque-type) proteins (like paxillin and talin) and crosslinked by myosin II. The core subdomain of the podosome is linked to the ECM via CD44 and contains dense network of branched actin (red). The cap subdomain rests on top of the F-actin dome of the core. Its function is not yet characterized (Linder *et al.*, 2011a).

III.4. Uncertainty about spatio-temporal order of podosome formation

The exact spatio-temporal order of recruitment of proteins to the site of nascent podosomes has not been fully dissected. In consequence, the chronological priority of cloud versus core formation during normal podosome assembly is still debated. A study made by Luxenburg and colleagues, however, suggested that the first step of podosome assembly is the recruitment of cloud-component paxillin followed by core-component cortactin (Luxenburg *et al.*, 2012b). This step, which represents the formation of the adhesion plaque at the

membrane-cytosol interface, is followed by the apparition of F-actin at the podosome core simultaneously with recruitment of α-actinin. β3 integrin would then be recruited to the podosome site. Although this data consolidates some aspects of the current podosome formation model, such as down-to-up assembly and inside-out activation of integrins, it raises a serious question: how are the site and the direction of actin nucleation in the core determined in the absence of integrins? A part of the answer could lie in the fact that, besides β3, other integrins subunits, such as αV, β1 and β2 and other non-integrin receptors such as CD44 are present at podosome site (Chabadel *et al.*, 2007; Schmidt *et al.*, 2011). These receptors, which have not been kinetically accounted for, can therefore participate in initial docking of the adhesion plaque and F-actin.

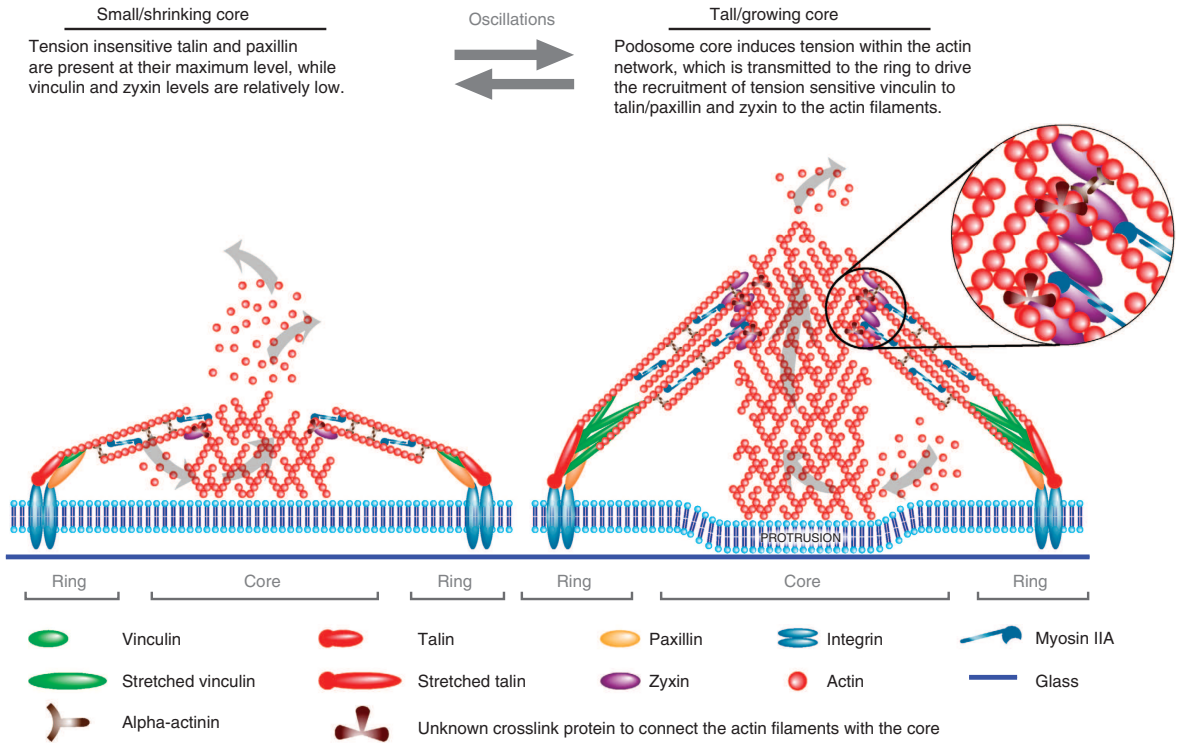

Figure 10. Model depicting the interplay of actin network and myosin IIA at podosomes. The amount of core and ring components in existing podosomes fluctuates, reflecting their variable protruding activity over time. Paxillin and talin are already present at their maximum levels in small podosome cores. As a reaction to matrix rigidity, podosomes grow vertically

by actin polymerization at the base of the core, tension is generated within the actin network and transmitted to talin and paxillin, thereby further driving the recruitment of the tension-sensitive vinculin and zyxin to reinforce the podosome and facilitate its protrusive activity. The connection of the actin network to the ring most likely occurs through talin and vinculin, whereas the main players crosslinking the network filaments to the core are still unknown. Myosin IIA cross-links the actin network filaments and is essential for core shrinkage by either generating contractility or directly unbundling and depolymerizing the actin network, thereby inducing podosome core instability. The delicate balance between actin polymerization in the core and myosin IIA activity in the ring facilitates core oscillations (van den Dries *et al.*, 2013b).

III.5. Podosome internal dynamics: interplay between polymerization and contractility

Once the podosome is "constructed", it has a lifespan of several minutes (2-10minutes). This seemingly long duration is however coupled with highly dynamic modulation, which is owed to intrinsic physical properties of its molecules.

First, the scaffold of the podosome, i.e. F-actin, is a polymer that constitutively undergoes fast treadmilling (Wanger *et al.*, 1985) and is entirely renewed every 20 to 60 seconds in OC podosomes, i.e. at least 2.5 times within the podosome lifespan (Destaing *et al.*, 2003). This fast actin turnover requires the presence of polymerization regulating molecules such as gelsolin. This protein is in fact an actin-capping and -severing protein with cleaves fast growing filament ends and thus creates new nucleation sites (Yin *et al.*, 1981; Southwick, 2000). Gelsolin localization at podosomes has been extensively documented (Zallone *et al.*, 1983; Marchisio *et al.*, 1984; Duong *et al.*, 2000) and its indispensability to podosome formation in OCs has been confirmed (Chellaiah *et al.*, 2000a) (Figure 11). Moreover, gelsolin depletion in mice results in mild osteopetrosis (Chellaiah *et al.*, 2000a). The presence of cofilin, another actin-severing protein at podosome sites has been recently described (Blangy *et al.*, 2012; Touaitahuata *et al.*, 2013). Cofilin is characterized with a lower affinity for actin compared to gelsolin (Southwick, 2000) but how it regulates podosomes is still unknown.

A second level of podosome dynamics is provided by acto-myosin contractility (Chabadel *et al.*, 2007) and elastic properties of vinculin and talin (Turner *et al.*, 1990) all present in the podosome cloud. These molecules convey to podosomes a property called "mechanosensitivity", which can be defined by modulation of contractility in parallel to F-actin polymerization in the core and, therefore, the adaptation of size and stiffness of the entire podosome to the extracellular matrix (Labernadie *et al.*, 2010; van den Dries *et al.*, 2013b) (Figure 10). Mathematical modeling of gelsolin-mediated actin polymerization in podosomes has predicted that F-actin growth can itself be a size-limiting factor of podosome core growth (Hu *et al.*, 2011a) (Figure 11). It is therefore conceivable that contractility and actin polymerization can interdependently modulate podosome mechanosensitivity.

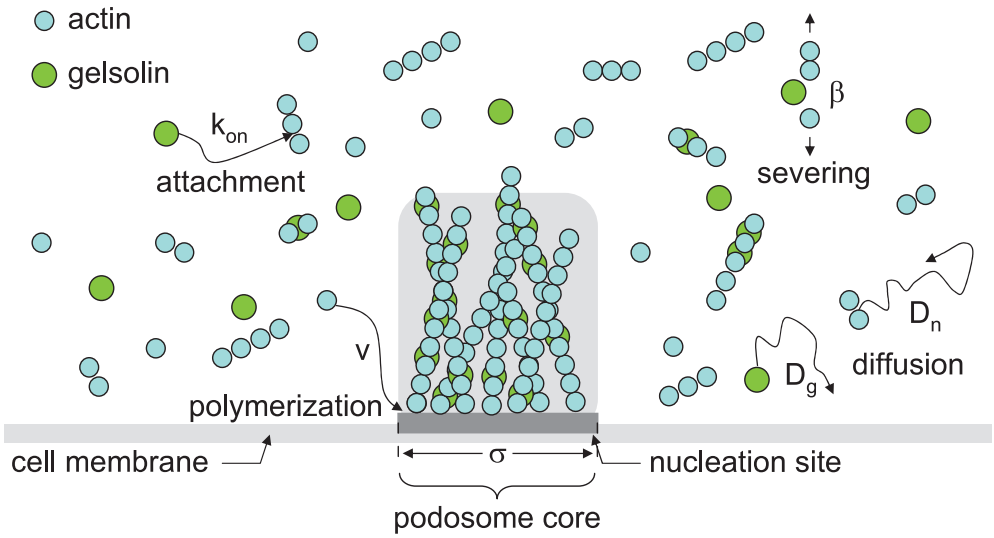

Figure 11. Schema of a mathematical model depicting steady-state actin turnover in the podosome. For simplification purposes, the model is considered as consisting of 2 dynamics elements: actin and gelsolin. Actin polymerization takes place at the base of the podosome core (with a diameter = σ) by recruitment of actin monomers at a characteristic speed *v*. After reaching an inherent limit of height, these polymers are severed by gelsolin thus releasing smaller polymers into the podosome cloud. In the cloud, gelsolin (diffusion rate = D_g) cleaves again the small polymers (diffusion rate = D_n) at a defined severing rate β (Hu *et al.*, 2011a).

III.6. OC-specific podosome properties

Podosomes are not exclusively present in OCs. Different cell types from a variety of lineages also exhibit these cytoskeletal structures. They include endothelial cells (Moreau *et al.*, 2003), smooth muscle cells (Kaverina *et al.*, 2003) and cells from the monocytic lineage such as DCs and macrophages (Linder *et al.*, 1999; Calle *et al.*, 2006). The fact that podosome-presenting cells have different physiological functions shows the high adaptability of podosomes to different microenvironments. Although the pool of structural proteins that builds the podosome is conserved between different cell types, the signals that transduce podosome formation are often different. It is therefore not surprising that some experimental observations depict differences between podosomes in different cells. This section will review some of these differences within the monocytic lineage, in other words between podosomes of OCs, DCs, and macrophages.

First, given that dynamic actin polymerization and depolymerization are necessary to maintain all podosomes, the genetic ablation of gelsolin, a high-affinity actin-severing protein that promotes actin turnover, in OCs results in their inability to form podosomes and SZs (Chellaiah *et al.*, 2000a) but has visibly no effect on podosome formation in DCs (Hammarfjord *et al.*, 2011). Second, several studies of podosomes of mature OCs seeded on culture-treated glass collectively evolve into circular patterns called rings and SZ-like structures (Jurdic *et al.*, 2006). In human and murine macrophages seeded on 2D substrates, podosomes also collectively organize into circular structures called “rosettes” (Cougoule *et al.*, 2012). In DCs however, podosomes do not exhibit such circular distributions but rather sustain their individual aspect (van den Dries *et al.*, 2013b). Third, cell migration has been shown to be mainly exerted by podosome rings in OCs. These observations suggest that there are yet unrevealed molecular pathways that induce the collective circular patterning of podosomes in OCs and in macrophage. A subset of such pathways could be exclusive to OCs to adequately support bone resorption through SZ formation. Furthermore, the role of WIP to integral podosome formation seems to be more indispensable to DCs compared to OCs. $WIP^{-/-}$ DCs do not exhibit podosomes at all (Banon-Rodriguez *et al.*, 2011) whilst $Wip^{-/-}$ OCs do form podosome clouds (i.e. podosomes without the core) although overall podosome formation is decreased compared to wildtype OCs (Chabadel *et al.*, 2007).

Interplay between the actin-containing podosomes and other components of the cytoskeleton, such as microtubules, can also be differently regulated between cells. Whilst chemical microtubule depolymerization (with nocodazole) severely abolishes podosome formation in

macrophages (Linder *et al.*, 2000), treatment with the same chemical at higher concentrations only partially blocks podosome formation in OCs but dramatically abrogates their collective patterning (Destaing *et al.*, 2005).

Finally, how podosomes dynamics and patterning could be regulated in an OC-specific manner is yet unknown. Interestingly, studies of Rho-Rock signaling in OC and OC-like cells (Ory *et al.*, 2000; Chabadel *et al.*, 2007) (reviewed in (Ory *et al.*, 2008b)) have shown that this pathway can temporally regulate podosome patterning during osteoclastogenesis and in a substrate-dependent manner. Signaling upstream of Rho and downstream of Rock though remain unclear.

III.7. Podosome patterning in osteoclasts

III.7.1. Structural and kinetic properties

Regardless of the debated importance of podosomes and adhesion in general to the OC differentiation process itself, these structures are undoubtedly crucial for the support of the mature function of OCs: bone resorption. As early as individual podosomes form within an OC, they are collectively and sequentially organized into patterns along the life of the same cell. These patterns evolve from apparently random groups of podosomes called “clusters” to circle of podosomes “rings” and, eventually to more massive circular structures, i.e. either “sealing zones” (SZ) or “SZ-like structures” (SZL, also known as “belts”) (Destaing *et al.*, 2003; Saltel *et al.*, 2004; Jurdic *et al.*, 2006; Luxenburg *et al.*, 2007) (Figure 12).

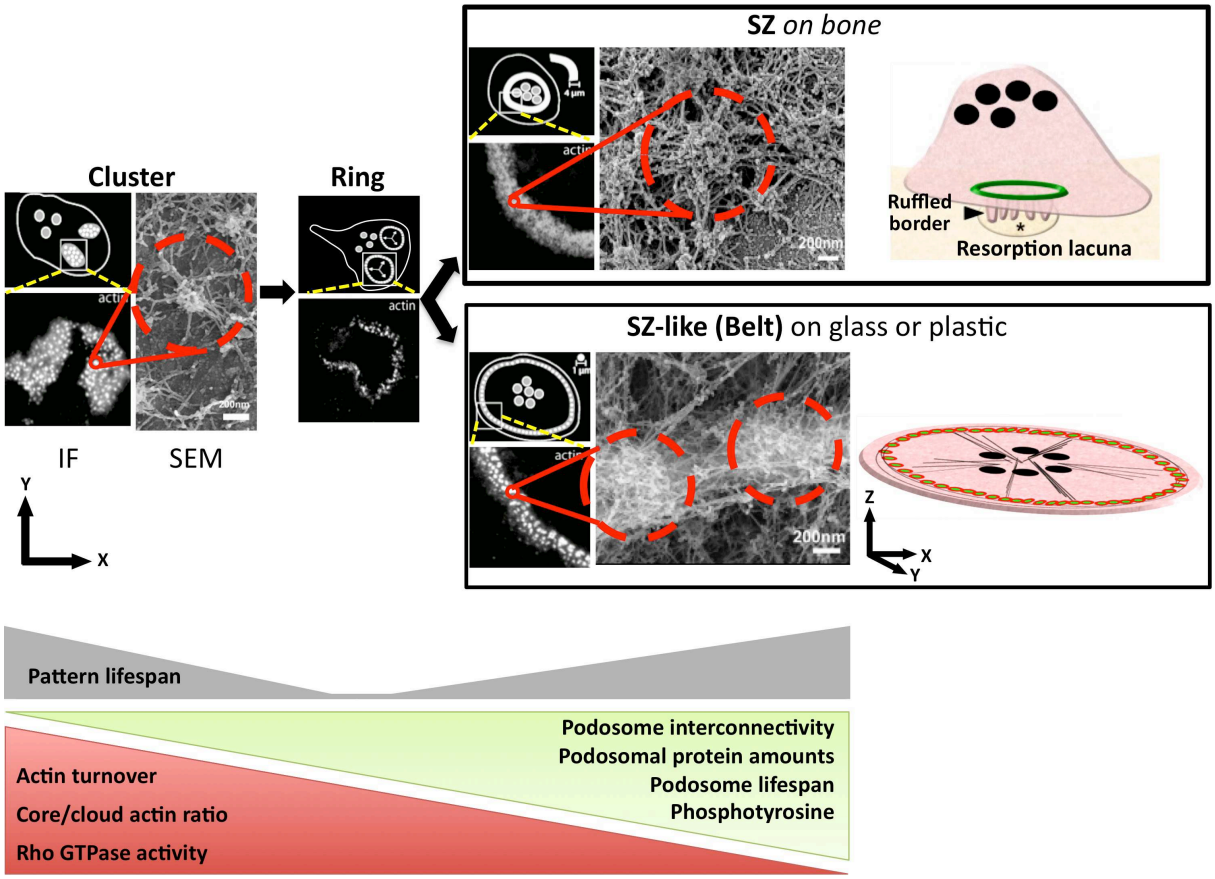

Figure 12. Current model of dynamic podosome patterning in OCs. Podosomes (surrounded by red dotted line) are collectively arranged into clusters the rings then finally either sealing zones (SZ) or SZ-like structures (also called "belts"). In the cluster, podosomes are grouped in close vicity as can be seen by immunofluorescence (IF) in a region of the cell and have a "relaxed" architecture as shown in the scanning electron micrograph (SEM). As podosomes transition from clusters to rings, transient cicrular patterns. Finally, rings can transform into SZs, if the osteoclast is seeded on bone or into SZ-like structures if the osteoclast is seeded on a non-mineralized substrate. The SZ ensures proper bone resorption by confining the degradation molecules secreted by the OC ruffled border into the resorption lacuna. The SZ-like structure is not associated with a functional activity and is at the extreme periphery of the cell. Note the increase in podosome density and interconnectivity in the SZ and the SZL compared to the cluster. Kinetic, biochemical and structural properties that accompany the patterning process are also displayed in this scheme: the pattern life span (grey), the increasing (green) and decreasing (red) factors (Adapted from (Luxenburg *et al.*, 2007; Saltel *et al.*, 2008; Novack and Faccio, 2011)).

The first pattern formed by a group of podosomes is the cluster. Several clusters can exist within an OC. At this point, individual podosomes have a "relaxed" conformation: the diameter of the core is ~300 nm, that of the cloud is 3µm and the average distance between the cores of two podosomes is 750nm (Luxenburg *et al.*, 2007). Podosomes being in this vicinity, the radial F-actin filaments of neighboring podosome clouds overlap in a common region yet without directly linking the cores to each other, suggesting the existence of some topological crosstalk between podosomes (Luxenburg *et al.*, 2007). The cluster pattern can last up to several hours in an OC while the lifespan of an individual podosome within the cluster is around 3 min (Destaing *et al.*, 2003; Luxenburg *et al.*, 2006a) (Figure 12). This means that podosome patterns are sustained by spatial commitment of *de novo* podosome formation through yet unknown mechanisms. Several non-exclusive hypotheses could explain this spatial confinement: (1) a local abundance of matrix-embedded or membrane-anchored molecules that directly stimulate podosome formation; (2) a wider microenvironment-induced cell-homing mechanism that induces migration or resorption in a given direction; (3) a cytoplasmic enrichment of podosomal proteins "left over" from disassembled podosomes thus shifting the balance from a diffusion-rate stochastic podosome formation anywhere at the cell-matrix interface in the favor of the region containing previous component.

As clusters grow, *de novo* podosomes are positioned towards the periphery of the clusters thus making transient circular structures that lasts for a few minutes: the rings (Figure 12). Although individual podosomes within a given pattern are not displaced, it has been suggested that, as a consequence of actin nucleation and polymerization at the base of the podosome core, nascent podosome repel each other while growing (Hu *et al.*, 2011a). The lifespan of individual podosomes in rings shortens down from 3 min to 1 min (Luxenburg *et al.*, 2006c), thus conveying a more dynamic aspect to this pattern compared to clusters (Figure 12). The shorter podosome lifespan is correlated with a fast ring expansion rate at 2 µm/s (Destaing *et al.*, 2003). A more detailed characterization of ring properties has been technically challenging because of the transient nature of this structure. However, what is visible by microscopy of fluorescently labeled actin is that if rings stabilize, i.e. exceed their typical lifespan without changing that of individual podosomes (Luxenburg *et al.*, 2006c), rings can give rise either to the SZ or to the SZL. When OCs are adherent to a non-mineralized substrate (glass, plastic), rings are transformed into SZL by fusing together and positioning podosomes at the very periphery of the OC (Luxenburg *et al.*, 2007). When OCs are on bone or on dentine, rings give rize to SZs by growing individually and making a thicker and more central and stable "super-ring" (D. Georgess, unpublished data).

The SZ and SZL are the most mature podosome patterns. The role of the SZ is to ensure osteoclastic bone resorption by confining OC-secreted degradation molecules at the vicinity of the bone matrix (see Section IV: Bone resorption processes). Its formation is substrate-exclusive, meaning that the SZ forms only on mineralized substrates such as bone or hydroxyapatite-coated glass (Saltel *et al.*, 2004). The SZL is thought to be the equivalent of the SZ that forms only on non-mineralized substrates such as culture-treated plastic or glass. Hence, the SZL is not affiliated with a specific function like the SZ, but it is used as an easier model to gather biochemical and microscopical data on collective podosome patterning in mature OCs.

The overall transition from clusters to SZs is marked not only by a collective displacement of podosomes but also by different internal actin dynamics and increased interconnectivity between podosomes (Figure 12). The amounts of actin and other structural proteins such as paxillin, vinculin and α-actinin recruited per podosome increases 3- to 4-fold in this transitions and neighboring podosomes become more tightly packed with a core-to-core distance that increases 2-fold on average, reaching 480 nm in the SZL and 210 nm in the SZ (Luxenburg *et al.*, 2007). With the increase of intimacy between podosomes, the density of the F-actin radial fibers that make the podosome cloud increases (Figure 12). This allows for clouds to form a continuous circular band with a thickness of 2-3 µm in the SZL and 3-6 µm in the SZ. The podosome cloud is therefore "accorded" 70 to 80 % of all the actin present in the podosome (with 20-30% of podosomal actin in the core) knowing that, at the cluster stage, the cloud only contained about 30% of actin present in the podosome (Luxenburg *et al.*, 2012a).

Although the rate of actin turnover might change from one pattern to another, it has been shown that individual actin turnover rates in the cloud and in the ring are similar and vary simultaneously (Destaing *et al.*, 2003). Even if these two podosomal subdomains might have different molecular architectures, the joint actin turnover rate attests for a common regulation of actin polymerization.

Finally, although all the mentioned podosomal patterns can appear within the lifetime of a single OC, the frequency of their formation varies as a function of OC maturation. In the early stages of osteoclastogenesis, the cluster is the most frequent pattern, making around 65% of all patterns. At the final stages of OC maturation, the SZL becomes the major pattern, constituting more than 60% of all patterns in OCs (Destaing *et al.*, 2003). This observation reveals that OCs, in order to organize these patterns, not only respond to instantaneous

extracellular cues but also commit very early along their differentiation to end-line functions such as resorption by reaching mature podosomal patterns. The fact that this differential patterning frequency occurs on the same substrate makes it tempting to speculate that the long-term regulation is directly dependent on genetic factors. Given that the frequency of SZL patterns coincides with increase OC fusion events, it would be interesting to investigate whether multinucleation is a direct genetic determinant of SZ formation.

III.7.2. Molecular mechanisms implicated in patterning

Podosome patterning is a complex molecular process that requires spatio-temporal regulation of signals and effector molecules. The molecular pathways that govern patterning were totally mysterious a decade ago but are now starting to be elucidated.

Tyrosine protein kinases: Src

During the collective patterning of scattered podosomes into the SZ/SZL, the apparent amount of certain structural proteins such as actin, vinculin, cortactin, α-actinin and paxillin increase within the individual podosome. The increase of these proteins is inversely correlated with global tyrosine phosphorylation in podosomes (Luxenburg *et al.*, 2006b; Luxenburg *et al.*, 2012a). This residue-specific post-translational modification has been associated with dynamic changes in adhesion structures. However, data on tyrosine kinases in OCs, albeit very revealing when available, is scarce.

In OCs, Src localizes to podosomes and is important for their assembly as well as their patterning (Destaing *et al.*, 2008). The dual importance of Src involves structural/docking activity and kinase activity. The first is necessary for the proper formation of the actin cloud in podosomes probably by binding the cytoplasmic tail of β3 and Pyk2 at the same time (Zou *et al.*, 2007; Destaing *et al.*, 2008). Interestingly, although Src kinase activity has also been shown important for podosome initiation, it is most crucial for rearrangement of podosomes by phosphorylating several downstream targets (Destaing *et al.*, 2008). Src can activate another tyrosine kinase Syk, which is involved in podosomal rearrangement by facilitating Rac GTPase activation (Faccio *et al.*, 2005). Indeed, mice lacking Src, Syk, or vav3 expression suffer from increased bone bass due to defective OC-resorption (Soriano *et al.*, 1991; Horne *et al.*, 1992; Lowell and Soriano, 1996; Faccio *et al.*, 2005). Another target of Src is cortactin, which induces slow actin turnover in podosomes in its phosphorylated form and thus contributes to SZL formation (Martinez-Quiles *et al.*, 2004; Luxenburg *et al.*, 2006c). Finally, Src expression, has been shown to increase during osteoclastogenesis

(Verollet *et al.*, 2013) thus suggesting that it is needed for mature podosome patterns. When other tyrosine kinases that are important for podosome patterning such as Hck are deleted, OCs compensate for this deletion by overexpressing Src which in fact re-establishes mature podosome patterning, i.e. SZL formation, and above-average OC resorptive capacity. However, Src is not expressed in OC precursors and therefore its overexpression cannot rescue defected precursor migration towards bone. As a result, $Hck^{-/-}$ mice, despite overexpressing Src in OCs, are ostepetrotic (Verollet *et al.*, 2013).

Rho GTPases

This family of molecular switches mediates signal transduction and cytoskeletal remodeling related to a broad spectrum of cellular processes in all cell types (Vega and Ridley, 2008; Hall, 2012). These molecules have been extensively studied *in vitro* and *in vivo* but the specificity of the OC cytoskeleton raises the difficulty in extrapolating their roles of into OCs. The comprehension of the roles of these proteins has been coincidently further complicated by several technical difficulties encountered by investigators as will be briefly discussed in the following paragraphs.

- ***Rho***

The importance of Rho to podosome organization and OC-mediated bone resorption has first been commented by Zhang and colleagues. In their study, the microinjection of C3 exoenzyme (a *Clostridium botulinum* toxin which inhibits RhoA/B/C) in murine OC-like cells resulted in the disassembly of the SZL structure after 20 min (Zhang *et al.*, 1995). The treatment of avian OCs with C3 lead, in the first 15 min, to transient growth of podosomes but eventually resulted in their complete dissolution 2 h after the treatment (Chellaiah *et al.*, 2000b). Also, avian macrophage polykaryons treated with TAT-C3 conjugated to the HIV TAT peptide (that ensure cell penetration) suffered from total podosomes disassembly (Ory *et al.*, 2000). This data shows a positive contribution of Rho to podosome stability. However, when the reversed experiments were performed, i.e. when avian OCs were transduced using a constitutively active Rho, they also suffered from podosome disassembly after 30 min (Chellaiah *et al.*, 2000b). The converging results of Rho overactivation and inhibition suggest the necessity for a precise and time-dependent Rho activation levels during podosome formation and patterning.

Even more, a discrepancy is observed between the C3-meditated podosome disassembly in avian macrophage polykaryons and C3-mediated stabilization of podosome rings and SZ

disassembly (Ory *et al.*, 2000; Destaing *et al.*, 2005). Whether this experimental contradiction is species-dependent and/or due to technical differences should be investigated.

Finally, the SZL-stabilizing role of Rho is dependent on the decrease of its GTPase activity during OC maturation. Indeed, lower levels of active Rho allow for less activation of its effector, mDia. In fact, active mDia can activate HDAC6 and thus lead to deactetylation and destabilization of microtubules (MTs). Therefore, lower levels of Rho allow for the stabilization of MTs by maintaining their acetylation, resulting in enhanced OC spreading and SZL formation at the cell periphery (Destaing *et al.*, 2005).

- ***Rac***

Rac1 and Rac2 are both expressed in OCs. These proteins are generally involved in organization of the cytoskeleton and are also important components of the NADPH, the enzyme that generates free radicals. The NADPH-related function of Rac has not been related with podosome organization.

A study of Rac functions in OCs using a murine Cre-recombinase-based genetic depletion model has depicted distinct roles of each of the two Rac proteins during OC precursor chemotaxis and differentiation *in vivo* (Wang *et al.*, 2008). This study has been contested by another group claiming the insufficient depletion of *Rac1* and *Rac2* genes in the first study (Croke *et al.*, 2011). In the more recent study, it is shown that Rac1 and Rac2 are not involved in osteoclastogenesis but have overlapping roles in podosome assembly and SZL formation by localizing Arp3 at podosome sites during osteoclastogenesis. The Rac double knockout therefore results in podosome disassembly, the absence of SZs and diminished bone resorption but only if Rac deletion occurs at early OC precursor stage. The abnormalities first observed in OCs due to Rac double knockout, strangely, were not reproduced when Rac deletion was driven by a different promoter corresponding to Cathepsin-K^+ differentiating OCs. As the cathepsin-K promoter activity is specific to committed OCs, it is thought that the absence of effect under this promoter is due to the incorporation of much less committed, upstream mononucleated precursors where Rac1/ 2 are not deleted (Croke *et al.*, 2011). The importance of Rac1/2 to the OC cytoskeleton and bone resorption is, however, confirmed by targeting them via intra-cellular blocking antibodies (Razzouk *et al.*, 1999).

Rac activity in OCs is regulated by its Guanine nucleotide Exchange Factors (GEFs) Dock5 and vav3 (Faccio *et al.*, 2005; Vives *et al.*, 2011b). Dock5 is increasingly expressed along osteoclastogenesis and localizes to podosomes in SZLs. The deletion of Dock5 in mice results in an osteopetrotic phenotype explained by decreased Rac activity, absence of podosome formation and SZL patterning leading to reduced adhesion and bone resorption (Vives *et al.*,

2011b). Distinctly from Dock5, the other Rac-specific GEF in OCs, vav3 is stably expressed during osteoclastogenesis but, like Dock5, promotes cell spreading and SZ formation (Faccio *et al.*, 2005). Physiologically, Vav3-null mice are osteopetrotic and protected from PTH- and RANK-stimulated bone loss indicating a role of this GEF in physiologically regulated bone remodeling.

IV. BONE RESORPTION PROCESSES

IV.1. Transmigration

At the latest stages of their differentiation/maturation, OCs are multinucleated giant cells with one main task: to resorb bone. In order to accomplish this function, the OCs needs to move to adequate regions of the bone and several possible hurdles can stand in its way. Because the *in vivo* trajectory undertaken by the OC to reach the bone surface is still uncertain, attempts have been made to better assess the tissue invasion potential of the OC by recreating the multicomponent bone microenvironment *in vitro*.

The surface of bone is largely covered by osteoblasts, bone-lining cells and, in some pathological situations, fibroblast-like cells (Pap *et al.*, 2003) and metastatic cells (Zhao *et al.*, 2006). These cells are able to secrete chemokines that attract OCs and locally promote bone degradation. At the same time, these cells can proliferate and/or differentiate abundantly in the vicinity of bone, thus representing a barrier between the OC and its resorption destination. OCs, similarly to highly invasive metastatic cells, express high levels of Src and Matrix Metalloproteiases (MMPs) (Yu *et al.*, 2003) are able to, first, transmigrate through such cells layers by forming large actin rich protrusions and, second, to spread over matrix and underneath the invaded cells (Figure 13) (Saltel *et al.*, 2006). The actin rich protrusion observed in transmigrating OCs reaches a diameter of at least 5µm (Figure 13) and therefore seems bigger than podosome-like structures observed in 3D-migrating macrophages (Van Goethem *et al.*, 2010) and invadopodia observed in metastatic cells (Linder, 2007). but could share similarities with the latter such as degradation-mediated invasion. Indeed, the chemical inhibition of either Src or MMPs hampers the transmigration process (Saltel *et al.*, 2006).

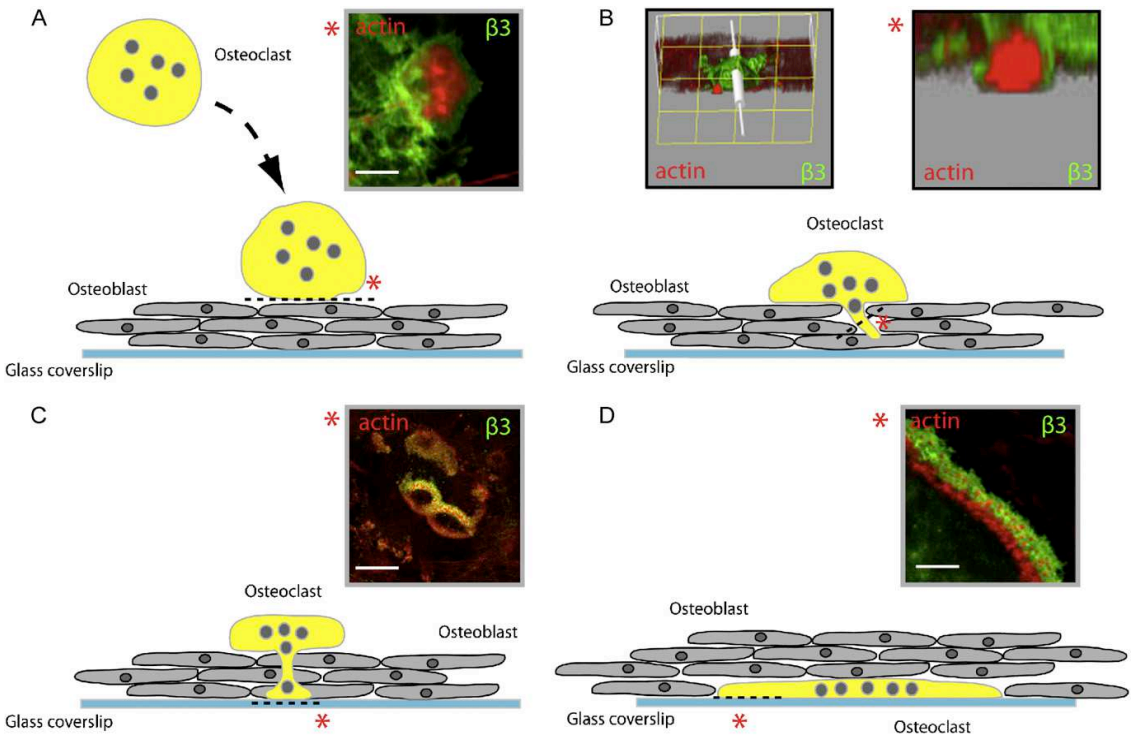

Figure 13. Model of osteoclast transmigration through cell layers. Multinucleated mature osteoclasts seeded on top of osteoblast layers (A) rapidly extend actin-rich protrusions through the stromal layer (B) until they contact the underlying substrate (C) on which they spread (D). Micrographs in insets: (*) show actin (red) and integrin β3 (green) in X/Y sections at the level indicated by black dotted lines. Left inset in (B) is a 3D reconstruction of the protrusion, bars: 5µm (Saltel *et al.*, 2006).

IV.2. Bone degradation: trafficking, acidification, proteolysis

Once it reaches the bone matrix, the fully differentiated OC can start resorbing bone. In order to fulfill its task, the OC become polarized and its membrane is reorganized into four distinct and unique membrane domains: the SZ, the ruffled border (RB), the basolateral domain (BL) and the functional secrectory domain (FSD) (Figures 14,15) (Salo *et al.*, 1996; Coxon and Taylor, 2008a). The RB is the resorptive organelle of the OC. Its function is to acidify the subjacent resorption lacuna therefore dissolving the mineral phase of the bone and to secrete proteases that will degrade the organic phase of the bone (Coxon and Taylor, 2008a). The RB is a convoluted membrane with a high surface area that forms as a consequence of active and directed transport of vesicles that fuse with the plasma membrane in the basal pole of the OC, facing the bone matrix (Abu-Amer *et al.*, 1997; Mulari *et al.*, 2003a; Mulari *et al.*, 2003b). In

fact, late endosomes/lysosomes originating from the BM are acidified by V-ATPases which pump protons into the lumen of vesicles. In parallel to this acidification, chloride channels such as ClC-7 transports chloride ions into the lumen to maintain the electroneutrality of the vesicles (Coxon and Taylor, 2008a). Along with acidification, the RD-delivered lysosomes are also responsible for the trafficking of proteolytic enzymes to the resorption lacuna. The cysteine protease Cathepsin-K, which is specific to OCs and most efficient in degrading type I collagen, is also delivered to the RB via acidic late endosomes/lysosomes (Zaidi *et al.*, 2001; Zhao and Vaananen, 2006). The matrix metalloprotease-9 (MMP-9) also contributes to the lysosome-mediated bone degradation but is activity is presumably specific to certain site of the bone tissue (Everts *et al.*, 1992)**.** This vectoral lysosome trafficking is dependent on prenylated Rab GTPases (Feng *et al.*, 1995; Bucci *et al.*, 2000) and mediated by via dynein anchorage to MTs (Jordens *et al.*, 2001). This dynamic transport of lysosome results in their delivery to the peripheral region of the RB, close to the SZ. The liberated acidic content upon fusion with the RB membrane allows therefore the liberation of protons that dissolve the mineral phase of the bone but also ensure acidic pH, optimal for Cathepsin-K activity (Zaidi *et al.*, 2001). Conversely, in the central region of the RB, the degraded matrix components are collected by clathrin-mediated endocytosis and trafficked via the transcytosis pathway to the FSB where they are excreted to the blood stream (Salo *et al.*, 1997; Hirvonen *et al.*, 2013) (Figure 15). Hence, the central region of the RB is called the "Uptake Zone". Interestingly, another osteoclastic protease, tartrate resistant acid phosphatase (TRAP), has not been found to be transported to the RB via the already described late endocytic pathway. The delivery of TRAP is therefore suggested to be part of the biosynthetic-secretory pathway, which, like the endocytic pathway, is derived from the Golgi apparatus (Vaaraniemi *et al.*, 2004) (Figure 15). Additionally, TRAP is also thought to be present in non-acidic biosynthetic vesicles that fuse with transcytotic (Vaaraniemi *et al.*, 2004). Because cathepsin-K can activate the phosphatase activity of TRAP by cleavage of its two subunits (Ljusberg *et al.*, 2005), the role of TRAP might be to further process collagen fragments inside transcytotic vesicles before their liberation through the FSD (Coxon and Taylor, 2008a). Finally, a new pathway called "Reverse Transcytosis" that consists of delivering vesicles from the FSD to the peripheral zone of the RB, thus compensating for the membrane loss during the matrix uptake process (Vaaraniemi *et al.*, 2004) (Figure 14).

It is hypothesized that first event of OC polarization is SZ formation (Coxon and Taylor, 2008a) probably because the polarization does not occur on non-mineralized substrates, where the OC has a completely flat morphology (sign of the absence of polarization) and forms a

SZL instead of a SZ (Saltel *et al.*, 2004). Adding further support to this hypothesis is the conceptual argument stating that RB formation and activity, i.e. secretion of degradation molecules, would be a waste of the cell's resources if the confinement of these molecules in the immediate vicinity to the bone surface were not ensured. However, the publication of few studies suggesting that protease secretion by OC is independent of polarization (Henriksen *et al.*, 2006; Hollberg *et al.*, 2008) or that morphological differences exist between OC at different bone sites highlight that there is still much to be learned about OC polarization during bone resorption.

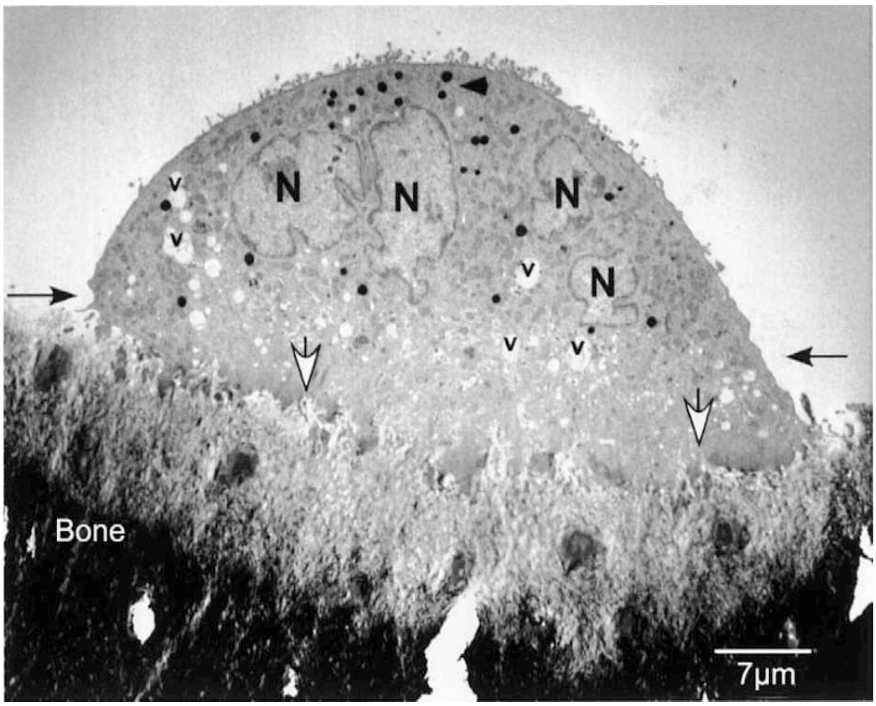

Figure 14. Transmission electron micrograph of a bone resorbing human osteoclast. The ruffled border (localised between the white arrows) penetrates deep into the bone matrix. An area of translucent vacuolar structures is visible directly adjacent to the ruffled border inside of the cell (indicated by the long black arrows). Numerous vacuolar (v) structures are also visible close to the basolateral plasma membrane; secretory-type vacuoles are also abundant (filled arrowhead). N: nucleus. (Stenbeck, 2002).

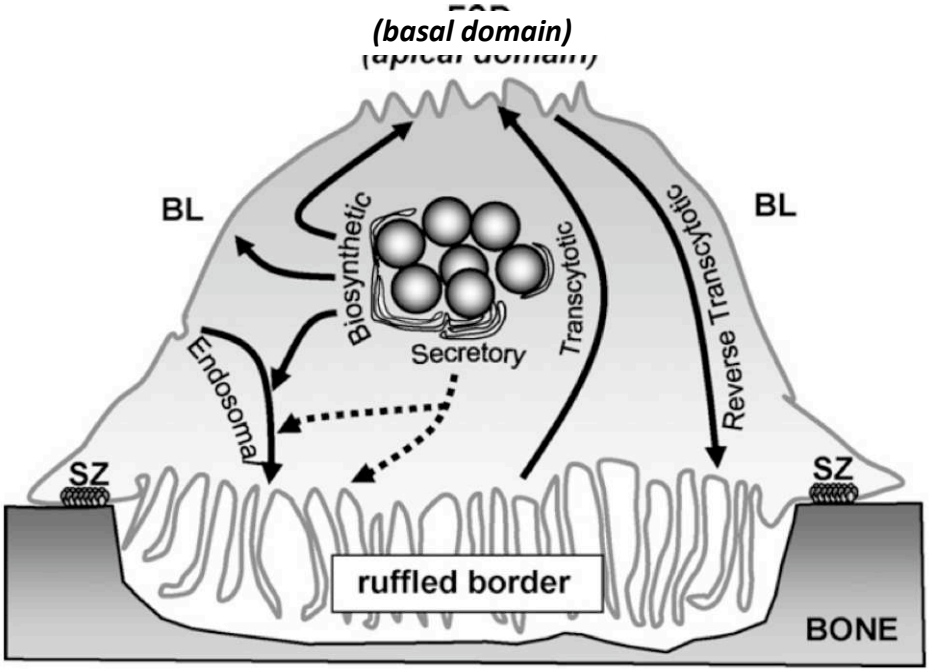

Figure 15. Vesicular trafficking pathways in osteoclasts. The ruffled border is formed as a consequence of trafficking of vesicles in the endosomal pathway, and therefore has characteristics of a late endosomal membrane. A distinct biosynthetic pathway may also contribute to the formation of the ruffled border. Degradation products from the resorption process are removed from the resorption lacuna by a transcytotic path- way and released at the FSD, which exhibits characteristics of an apical membrane. Recently, a reverse pathway from the FSD to the ruffled border has been identified. FSD, functional secretory domain; BL, basolateral domain; SZ, sealing zone (Coxon and Taylor, 2008a).

IV.3. The resorption-migration cycle

While adherent on the bone surface, the OC needs to search for news spots to degrade. It is thought that its migration is driven by podosomes because of their role in migration of other cells such as macrophages (Linder and Kopp, 2005) but a mechanism depicting how podosomes exactly promote this 2D displacement during resorption is yet to be provided. One plausible hypothesis assumes that cyclic podosome switching between two categories of patterns, the SZ-state and a non-SZ state (i.e. cluster or ring), allows the OC to alternate between bone resorption and motility, respectively (Saltel *et al.*, 2008; Novack and Faccio, 2011). This model is derived from two *in vitro* observations: (1) the SZ, which is the podosomal arrangement that is maintained during bone degradation, stays in a relatively

stable position; (2) the "resorption tracks" made by OC cultured on bone, dentine, ivory and hydroxyapatite slices consist of several individual resorption lacunae that overlap to make form of what could be described as a "chain" or also a trail of partially overlapping pits (Figure 16).

If this model were true, the OC would have to undergo fast transitioning also between two different directions of polarization. While migrating, the OC should be horizontally polarized, i.e. parallel to the substrate and with a leading edge and a trailing edge. While resorbing, the OC should be vertically polarized, in order to degrade the matrix and export its components to the systemic blood stream.

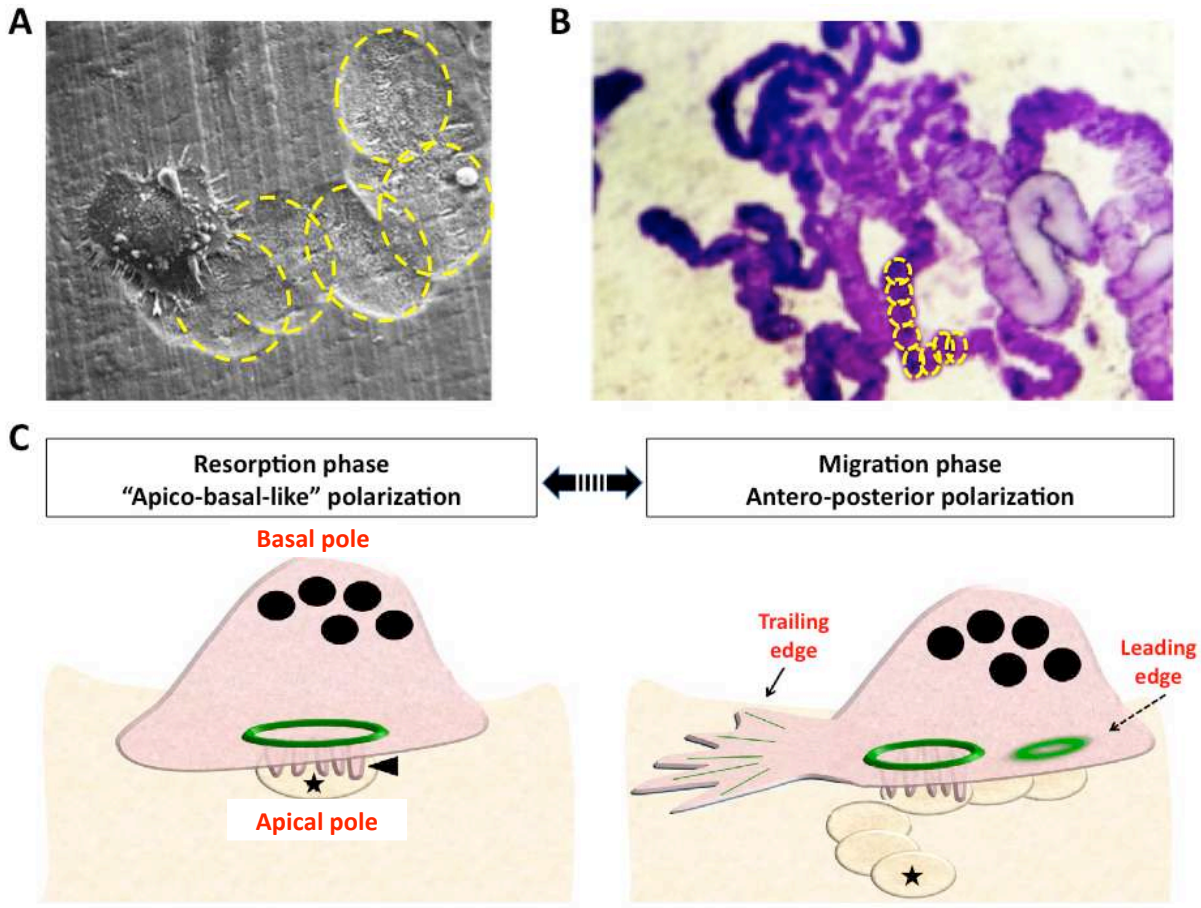

Figure 16. The osteoclast resorption-migration model. (A) Scanning electron micrograph of a resorbing osteoclast on dentine showing consecutive and partially overlapping circular resorption pits/lacunae (dotted yellow circles). (B) Resorption tracks of osteoclasts seeded on dentine, then removed for the staining of resorption tracks with Toluidine blue, again showing overlapping circular resorption pits/lacunae (small dotted yellow circles) (Susa *et al.*, 2004). (C) Schematic representation of the current working model that depict OC-switching between

an apico-basal-like polarization and an antero-posterior polarization during resorption and migration, respectively. Schema in (C) is adapted from (Novack and Faccio, 2011).

CHAPTER 2: RESULTS

I. OC MIGRATION

I.1. Introduction and rationale: How do podosomes drive OC migration?

OCs are adherent and motile cells. During their migration, they form dynamic multimolecular adhesive structures called podosomes, which are not only characterized by internal turnover, but also by collective patterning from clusters to rings. Because podosomes bridge (a) the cell to (b) its substratum, we investigated whether these structures had a particular role in mediating the mechanical interplay between the two elements (a and b). In other words, are podosomes the cause or the consequence of cell adhesion and displacement?
The cell-matrix relationship is continuous but involves several different processes: adhesion, spreading and, migration. Our broad question was therefore divided into several distinct parts to obtain experimental insight into each of these processes.

Timelapse micrographs of OCs in culture have shown that these large cells, as soon as they contact the matrix, first need to spread and, once properly spread, they start migrating in a given direction. We therefore first inspected the timing of podosome formation during the initiation of cell spreading and cell retraction using fluorescence and Nomarski contrast microscopy. By detaching and reseeding OCs, we observed that the OC first adheres then starts exhibiting podosomes concomitantly with its spreading. Inversely, the inhibition of integrin-mediated adhesion in already spread OCs resulted in podosome disassembly before subsequent cell retraction and detachment. These results indicated that podosomes are needed for maintaining adhesion during spreading but are not the exclusive mediators of these processes. Podosome exert forces to initiate and maintain the spreading of the OC.
We also sought to identify the leading podosome patterns during these sequential events. We found that podosome ring expansion is what initiates and maintains OC migration.

During the migration phase *per se*, we aimed at a qualitative description of the short-term forces exerted by the cell on the matrix and of the typical OC migration trajectory. To this end, we imaged short-term podosome ring movement on a fluorescently labeled substrate. We could therefore correlate the outward expansion of the podosome ring to the displacement of the substrate and we concluded that podosome rings exert on the substrate the tension needed for cell displacement.

Finally, we described the typical long-term OC migration trajectory and quantified displacement parameters in the perspective of establishing a physical correlation between the cell and its actin cytoskeleton. The displacement of the cellular actin mass always preceded the global cell displacement by a characteristic lag time, demonstrating once again that the actin-based structures are at the basis of OC movement. Moreover, the ring-dependent trajectory was characterized by periodic lateral “jumps” resulting from asymmetrical stability of rings in the migrating OC.

Finally, the mechanical data obtained from this study, combined with previously demonstrated data on podosome dynamics, allowed us to form a working model that governs OC motility. The model elaborates that podosomes grow in close vicinity during assembly on a confined area, such as the area of a cluster or a ring. Hence, because of a steric frustration event that accompanies their growth, podosomes repel each other and create the tension needed for migration.

I.2. Publication: Podosome rings drive saltatory osteoclast migration

MBoC | ARTICLE

Podosome rings generate forces that drive saltatory osteoclast migration

Shiqiong Hu[a,b], Emmanuelle Planus[c], Dan Georgess[d], Christophe Place[a,e], Xianghui Wang[b], Corinne Albiges-Rizo[c], Pierre Jurdic[d], and Jean-Christophe Géminard[a]

[a]Laboratoire de Physique, UMR 5672, Lyon 69364, France; [b]Department of Physics, State Key Laboratory of Precision Spectroscopy, East China Normal University, Shanghai 200062, China; [c]Institut Albert Bonniot, Université de Grenoble, Centre de Recherche INSERM-UJF U823, Equipe 1 DySAD–CNRS ERL 5284, Grenoble 38042, France; [d]Institut de Génomique Fonctionnelle de Lyon, Université de Lyon, UMS 3444 Biosciences, Gerland-Lyon Sud 69364, France; [e]Laboratoire Joliot-Curie, USR 3010, Ecole Normale Supérieure de Lyon, Centre National de la Recherche Scientifique, Lyon 69364, France

ABSTRACT **Podosomes are dynamic, actin-containing adhesion structures that collectively self-organize as rings. In this study, we first show by observing osteoclasts plated on bead-seeded soft substrates that podosome assemblies, such as rings, are involved in tension forces. During the expansion of a podosome ring, substrate displacement is oriented outward, suggesting that podosomal structures push the substrate away. To further elucidate the function of forces generated by podosomes, we analyze osteoclast migration. Determining the centers of mass of the whole cell (G) and of actin (P), we demonstrate that osteoclasts migrate by "jumps" and that the trajectories of G and P are strongly correlated. The velocity of the center of mass as a function of time reveals that osteoclasts rapidly catch up with podosomal structures in a periodic pattern. We conclude that actin dynamics inside the cell are not only correlated with cell migration, but drive it.**

Monitoring Editor
Alexander Mogilner
University of California, Davis

Received: Feb 1, 2011
Revised: Jun 24, 2011
Accepted: Jun 29, 2011

INTRODUCTION

Podosomes are structures, mainly made of actin, found in the contact region between cells and solid substrates. They consist of a dense, polymerized actin core surrounded by a "cloud," a loose, polymerized actin meshwork (Destaing *et al.*, 2003). Numerous proteins, such as actin regulators or focal adhesion proteins, are associated with these actin structures (Linder, 2009). Podosomes are typically formed in monocyte-derived cells (osteoclasts, macrophages, dendritic cells), endothelial cells, and smooth muscle cells. Studies of their molecular components have related them to invadopodia, which are mostly found in highly metastatic cancer cells. Even though there are some differences between these two actin-containing structures, they are very similar and are often referred to as *invadosomes* (Linder, 2009).

The main functions of invadosomes are considered to be cell adhesion and matrix degradation. They establish close contact with the substrate, and their formation requires integrins (Destaing *et al.*, 2010, 2011). Indeed, total internal reflection fluorescence (TIRF) microscopy has shown that podosomes are enriched in adhesion-mediating integrins and form only on the substrate-bound side of the cell (Linder and Aepfelbacher, 2003). Furthermore, there is increasing evidence that invadosomes are able to degrade extracellular matrix (Saltel *et al.*, 2008; West *et al.*, 2008; Linder, 2009). It recently has been proven that the invadosome-like structures of lymphocytes are involved in transcellular diapedesis, which has led to the suggestion that these structures could probe the endothelial cell surface to allow invasion (Carman *et al.*, 2007; Carman, 2009). Finally, podosomes are thought to play a role in cell migration and invasion by establishing localized anchorage, stabilizing sites of cell protrusion, and enabling directional movement (Linder and Kopp, 2005). However, there is no direct evidence proving the latter mechanism, and the role played by the podosomes in cell migration is still unknown.

This article was published online ahead of print in MBoC in Press (http://www.molbiolcell.org/cgi/doi/10.1091/mbc.E11-01-0086) on July 14, 2011.

Address correspondence to: Jean-Christophe Géminard (jean-christophe.geminard@ens-lyon.fr) or Pierre Jurdic (pierre-jurdic@ens-lyon.fr).

Abbreviations used: EDTA, ethylene diamine tetraacetic acid; FBS, fetal bovine serum; GFP, green fluorescent protein; M-CSF, macrophage colony–stimulating factor; αMEM, α-minimal essential medium; PBS, phosphate-buffered saline; PIV, particle image velocimetry; RANK-L, receptor activator of nuclear factor κB-ligand; SEM, scanning electron microscopy; TEMED, tetramethylethylenediamine; TIRF, total internal reflection fluorescence.

Osteoclasts, the bone-resorbing cells, are large, multinucleated hematopoietic cells that exhibit podosomes when adherent, for instance, on plastic or glass. We have previously shown that podosomes can collectively self-assemble in osteoclasts. They can aggregate in clusters that later form rings. In a transient regime, the rings grow before they dissociate. Podosome rings eventually end up forming belts at the periphery of mature osteoclasts at rest. These belts require an intact microtubule network (Destaing *et al.*, 2003, 2005), contrary to clusters and rings that are microtubule-independent. When adherent on a mineralized extracellular matrix, osteoclasts polarize and podosomes condense to form a large sealing zone delineating the resorption area (Luxenburg *et al.*, 2007; Saltel *et al.*, 2011). This dynamic patterning of podosomes in osteoclasts recently has been shown to depend on the topography of the substrate (Geblinger *et al.*, 2010). These latter data correlate well with previously described results that provided the first evidence that invadosomes in rosettes, found in either NIH3T3 fibroblasts or src-transformed BHK cells, are major sites through which cells sense mechanical forces and exert traction forces (Collin *et al.*, 2006, 2008). Nonetheless, the molecular mechanisms governing these forces remain unknown (Destaing *et al.*, 2003; Saltel *et al.*, 2004).

In this study, we describe a series of experiments designed to elucidate the role played by podosomes in the spreading, migration, and retraction of osteoclasts. At one end of the spectrum, we report observations of actin structures at a short time scale: we describe the spatial organization of podosomes during early adhesion and retraction. We also report the evolution of the three-dimensional shape of an osteoclast in relation to the organization of podosomes in the contact region between the cell membrane and the substrate. We also qualitatively characterize the force applied by the osteoclast onto the substrate. At the other end of the spectrum, we report a study of the migration process of a single osteoclast at a long time scale, and investigate how the motion of the cell is related to the collective organization of actin. The whole set of experimental results makes it possible to discuss the role of the podosomal structures in osteoclast motility and adhesion processes.

RESULTS

Podosomes are involved in maintaining tension in osteoclasts

To further characterize the role of podosomes in osteoclast adhesion, we first observed their behavior during spreading and, inversely, detachment. We used a RAW macrophage cell line stably expressing actin fused to GFP (Destaing *et al.*, 2003) and differentiating into osteoclasts in presence of the two cytokines macrophage colony–stimulating factor (M-CSF) and receptor activator of nuclear factor κB-ligand (RANK-L). In our first experiment, we observed the dynamics of the GFP-actin during the early adhesion process: mature osteoclasts were detached and then seeded on glass. The experiment consisted of observing the attachment and spreading by Normarski contrast and fluorescence time-lapse microscopy (Figure 1A and Supplemental Movie 1). We observed that the osteoclast, which was initially round before adhering, rapidly spread by forming membrane protrusions, reminiscent of corollas, around the central part of the cell. Simultaneously, GFP-actin, which was initially scattered throughout the cell, concentrated at the periphery of the spreading areas and started forming clearly recognizable podosomes marked by dense actin cores within 12 min of seeding. Additional immunofluorescence staining of actin and vinculin, a podosome cloud component, confirmed the osteoclast is adherent but does not make podosomes during the first 10 min after seeding; actin is loosely distributed in the cytoplasm and vinculin localizes at the periphery of the cell but does not participate in any organized structures. However, when the osteoclast starts spreading, typical podosomes with F-actin cores and vinculin-containing clouds start to form (Figure 1B). These observations revealed that a reorganization of actin results from or drives the spreading process. In a second experiment, adherent osteoclasts were slowly detached by ethylene diamine tetraacetic acid (EDTA) treatment. We observed that membrane retraction occurred right after the disappearance of podosomes (Figure 1C and Supplemental Movie 2). Indeed, within 2 min of EDTA treatment, all the podosomes dismantled, whereas osteoclasts retracted slowly but remained adherent. From these observations, we concluded podosomes are not strictly necessary

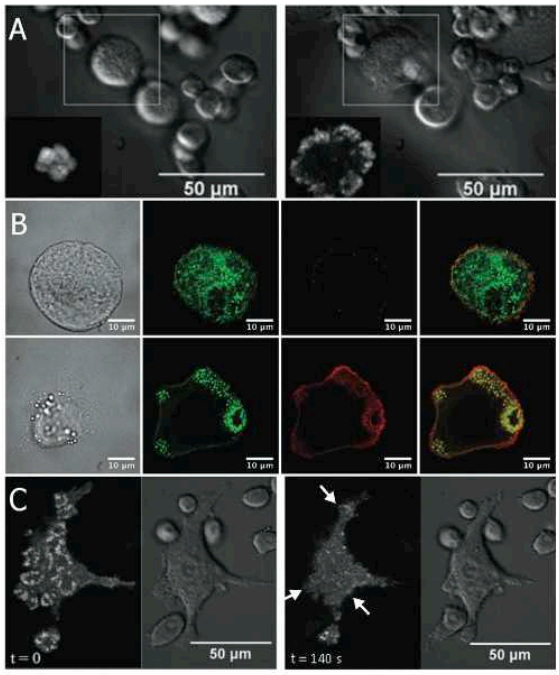

FIGURE 1: Podosomes are involved in maintaining tension in osteoclasts. (A) During adhesion and spreading processes, the podosomes accumulate along the periphery of the cell, in the expanding regions. Several mature osteoclasts expressing GFP-actin are seeded onto a glass coverslip and observed under the microscope using a Nomarski contrast. Insets, fluorescence image of the cell, which is indicated by the white square. Left, 5 min after seeding, the cell is round and actin is scattered in the cytoplasm (inset). Right, 20 min after seeding, the considered cell starts spreading. The fluorescence image (inset) reveals that actin becomes concentrated in podosomes along the periphery of the contact region, where the cell is expanding. (B) Immunofluorescence labeling of adherent osteoclasts spreading on glass: actin stained with phalloidin (green) and vinculin stained with anti-vinculin (red). Top, 10 min after seeding, actin is loosely distributed in the cytoplasm of the osteoclast and vinculin staining confirms the absence of podosomes. Bottom, 25 min after seeding, podosomes form where the cell is expanding. Vinculin marks the periphery (surrounding cloud) of the podosomes. (C) Osteoclasts remain adherent even in the absence of podosomes. At t = 0 s, the cell is spread, in close contact with the substrate (right), and the fluorescence image (left) reveals several rings of podosomes (bright spots). At t = 40 s, the addition of EDTA produces a rapid dissociation of podosomes associated with cell retraction (white arrows).

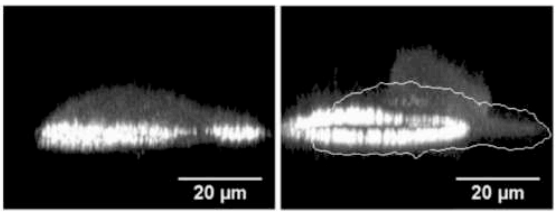

FIGURE 2: The podosome ring expansion correlates with the direction of migration. One osteoclast expressing the GFP-actin adherent on glass is imaged under the confocal microscope. The actin organization in the contact area with the substrate is revealed by slightly tilting the reconstructed images along the *z*-axis. Left, actin, concentrated in the base plane, is organized in two rings, with the largest ring located on the left-hand side. The fluorescence signal from the actin monomers ubiquitously invading the cytoplasm clearly reveals the shape of the cell. Right, 75 min later, the largest ring grows and the smallest disappears. Simultaneously, the cell flattens above the remaining ring, expanding in that region, and also moving to the left (white contour corresponds to the initial shape of the cell shown on the left).

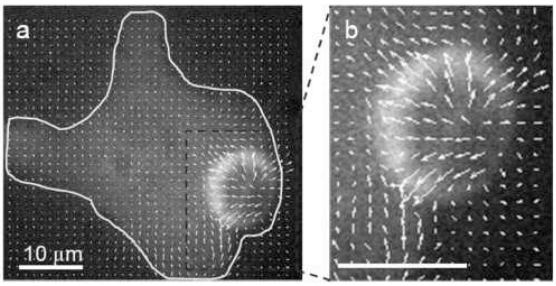

FIGURE 3: Actin ring structures exert tension forces on the substrate. The dynamics of a live osteoclast, expressing GFP-actin moving on the surface of a soft polyacrylamide gel (stiffness: 0.5 kPa) are shown. The gel containing fluorescent beads (rhodamine, diameter 210 nm) is coated with vitronectin. Images of GFP-actin and of the rhodamine beads were taken every minute. The substrate displacement field is reconstructed by tracking the displacements of the fluorescent beads. (A) The merge of the osteoclast image (GFP-actin) and of the displacement field (arrows indicate the local displacement with respect to the substrate at rest) reveals displacement is significant solely around the podosomal structure (ring). (B) Enlargement of the podosomal structure as delineated by the rectangle in (A). The displacements of the beads clearly reveal that the ring pushes the substrate outward.

for osteoclast adhesion but rather play a role in exerting tension needed for spreading.

The expansion of a podosome ring induces cell displacement

To further determine the interaction between actin dynamics and osteoclast migratory behavior, we assessed the three-dimensional shape of an osteoclast vis-à-vis the organization of actin in the contact region between the cell and the substrate. As an osteoclast migrated on a glass dish, we used confocal time-lapse microscopy to image *z*-planes every 15 min. Then Z-stacks were used to reconstruct the three-dimensional shape of the cell based on a fluorescence signal from G-actin diffusing ubiquitously in the cytoplasm (Figure 2 and Supplemental Movie 3). These observations revealed that the growth of a podosome ring in the contact region is associated with a rapid flattening and migration of the cell. Again, the dynamics of the actin structure inside the cell were proven to be strongly correlated with the spreading and migration processes.

Podosome structures exert tension on the substrate

To assess the forces exerted by an adherent osteoclast, we observed the deformation of the substrate induced by the cell. To do so, we used a soft polyacrylamide gel (stiffness: 0.5 kPa) coated with vitronectin to allow adhesion (Figure 3). The experiment revealed that the displacement of the fluorescent beads in the gel is concentrated around the podosome ring, whereas no displacement was ever observed in the regions devoid of podosomes (Figure 3A). Furthermore, when the podosome ring grew and spread, the substrate displacement was mainly oriented outward from the ring (Figure 3B, white arrows). Thus the podosome ring is subjected to an internal tension that tends to increase its perimeter and extend the ring toward the periphery (negative tension). As a consequence, the substrate exerts a compressive force and tends to reduce the size of the ring. To conclude, the podosome ring is clearly associated with a tensional effect that stretches the cellular membrane.

Podosome ring expansion drives osteoclast migration

To comprehend the role played by podosome rings in cell motility, we observed the motion of several mature osteoclasts expressing GFP-actin, seeded on a vitronectin-coated soft polyacrylamide gel (stiffness: 3 kPa). (We chose to work with the same substrate as the one used for the force measurement to obtain a complete set of experiments under similar conditions). Images were obtained using time-lapse microscopy every 5 min for ~8 h (Figure 4 and Supplemental Movie 4). Qualitatively, in the whole set of experiments (four mature osteoclasts on polyacrylamide gel), we observed that the cell migrates randomly. More precisely, the formation of podosome rings inside the osteoclast accompanies its elongation in one given direction. When the maximal length (L) of the cell is about twice its typical size, the actin structure disappears from one side, and the cell retracts toward the remaining structure on the opposite side, which becomes the leading edge (Figure 4; t = 120 min). This results in a "jump" of the cell in the corresponding direction (Figure 4; t = 150–180 min). Subsequently, the cell elongates in an almost perpendicular direction due to the growth of two new rings from the remaining structure at the leading edge (Figure 4; t = 120 min). In the following paragraphs, we report a representative quantitative study of the cell motion.

First, we focused on the dynamics of the cell's center of mass, G (see *Materials and Methods*). We reported the trajectory of G in the sample plane (*x*, *y*) during the whole experimental time (Figures 4, Bottom, right, and 5). The first striking result is that the cell moves in a series of straight jumps separated by spatially localized changes in direction. To get information about the dynamics, we reported the velocity of the center of mass, V_G, as a function of time, t (Figure 6A), and noticed V_G exhibits large peaks (A to D) almost periodically every 2 h.

Then, in order to account for the potential coupling between the motility of the cell, characterized by the motion of the center of mass G, and the internal dynamics of actin, we defined a point, P, summarizing the position of all actin inside the cell (see *Materials and Methods*). We also defined the vector $\vec{f} \equiv \overrightarrow{GP}$, which accounts for the distance and direction between the center of mass G and the location of actin P (Figure 4). Reporting the trajectory of P in the (*x*, *y*) plane (Figure 5), we observed first that G and P experience the same trajectories. To provide information about the dynamics, we

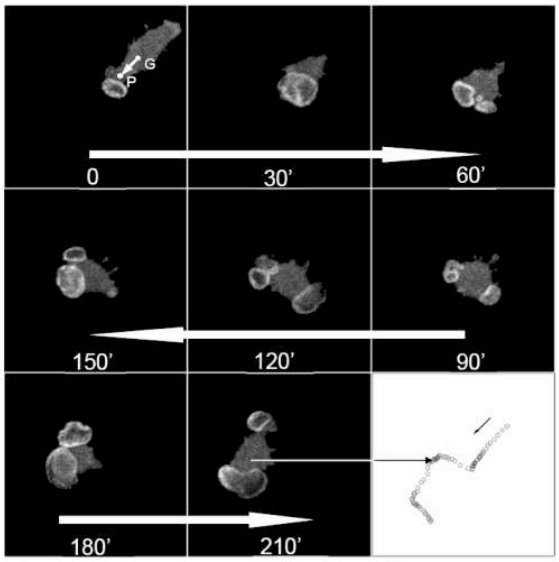

FIGURE 4: Podosome ring expansion and osteoclast migration are correlated. The dynamics of an osteoclast expressing GFP-actin moving on the surface of a polyacrylamide gel (stiffness: 3 kPa) are shown using time-lapse fluorescence microscopy (Supplemental Movie 4). Eight successive images separated by 30 min are displayed. The center of mass of the cell G, the position of the actin structure P, and defined the vector $\vec{f} \equiv \overrightarrow{GP}$ were determined from such images (see *Materials and Methods*). The points G and P for the first image (t = 0, top, left) are indicated. Bottom, right, successive positions, separated by 5 min, of the center of mass G determined from this image sequence (same scale).

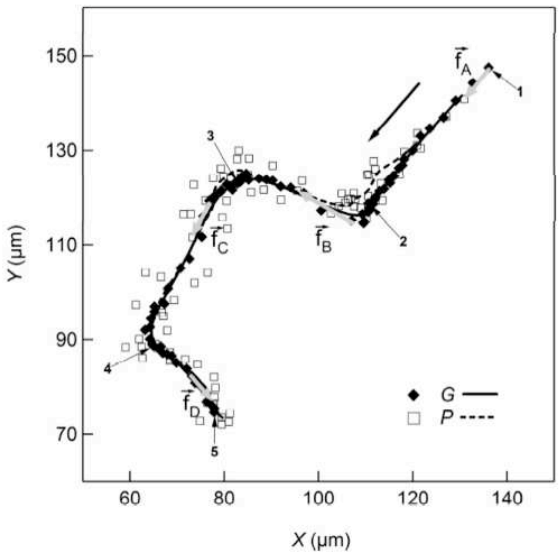

FIGURE 5: Successive positions of the center of mass G and of actin P in the sample plane (*x*, *y*). The time difference between two successive points is 5 min. The black arrow indicates the direction of the motion. The continuous and dashed lines correspond to the trajectory of G and P, respectively, averaged over 10 successive positions. The trajectories of G (full diamonds) and P (open squares) are strongly correlated. The vectors $\vec{f}_A$, $\vec{f}_B$, $\vec{f}_C$ and $\vec{f}_D$ (gray arrows) are associated to the events A, B, C, and D, and labels 1–5 indicate the minima in the velocity V_G, as defined in Figure 6.

reported the distance $\vec{f} \equiv \|\overrightarrow{GP}\|$ between G and P as a function of time t (Figure 6B). We then observed that f and V_G are also strongly correlated in time, a large peak in f preceding each large peak in V_G. The temporal correlation between f and V_G, and especially the delay τ between the peak in f and the peak in V_G, can be assessed by calculating the cross-correlation function $\chi(t) \equiv \int f(t'-t)V_G(t')dt$, where the integral is estimated over the whole experimental time (Figure 7). The experimental correlation function $\chi(t)$ exhibited a maximum for $t \equiv \tau \approx 10$ min, whereas the oscillations pointed out the period of the cell motion, $T \approx 2$ h. In the same way, we reported the cell length L as a function of time t (Figure 6C). We observed that the cell length L increased almost linearly between two successive jumps. The disappearance of one of the actin structures on one side leads to a peak in f when L is maximum (Figure 6B).

We considered the direction of the jumps by identifying first the peaks A, B, C, and D, as defined in Figure 6, and the associated minima in the velocity (numbered from 1 to 5, such that peak A is associated with the jump from G_1 to G_2, etc.). We denoted $\vec{f}_A, \vec{f}_B, \vec{f}_C$, and $\vec{f}_D$, the values of $\vec{f}$ at the peaks A, B, C, and D, and $\overrightarrow{\Delta G}_{ij} \equiv \overrightarrow{G_iG_j}$, the vector associated to the displacement of G during the jumps from i to j. Reporting the values of $\vec{f}$ at the maxima and the corresponding displacements $\overrightarrow{\Delta G}$, we observed that these quantities are correlated in both length and direction (Figure 8). First, the angles θ_P and θ_G that $\vec{f}$ and $\overrightarrow{\Delta G}$ make with the *x*-axis are equal (Figure 8A), which proves the jumps occur in the direction of $\vec{f}$. Second, the amplitude ΔG of the jumps is proportional to f (or, equivalently, to L; Figure 8B). Finally, note that successive jumps occur in directions making angles of ~90 degrees between them (Figure 8).

As a conclusion of this last experiment, the osteoclast jumps follow the internal organization of actin. We maintain that the point P refers to all G-actin monomers in the cell, including the ones present in structures made of F-actin polymers. We show that the growth of rings induces the elongation of the cell. When the length L of the cell in a given direction is about twice its initial size before expansion, one of the actin rings takes the lead at one end, whereas the others disassemble. Subsequently, the cell retracts toward the remaining structures, which leads to a jump of the cell in the given direction ~10 min after f (or L) has reached a maximum. The process repeats itself almost periodically every 2 h. Thus the motion of the cell occurs by seemingly periodic jumps, the length of each jump correlating to the cell's length, during which the cell moves rapidly in a given direction, resulting in saltatory migration.

DISCUSSION

We have investigated the role played by podosomes in the migratory behavior of osteoclasts. In summary, podosome rings exert tension forces that tend to extend the cellular membrane and push the substrate outward. Podosome assemblies, even in close contact with the substrate, do not play a direct role in cell adhesion; rather, they exert forces where tension is needed, forming in expanding regions and disappearing from retracting regions. Discussing in detail the migration of a set of osteoclasts from a RAW monocytic cell line expressing an actin green fluorescent protein (GFP), we showed that osteoclasts move by jumps, rapidly catching up with podosomal structures in a periodic pattern.

We wish to emphasize that our experimental observations are not too specific and do correspond to a general pattern. First, we can state that all the RAW-derived osteoclasts we observed were

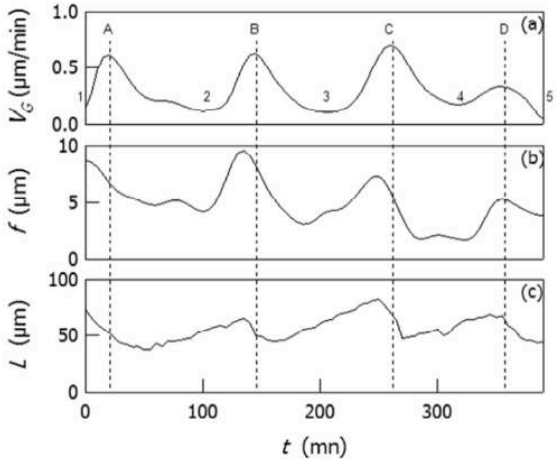

FIGURE 6: Velocity of the center of mass V_G, distance f, and cell length L as a function of time t. (A) The velocity V_G exhibits peaks, which correspond to a rapid motion of the cell in a given direction (jump). The minima in the velocity V_G are labeled 1–5. (B) The distance f interestingly exhibits the same type of temporal evolution. (C) The cell length L increases slowly when the cell velocity is small, and rapidly decreases during the jumps. Note that the cell jumps ~10 min after f or L have reached a maximum. Identified here are four events: A, B, C, and D. Successive jumps are separated by ~2 h.

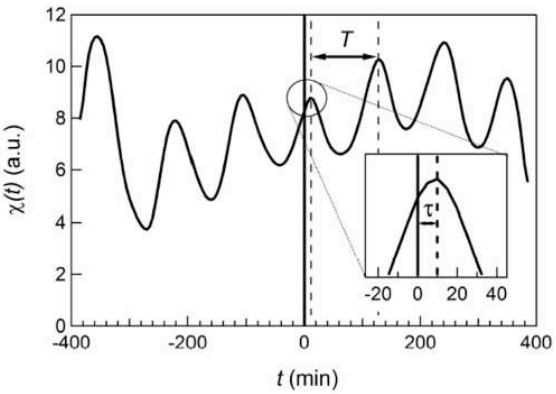

FIGURE 7: Temporal cross-correlation (t) between the distance f and the cell velocity V_G. The oscillations of the correlation function confirm the almost periodic character of the jumps, with a period T ≈ 2 h. Inset, enlargement of the central peak. The correlation (t) is maximum for t ≡ τ ≈ 10 min, which shows that the cell jumps ~10 min after f has reached a maximum.

exhibiting qualitatively the same type of motion as proven by cells exhibiting mainly two or more podosome rings, and even podosome clusters (Supplemental Movie 5). Second, in order to confirm results with different substrate and osteoclast origins, we also studied the dynamics of primary osteoclasts expressing LifeAct-eGFP moving on glass. We observed the exact same migration pattern (Supplemental Data 6 and Supplemental Movie 6). These experiments demonstrate that the observed pattern is not specific to the RAW cell line and substrate (vitronectin-coated polyacrylamide) and that the dynamics of actin inside the osteoclast are not only correlated with cell migration, but drive it.

We propose a potential mechanism that accounts for osteoclast migration. The migration of osteoclasts involves their elongation, which is correlated with the growth of podosome rings. Podosomes collectively push the cell membrane outward, as already observed during the early spreading process. From the observation of substrate displacement, we concluded, in agreement with previous investigations on BHK-RSV cells showing torsional tractions underneath the podosome rings (Collin *et al.*, 2008), that podosome rings exert forces onto the substrate. We propose that the associated substrate displacement, which points outward, subjects the ring to an internal tension that tends to extend the ring. Thus the formation and growth of a podosome ring can account for the spreading of the contact region. Indeed, a podosome ring that encounters the cell periphery pushes the membrane outward. The process can take place until the membrane has reached its maximum possible extension (the cell is then flat). If two rings are pushing the cell in opposite directions, the cell length increases until the weakest ring loses its mechanical stability because of excessive stress. Then the weaker disappears and the cell jumps in the direction of the remaining ring.

Finally, we discuss the physical origin of the tension force. Individual podosomes are associated with a dense actin core formed by cross-linked actin filaments, as demonstrated by scanning electron microscopy (SEM) observation experiments (Luxenburg *et al.*, 2007).

We have previously proposed that actin cores have a conical shape (Destaing *et al.*, 2003; Jurdic *et al.*, 2006; Hu *et al.*, 2011); they are dynamical structures growing from the cell membrane at the substrate interface and dissociating from the top (Figure 9A). Considering the sketch in the Figure 9B, one can easily see that, because of a steric frustration effect, the base of the cone tends to extend if the structure grows from the base and the filaments are linked to one another. As a consequence, two neighboring podosomes tend to repel each other, which naturally explains why a ring structure is subjected to an internal tension that tends to increase the length of a podosome line (negative tension) and, accordingly, the ring diameter. In such a scenario, the podosomes are responsible for the membrane tension. What remains unexplained are the molecular mechanisms involved in the transmission of tension from the membrane to the substrate at the podosome base.

The mechanism we propose is based on several assumptions (for instance, the cell adheres to the substrate in the contact region and the podosomal structure becomes unstable when the stress is

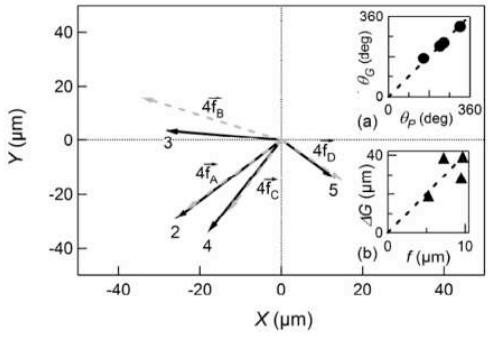

FIGURE 8: Vectors $\vec{f}_A, \vec{f}_B, \vec{f}_C$ and associated displacements $\Delta\vec{G}$. The cell center of mass G jumps toward P, as pointed out by the strong correlation between at the maximum (gray dotted arrows) and the corresponding $\Delta\vec{G}$ (black arrows). (A) Angle θ_G vs. angle θ_P. The dotted line corresponds to the slope 1, showing that $\theta_G \approx \theta_P$. (B) Jump length $\Delta\vec{G}$ vs. maximum distance f. The cell moves over a larger distance when the distance f at the maximum is larger.

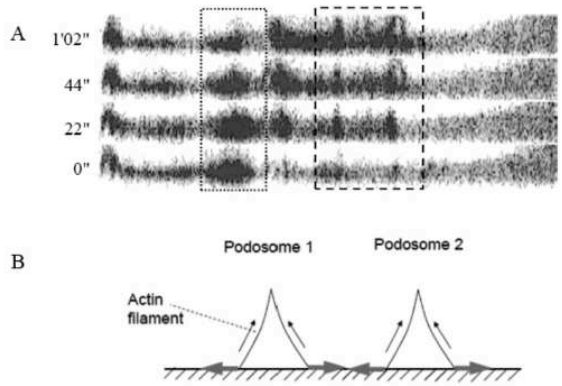

FIGURE 9: Sketch of forces exerted by two growing podosomes. (A) Podosomes in the contact region between an osteoclast and a glass bottom dish were imaged under the confocal microscope. Stacks of pictures were then used to reconstitute a Z-image, rendering the profiles of the podosomes in a vertical plane (t = 0, 22, 44, and 62 s). The sequence shows that the podosomes consists of actin filaments growing rapidly from the cell membrane (thick dotted rectangle on the right) and disappearing from the top (dotted rectangle on the left). (B) We have previously proposed that the actin cores of podosomes are organized in a conical brush (Destaing *et al.*, 2003; Jurdic *et al.*, 2006, Hu *et al.*, 2011). Because actin filaments are cross-linked and growing from the membrane, the actin filaments, due to steric constraints, repel each other in the base plane. Thus two neighboring podosomes tend naturally to repel each other, and generate the negative tension associated with the podosomal structure. Gray arrows, forces exerted by neighboring podosomes on the substrate.

released), but it is compatible with the seemingly periodic movement of the cell in the direction of $\overrightarrow{GP}$, thus toward the actin structure. First, as explained above, the cell moves in the direction of $\overrightarrow{GP}$. One can estimate the growth velocity of the ring from the period T, which corresponds to the time needed for two rings to push the cell membrane over a distance that compares to the cell size. From the slope $\frac{dL}{dt}$ (Figure 6C), we have estimated that the ring growth velocity is on the order of $v \approx 0.25$ µm/min (L increases by ~50 µm in 100 min due to the action of two rings). From the growth velocity v, taking into account the typical distance between two podosomes (~1 µm), we estimate the typical lifespan of one podosome is ~4 min. The latter estimate agrees reasonably with previous results (Destaing *et al.*, 2003; Geblinger *et al.*, 2010), which again sustains our model. Second, it is interesting to note that the assumption that the podosomal structure becomes unstable when the stress is released would be compatible with the fact that successive jumps make a 90-degree angle between them, at least when two rings develop in opposite directions. Indeed, when the cell reaches its maximum elongation, the disappearance of one of the podosomal structures releases the stress along $\vec{f}$. As a consequence, the remaining podosomal structure becomes unstable along $\vec{f}$. This instability could explain why two secondary rings, aligned in a perpendicular direction, form and grow from the remaining ring.

The saltatory migration of osteoclasts described here is reminiscent of the saltatory migration of oligodendrocyte precursors dispersing from the ventricular zone during early brain development and described as existing in alternating stationary and fast-moving phases (Tsai *et al.*, 2009). It could reflect the inchworm-like progression of bone-resorbing osteoclasts we described earlier (Saltel *et al.*, 2004).

MATERIALS AND METHODS

Osteoclast differentiation

To image podosomes in osteoclasts, we have used the RAW monocytic cell line expressing an actin GFP (Destaing *et al.*, 2003). The RAW 264.7 cells, from the American Type Culture Collection (Manassas, VA), were transfected in our lab with FuGENE 6 following manufacturer's recommendations (Roche Diagnostics, Indianapolis, IN). The cells then were regularly selected by flow cytometry (FACScan, Becton Dickinson, San Jose, CA) to maintain a stable RAW cell line expressing GFP-actin. The GFP-actin RAW cells were cultured with a density of ~50 cells/mm^2 in a 12-well plate for 6 d, which is the optimum time for differentiation into osteoclasts. Primary murine osteoclasts were differentiated from the bone marrow of 8-wk-old mice, as described in Destaing *et al.* (2003). The differentiation medium was α-minimal essential medium (αMEM; Invitrogen, Carlsbad, CA) containing 10% fetal bovine serum (FBS; Biowest, Nuaillé, France), 30 ng/ml M-CSF, and 35 ng/ml RANK-L. Recombinant human RANK-L and human M-CSF were produced in our laboratory as previously described (Destaing *et al.*, 2003). Culture medium was changed every 2 d. After 6 d of differentiation, mature osteoclasts were washed twice with phosphate-buffered saline (PBS; Invitrogen) and detached by using 0.25 µM EDTA (Invitrogen) in PBS for 5 min (EDTA chelates divalent ions essential for activating membrane receptors involved in cell adhesion). After centrifugation, osteoclasts were seeded with a density of ~100 cells/mm^2, either on a glass bottom dish (MatTeK, Ashland, MA) or on a polyacrylamide gel.

Transient transfection

For video microscopy of the actin cytoskeleton in primary osteoclasts, day 4 osteoclasts were transfected with pEGFP-N1-LifeAct (Riedl *et al.*, 2008) using Lipofectamine LTX with PLUS Reagent (Invitrogen) following the manufacturer's instructions. After 48 h, cells were detached using EDTA, and replated on a glass bottom dish, as described in the preceding section.

Indirect immunofluorescence

To observe podosome formation during spreading, we reseeded osteoclasts derived from RAW 264.7 cells on a glass bottom dish as previously described. Briefly, cells were fixed with 4% paraformaldehyde (pH 7.2) at 10 min and 25 min after reseeding. They were permeabilized with 0.2% Triton-X-100 in PBS, and then incubated for 1 h with anti-Vinculin antibody (Clone hVIN1, #V9264; Sigma-Aldrich, St. Louis, MO) at 10 µg/ml final concentration. Cells were then washed three times with PBS and incubated with Alexa Fluor 488 phalloidin (Life Technologies) and Alexa Fluor 647 goat anti–mouse immunoglobulin G (A21236; Life Technologies) at 2 µg/ml for 45 min. Samples were washed and kept in PBS for microscopy.

Confocal microscopy

Living cells were imaged in an inverted microscope (DMI 4000; Leica) equipped with a confocal spinning-disk unit (CUS22; Yokogawa, Tokyo, Japan) and an incubating chamber at 37°C with 5% CO_2 and humidity-saturated atmosphere. The light source consisted of a laser diode (excitation wavelength 491 and 647 nm; Roper Scientific) and an emission filter with a 500- to 550-nm or 641- to 708-nm bandpass (Semrock, Lake Forest, IL). For time-lapse microscopy, we recorded, during 8 h, one image from a QuantEM camera (Photometric, Tucson, AZ) every 5 min using a 20× objective. For fixed samples, we used a 100× oil immersion objective.

Soft-gel substrate

Polyacrylamide gels were prepared at the bottom surface (14-mm diameter) of glass bottom dishes (MatTeK). First, the glass bottom surfaces of the MatTek culture dishes were pretreated with 500 µl Bind-Silane (g-methacryloxypropyltrimethoxysilane; GE Healthcare, Waukesha, WI) by applying the solution with a cotton swab and then drying the surface under a hood. At the same time, glass coverslips (12-mm diameter) were quickly treated with 15 µl Sigmacote (Sigma) and then dried under the hood.

Polyacrylamide gels exhibiting two different rigidities were obtained, according to the ratio 8% acrylamide/0.05% bis-acrylamide for a very soft gel (stiffness: 0.5 kPa) or the ratio 8% acrylamide/0.1% bis-acrylamide for a soft gel (stiffness: 3 kPa). Fluorescent beads (210-nm diameter; Molecular Probes, Invitrogen) were seeded in the softer gel. A 2.5 ml solution was obtained by mixing 500 µl acrylamide 40%, 62.5 µl bis-acrylamide 2%, 25 µl HEPES (1M, pH 8.5), 80 µl 2% bead solution, and water. Then 12.5 µl ammonium persulfate and 1.25 µl tetramethylethylenediamine (TEMED) were added to allow polymerization. The final solution (8 µl) was dropped on a Bind-Silane–treated MatTek dish coverslip, which was then covered by a Sigmacote-treated coverslip. After 20 min of polymerization, the upper coverslip was removed.

Finally, the gel surface was activated with vitronectin (BD Biosciences; Damljanovic *et al.*, 2005). Briefly, pure hydrazine hydrate (Sigma) was added to the gels for 2 h; the gels were then washed first with 5% glacial acetic acid for 1 h and then with distilled water for 1 h. Vitronectin solution (10 µg/ml) was diluted in 50 mM sodium acetate buffer at pH 4. The oxidation of vitronectin was achieved by adding 3.6 mg/ml sodium periodate crystals (Sigma) and incubating the gels at room temperature for 30 min. Oxidized vitronectin (150 µl) was added on the polyacrylamide-treated gel, which was incubated at room temperature for 1 h and then washed with PBS.

Analysis of the substrate displacement field

We used the open software package JPIV for particle image velocimetry (PIV; www.jpiv.vennemann-online.de) to determine the displacements of the fluorescent beads in the (x, y) plane with respect to their initial positions.

Cell-tracking image analysis

Stacks of images and associated data were analyzed using the image processing and analysis software ImageJ (Abramoff *et al.*, 2004) and the technical graphing and data analysis software Igor Pro (WaveMetrics, Lake Oswego, OR). We denoted M and N the dimensions in pixels of the image in the directions m and n, respectively. We determined the position (m_G, n_G) of the center of mass of a cell, G.

From one raw fluorescence image I_{mn}, using an intensity threshold, we obtained a binary image B_{mn} of the cell such that $B_{mn} = 1$ if the indices m and n correspond to a point inside the cell and $B_{mn} = 0$ otherwise. By definition, $m_G \equiv \frac{1}{NM}\sum_{n=1}^{N}\sum_{m=1}^{N} mB_{mn}$ and $n_G \equiv \frac{1}{NM}\sum_{n=1}^{N}\sum_{m=1}^{N} nB_{mn}$ are the position (m_P, n_P) of actin, P.

To obtain a point P, which characterizes the position of actin inside the cell, from one raw fluorescence image, we defined $m_P \equiv \frac{1}{NM}\sum_{n=1}^{N}\sum_{m=1}^{N} mI_{mn}^{\alpha}$, and $n_P \equiv \frac{1}{NM}\sum_{n=1}^{N}\sum_{m=1}^{N} nI_{mn}^{\alpha}$. We introduced the exponent α in order to increase the contrast. We checked that the experimental results did not depend significantly on α, and report results obtained with $\alpha = 3$.

Finally, scaling factors were applied to convert (m_G, n_G) and (m_P, n_P) to the positions (x_G, y_G) and (x_P, y_P) in the sample plane (x, y).

ACKNOWLEDGMENTS

We thank C. Chamot and C. Lyonnet from the Imaging Platform (PLATIM) of UMS3444/US8 Biosciences, Lyon, France, for their help and advice; C. Domenget and all members of P. Jurdic's team for their support and assistance in osteoclast cultures; and O. Destaing (Institut Albert Bonniot, Université de Grenoble, Centre de Recherche INSERM-UJF U823, Equipe 1 DySAD—Centre National de la Recherche Scientifique ERL 5284, Grenoble, France) and F. Saltel (Institut Européen de Chimie-Biologie, Université de Bordeaux, Pessac, France & INSERM Unité 889, Bordeaux, France) for Figure 9A. This work was supported by recurrent grants from Centre National de la Recherche Scientifique and Ecole Normale Supérieure de Lyon and grants from the Association pour la Recherche sur le Cancer (ARC), the Agence Nationale de la Recherche ("ANR-podosomes"), and the Fondation pour la Recherche Médicale (DEQ20051205752). D.G. is supported by Marie Curie Actions (FP7, T3Net).

REFERENCES

Abramoff MD, Magelhaes PJ, Ram SJ (2004). Image processing with ImageJ. Biophotonics Int 11, 36–42.

Carman CV (2009). Mechanisms for transcellular diapedesis: probing and pathfinding by "invadosome-like protrusions." J Cell Sci 122, 3025–3035.

Carman CV, Sage PT, Sciuto TE, de la Fuente MA, Geha RS, Ochs HD, Dvorak HF, Dvorak AM, Springer TA (2007). Transcellular diapedesis is initiated by invasive podosomes. Immunity 26, 784–797.

Collin O, Na S, Chowdhury F, Hong M, Shin ME, Wang F, Wang N (2008). Self-organized podosomes are dynamic mechanosensors. Curr Biol 18, 1288–1294.

Collin O, Tracqui P, Stephanou A, Usson Y, Clement-Lacroix J, Planus E (2006). Spatiotemporal dynamics of actin-rich adhesion microdomains: influence of substrate flexibility. J Cell Sci 119, 1914–1925.

Damljanovic V, Lagerholm B, Jacobson K (2005). Bulk and micropatterned conjugation of extracellular matrix proteins to characterized polyacrylamide substrates for cell mechanotransduction assays. Biotechniques, 39, 847–851.

Destaing O, Block M, Planus E, Albiges-Rizo C (2011). Invadosome regulation by adhesion signaling. Curr Opin Cell Biol 23, 1–10.

Destaing O, Planus E, Bouvard D, Oddou C, Badowski C, Bossy V, Raducanu A, Fourcade B, Albiges-Rizo C, Block MR (2010). 1A integrin is a master regulator of invadosome organization and function. Mol Biol Cell 21, 4108–4119.

Destaing O, Saltel F, Geminard JC, Jurdic P, Bard F (2003). Podosomes display actin turnover and dynamic self-organization in osteoclasts expressing actin-green fluorescent protein. Mol Biol Cell 14, 407–416.

Destaing O, Saltel F, Gilquin B, Chabadel A, Khochbin S, Ory S, Jurdic P (2005). A novel Rho-mDia2-HDAC6 pathway controls podosome patterning through microtubule acetylation in osteoclasts. J Cell Sci 118, 2901–2911.

Geblinger D, Addadi L, Geiger B (2010). Nano-topography sensing by osteoclasts. J Cell Sci 123, 1503–1510.

Hu S, Biben T, Wang X, Jurdic P, Géminard J-C (2011). Internal dynamics of actin structures involved in the cell motility and adhesion: modeling of the podosomes at the molecular level. J Theor Biol 270, 25–30.

Jurdic P, Saltel F, Chabadel A, Destaing O (2006). Podosome and sealing zone: specificity of the osteoclast model. Eur J Cell Biol 85, 195–202.

Linder S (2009). Invadosomes at a glance. J Cell Sci 122, 3009–3013.

Linder S, Aepfelbacher M (2003). Podosomes: adhesion hot-spots of invasive cells. Trends Cell Biol 13, 376–385.

Linder S, Kopp P (2005). Podosomes at a glance. J Cell Sci 118, 2079–2082.

Luxenburg C, Geblinger D, Klein E, Anderson K, Hanein D, Geiger B, Addadi L (2007). The architecture of the adhesive apparatus of cultured osteoclasts: from podosome formation to sealing zone assembly. PLoS One 2, e179.

Riedl J *et al.* (2008). Lifeact: a versatile marker to visualize F-actin. Nat Methods 5, 605–607.

Saltel F, Chabadel A, Bonnelye E, Jurdic P (2008). Actin cytoskeletal organisation in osteoclasts: a model to decipher transmigration and matrix degradation. Eur J Cell Biol 87, 459–468.

Saltel F, Daubon T, Juin A, Ganuza IE, Veillat V, Genot E (2011). Invadosomes: intriguing structures with promise. Eur J Cell Biol 90, 100–107.

Saltel F, Destaing O, Bard F, Eichert D, Jurdic P (2004). Apatite-mediated actin dynamics in resorbing osteoclasts. Mol Biol Cell 15, 5231–5241.

Tsai HH, Macklin WB, Miller RH (2009). Distinct modes of migration position oligodendrocyte precursors for localized cell division in the developing spinal cord. J Neurosci Res 87, 3320–3330.

West MA, Prescott AR, Chan KM, Zhou Z, Rose-John S, Scheller J, Watts C (2008). TLR ligand-induced podosome disassembly in dendritic cells is ADAM17 dependent. J Cell Biol 182, 993–1005.

II. NOVEL REGULATORS OF BONE RESORPTION: FOCUS ON RHOE

II.1. Introduction and rationale: Finding new regulators of the actin cytoskeleton in osteoclast-mediated bone resorption

Ring-driven migration and SZ formation are essential to OC-mediated bone resorption. Podosomes are the structural units of the ring and the SZ but the molecular signaling that governs their collective organization into these superstructures remains elusive. In this study, our goal was to find new genes that would be relevant to this OC-exclusive functional patterning. The investigation was therefore comprised of two main parts:

We first aimed at finding a new list of candidate genes possibly involved in cytoskeletal processes during bone resorption. Such a list would be considered as grounds for selection for functional investigation of individual genes. To that end, we established an original comparative model that takes advantage of the differentiation plasticity of monocytic lineage cells. Since OCs are multinucleated cells derived from the differentiation and fusion of mononucleated monocytic precursors, we differentiated the same precursors into another type of multinucleated giant cells (MGCs) that shares several OC traits. These MGC formed podosomes and expressed osteoclastic degradation enzymes, but were unable to resorb. Based on these phenotypical properties, we used Affymetrix Genechip technology to perform a transcriptome-wide comparison between OCs and their non-resorbing counterparts with the objective of sorting out the genes that are exclusively expressed in OCs. We therefore obtained a list of genes that were highly expressed in OC. We validated this list using the Taqman Low Density Array, a method of highthroughput qPCR that provided more reliable quantification of gene expression levels. At each of these two screening steps, we observed a significant enrichment of actin-regulating genes, most of which where not studied in OCs. This reinforced the importance of the actin cytoskeleton for OC function and suggested new possible regulators for it. We therefore chose to functionally investigate RhoE because it is a constitutively active GTP-binding protein that was previously shown to regulate actin-based structures such as focal adhesions and stress fibers.

Using primary culture of OCs derived from a $RhoE^{gt/gt}$ (knockout by gene trap) mouse, we observed that this gene was dispensable for OC differentiation but essential to bone resorption. Given its previously described actin-regulatory functions in other cells, we hypothesized that its role in bone resorption could be played via regulation of the OC cytoskeleton. Using confocal microscopy and Fluorescence Recovery After Photobleaching, we showed that RhoE expression maintains fast actin turnover in podosome clusters and rings and therefore regulates their patterning. Consequently, RhoE-deficient OCs suffered from impaired migration and suboptimal SZ formation, two crucial processes for bone resorption. Finally, we proposed a molecular pathway accounting for the participation of this gene to actin remodeling in OC podosomes: in wildtype OCs, RhoE inhibits Rock-mediated phosphorylation of a recently identified podosomal component: cofilin. The reduced levels of non-phosphorylated cofilin, the active form of this protein, would therefore ensure fast actin turnover in podosomes and ultimately facilitate their patterning.

Altogether, the data provided in this study depict a new role for RhoE in the control of actin dynamics in podosomes through Rock-antagonism. It also provides a new molecular link between podosome patterning in OCs and bone resorption.

II.2. Publication: Comparative transcriptomics reveals RhoE as a novel regulator of bone resoption by OCs

Title:

Comparative transcriptomics reveals RhoE as a novel regulator of actin dynamics in bone resorbing osteoclasts.

Authors:

Dan GEORGESS[†], Marlène MAZZORANA[*†], José TERRADO[*‡], Christine DELPRAT[§], Christophe CHAMOT[‖], Rosa M. Guasch[¶], Ignacio PÉREZ-ROGER[#], Pierre JURDIC[†], Irma MACHUCA-GAYET[†].

*Equally contributed

† Institut de Génomique Fonctionnelle de Lyon, Université de Lyon, Université Lyon 1, CNRS, Ecole Normale Supérieure de Lyon, 32-34 Avenue Tony Garnier Lyon cedex 07, France

‡ Departamento Medicina y Cirugía Animal, Facultad de Veterinaria, Universidad CEU Cardenal Herrera, C Tirant lo Blanc, 7. 46115 Alfara del Patriarca – Valencia – Spain

§ Laboratoire de Biologie Moléculaire de la Université de Lyon, Université Lyon 1, CNRS, Ecole Normale Supérieure de Lyon, 46, allée d'Italie 69364 Lyon cedex 07, France

|| Platim facility, SFR Biosciences (UMS3444/US8), Ecole Normale Supérieure de Lyon, 46, allée d'Italie 69364 Lyon cedex 07, France

¶ Laboratory of Cellular Pathology, C/ Eduardo Primo Yúfera 3, 46012 Valencia, Spain

Departamento Ciencias Biomédicas - Seminario Salud, Avda. Seminario s/n. 46113 Moncada – Valencia - Spain

KEYWORDS

Osteoclast, bone resorption, RhoE, podosomes, migration, transcriptomics

ABBREVIATIONS

BM: bone marrow

OC(s): osteoclast(s)

DC(s): immature dendritic cell(s)

DC-MGC(s): multinucleated giant cell(s) derived from dendritic cells, not including OCs

DC-17-MGC(s): multinucleated giant cell(s) derived from dendritic cells by stimulation with IL-17

DC-17 γ -MGC(s): multinucleated giant cell(s) derived from dendritic cells by stimulation with IL-17 and IFN-γ

DC-OC: dendritic-cell derived osteoclast

FL: Foetal liver

FRAP: Fluorescence recovery after photobleaching

IL-17: interleukin-17

IFN-γ: interferon-γ

M-CSF: macrophage colony stimulating factor

MGC(s): multinucleated giant cell(s)

Mo: monocytes

Mo-OC: monocyte-derived osteoclast

RANKL: receptor activator of nuclear factor κB

SZ: sealing zone

TRAP: tartrate-resistant acid phosphatase

gt: gene trap

Abstract

Osteoclasts (OCs) are multinucleated giant cells (MGCs) of the monocytic lineage, responsible for bone resorption. Podosomes are actin-rich adhesive structures important for OC functions because they pattern into “rings”, that drive osteoclast migration, and into “sealing-zones” (SZs) that ensure optimal enzyme and proton confinement in the resorption lacuna. Although changes in actin dynamics during podosome patterning have been documented, the mechanisms that regulate these changes are largely unknown. From human monocytic precursors, we differentiated MGCs that express OC degradation enzymes, but are unable to resorb the mineral matrix. We demonstrated that, despite exhibiting bona fide podosomes, these cells presented dysfunctional SZs. We then performed two-step differential transcriptomic profiling of bone resorbing OCs versus non resorbing MGCs to generate a list of genes implicated in bone resorption. Among the generated list of candidate genes, we investigated the role of RhoE/Rnd3. Using primary RhoE-deficient OCs, we demonstrated that RhoE is indispensable for OC migration and bone resorption. Using FRAP analysis, we found that RhoE is required for maintaining fast actin turnover in podosomes probably by inhibiting Rock-dependent cofilin phosphorylation. Consequently, the role of RhoE in podosome dynamics is central for OC migration and SZ formation and therefore to bone resorption.

INTRODUCTION

OCs are giant multinucleated cells (MGCs) of the monocytic lineage that are responsible for bone resorption. They differentiate and fuse from mononucleated precursors such as monocytes (Mo) or immature dendritic cells (DCs) in the presence of receptor activator of nuclear factor κB ligand (RANKL) and macrophage colony stimulating factor (M-CSF) (Rivollier *et al.*, 2004; Speziani *et al.*, 2007; Boyce, 2013). Once differentiated, mature OCs resorb the bone matrix by secreting protons and proteases, such as tartrate-resistant acidic phosphatase (TRAP), cathepsin-K and matrix metalloprotease 9 (MMP9) onto the underlying bone matrix. A circular adhesive superstructure called "sealing zone" (SZ) allows these molecules to be within the resorption pit (lacuna) for efficient bone degradation.

Other types of MGCs can be also generated from immature DCs under various conditions. DCs stimulated by interleukin-17 (ll-17), potentiated by IFN-γ, leads to DC-17γ-MGCs (Coury *et al.*, 2008). Besides resulting from cell-cell fusion of the same precursors (i.e. DCs), DC-17γ-MGCs have OC-like characteristics namely the expression of bone-degrading proteases such as TRAP, MMP9 and Cathepsin-K (Coury *et al.*, 2008) as well as forming adhesive structures called "podosomes" (Olsson Akefeldt *et al.*, 2013).

Podosomes are integrin-based actin-rich dot-like structures, which are present in OCs, DCs and macrophages (Linder and Kopp, 2005). They are the structural units of OC SZ (Luxenburg *et al.*, 2007). A model of intra-podosomal architecture in monocytic cells that is currently widely accepted depicts two distinct domains within podosomes: a peripheral domain made of a loose F-actin meshwork with adhesion and adaptor molecules like αVβ3 integrin, paxillin, vinculin, myosin II, and a central domain comprised of a tightly connected F-actin network with adaptor molecules like cortactin and Arp2/3 (Linder and Aepfelbacher, 2003; Chabadel *et al.*, 2007). When formed in OCs, podosomes are first assembled in clusters that self-organize into "rings" and finally into SZs on mineralized substrates or into "SZ-like" structures (also known as "podosome belts") on non-mineralized substrates. Besides driving the saltatory migration typical of OCs, podosome rings have been described as short-lived patterns, with life spans of 10-15 minutes, that mediate the transition from clusters to SZ–like patterns, more stable structures with life spans of several hours (Destaing *et al.*, 2003; Saltel *et al.*, 2004; Jurdic *et al.*, 2006). Interestingly, the life span of individual podosomes decreases by at least two folds with the transition from clusters to rings/SZ-like structures indicating differential regulation during podosome "remodeling" (Luxenburg *et al.*, 2007). The regulation of podosome assembly and disassembly as well as their inner architecture and

stability are of central importance to their patterning. Therefore, fast and dynamic polymerization and depolymerization of actin, the scaffold of podosomes, has to be tightly regulated in OCs. For example, knockout of gelsolin, a high-affinity actin severing and capping protein, results in the inability of OCs to form podosomes (Chellaiah *et al.*, 2000a). In the same context, slowing the rate of actin turnover in OCs using cytochalasin D, an actin capping molecule, leads to overstabilized podosomes with longer life spans and seemingly larger podosome cores (Luxenburg *et al.*, 2012b). Another important mechanism that regulates podosome size, stability and patterning is acto-myosin-II contractility around podosome cores (Meddens *et al.*, 2013).

Some studies have provided data as to how these processes are regulated at the molecular level in OCs. Src has been shown as an indispensable regulator of phosphorylation of podosomal proteins such as cortactin and gelsolin (Luxenburg *et al.*, 2006b; Destaing *et al.*, 2008). Control of podosome patterning by small GTPases, namely RhoA and Rac1/2 in OCs has been well documented. Rac activation following integrin-dependent signaling is essential to form a functional SZ. Indeed, mice lacking both Rac1 and Rac2 display massive osteopetrosis due to the inability of OCs to form SZs and subsequently resorb bone (Croke *et al.*, 2011). Supporting this result, deletion of Rac GTPase Exchange Factors (GEFs) Vav3 and Dock5 in mice also present osteopetrotic phenotypes explained by an osteoclast functional defect (Faccio *et al.*, 2005; Vives *et al.*, 2011a). RhoA is critical for maintaining OC polarization and SZ formation on a mineralized matrix (Chellaiah *et al.*, 2000b; Destaing *et al.*, 2005). The complete molecular scheme of actin cytoskeleton regulation in OCs that is needed to adequately support bone resorption is still largely incomplete. Studies of Rho-Rock signaling in OC and OC-like cells have shown that this pathway can temporally regulate podosome arrangement during osteoclastogenesis and in a substrate-dependent manner but Rock-downstream signaling in OC remains unclear (Chellaiah *et al.*, 2000b; Ory *et al.*, 2000; Ory *et al.*, 2008a).

In this study, we aimed at finding new genes implicated in actin-related control of bone resorption by OCs, we have compared transcriptomic profiles of human primary Mo-derived OCs (Mo-OCs) and DC-derived OCs (DC-OCs), on one side, with those of Mo, DCs and DC-17 γ -MGC(s) with OC-like traits, on the other, to find genes that were highly upregulated in mature OCs. As a result, we obtained a short list of actin-regulating genes that were up regulated in mature OCs, considered as candidates for functional studies. We focused on the role of one candidate, RhoE (also known as Rnd3), in bone resorption using a genetic knockout model. Given its already described function in other actin structures such as focal

adhesions and stress fibers, we investigated its implication in OC podosome-related aspects such as size, actin dynamics, patterning and cell migration. Finally, given that RhoE interaction with Rock-I has been widely shown to be a central pathway of RhoE function (Riento *et al.*, 2003; Riento *et al.*, 2005), we checked whether RhoE function in OCs was Rock-dependent.

RESULTS

Non-resorbing human multinucleated giant cells exhibit osteoclast-like characteristics but are unable to resorb bone.

Knowing that DC-17γ-MGCs are multinucleated giant cells expressing OC degradation markers such as TRAP, cathepsin-K and MMP9, we first asked whether they were able to resorb the mineral matrix in comparison with bone-resorbing DC-OCs. Then, we investigated their actin containing adhesion structures. Initially differentiated on tissue culture dishes, mature DC-OCs and mature DC-17γ-MGCs on day 5 and 13 of culture, respectively, were detached and seeded on apatite-collagen complexes (ACC), a bone-mimicking substrate (Shibutani *et al.*, 2000; Saltel *et al.*, 2004), and stimulated with M-CSF and RANKL to promote resorption. Confocal microscopy of these cells fixed and stained for actin showed, as expected, that DC-OCs exhibited circular actin-rich sealing zone (SZs) and were able to resorb the mineralized matrix. DC-17γ-MGCs, however, were unable to resorb the matrix and displayed circular actin structures that were significantly less frequent and smaller in size compared to OC SZs **(Figure 1A,B)**. We therefore named the latter actin structures "dysfunctional SZs" because of their inability to ensure proper degradation of the mineral matrix.

To gain further insight into cytoskeletal organization in DC-17γ-MGCs, we compared their actin organization with that of human Mo-OCs and DC-OCs on glass. We labeled these cells for actin, cortactin, a component of the podosome core as well as for paxillin and vinculin, components of the podosome cloud. We acquired images with a confocal microscope and visualized protein colocalization of one podosome marker at a time with actin by displaying channel merges and pixel-to-pixel multiplication of normalized and non-saturated micrographs. We found that cortactin colocalized perfectly with actin in podosome cores of Mo-OCs, DC-OCs as well as in DC-γ17-MGCs. Vinculin and paxillin also colocalized with actin in podosome clouds in all three cell types **(Figure 2)**. These results showed that DC-17γMGCs, albeit displaying *bona fide* podosomes, are unable to efficiently organize SZs, which may participate to their inability to resorb bone.

Comparative transcriptomics revealed bone resorbing OC-specific genes

In order to identify new genes involved in osteoclast-mediated bone resorption, excluding ones involved in myeloid cell-cell fusion, we performed transcriptomic profiling of human

bone resorbing Mo-OCs, DC-OCs as well as their precursor cells, Mo and DCs, and non-resorbing DC-derived MGCs. These latter MGCs included DC-17-MGC(s) and DC-17γ-MGCs **(Figure 3A)**. Practically, blood monocytes from healthy human donors were differentiated in either DCs with M-CSF and IL4, or OCs with M-CSF and RANKL. DCs were then further differentiated in OCs (DC-OCs) with M-CSF and RANKL or DC-17γ-MGCs with IL17 and INF- γ. Total RNAs were extracted from these six culture conditions for two to four independent healthy donors and separately analyzed analyzed by GeneChip® Microarray technology by using 54675 distinct probes. Given the high number of probe sets used, a gene was considered as expressed in a cell type if its mean expression was superior to the overall gene expression in the same cell type (see Mat and Methods). This allowed us to establish a differential list of 115 genes that were expressed only in OCs **(Figures 3, S1, S2**). The presence in this list of RNAs for NFACT1, the OC-specific transcription factor (Takayanagi, 2007) (reviewed in (Takayanagi *et al.*, 2002a)) and ATP6v1c1, a proton pump needed for OC podosome ring formation (Feng *et al.*, 2009), validated our approach. Both resorbing and non-resorbing group of cells were maintained in cell fusion culture conditions, consequently any genes known for roles in cell-cell fusion (such as DC-STAMP, ATP6v0d2, or OSCAR) were eliminated from this analysis. We therefore considered these 115 genes as new potential candidates for the investigation of OC functions. The "molecular functions" of this list compared to the human genome as determined by Gene Ontology (GO) vocabulary underlined enrichment in "Cytoskeletal protein binding" and its sub-category "Actin binding" **(Figure 3B)**.

We aimed at further validating candidates that would be preferentially involved in cytoskeletal regulation of bone resorption as opposed to genes rather implicated in other OC mechanisms. DC-17γ-MGCs were used as MGCs reference model. We then determined RNA expression values of the previously identified 115 genes in Mo-OCs, DC-OCs, DC-17γ-MGCs and their Mo and DC precursors by Taqman Low Density Array (TLDA), a high throughput quantitative real-time PCR. We then averaged the mean expression of a gene (X_c) from several human blood donors and determined if X_c was significantly higher in both Mo- and DC-OCs compared to non-resorbing Mo, DCs and DC-17γ-MGCs by using the limma test. This method allowed us to spot 6 genes that were highly expressed in OCs **(**marked in red in **Figure 3A),** but were not even detected in the other cells types, namely TM4SF1, PLS3 (also known as T-fimbrin), ARHE (also known as RHOE or RND3), LNX1, AK5 and MYO1B. Three out of these six genes (PLS3, MYO1B and RHOE) have been already described as regulators of actin structures in several cell types whereas PLS3 protein has been

shown as a component of podosomes in Mo-OCs (Babb 1997 Cell Motility and Cytoskeleton). Given the importance of Rho-GTPases in the regulation of podosomes in OCs, we aimed at further investigating RhoE role in OCs.

RhoE is essential for bone resorption but not for OC differentiation

RhoE has been previously shown as a regulator of focal adhesions and stress fibers in different cell types. We first investigated the implication of RhoE in osteoclastogenesis using primary murine precursors isolated from a RhoE genetrap mouse model (Mocholi *et al.*, 2011). Because these animals rarely surviving 15 after birth, we used either fetal liver (FL) or P14 bone marrow as a source of OC precursors. We differentiated primary OCs from fetal liver (FL) precursors from $RhoE^{+/+}$, $RhoE^{+/gt}$ and $RhoE^{gt/gt}$ E15.5 littermates in the presence of M-CSF and RANKL on culture-treated dishes and on cortical bone slices. Differentiation of FL-derived OCs (FL-OCs) on days 5, 6 and 8 post seeding was assayed by TRAP staining. On both substrates, no difference in the number of TRAP-positive cells with 3 or more nuclei were observed between these different genotypes **(Figure 4A)**. In the same assay, we also counted the number of nuclei per OC on days 5 and 8 of culture on plastic wells as a measure of OC precursor fusion **(Figure 4B)**. Again, we observed no difference in the absence of RhoE expression. We therefore concluded that RhoE does not play a role in osteoclastogenesis.

To evaluate the role of RhoE in OC-mediated bone resorption, we performed resorption assays in two different conditions. First, precursors from $RhoE^{+/+}$ and $RhoE^{gt/gt}$ littermates were differentiated directly on cortical bone slices. On day 8 of differentiation, the cultures were stopped and the resorption index was determined from surface area measurement of toluidine blue-positive resorption pits and TRAP staining of OCs on the same slices. $RhoE^{gt/gt}$ OCs resorbed bone about 25 times less than wildtype OCs **(Figure 4C,** upper panel**)**. In the second condition, we detached day-4 $RhoE^{+/+}$ and $RhoE^{gt/gt}$ FL-derived OCs (FL-OCs) that were initially differentiated on culture-treated plates and seeded them for 48h on OsteoAssay substrate (OAS) plates, a bone-mimicking substrate. We counted the number of TRAP-positive OCs per well and, in replicate wells, quantified the total resorbed area per well with Silver Nitrate staining. Hence, we calculated the mean resorption index per OC. Again, $RhoE^{gt/gt}$ OCs resorbed the OAS matrix about 12 times less than $RhoE^{+/+}$ OCs **(Figure 4C,** lower panel**)**. These results accounted for an essential role of RhoE in bone resorption *in vitro.*

Small SZs and actin based defective structures in RhoE-lacking OCs

RhoE has been involved in the control of actin cytoskeleton in other cell types (Guasch *et al.*, 1998)**.** We therefore investigated its role in SZ formation, given the critical importance of this actin structure in the bone resorption process. Day-4 FL-OCs expressing or not RhoE were lifted from culture-treated plates and seeded for 24h on bone slices. These OCs were then fixed, stained for actin and imaged using confocal microscopy. Using ImageJ software, peripheral outlines of SZs were then manually determined from acquired micrographs allowing the quantification of the surface areas of SZs. There was a slight yet significant 15% decrease in mean SZ size in $RhoE^{gt/gt}$ OCs compared to $RhoE^{+/+}$ OCs **(Figure 5)**. This result indicated that RhoE expression was dispensable for SZ formation but was needed to maintain normal SZ size.

Because of the observed effect of RhoE knockdown on SZ size, we investigated its importance for podosome formation and patterning into cluster, ring and SZ-like superstructures. Fixed day-4 BM-derived OCs (BM-OCs) were stained with fluorescently labeled phalloidin and imaged with confocal microscopy. Based on observed local fluorescence intensity, actin staining of OC allowed not only the identification of individual podosomes within an OC but also the discrimination between the two subdomains of podosomes: the core with high fluorescence intensity and the cloud with low intensity according to (Chabadel *et al.*, 2007) and (van den Dries *et al.*, 2013c) **(Figure 6A)**. We therefore applied a method of fast and curated fluorescence intensity-based quantification of podosome core surface area. Briefly, once OC cell periphery was drawn manually, we used the "Find Peaks" plugin of ImageJ software with a set of fixed parameters (see Material and Methods) to count podosome numbers per cell and the size of individual podosome cores. We found that the mean number of podosomes per OC was decreased in $RhoE^{gt/gt}$ OCs (645podosomes/cell) compared to $RhoE^{+/+}$ OCs (1018 podosome/cell). Podosome core size was, however, increased in the absence of RhoE expression as shown by mean values and frequency distribution of size **(Figure 6B)**. This suggested that RhoE is not necessary for initial podosomes formation but is important for maintaining proper podosome size.

We then, quantified the number of OCs with clusters, rings and SZ-like structures per well. The total number on average per well of OC exhibiting these podosomal structures was significantly decreased in $RhoE^{gt/gt}$ OCs (45 per well) compared to $RhoE^{+/+}$ OCs (75 per well) whilst the mean OC number per well was not altered as previously shown by the TRAP assay. In more detail, the mean number of OC with clusters was decreased from 20 per well in wildtype cultures to 10 per well in $RhoE^{gt/gt}$ and SZ-like structures from 47 per well to 21 per

well, in that same order. The number of OC with rings was however increased up to 14 per well in $RhoE^{gt/gt}$ OCs compared to 6 per well for wildtype OCs **(Figure 6C)**.
Combining these data with the results from podosome size and number assays suggested that, as a result of RhoE depletion, podosomes were bigger therefore unusually stable but their number was insufficient to properly form clusters. This increase in podosome stability was also depicted by the enrichment in rings, normally transient structures required for SZ-like formation, resulting in fewer SZ-like counts per well. We concluded that RhoE is required for podosome organization and patterning.

RhoE controls actin turnover in podosome clusters and rings

The abnormalities of podosome size, number, superstructure patterning and OC-mediated bone resorption observed in $RhoE^{gt/gt}$ OCs raised the question of RhoE effect on actin turnover in podosomes. To address this point, we performed FRAP experiments on actin in podosome rings and clusters of day-5 FL-OCs 48h after their infection with a LifeAct-mCherry-coding lentivirus to label actin **(Figure 7A)**. We fitted relative fluorescence intensity data with a non-exponential equation of recovery (Negi and Olson, 2006) to minimize constraints by mathematical functions (such as exponential growth). In wildtype OCs, mean actin turnover half times in clusters and rings were 9.8 sec ± 1.4 and 19.7sec ± 3.5, respectively. This showed that rings normally exhibit slower actin turnover. These values were significantly increased in $RhoE^{gt/gt}$ OC for both structures: 24 sec ± 3 in clusters and 34.4 sec ± 3.8in rings (**Figure 7B)**. These data indicated that RhoE is involved in maintaining a fast actin turnover in podosomes.

Depletion of RhoE results in impaired OC migration

Having demonstrated a role of RhoE in actin dynamics in podosomes and in podosome stability and patterning, we hypothesized that RhoE would be implicated in OC migration. To test this hypothesis, we performed a random migration assay on OC. Differentiating FL-OCs expressing or not RhoE were detached on day 4 of culture and replated on culture-treated dishes at identical low confluence ($5x10^4$ cells per well) to minimize OC fusion events. Timelapse movies were then acquired with phase-contrast microscopy and randomly migrating OCs were manually tracked. As visualized in single OC migration tracks **(Figure 8A)**, wildtype OCs displayed typical saltatory migration consisting of displacement in a straightforward direction followed by a recognizable angular turn as we had published in a previous study (Hu et al). This pattern of migration allowed OCs to randomly cover a large

surface area. RhoE$^{gt/gt}$ OCs displayed aberrant migration tracks where they turned in circles because of frequent consecutive angular turns to one side **(Figure 8A)**. The frequency distribution of the instantaneous angle change ($\Delta\alpha_i$) of several wildtype OC migration tracks nicely fitted a Gaussian distribution (R^2 = 0.91) in which the amplitude, indicating the frequency of straightforward movement (i.e. when $\Delta\alpha_i$ is close to 0°), was 2.85% ± 0.07 and the absolute standard deviation (SD, i.e. the interval containing the most frequent 34% single-sided angle changes close to the mean) of 68.4° ± 2.01. Interestingly, values from RhoE$^{gt/gt}$ OCs deviated from the Gaussian distribution (R^2 = 0.58) with an amplitude of 1.97% ± 0.08 and an absolute standard deviation of 115° ± 6.51. The mean of $\Delta\alpha_i$ Gaussian distributions did not vary between the two genotypes (-2.35° ±1,99 for RhoE$^{+/+}$ OCs and -8.76° ± 5.31 for RhoE$^{gt/gt}$ OCs) because we pooled in our quantification several individual tracks which had negative or positive $\Delta\alpha_i$ values. However, amplitudes and SDs were significantly different denoting a decrease of the frequency of straightforward displacements and the increase of the frequency of angular turns during OCs migration in the absence of RhoE expression. This aberrant distribution of angle changes therefore resulted in a significantly lower instantaneous persistence of RhoE$^{gt/gt}$ OCs (P_i=0.335) compared to that of RhoE$^{+/+}$ OCs, (P_i = 0.419) **(Figure 8B)**. Additionally, quantification of the instantaneous velocity of displacement (V_i) showed a significant decrease from 0.86 µm/sec ± 0.01 in RhoE$^{+/+}$ OCs to 0.57 µm/sec ± 0.38 in RhoE$^{gt/gt}$ OCs **(Figure 8B)**. These data showed that RhoE plays an essential role in the directionality as well as velocity of OC migration.

RhoE inhibits Rock−mediated cofilin phosphorylation

Having shown a role of RhoE in podosome dynamics and organization, we sought to find its subcellular localization and the molecular mechanism through which RhoE could perform this function. Day-5 BM-OCs overexpressing RhoE-GFP were fixed, stained with phalloidin and imaged with a confocal microscope. Interestingly, RhoE did not colocalize with podosomes *per se* but was rather ubiquitous in the cytoplasm with certain enrichments at membrane borders **(Figure 9A)**. We therefore considered that RhoE probably acts indirectly on actin in podosomes.

It has been shown for focal adhesions and stress fibers that RhoE acts on the actin cytoskeleton through its inhibition of Rock-I kinase activity. Hence, we searched in mature OCs, phosphorylation targets downstream of Rock-I, such as Mypt1, a regulator of myosin-II (Van den Dries), and cofilin, that could mediate the effects of RhoE on podosome size and actin dynamics. We blocked Rock kinase activity in day-5 BM-OCs for 2h using an inhibitor,

Y-27632, and probed by immunoblotting of total lysates the canonical phosphorylation sites of each of the two Rock targets: cofilin phosphorylation on serine 3 and Mypt1 phosphorylation on threonine 696 **(Figure S3)**. We observed a decrease in p(Ser3)-Cofilin but not p(Th696)-Mypt1 ratios normalized to their respective total protein controls. Thus we validated cofilin as a downstream target of Rock in mature OCs.

Then, to investigate whether cofilin phosphorylation was altered in the absence of RhoE expression in a Rock-dependent manner, we probed p(Ser3)-cofilin levels in $RhoE^{+/+}$ and $RhoE^{gt/gt}$ BM-OCs with or without inhibition of Rock activity by Y-27632. In the absence of Y-27632 treatment, p(Ser3)-cofilin was 2.3 times higher in OCs lacking RhoE expression than in wild type OCs. The addition of Y-27632 reduced cofilin in both situations whilst Rock-I levels did not vary in any of these conditions **(Figure 9B)** suggesting that the observed changes in cofilin phosphorylation were independent of Rock-I expression levels but dependent on its kinase activity. Taken together, these experiments revealed that, when expressed in OCs, RhoE partially blocks Rock-mediated cofilin phosphorylation and therefore the presence of active i.e. non-phosphorylated cofilin.

DISCUSSION

Actin organization during podosomes patterning is central for osteoclast migration and bone resorption. In order to further decipher the mechanisms involved in actin remodeling in bone resorbing osteoclasts, we took advantage of human monocytic plasticity. Indeed, we are able to generate, from human blood cells, either two types of OCs derived from Mo or from DCs (Rivollier *et al.*, 2004), or two different types of MGCs derived from DCs (Coury *et al.*, 2008 and unpublished data). Characterization of DC-derived MGCs, revealed that, despite expressing osteoclastic proteases (Coury *et al.*, 2008), they were unable to resorb the mineral matrix. Moreover, their actin cytoskeleton was organized into circular superstructures reminiscent of SZs that were named "dysfunctional SZs" because of their inability to ensure resorption of a mineralized matrix in comparison with OC SZs. We have showed that, in MGCs, vinculin, as previously reported (Olsson Akefeldt *et al.*, 2013), but also cortactin and paxillin perfectly colocalize with actin in podosomes. This indicated that the existence of *bona fide* podosomes in DC-derived MGCs is insufficient for SZ formation and, more importantly, it suggested that there are yet unknown SZ-specific molecular regulations which are absent in non-patterned individual podosomes.

A Comparative transcriptomics analysis between the two bone resorbing OC populations versus the two MGCs allowed us to provide a list of 115 genes that were highly expressed in OCs but not in MGCs. We hypothesized that these genes would be relevant to mature osteoclast functions. Among these, we validated six genes that were highly and exclusively expressed in OCs, namely TM4SF1, AK5, LNX1, MYO1B, RHOE/ARHE/RND3 and PLS3/T-PLASTIN/T-FIMBRIN. Previous studies have provided data linking these genes either with OCs and/or with the actin cytoskeleton. PLS3, a member of the fimbrin family, has been shown to colocalize with OC podosomes (Babb *et al.*, 1997). AK5 expression is stimulated by RANKL in osteosarcoma cells (Mori *et al.*, 2007). TM4SF1, a member of the tetraspanin family described for their interaction with integrins at the cell surface, is involved in nanopodia formation and cell migration (Zukauskas *et al.*, 2011). LNX1 is responsible for the ubiquitinilation of Src, a known OC regulator (Weiss *et al.*, 2007). Myo1B, a member of the myosin superfamily, is localized in filopodia in HeLa and Cos-7 cells (Almeida *et al.*, 2011) and regulates Arp2/3 in Golgi-related actin foci. Finally, RhoE, a constitutively active RhoGTPase, inhibits stress fibers and focal adhesions by inhibiting the Rho-Rock pathway. Considering the importance of Rho signaling pathways in OCs (Zou and Teitelbaum, 2010), we focused our interest on RhoE.

RhoE depletion did not affect primary OC differentiation nor fusion but greatly decreased bone resorption. $RhoE^{gt/gt}$ OCs were still able to form podosomes but those were fewer in numbers per cell and with smaller cores compared to $RhoE^{+/+}$ OCs. FRAP experiments targeting actin in podosomes revealed a significantly slower actin turnover in clusters and rings of RhoE deficient OCs. Such an increase in podosome stability and core size in OCs has been observed when actin turnover rate was reduced with cytochalasin-D treatment (Luxenburg *et al.*, 2012a). Furthermore, lack of RhoE expression resulted in smaller SZs in OCs seeded on bone. Besides RhoE, RhoA is also dispensable for podosome formation but required for their patterning and SZ spreading (Chellaiah *et al.*, 2003; Destaing *et al.*, 2005). However, conversely to the results of RhoE knockdown, the chemical inhibition of Rho resulted in the spreading of SZ to a belt at the cell periphery of OCs seeded on ACC (Saltel *et al.*, 2004). The reversed consequences of RhoA and RhoE inhibitions suggest antagonistic functions of these proteins in OCs.

The increase in the number of OCs with rings provoked us to investigate typical ring-driven saltatory OC migration in the RhoE-depleted OCs. We have previously described OC random migration as a long phase of movement in the same direction followed by a short phase consisting of a 90°-switch in direction (Hu *et al.*, 2011b). In the herein study, we provide new quantifiable parameters of migration demonstrating that it is considerably altered in $RhoE^{gt/gt}$ OCs, namely by a decrease in displacement velocity and an increase in the frequency of 90°-angle turns. This resulted in global loss of persistence of OC movement. These observations make it tempting to speculate that slow actin turnover rate in rings causes increase in rings stability and results in impaired migration and SZ organization.

To find the molecular pathway in which RhoE could take part to modulate actin kinetics in OCs, we investigated downstream phosphorylation targets of a well-described RhoE partner, Rock-I (Riento *et al.*, 2003). Contrary to its upstream activator Rho (Chellaiah *et al.*, 2000b; Ory *et al.*, 2008a), Rock-I downstream signaling towards podosomes has been poorly studied. However, in non-myeloid cells, RhoE direct binding in 1:1 complex dimers, inhibits kinase activity of Rock-I, but not of its isoform Rock-II,

(Komander *et al.*, 2008). This Rock-I-RhoE interaction destabilizes actin-based focal adhesions and stress fibers when RhoE is over expressed (Klein and Aplin, 2009). We investigated two known Rock-I phosphorylation targets, namely Mypt1 and cofilin. Mypt1 is the main subunit of the myosin light chain phosphatase (MLCP) that activates acto-myosin-II contractility (Ito *et al.*, 2004)**.** We asked if Mypt1 was a Rock-I target in OCs and could explain a myosin-II-dependent regulation of podosome size and patterning as suggested in

previous studies (van den Dries *et al.*, 2013a) (Luxenburg *et al.*, 2012b) (Linder and Kopp, 2005). The chemical inhibition of Rock activity revealed that Mypt1 phosphorylation status at its primary phosphorylation site is not Rock-dependent in OCs. Similarly, when myosin-II contractility was blocked in OCs, the size and stability of clustered podosomes were not affected (Luxenburg *et al.*, 2012b). On the other hand, cofilin is an actin severing and capping protein that regulates F-actin assembly and disassembly thus promoting fast actin turnover (Lappalainen and Drubin, 1997; Maekawa *et al.*, 1999). Non-phosphorylated cofilin has been shown as the active form whilst its phosphorylation on Serine 3 blocks its activity (Arber *et al.*, 1998) (Abe *et al.*, 1996). Furthermore, both total and phosphorylated cofilin have been already shown to localize at podosome clusters and SZ-like structures but how they regulates these structures was still unknown (Blangy *et al.*, 2012; Touaitahuata *et al.*, 2013). We did not investigate gelsolin, another actin-severing molecule, because gelsolin$^{-/-}$ OCs, contrarily to RhoE$^{gt/gt}$ OCs, are totally unable to form podosomes (Chellaiah *et al.*, 2000a). This drastic effect of gelsolin depletion on the cytoskeletal phenotype of OCs is probably due to its much higher affinity to actin compared with cofilin (Ressad *et al.*, 1998; Southwick, 2000). This suggests that gelsolin is likely to be implicated in podosome formation rather than their patterning. Inhibition of Rock severely reduced cofilin phosphorylation at serine 3. We found that p(Ser3)-cofilin levels in RhoE$^{gt/gt}$ OCs were much higher than in RhoE$^{+/+}$ OCs. RhoE could therefore be responsible for the inhibition of Rock-mediated cofilin inactivation, thus ensuring fast actin turnover in OCs.

This Rock-RhoE-cofilin pathway highlights once again the importance of actin cytoskeleton organization in mature OC processes implicated in bone resorption such as migration and sealing zone formation. It also consolidates the emerging model that dissociates podosome dynamics from OC adhesion (Hu *et al.*, 2011b) and differentiation (Touaitahuata *et al.*, 2013).

MATERIALS AND METHODS

Ethics Statements

All animal procedures were approved by local ethics comitee for animal welfare of the Universidad CEU Cardenal Herrera, ID#CEBA03/2007,met the local guidelines, European regulations (EUdirective86/609) and standards for Use of Laboratory Animals nu 5388-01 (NIH).

Primary human cell cultures

All the human cell types used in this study were differentiated directly or indirectly from peripheral monocytes from healthy donor blood (Etablissement Français du Sang, Lyon Gerland, France). All the human recombinant cytokines used for human cultures were obtained from Peprotech (USA). Briefly, $CD14^+$ Mo were isolated from blood after two successive gradient centrifugations in Leukocyte Separation Medium (CMSMSL01-01, Eurobio, France) and 50% Percoll (Gallois *et al.*, 2010), respectively, followed by negative antibody selection. $CD14^+$ $CD16^+$ Mo were then differentiated into OCs in α-minimal essential medium (α-MEM) (22561, Life Technologies, USA) with 10% fetal bovine serum (Bio West, France), 100units/ml Penicillin, 100µg/ml Streptomycin (#15070-063, Life Technologies, USA), 2mM L-glutamine (#25030081, Life Technologies, USA) 50ng/ml human recombinant M-CSF and 30ng/ml human recombinant RANKL. After the first 3 days of culture, medium was changed every 48h with 25ng/ml M-CSF and 100ng/ml RANKL until the end of the culture (5 to 6 days). Mo were also differentiated in suspension into immature (i.e. $CD1a^+$, $CD14^-$, $CD16^-$) DCs in RPMI with 10% fetal bovine serum, 10mM HEPES, 2mM L-glutamine, 100ng/ml GM-CSF and 10ng/ml IL-4 for 6 days. Experimental details of Mo isolation and differentiation and DC differentiation can be found in (Gallois *et al.*, 2010). DCs were then differentiated into either OCs using the same conditions as for Mo-OCs (Rivollier *et al.*, 2004) or into different MGCs such as DC-γ17-MGC (Coury *et al.*, 2008) with or without IFN-γ.

Affymetrix GeneChip® assays and comparative analysis

Primary human cultures of the following cell types were performed from several donors: Mo (2), DCs (4), Mo-OCs (2), DC-OCs (2), DC-derived MGCs with IL-17 (2), with IL-17 and IFN-γ (3). RNA extraction, anti-sense cRNA target labeling, array hybridization and scanning

were performed as shown previously (Gallois *et al.*, 2010). Intra- and inter-assay normalizations were performed according to manufacturer's instructions and gene expression values were averaged per cell type over all donors. When the mean expression value of a gene in a given cell type was superior to the average of all gene means in the same cell type, the gene was considered as expressed. As such, genes commonly expressed in both Mo-OCs and DC-OCs but not expressed in any other cell type used in this study were considered for further investigation.

For the mathematical analysis, after intra- and inter-chip normalization, we calculated the mean expression level of a specific RNA in a given cell type (X_c) as follows:

$$X_c = \frac{1}{n}\sum_{i=1}^{n} X_{(i)} \quad \text{where}$$

X_c is the mean expression of a RNA "$X_{(i)}$" in a cell type "c"

i is the number of donors for this cell type

Then, we calculated the overall RNA expression per cell type ($\overline{X}_c$) as follows:

$$\overline{X}_c = \frac{1}{n}\sum_{i=1}^{n} X_{c(i)} \quad \text{where}$$

$\overline{X}_c$ is the average expression of all probed genes "$X_{c(i)}$" in a cell type "c"

i is the number of probe sets (i = 54 675 for all cell types)

Gene Ontolgy molecular function enrichment

Molecular functions of 115 genes resulting from the transcriptomic assay were annotated according to Gene Ontology and their percentages were compared against the human genome using the online software FatiGO (Al-Shahrour *et al.*, 2006). Only statistically over expressed functions in our specific gene set were represented. Statistical relevance was determined using the Fischer test.

Taqman Low Density Array (TLDA)

Mo, DCs, Mo-OCs, DC-OCs and DC-17 γ -MGCs triplicate cultures were obtained from 3 different human blood donors. RNA was extracted as mentioned in the previous paragraph, quantified with a Nanodrop (ThermoFischer Scientific, USA), quality-checked with an Agilent 2100 Bioanalyzer (Agilent Technologies, USA) and finally reverse-transcribed using iScript™ cDNA Synthesis Kit (#170-8891, Bio-Rad, USA) following kit protocol. Amplification was performed using a made–to-order Taqman Gene Expression Assay (Agilent Technologies, USA) according to manufacturer's instructions. After verification with

of 18S (Hs99999901_s1) amplification (standard microfluidics technical control for amplification runs), relative cDNA quantities (RQs) calculated based on cycle thresholds (Ct) were normalized with SEC61B (Hs00606455_m1) and TBP (Hs00920494_m1) housekeeping genes. Then, differential expression for each gene in resorbing cells (i.e Mo-OCs and DC-OCs) was compared with that of non resorbing cells (i.e. Mo, DC and DC-17 γ -MGCs) by using the latter as background in the limma parametric test (Limma package, Affymetrix, USA) combined with the Benjamini-Hochberg False Discovery Rate p-value adjustment. Adjusted p-values <0.05 were considered significant.

Primary murine osteoclast cultures and transfection

OCs were differentiated from myeloid precursors extracted from either E15 to E18 fetal liver (FL) or from neonatal bone marrow (BM) or spleen (Sp) of $RhoE^{+/+}$, $RhoE^{+/-}$ and $RhoE^{gt/gt}$ mice of exactly the same age respectively described in (Schmidt JCB 2011, Destaing MBoC 2003, (Chabadel *et al.*, 2007). For each experiment, all cultures were started from the same source tissue (i.e. FL, BM or Sp) from littermates sacrificed at the same time. Once extracted from their respective tissues by flushing (in the case of BM) or grinding against a 100µm-pore nylon cell strainer (in the case of FL and Sp), these precursor cells were purified with a gradient of Leukocyte Separation Medium at 1250g for 20min and 20°C by aspiration of the gradient interface. Cells were then washed by centrifugation and put into culture with αMEM with 10% fetal bovine serum, 100 units/ml Penicillin, 100µg/ml Streptomycin, 2mM L-glutamine, 20ng/ml murine recombinant M-CSF (produced by the "Production d'analyse des protéines" platform, UMS3444, Lyon-Gerland, France) and murine RANKL. The source of precursors for each experiment is mentioned in the Results section. For transfection, day-4 OCs were detached with 0.25mM EDTA in warm PBS and transfected using the Neon® MP-100 electroporator (Life Technologies, USA). Briefly, $0.5x10^6$ cells were resuspended with 2µg of pEGFP-C-RhoE (#23229, Addgene) plasmid DNA in 10µl of Buffer "R" (see kit protocol) then jolted with a 1720V current in 2x10ms pulses. Electroporated cells were then seeded on coverslips with pre-warmed medium and kept overnight. Medium was renewed the following day.

Differentiation assays

To quantify differentiation and fusion of FL-derived OCs (FL-OCs) from $RhoE^{+/+}$, $RhoE^{+/gt}$ and $RhoE^{gt/gt}$ mice (Mocholi *et al.*, 2011), the same number of precursors ($2x10^4$ cells/well) from E15.5 littermates was seeded in 96-well culture-treated plates and on bones slices of the

same size. They were then fixed at several time points (day 5, day 6 and day 8 post-seeding) with 4% (m/v) parafolmaldehyde in PBS for 15 min at room temperature then stained at 37°C using a TRAP assay kit (Sigma-Aldrich, USA) according to manufacturer's instructions. Cells with 3 or more nuclei that turned violet were counted as OCs.

Resorption assays

To quantify the resorbed surface per murine OC (i.e. resorption index), two methods were used. For resorption on bovine cortical bone slices, day-8 FL-OCs were assayed for differentiation then resorption was measured as mentioned in (Harre *et al.*, 2012) (Destaing *et al.*, 2003). For resorption on bone-mimicking OsteoAssay Surfaces® (OAS) (#3988, Corning, USA), day-4 FL-OCs were detached from plastic wells by flushing after incubation at 37°C for 5min in PBS + 0.25mM EDTA, counted then seeded at the same number ($2x10^4$ cells/well in 96-well plates) in replicate plates and cultured for 48h. To measure the total surface of the resorbed matrix, OCs were washed off with distilled water then the matrix was stained with a 5% (m/v) Silver Nitrate solution. In parallel wells, the number of OCs was determined by TRAP staining as mentioned previously. Finally, the resorption index was obtained by diving the total resorbed area per well by the total number of OCs per well.

To determine the resorption index of human DC-OCs and DC-17Ɣ-MGCs on coverslips coated with apatite-collagen complexes (ACC) (Shibutani *et al.*, 2000) (Saltel *et al.*, 2004), day-4 DC-OCs and day-14 DC-17Ɣ-MGCs (i.e. stages of differentiation where both cell types a terminally differentiated (Coury *et al.*, 2008) (Rivollier *et al.*, 2004) were detached using 1X Accutase® (Sigma Aldrich, USA), replated on ACC coverslips with RANKL and M-CSF stimulation to promote resorption. The resorbed area per cell was determined by the absence of matrix crystal complexes subjacent to the cell.

Images of all substrates were captured with an AxioImager microscope (Carl Zeiss, Germany) topped with a CCD Coolsnap color camera (Photometrics, USA) and manually quantified with ImageJ software.

Random migration assay

Day-5 Sp-OCs were detached and replated at low confluence ($5x10^4$ cells/well in a 24-well plate) to solicit random (non-directed) OC migration. Cells were given 2h to adhere then were imaged in phase contrast on an inverted microscope Axiovert 100M (Zeiss) for 14 hours at 37°C with saturated humidity. Images were acquired every 5min. Consecutive cell positions were determined manually using the MTrackJ plugin in ImageJ at 20min intervals so that

displacements were significantly greater than imprecisions due to manual tracking. Small front-to-back polarized OCs that< were not in contact with other cells were tracked. In other words, OCs that were fusing or without visible leading and trailing edges were not considered for this assay. Instantaneous velocity (V_i) was defined as the distance travelled between two consecutive points divided by the corresponding time interval (20min). Instantaneous angular change ($\Delta\alpha_i$) was defined as the result of the subtraction between the angles of velocity vectors of two consecutive displacements. Persistence of movement "P_i" was defined as the ratio of "d_i" divided by "D_i", with "d_i" defined as the direct distance between the position "i" and the position at the start of the track and D_i defined as over the length "D" of the track at a given position "i".

Fluorescent labeling and confocal microscopy of fixed cells

OCs in culture on coverslips or glass-bottom plates (Mattek Corp., USA) were fixed with 4% parafolmaldehyde in phosphate buffered saline (PBS) for 10min at 37°C and permeabilized using PBS + 0.2% Triton-X-100 Triton-X-100 in PBS. All antibody dilutions and washes were thereafter performed with PBS + 0.1% Triton-X-100. Used primary antibodies were: anti-vinculin (5µg/ml final, clone hVIN-1, #V9264, Sigma-Aldrich, USA), anti-cortactin (10µg/ml final, #05-180, Clone 4F11, Millipore, USA), anti-paxillin (10µg/ml final, #610051, BD Biosciences, USA). Secondary antibodies Alexa Fluor® 488 anti-Mouse IgG (A11029, Life Technologies) and Alexa Fluor® 488 anti-Rabbit IgG (A-21245, Life Technologies, USA) were used at 2µg/ml. Then Alexa Fluor® 647 Phalloidin (A22287, Life Technologies, USA) was diluted 1:100. Image acquisition was performed with either a DMI4000 microscope (Leica Microsystems, Germany) equipped with a spinning disk unit CUS22 (Yokogawa, Tokyo, Japan) or an SP7 spectral confocal microscope (Leica Microsystems, Germany). For podosome colocalization studies, all images were acquired with the same excitation and detection parameters without reaching signal saturation. To perform pixel-to-pixel multiplication of 16-bit images using ImageJ, non-specific signal obtained from negative control micrographs (cells with only secondary antibodies) was subtracted from the "green micrographs" on coverslips treated with primary and secondary antibodies. Background noise in "red micrographs" (where Alexa Fluor® 647 Phalloidin was used) was measured outside the cells and subtracted from each image. For each cell, the "green channel image" was multiplied with the red channel using the "multiplication" option of the Image Calculator plugin in ImageJ and the result was represented as a "32-bit float" image with a "Ratio" lookup table. In the resulting image, the intensity value of a given pixel is therefore

the results of the multiplication of the intensity values of the pixels with the same coordinates from the "red channel" and the "green channel". For the measurement of SZ sizes on bone slices, contrast minima per field were raised so that bone autofluorescence was no more observed. For podosome core size measurement, background noise was measured outside of the cells and subtracted from entire images. The podosome core was delimited based on local intensity thresholds using the Find Peaks plugin in ImageJ with the following parameters: Gaussian blur "0.72", Background method: "Std.Dev above mean", Background parameter "0", Statistics mode "Both", Background level "24", Search method "Half peak value", Remove edge maxima "On".

Fluorescence recovery after photobleaching (FRAP) acquisition and analysis

Day-4 FL-OCs were infected with 2nd generation packaging viral particles (provided by the "Anira-Vectorologie" platform, UMS3444, Lyon-Gerland, France) containing a pLVX-LifeAct-mCherry lentiviral construct (obtained by inserting LifeAct coding sequence between EcoR1 and BamH1 site in pLVX-mCherry-N1 vector, #632562, Clonetech, USA) at a multiplicity of infection of 10:1 in 1ml per well of a 6-well plate. OCs were incubated overnight and medium was changed in the morning. OCs with clusters and rings were fluorescent on day 6 (48h post infection) and imaged using a DMI4000 microscope (Leica Microsystems, Germany) equipped with a spinning disk unit and a FRAP module piloted by iLas2 software (Roper Scientific, USA). mCherry was excited with a 561nm laser and bleached with a 473nm laser at 100% in 3 iterations. Acquisition was optimized to obtain maximal signal without any saturated pixels and defined in 3 temporal phases: Prebleach phase (5 acquisitions, 5sec time interval between consecutive acquisitions), first postbleach phase (20 acquisitions, 3sec interval) and second postbleach phase (11 acquisitions, 30sec interval). The mean relative fluorescence intensity (RFI) of a given region of interest was measured and normalized as mentioned in (Negi and Olson, 2006). The obtained RFIs were curve fitted and plotted using the formula in (Negi and Olson, 2006) with consideration of the guidelines in (Hardy, 2012). Statistical analysis of recovery half-times was calculated from data fitting using the "Do the best fit values of selected parameters differ between datasets differ" function in Prism 6 (Graphpad software, USA) (Weisswange *et al.*, 2009).

Immunoblotting

Day-5 BM-derived OCs (BM-OCs) were lysed in 2X Lameli sampling buffer, ran on SDS-PAGE and blotted on PVDF membranes. Primary antibodies were: anti-cofilin (1:1000, clone

D3F9, #5157, Cell Signaling Inc, USA), anti-phospho(Ser3)-Cofilin (1:1000, clone77G2, #3313,Cell Signaling Inc., USA), anti-β-tubulin (0.3 mg/ml final, T4026, Sigma-Aldrich, USA), anti-Rock-I (1:1000, clone C8F7, #4036, Cell Signaling), anti Mypt1 (10µg/ml, A300-888A, Bethyl Laboratories Inc., USA), anti-p(696)-Mypt1 (1:1000, STA415, Cell Biolabs Inc, USA). Enhanced chemiluminescence detection was performed using Amersham ECL Prime Western Blotting Detection Reagent (RPN2232, GE Healthcare, USA).

Statistics

Comparison of means was performed with the two-tailed Mann-Whitney non-parametric test in Prism 6 (Graphpad). Unless noted otherwise, values mentioned in the text are Mean ± SEM. confidence level for all tests was 95%. A p-value < 0.05 was considered as significant (*), $p < 0.01$ as highly significant (**), $p<0.001$ as very highly significant (***). Error bar annotation for each sample is defined in figure legends.

ACKNOWLEDGMENTS

The authors would like to acknowledge the contribution of the following members of SFR Biosciences Gerland-Lyon Sud (UMS344/US8) facilities: C. Lionnet at PLATIM platform for valuable input on microscopy, AniRA-PBES for animal care, AniRA-Vectorologie for lentiviral particle production, PAP platform for murine RANKL production. D.G. is an Early Stage Researcher at Tissue Transmigration Training Network (T3-Net) funded by the European Commission under Framework Program 7. D.G is also funded by Fondation-ARC (“Aides individuelles jeunes chercheurs”, ref. DOC20120605264). This project has received research grants from Fondation-ARC (“Subvention fixes”, ref. SFI20101201877), Fondation Arthritis Courtin and PRCEU-UCH22/12.

FIGURE LEGENDS

Figure 1. DC-17 γ -MGC, like OCs, are able to make podosomes but not functional SZs for resorption. (A) Cells seeded on a resorbable apatite-collagen coated matrix. As expected, DC-OCs form SZs (actin is in white in the left panel, in red in the middle panel) and are able to resorb bone (resorbed area in outlined with a white dotted line, right panel). DC-17 γ -MGCs make dysfunctional SZ structures and are unable to resorb the matrix. Yellow line outlines the cell periphery. Scale bar is 20µm. (B) Quantification of actin-containing structures and resorption areas per cell. Left: Percentage of fixed DC-OCs exhibiting SZs compared with DC-17 γ -MGCs exhibiting dysfunctional SZ structures. Middle: box-and-whiskers plot showing surface area of SZ and dysfunctional SZs. Represented on the plot are minimum and maximum values (whiskers), mean (+), median (middle line in grey box), and 25% and 75% quartiles (limits of grey box). Right: histogram of the resorption index (area of resorbed matrix per cell) of the two cell-types. Error bars are SEM.

Figure 2. Cytoskeleton organization in DC-17 γ -MGC compared to Mo and DC-Ocs. Cells seeded on glass showing colocalization of paxillin or vinculin (green) with actin (red) at the podosome cloud (upper panel and middle panel, respectively) and cortactin (green) with actin (red) at the podosome core. Multiplication images where calculated pixel-to-pixel from actin combined with one podosomal protein at a time and are represented in 32-bit float images with "Ratio" lookup table. The calibration bar indicates the correspondence of false color to 32-bit pixel fluorescence intensities. Scale bar is 10µm in first 4 columns and 2µm in magnified square insets.

Figure 3. Workflow and results of the comparative transcriptomic study used to probe for OC-specific genes. (A) *In vitro* treatments used for differentiation and fusion of human Mo into resorbing OCs, of immature DCs into resorbing OCs and of DCs into non resorbing MGCs by addition of IL-17 and/or IFN-γ. Genechip® Microarray technique was applied to total RNAs obtained from each of cell type followed by mathematical comparison to sort out 115 mRNAs highly and exclusively expressed in Mo-OCs and DC-OCs. Validation of the upregulation of the 115 genes in OCs by Taqman Low Density Array performed on cDNAs from Mo, DCs, Mo-OCs, DC-OCs, and DC-17ϒ-MGCs. Due to the high cut-off value for detection, only 56 genes out of 115 were found to be expressed in OCs. Among the these, 6 genes (grey columns, names in red) were undetected neither in Mo, DCs nor in MGCs. (B) Enriched Gene Ontology Molecular functions in the 115 OC-speficic genes compared to the

human genome identified by the online tool FatiGO. Second: secondary, TA: transporter activity, TTA: transmembrane transporter activity, NT: neurotransmitter.

Figure 4. RhoE is dispensable for primary murine OC differentiation and fusion but is required for bone resorption. (A) Micrographs showing TRAP staining of FL-OCs differentiated with M-CSF and RANKL on tissue culture-treated plates after 5, 6 and 8 days of culture. Scale bars are 200µm. Histogram shows a time-scale quantification of the number of OCs (TRAP-positive cells with 3 or more nuclei) per well on tissue culture plastic and bone slices. (B) Plot of the number of nuclei per OC as indicator of OC fusion on tissue culture-treated plastic. (C) Upper panel: micrographs and plot showing resorption index of OCs seeded for 8 days on bone. Resorbed bone is stained with toluidine blue (violet surface outline with white dotted lines). Scale bar is 200µm. Graphs shown mean ± SEM. Lower panel: micrographs and plot showing resorption index of OCs seeded for 48 hours on a bone-mimicking substrate (OsteoAssay plates). Unresorbed matrix is stained with silver nitrate (grey). Resorbed surface is not stained (white). Scale bar is 500µm.

Figure 5. RhoE$^{gt/gt}$ OCs exhibit smaller SZs. Micrographs of actin-stained OC seeded on cortical bone slices showing smaller SZs sizes. Yellow lines show cell periphery inferred from overcontrasted images. SZs were determined by their circular shape and strong fluorescence. SZ outlines were manually drawn and inner surface areas where quantified and calculated mean ± SEM was plotted in the graph. Scale bar is 50µm.

Figure 6. Podosome size, number and superstructure patterning are regulated by RhoE in OCs. (A) Upper lane: micrographs of FL-OC podosomes stained with actin showing a reduced number of podosomes in RhoE$^{gt/gt}$ OCs Yellow line in the zoomed images (lower lane) shows cell periphery (Upper lane). Lower lane: zoom of white insets in upper lane using "Ratio" lookup table colors. White circles depict peripheries of podosome cores as identified by local intensity thresholds using ImageJ (see Materials and Methods) followed by manual curating. The calibration bar indicates the correspondence of false color to 16-bit pixel fluorescence intensities (B) Left: Whisker-box plot depicts minimum and maximum number of podosomes per cell (whiskers), 25% and 75% quartiles (lower and upper limits of boxes) and median (midline of boxes). Middle: Histogram showing mean podosome core size with SEM bars. Left: Frequency distribution histogram of podosome core sizes showing a shift toward bigger sizes in RhoE$^{gt/gt}$ OCs. Horizontal axis shows the centers of intervals. (C)

Micrographs of actin-stained OC cultures. # indicates OCs with SZ-likes. Yellow lines delineate the periphery of cells with podosome rings. Histogram shows counts of clusters, rings and SZ-likes per well. Note the decrease in $RhoE^{gt/gt}$ OCs in stable and metastable podosome superstructures i.e. clusters and SZ-likes, respectively, as well as the increase of transient superstructures, i.e. rings. Scale bar is 100µm.

Figure 7. FRAP of LifeAct-mCherry reveals slower turnover in podosome clusters and rings in $RhoE^{gt/gt}$ FL-OCs. (A) Micrographs of timeframes pre- and post-photobleaching of LifeAct-mCherry-expressing FL-OCs on day 5. Yellow insets show bleached areas. Scale bar is 10µm. (B) Mean fluorescence recovery of photobleached areas normalized to mean fluorescence of the same area before photobleaching and to the non-bleached remainder of the cell during recovery. Data was gathered from n>12 samples per genotype and per structure from 2 independent cultures. Each culture was differentiated using a pool of precursors from at least 3 animals of the same genotype. Dots are means of mean relative fluorescence. Lines are fitted curves. Bars are SD. (C) Actin recovery half-times calculated from recovery curves. Recovery half-times are increased in clusters from 9.8 sec ± 1.4 in $RhoE^{+/+}$ to 19.7sec ± 3.5 in $RhoE^{gt/gt}$ OCs and in rings from 24 sec ± 3 in $RhoE^{+/+}$ to 34.4 sec ± 3.8 in $RhoE^{gt/gt}$.

Figure 8. $RhoE^{gt/gt}$ OCs show impaired migration. (A) Upper panel: micrographs of timelapse imaging showing day-5 Sp-OC migration tracks (red). Scale bar is 40µm. Lower panel: Representative rose plots of 5 $RhoE^{+/+}$ and 5 $RhoE^{gt/gt}$ OC migration tracks for a total duration of 8h per track. (B) Plots of migration parameters of migrating OCs ($RhoE^{+/+}$: n-=84 tracks, 1870 time points; $RhoE^{gt/gt}$: n=39 tracks, 1214 time points). Left: instantaneous velocity of displacement (i.e. speed between 2 consecutive positions). Middle: instantaneous persistence of OC migration ($P_i=D_i/d_i$). Right: Frequency distribution of angle change between 2 consecutive movements. Raw values are represented with dots and fitted with a Gaussian function. Error bars are SEM

Figure 9. RhoE is cytoplasmic and inhibits Rock-I from phosphorylating Cofilin. (A) Micrograph of a day-5 BM-OC expressing RhoE-GFP (green) 24h post-transfection and stained for actin (red) showing ubiquitous cytoplasmic localization of RhoE. (B) Immunoblotting of total Cofilin, phosphorylated Cofilin at Serine 3 (p(Ser3)-Cofilin), Rock-I and β-tubulin of serum-induced day-5 BM-OCs treated or not with 10µM Y-27632 (a Rock inhibitor) after 2h of serum starvation. Quantification of protein expression of p(Ser3)-Cofilin

normalized to total Cofilin reveals a 2.3 fold increase in $RhoE^{gt/gt}$ OCs compared to $RhoE^{+/+}$ OCs without affecting overall Rock-I levels.

SUPPLEMENTARY DATA LEGENDS

Figure S1. Expression ratios of the 115 genes highly expressed in OCs and not expressed in Mo, DCs and DC-MGCs as quantified by GeneChip® microarray. The value of each gene corresponds to the $\log_{10}$ of the ratio resulting from dividing the average expression in OCs by the average expression in Mo, DCs and DC-MGCs described in Fig. 2A.

Figure S2. **Expression values (arbitrary units) of the 115 genes highly expressed in OCs** (Mo-OCs in green; DC-OCs in violet) and not expressed (i.e. below average gene expression within each cell type) in Mo (blue), DCs (red) as quantified by GeneChip® microarray. Stacked bars depict the mean values of expression of a given gene per cell type.

Figure S3. Mypt1 phosphorylation is not Rock-dependent in OCs
OCs were serum-starved for 2h then treated or not with Y-27632 (30µM). Rock-I inhibition resulted in decreased phosphorylation of Cofilin on Serine 3 (normalized over total Cofilin) and did not affect Mypt1 phosphorylation on Threonine 696 (normalized over total Mypt1).

Figure 1.A

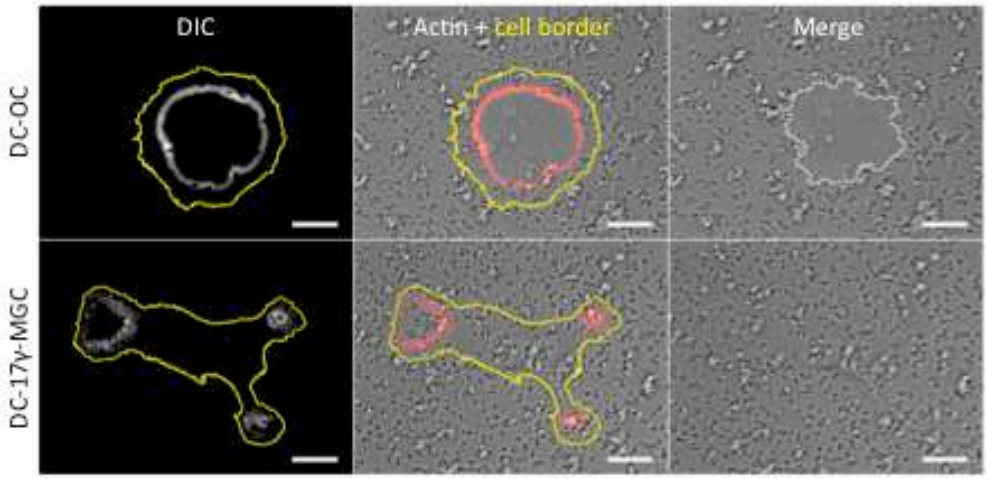

Figure 1.B

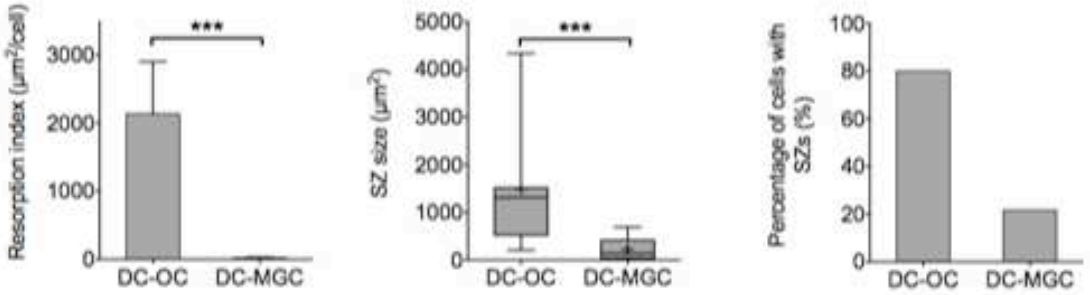

Figure 2

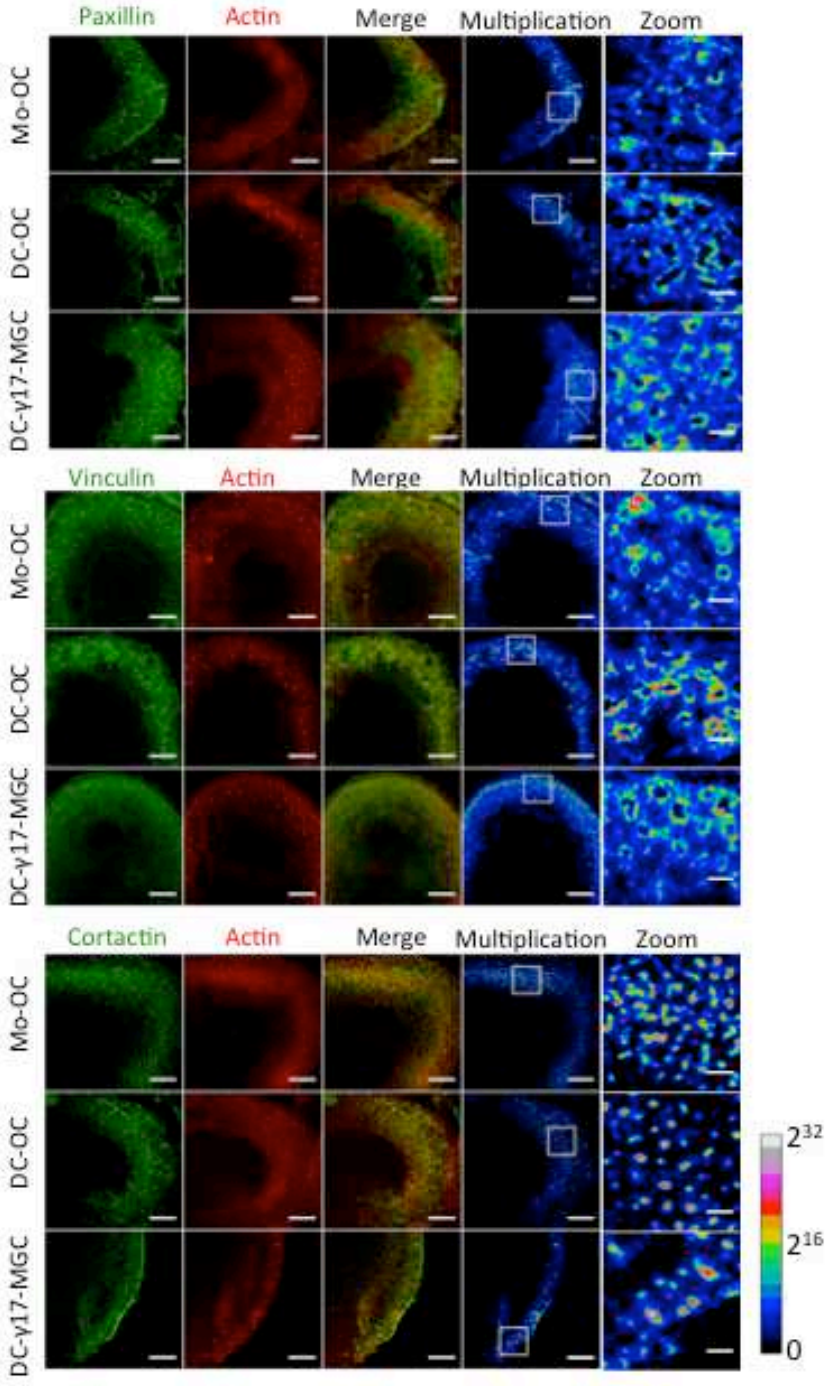
Paxillin
Actin
Merge
Multiplication
Zoom
Mo-OC
DC-OC
DC-γ17-MGC
Vinculin
Actin
Merge
Multiplication
Zoom
Mo-OC
DC-OC
DC-γ17-MGC
Cortactin
Actin
Merge
Multiplication
Zoom
Mo-OC
DC-OC
DC-γ17-MGC
2^{32}
2^{16}
0

Figure 3A

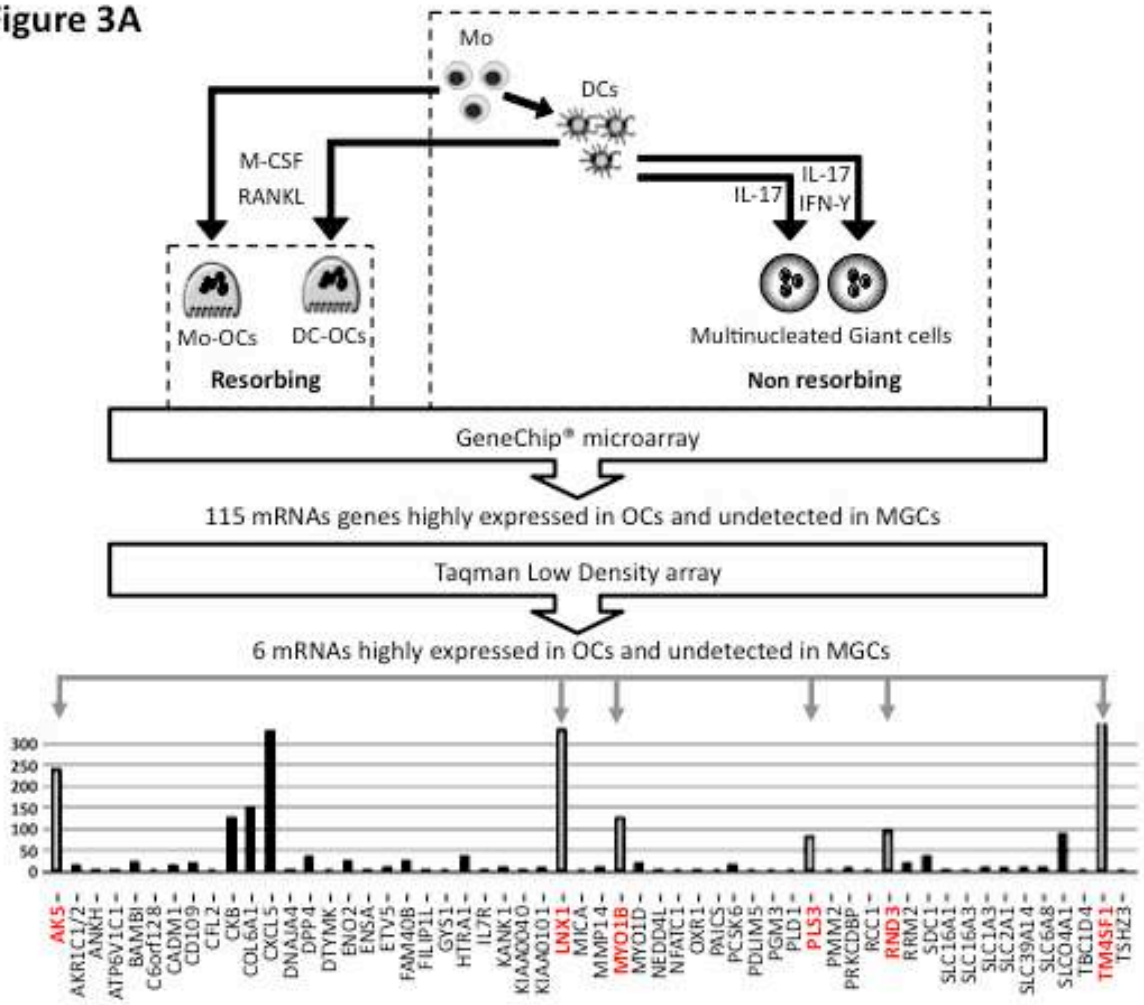

Figure 3B

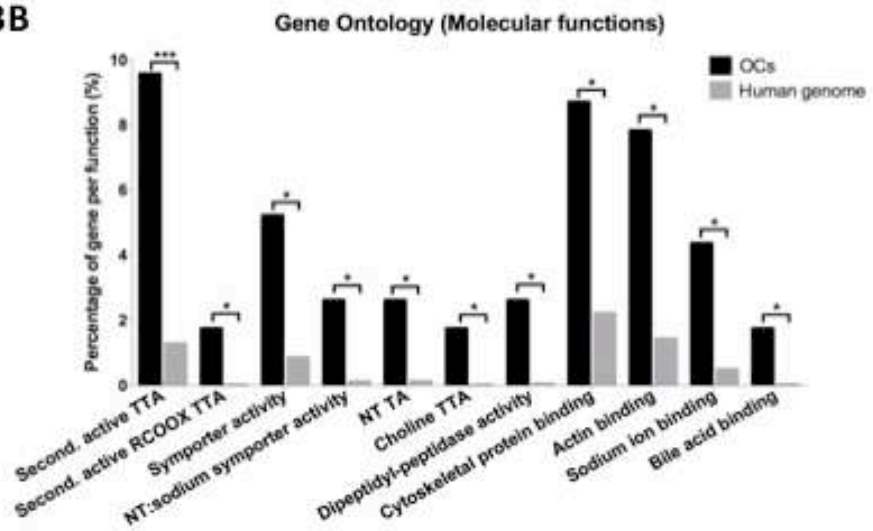

Figure 4.A

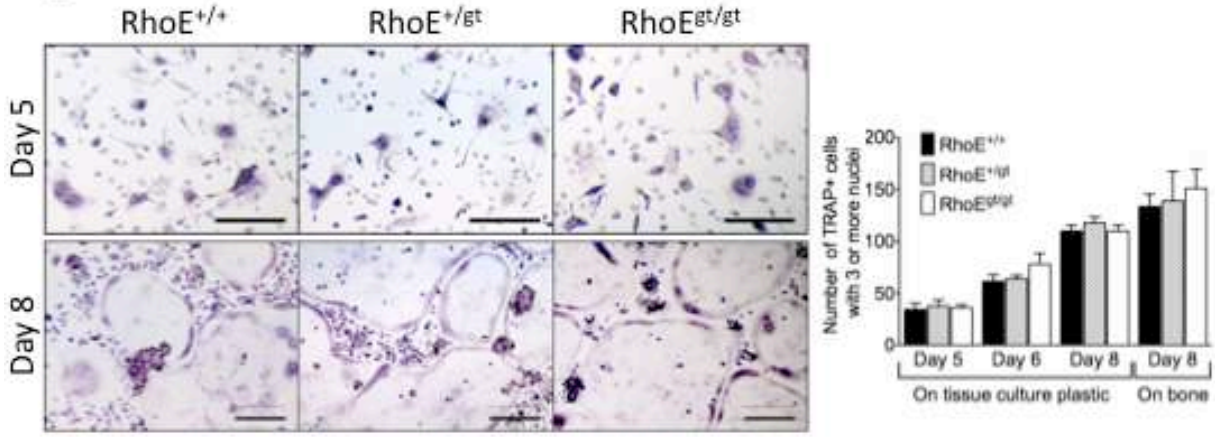

Figure 4.B

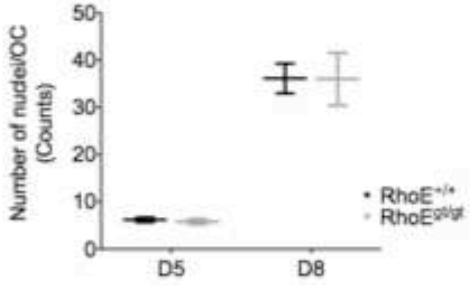

Figure 4.C

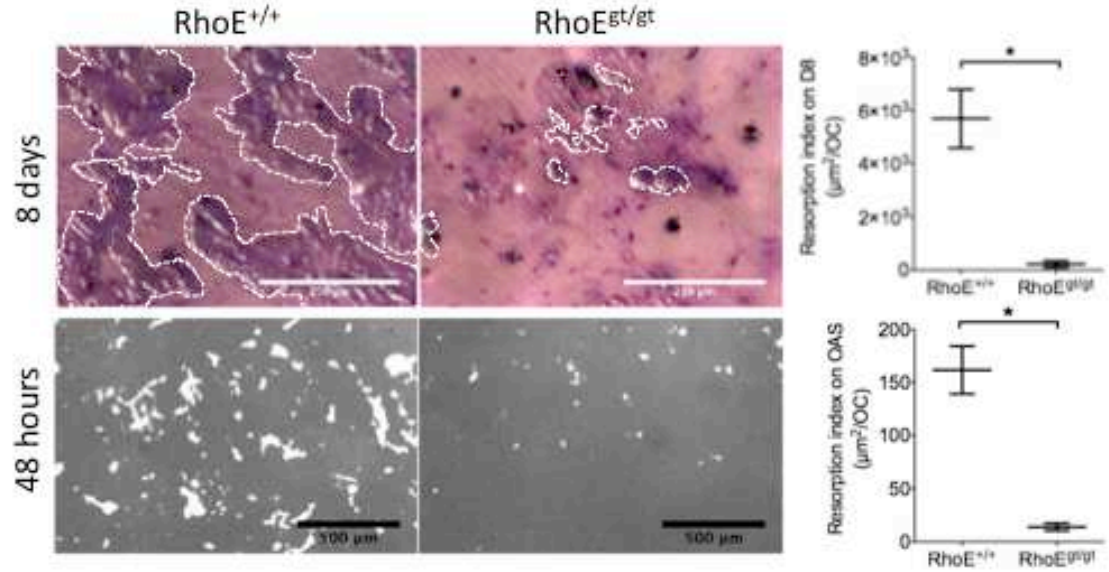

Figure 5

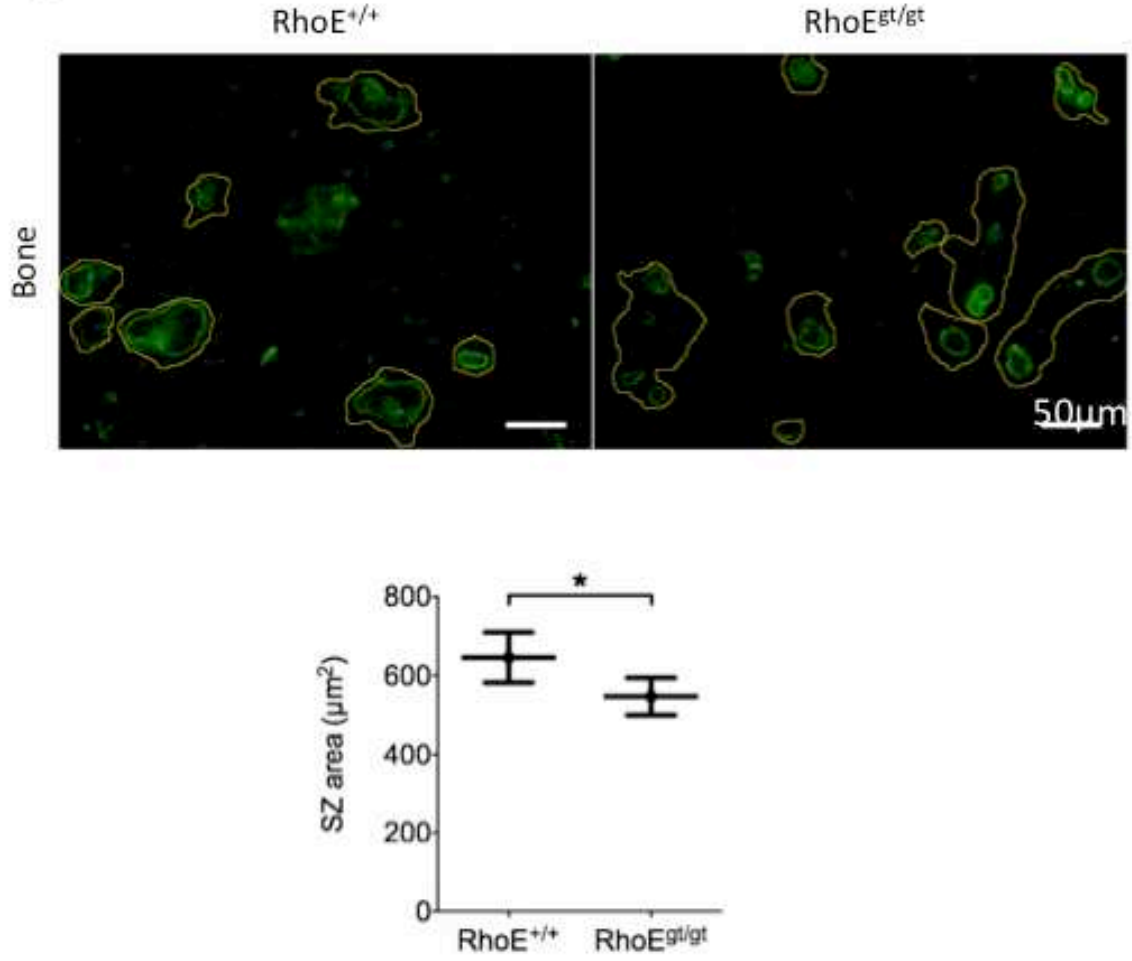
RhoE+/+
RhoEgt/gt
Bone
50µm
SZ area (µm2)
800
600
400
200
0
*
RhoE+/+
RhoEgt/gt

Figure 6.A

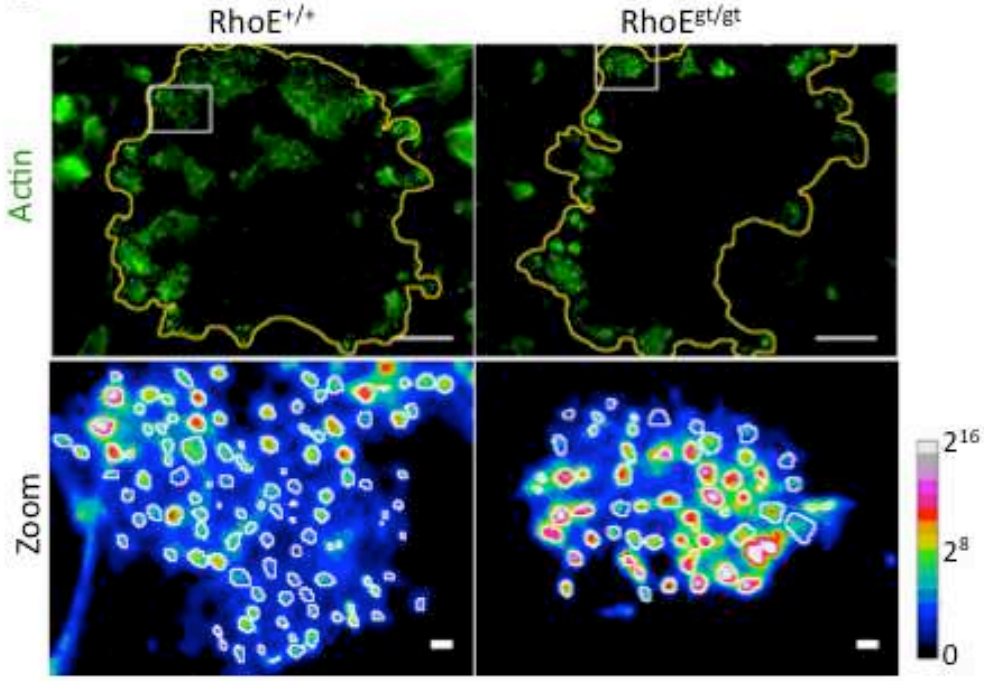

Figure 6.B

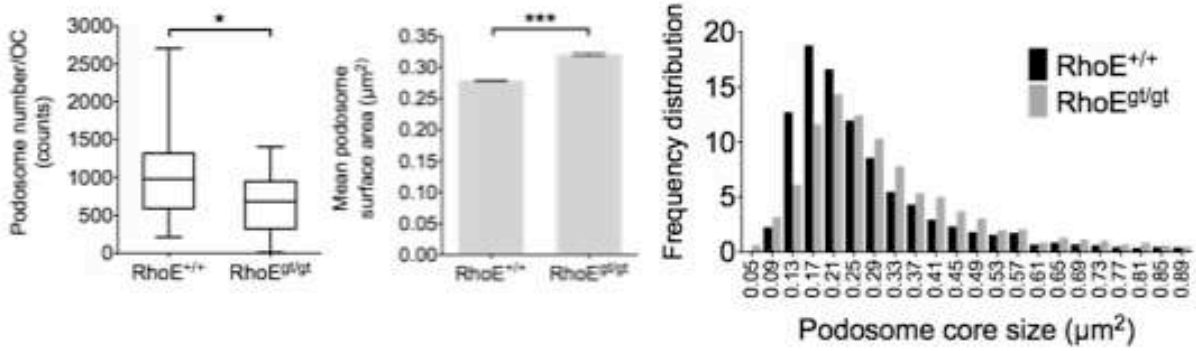

Figure 6.C

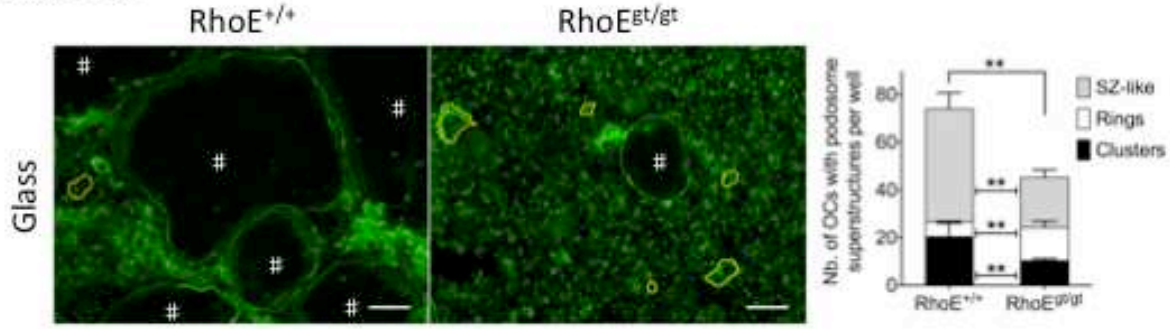

Figure 7.A

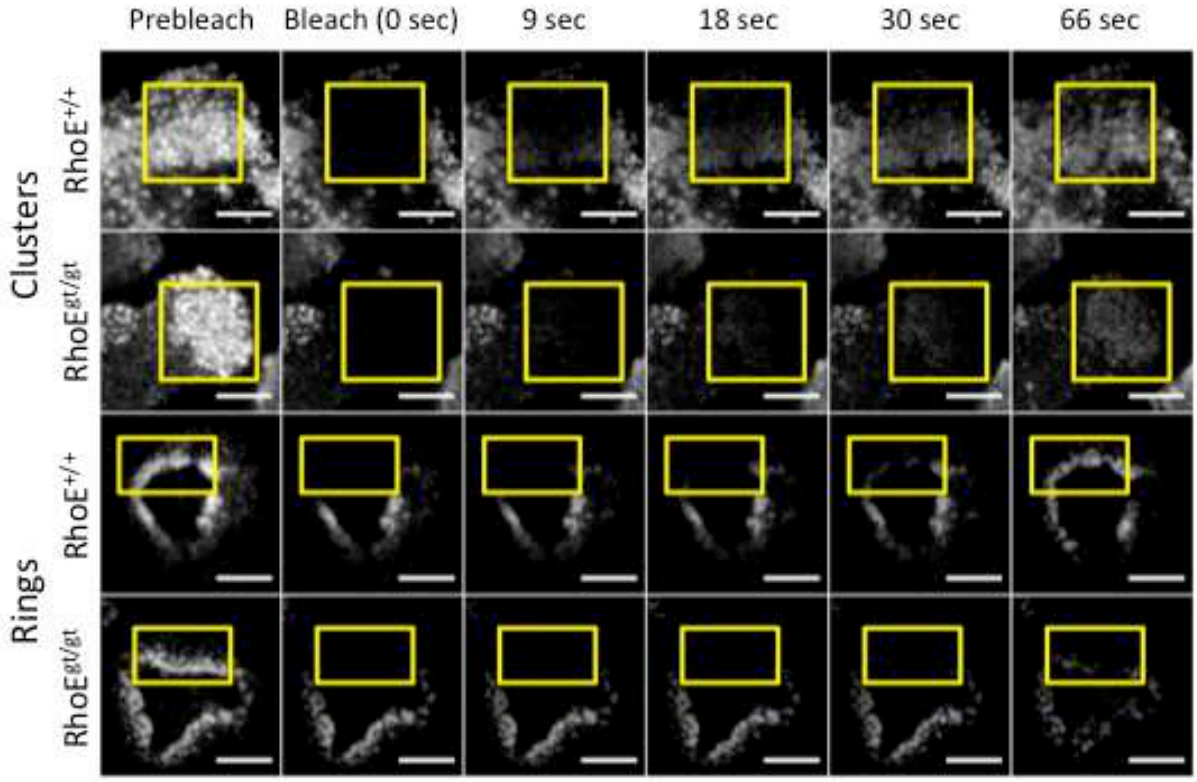

Figure 7.B

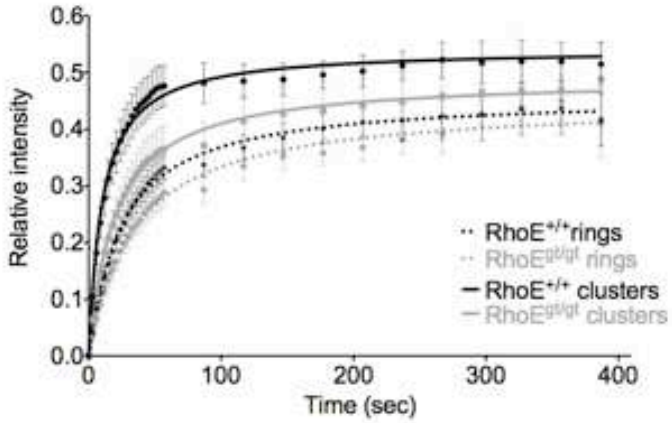

Figure 6.C

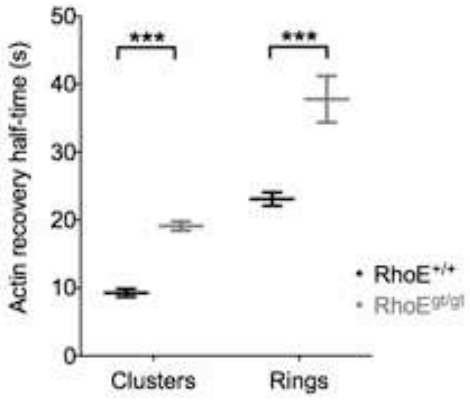

Figure 8.A

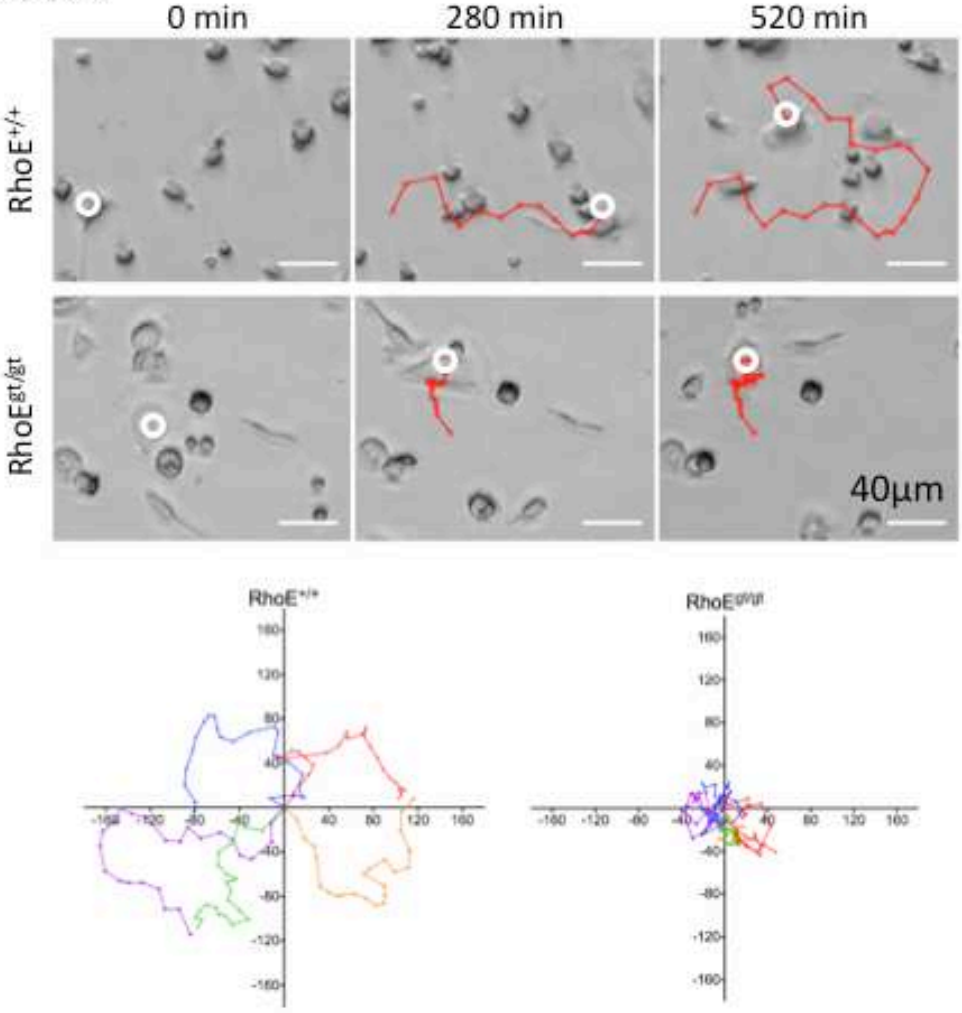

Figure 8.B

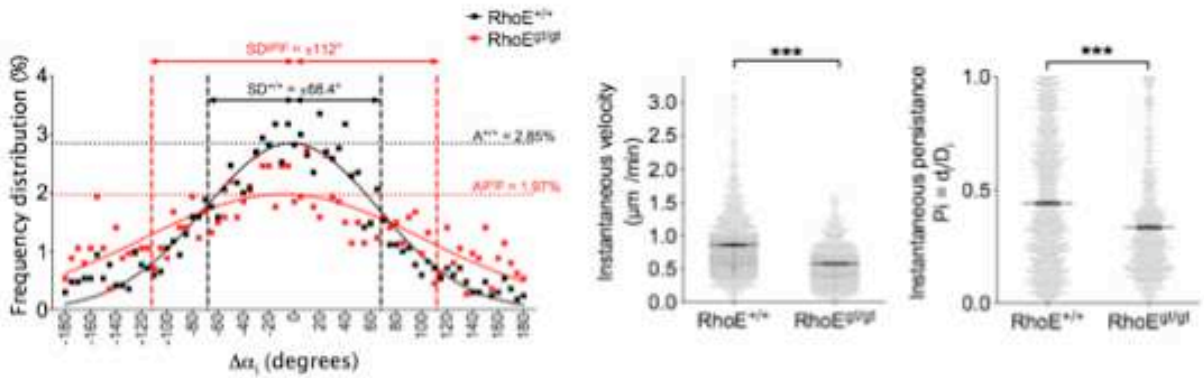

Figure 9.A

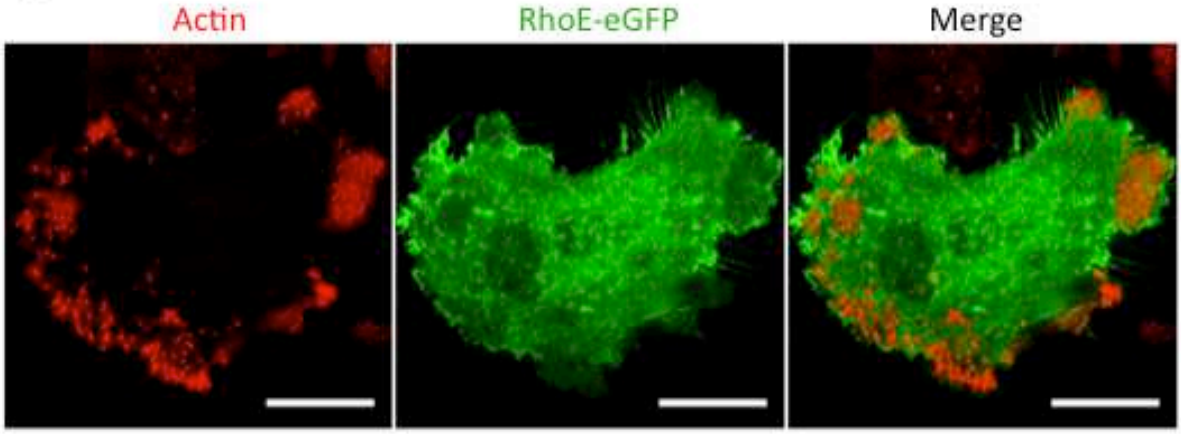

Figure 9.B

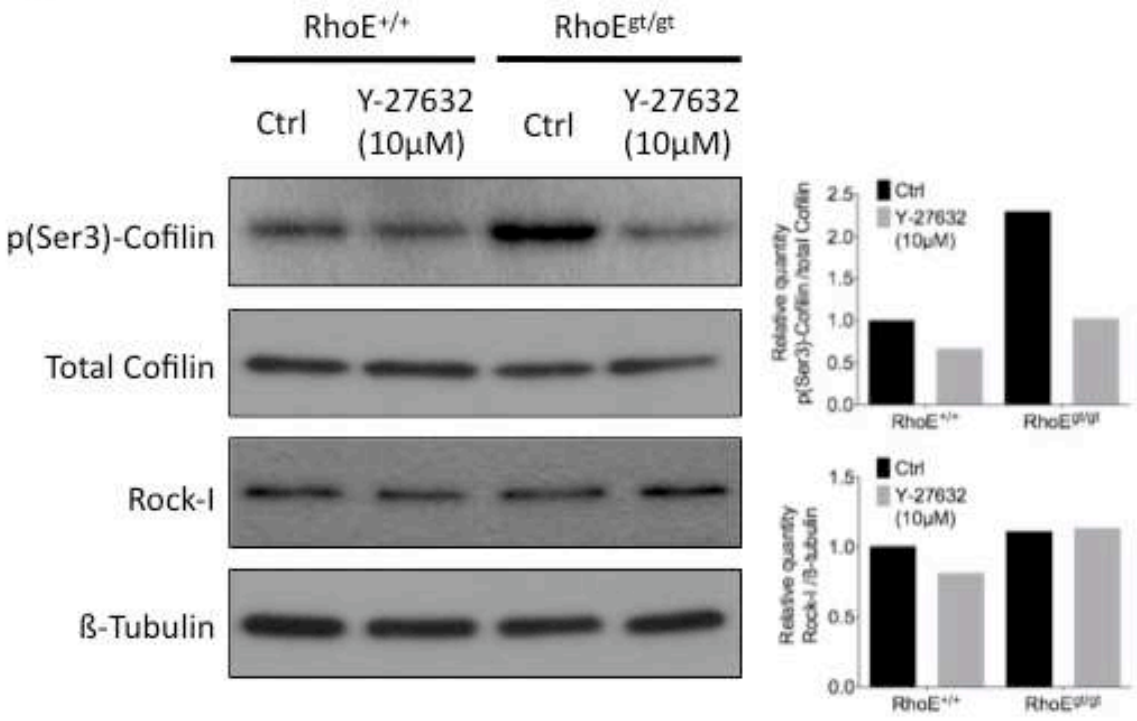

Figure S.1

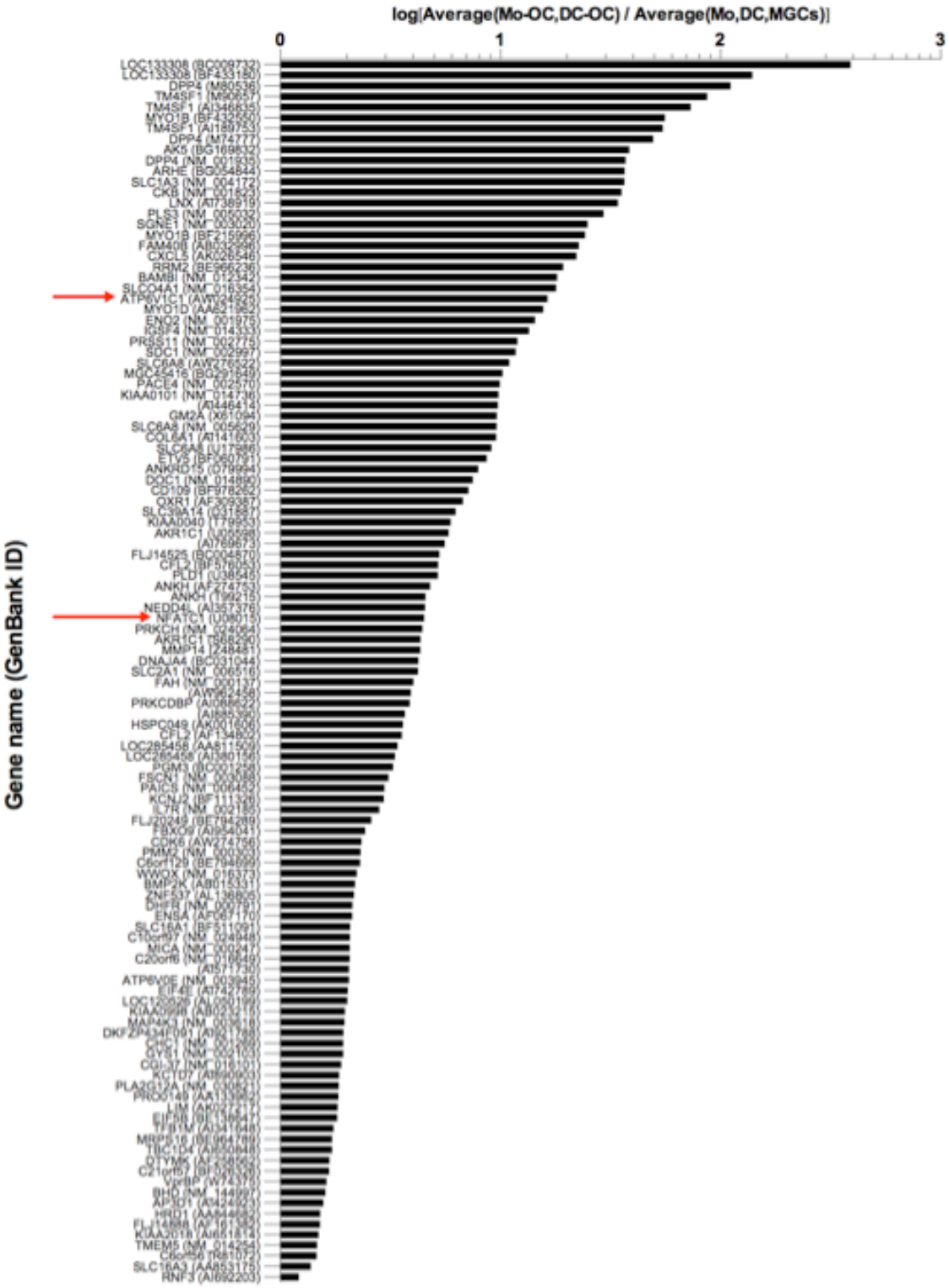
log[Average(Mo-OC,DC-OC) / Average(Mo,DC,MGCs)]
0
1
2
3
Gene name (GenBank ID)

Figure S.2

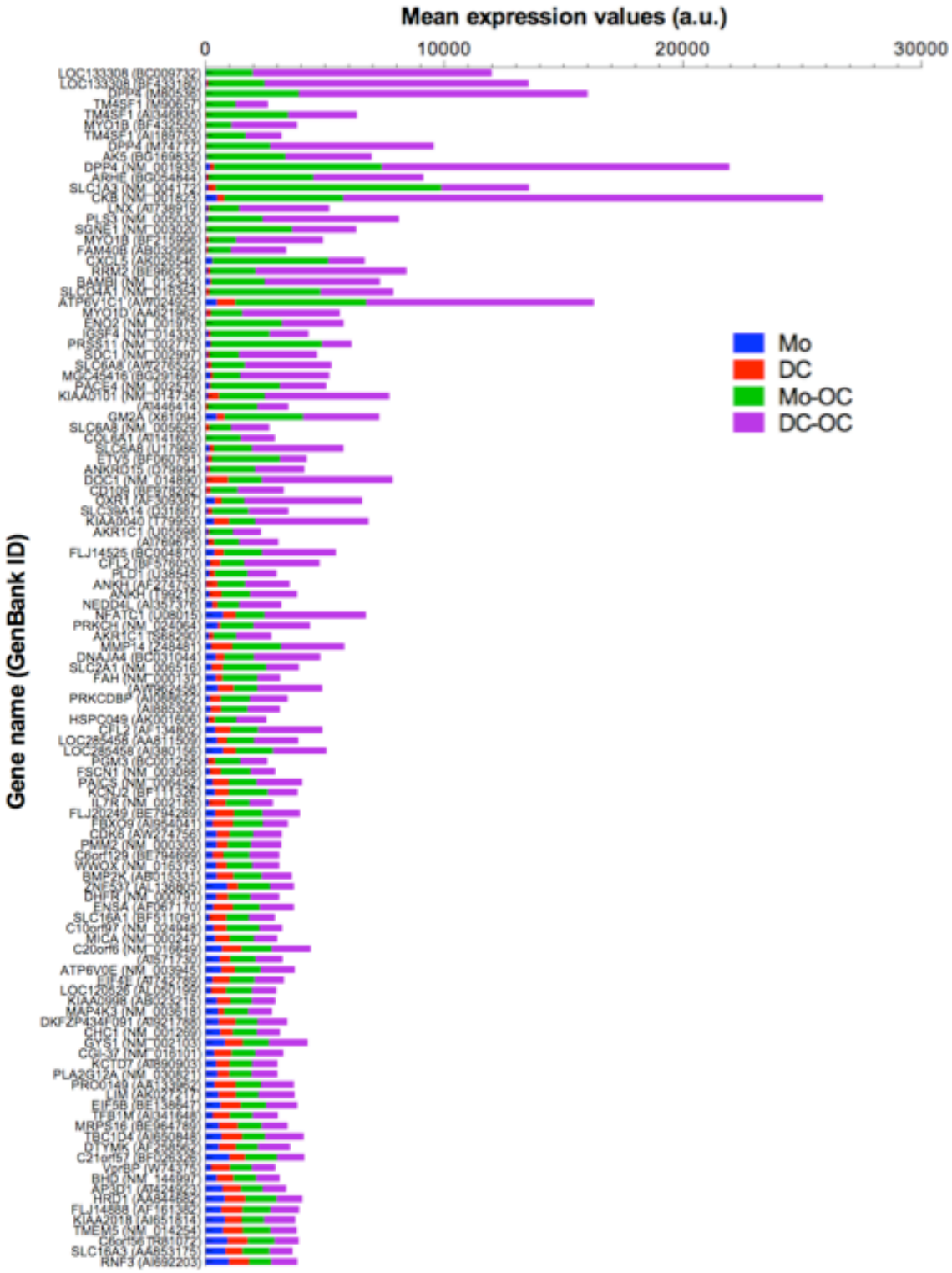
Mean expression values (a.u.)
0
10000
20000
30000
Gene name (GenBank ID)
Mo
DC
Mo-OC
DC-OC

Figure S.3

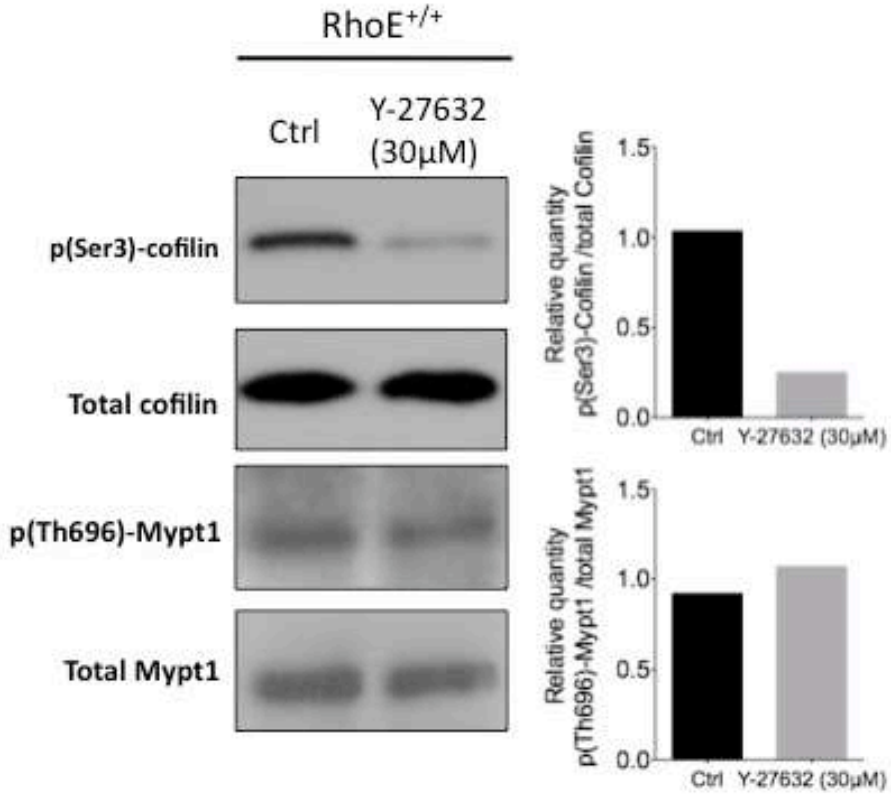
RhoE+/+
Ctrl
Y-27632 (30µM)
p(Ser3)-cofilin
Total cofilin
p(Th696)-Mypt1
Total Mypt1
Relative quantity p(Ser3)-Cofilin /total Cofilin
1.5
1.0
0.5
0.0
Ctrl
Y-27632 (30µM)
Relative quantity p(Th696)-Mypt1 /total Mypt1
1.5
1.0
0.5
0.0
Ctrl
Y-27632 (30µM)

CHAPTER 3: DISCUSSION AND PERSPECTIVES

The cell biology of the OC is an exciting field of research. It allows the understanding of fundamental processes such as cell migration, fusion, matrix degradation, and cytoskeletal remodeling in a physiologically relevant context, that of bone remodeling and homeostasis. OCs differentiate and fuse from mononuclear monocytic precursors to become large multinucleated giant cells. After reaching maturity, these "big" cells roam on the bone surface and degrade it. Meticulous regulation of OC differentiation and mature function is necessary for a healthy bone tissue and, therefore, a healthy organism. Conversely, deregulations of OC processes can lead to bone pathologies. The general purpose of my thesis was to indentify new molecular mechanisms that regulate OC-mediated bone resorption with particular interest to OC differentiation and OC cytoskeletal organization.

OSTEOCLAST DIFFERENTIATION IN PATHOLOGY: THE LINK BETWEEN AUTOIMMUNITY AND BONE LOSS

Osteoclastogenesis is the first rate-determining step in bone resorption. While studying the mechanisms promoting massive bone loss in Rheumatoid Arthritis (RA) *in vivo* and *in vitro*, we found that increased differentiation but not resorption capacity of OCs was the reason behind this bone loss. RA-induced osteoclastogenesis mainly consisted of three phases. First, autoantibodies that rise years before the onset of RA recognize a genetically mutated and post-translationally modified protein, mutated citrullinated vimentin (MCV), in OCs. This recognition stimulates OC secretion of an immune cytokine TNF-α, which known for its acute osteoclastogenic potential. Finally, by an amplified autocrine loop, TNF-α not only induces OC precursor proliferation and differentiation, but also promotes its own expression in these cells (Harre *et al.*, 2012). Therefore, this study constituted the first link between the three main elements in RA: the major autoantibody (anti-MCV), the prevalent clinical aspect (bone loss) and the dominant cytokine (TNF-α) (Figure 17).

Although it is now clear that MCV can be exported to the surface of OC, future efforts should be made to elucidate the molecular mechanisms induced by these autoantibodies after they bind MCV at the surface of the cell.

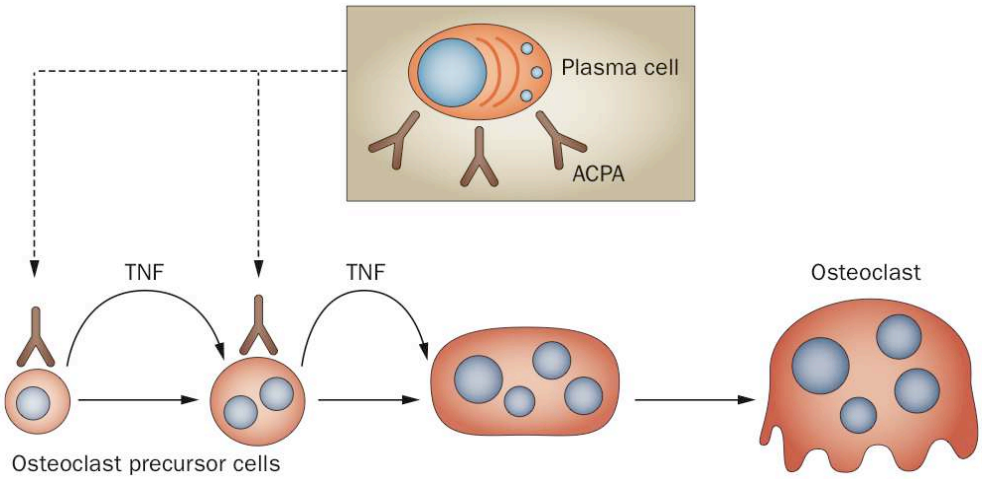

Figure 17. The current model of autoantibody-induced osteoclastogenesis in RA. Autoantibodies against citrullinated proteins (ACPAs), with high specificity against citrullinated vimentin are produced by plasma cells. These ACPAs bind to osteoclast precursor cells and induce the release of TNF, which in turn enhances the differentiation of these cells into mature osteoclasts (Schett and Gravallese, 2012).

ORGANIZATION OF THE OSTEOCLAST CYTOSKELETON DURING BONE RESORPTION

Differentiated OCs dispose of a unique cytoskeletal machinery that allows them to degrade bone. Although podosome formation is not exclusive to OCs, these cells are the only ones that arrange their podosomes to form sealing zones (SZs). As its name suggests, the role of the SZ is to ensure proper confinement ("sealing") of degradation molecules secreted via the ruffled border into the subjacent resorption lacuna. In fact, the formation of the SZ is concomitant with OC apico-basal polarization and subcellular compartmentalization. Not only does the OC form a ruffled border that is characterized by vesicular secretion and proton pump activity and surrounded by a SZ, the cell also commits to other resorption-related functions such as microtubule stabilization and transcytosis through the apical pole. Furthermore, the OC also transitions into an active podosome-driven migration phase between two resorption phases, thus adding a second type of polarization, i.e. antero-lateral, to the dynamic process of bone resorption. Given its involvement in all the processes of resorption, the OC cytoskeleton was the main subject of research in this thesis. Discussed below are the significant findings from the two main studies, Hu *et al* and Georgess *et al*: how they elucidate some aspects of OC function but also why they make grounds for new perspectives.

Novel actin-organizing genes indentified in osteoclasts

With the perspective of finding new pathways involved in OC function, we have performed a differential transcriptomic screen comparing, on one hand, bone resorbing human OCs and, on the other hand, non-resorbing multinucleated cells from the same OC precursors. We were then able to establish a list of 115 genes that were highly and exclusively expressed in OCs.

Gene Ontology annotation of these genes has revealed that this list contained an enrichment of certain cellular functions in OCs compared to the percentage of the functions in the Human genome. One of the enriched functions was "Cytoskeleton binding" including is sub-category "Actin binding", thus highlighting the importance of the cytoskeleton in general and actin filaments in particular to OCs. Additionally, other enriched functions never before addressed in OC have been identified, e.g. "Active transporter activity".

In a second step of this comparative study, we verified with higher quantitative precision the expression levels of the 115 genes in the same set of cells used for the transcriptome analysis. This allowed the validation of 6 candidate genes (out of the original 115) as OC-exclusive genes in our model: Tm4sf1, Pls3, Myo1b, AK5, LNX1 and RhoE. Previous studies have provided data linking these genes either with OCs and/or with the actin cytoskeleton in other cells. This highlights once more the necessity of tight cytoskeletal regulation in OCs. PLS3, a member of the fimbrin family known for organizing actin filaments, has been shown to colocalize with OC podosomes but how it might actually regulate podosomes is unknown. AK5 expression is RANKL-dependent in osteosarcoma cells but its function in OCs has not been addressed. TM4SF1, a member of the tetraspanin family described for their interaction with integrins at the cell surface, organizes adhesion structures and cell migration. It would be interesting to find if it is implicated in integrin signaling during OC migration. LNX1 is responsible for the ubiquitinilation of Src, a major podosome regulator. Myo1B, a member of the myosin superfamily, is localized in filopodia, protrusive adhesion-type structures, and regulates Arp2/3, a known podosome component, in Golgi-related actin foci. Finally, RhoE, a constitutively active GTP-binding protein of the Rho family, inhibits stress fibers and focal adhesions by inhibiting the Rho-Rock pathway. In summary, our comparative model has provided new putative regulators of OC pathways.

Because of their high expression in OC and the cytoskeletal functions that these gene play in other cell types, their study should bring new information on the regulation of OC cytoskeleton.

Considering the importance of RhoGTPase signaling pathways in OCs, we focused our interest on RhoE. We confirmed the importance of RhoE for podosome organization during

bone resorption by its ability to inhibit Rock-activity *in vitro*. Details of the cellular and molecular mechanisms controlled by RhoE and how they have provided new insight into the OC mode of function are given in the subsequent sections of this chapter. In the future, investigation of the role of RhoE will evolve around its function as a physiological regulator of bone remodeling. Two distinct *in vivo* models should be used to investigate the physiological role of RhoE. First, RhoE OC-specific deletion in mice could be achieved by crossing RhoE-floxed mice with mice expressing Cre recombinase under the Cathepsin-K promoter, which is specific to OCs. Both mouse lines are available. The finding of an osteopetrotic bone phenotype in OC-specific RhoE-deleted mice would then be the ultimate proof of the dependency of bone resorption on this gene. The second model, which already exists and should be used for the *in vivo* investigation, is the RhoE ubiquitous knockout by genetrap ($RhoE^{gt/gt}$). These mice present severe developmental defects which lead to their premature postnatal death. Among the existing abnormalities, $RhoE^{gt/gt}$ mice are strikingly smaller at birth and display growth retardation compared to wildtype littermates. The underlying causes of this smaller size could be arrested chondrogenesis, arrested osteogenesis, and/or the absence of bone resorption, which is the first step of the cartilage-to-bone transition. Thus, to uncover the global role of RhoE in bone, its tissue-specific functions should be assessed. Histological analysis of bone sections should provide indications of RhoE-depleted OB differentiation and bone formation. Furthermore, micro-computed tomography (μCT) studies of bone tissues in each of the proposed murine models would finalize the analyses by allowing accurate quantification of bone histomorphometric parameters.

The role of podosomes in adhesion and spreading

Before the OC migrates and resorbs bone, it needs to adhere the extracellular matrix. The relationship between cell adhesion and podosome organization has been long admitted by scientists, but its details were poorly understood. We have shown that, as soon as the OC contacts it substrate but before it is properly spread, intracellular waves of unorganized actin are pooled in membrane protrusions at the edge of the cells. After 10-20 minutes, podosome assembly begins and the cell membrane is laterally stretched to make even bigger protrusions than ensure the complete spreading of the cell. Now given the fact that actin recruitment in podosomes occurs at the level of the adhesion plaque at the immediate vicinity of the cell membrane (see Chapter I - sections III.2 and III.3), it would mean that podosome assembly (and namely podosome core growth) in a bottom-up manner exerts a force on the membrane

itself, pushing it away from the center of the cell and thus induces spreading. Our findings converge with other data describing matrix-dependent podosome dynamics (Labernadie *et al.*, 2010; van den Dries *et al.*, 2013b).

Conversely, the inhibition of integrins in an already-spread OC results in two sequential phases of detachment: (1) within the first seconds, podosomes disassemble but the cell remains spread, then (2) the cell retracts and detaches from the substrate. These observations allow the conclusion that podosomes are not the only mediators of adhesion in OCs, at least in a short period of time, but that they greatly enhance and maintain it.

Osteoclast saltatory migration

An adherent and spread OC forms podosomes that grow in a confined space during their assembly phase. The growth of podosomes in close vicinity within a cluster leads to them "pushing" each other, thus resulting in a ring pattern. While rings expand by rapid podosome assembly and disassembly in an outward radial direction, they apply traction forces on the matrix thus steering a part of the cell that becomes a leading edge. Our observations have shown that, within one OC, at least two podosome rings grow simultaneously, hence creating two leading edges at opposite directions. At this point, the migratory OC adopts a triangular form with two tips occupied by podosome rings and the third tip constituting the trailing edge of the cell. Due to the transient nature of rings, one of the two migratory rings eventually collapses before the other. The most stable ring then determines the migratory direction of the entire cell, after a characteristic delay period, in following that of its proper growth. These events translate into a cyclic biphasic migration scheme: (1) Straightforward movement: while the two rings grow at the front of the cell (in positions similar to two tips of a triangle) and the trailing edge of the OC passively follows behind (positioned at the third tip of the triangle), the OC moves forward in a straight direction, then (2) Angular switch: the rings reach a maximal distance between them, they stretch and flatten the triangle, one rings collapses and the other determines the sudden “jump” of the entire cell in its direction. This jump has a characteristic deviation of 90° from the previous straightforward phase direction and marks the start of a new straightforward phase which will eventually perpendicularly deviate from itself. The cycling of angular switching in the OC trajectory allows for a large mean squared displacement, which is probably needed by the OC to cover a maximal surface area in the search for spots to degrade.

Although the saltatory migration of OC is intrinsically heterogeneous, its characteristic parameters can be experimentally quantified. In the normal situation, the OC migrates at an

average instantaneous velocity of 0.8μm/sec and with a track persistence value of 0.45 ("0" being a constant rotation of the cell around itself and "1" being a perfectly straight line). From now on, these parameters can be used by OC biologists for quantitative assessment of OC migration in different experimental conditions. We have used them to assay for the role of RhoE in OC migration. For example, while investigating the function of RhoE in OCs, we saw that $RhoE^{-/-}$ OCs migrated with reduced instantaneous velocity compared to wildtype OCs, but also that their persistence was reduced due to increased angular turns and decreased straightforward motion. Therefore RhoE deletion in OCs changed their migration from saltatory to simply "turning in circles" around themselves.

Regulation of podosome internal dynamics and collective patterning

Podosome dynamics need to be tightly regulated by the OC in order to properly organize into a SZ. The presence of classical structural markers such as actin, vinculin, paxillin and cortactin within podosomes of OCs or of other multinucleated giant cells from the same lineage can lead to circular patterning of podosomes but is insufficient to form a functional SZ capable of ensuring bone resorption. This finding supports the existence of OC-specific molecular mechanisms to podosomes that distally support SZ formation by upstream regulation of podosomal proteins. Indeed, although their upstream distal regulators are not always known, some podosomal proteins like cortactin and cofilin have been previously shown to undergo posttranslational modification, such as tyrosine phosphorylation, which have consequences on actin dynamics in podosome. The idea of "distal upstream regulation" is further confirmed by data derived from a single bone marrow-derived OC population. In absence of the expression of RhoE, which is not a structural component of the podosome, podosomes can still assemble but SZ formation is abnormal. In fact, RhoE regulates podosomes by modulating cofilin-mediated actin turnover.

The resorption-migration cycle

In order for OCs to efficiently degrade bone and ensure its renewal, this cell needs to fulfill two functions: resorption and migration to find new resorption target sites. This would mean that the podosomes in OCs needed to maintain dynamic patterning transition between SZs rings. The data obtained on the role of RhoE in OCs has demonstrated how one molecular pathway links internal podosome dynamics to both ring-driven migration and SZ-mediated resorption. This provides proof, additionally to that already found in the literature, of the necessity of podosomes to these cellular processes. However, the gathered data did not bring

new insight as to the spatio-temporal regulation of the hypothetical resorption-migration cycle. To address this aspect, one would need to distinguish podosome migratory rings from SZs, which is not possible in a static, fixed setting because they are both circular podosomal patterns that contain the same proteins. However, the discrimination between rings and SZ could be addressed by timelapse microscopy of OCs with fluorescently labeled actin and seeded on bone (Figure 18). The quantification of morphological and kinetic parameters such as pattern lifespan and size, circular expansion rate, pattern displacement, cell displacement, etc…, followed by principal component analysis should allow the identification of two subsets (rings and SZ) within these circular podosome patterns. This approach might provide, once and for all, a clear demonstration of how the OC coordinates displacement with resorption.

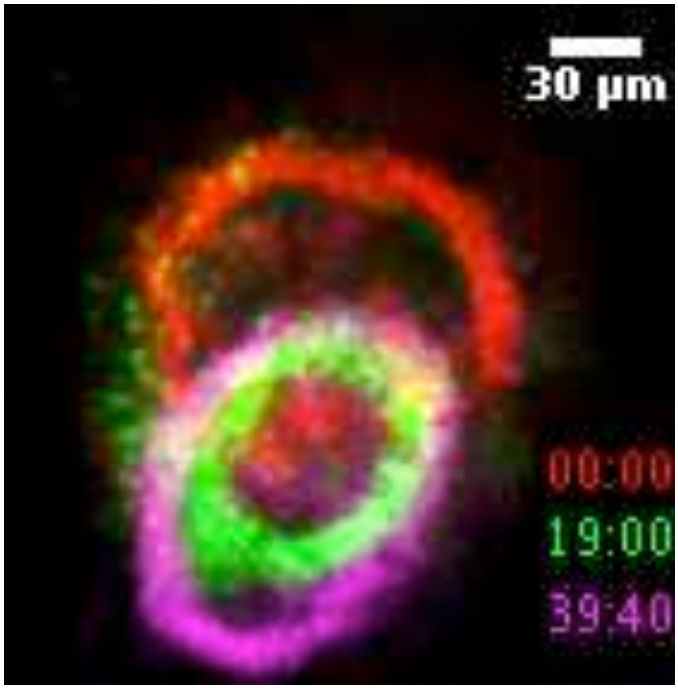

Figure 18. Merged micrographs of the actin cytoskeleton in a primary osteoclast in three time points. A murine bone marrow-derived OC expressing fluorescent LifeAct (an F-actin probe) displays evolving circular podosome patterns (either ring or SZ) during resorption of bovine bone. Between the 1st position at 0 min (red) to the 2nd position at 19 min (green), *de novo* podosome assembly sites have moved suggesting a ring-driven migration phase. Between the 2nd to the 3rd position (magenta), at 19 min and 39 min 40 sec, respectively, podosome assembly site have been partially conserved and the circular pattern has expanded. This suggests ring stabilization and transition to SZ.

Signaling in osteoclasts

Given the dynamic nature of the "OC cytoskeleton in action", its study using biophysical approaches is both intriguing and insightful. However, the increasingly acquired data demands biochemical explanations: What are the signals transmitted to the OC cytoskeleton? What are the genes and proteins that transmit them? How does the OC synchronize its cytoskeleton with its entire polarization?

Although these questions are very broad, partial answers might be provided by identifying new molecular pathways in OCs. The list of candidate genes that we have provided could serve as starting points for the identification of such pathways.

Another source of insight into OC signaling might be the characterization of the interplay between members of the Rho GTPase family in OCs. These small proteins are involved in a variety of cellular mechanisms and act as differential molecular switches in different parts of the cell in response to different intra- and extracellular stimuli.

We have provided a new molecular mechanism depicting the role of RhoE in the regulation of podosome dynamics and, subsequently, bone resorption. RhoE acts as an inhibitor of Rho kinase (Rock) and thus prevents Rock-mediated cofilin phosphorylation. Finally, non-phosphorylated cofilin ensures fast actin turnover in podosomes. Although cofilin has been confirmed as a Rock target and therefore an indirect target of RhoE, Rock has other downstream targets in OCs and differentially modulated by binding to Rho or to RhoE. In fact, while RhoE inhibits Rock, Rho promotes its. Besides Rock, Rho (A/B/C) can also act via other effectors in the OC such as mDia to regulate microtubules and podosome patterning. Another GTPase that has been shown important in OCs is Rac. Rac has been shown to be essential for OCs and to be activated by Dock5 in OCs.

These three GTPases, Rho, RhoE and Rac, are present in OCs. The functions of Rho and Rac is conveyed by their ability to catalyze GTP to GDP and can be therefore be induced or repressed in different parts of the cell. These 2 GTPases are also known for their antagonistic functions vis-à-vis one another. RhoE, on the other hand, is an atypical Rho family member, that is constitutively active. Its lack of GTPase activity allows is be continuously linked to GTP and therefore remains active, although post-translational modifications have been shown to modulate its activity. RhoE and Rho are also known to have antagonistic functions pertaining to the actin cytoskeleton, mainly through modulating Rock activity.

A more detailed molecular scheme is needed for a full understanding of the GTPases in OCs: how they are spatially and temporally expressed, activated and localized along the OC lifespan.

REFERENCES

Abe, H., Obinata, T., Minamide, L.S., and Bamburg, J.R. (1996). Xenopus laevis actin-depolymerizing factor/cofilin: a phosphorylation-regulated protein essential for development. J Cell Biol *132*, 871-885.

Abu-Amer, Y., Ross, F.P., Schlesinger, P., Tondravi, M.M., and Teitelbaum, S.L. (1997). Substrate recognition by osteoclast precursors induces C-src/microtubule association. J Cell Biol *137*, 247-258.

Aigner, E., Schmid, I., Osterreicher, C.H., Zwerina, J., Schett, G., Strasser, M., Niksic, F., Hohla, F., Ramsauer, T., Dorn, U., Patsch, W., and Datz, C. (2007). Contribution of anti-cyclic citrullinated peptide antibody and rheumatoid factor to the diagnosis of arthropathy in haemochromatosis. Ann Rheum Dis *66*, 1249-1251.

Akashi, K., Traver, D., Miyamoto, T., and Weissman, I.L. (2000). A clonogenic common myeloid progenitor that gives rise to all myeloid lineages. Nature *404*, 193-197.

Al-Shahrour, F., Minguez, P., Tarraga, J., Montaner, D., Alloza, E., Vaquerizas, J.M., Conde, L., Blaschke, C., Vera, J., and Dopazo, J. (2006). BABELOMICS: a systems biology perspective in the functional annotation of genome-scale experiments. Nucleic Acids Res *34*, W472-476.

Almeida, C.G., Yamada, A., Tenza, D., Louvard, D., Raposo, G., and Coudrier, E. (2011). Myosin 1b promotes the formation of post-Golgi carriers by regulating actin assembly and membrane remodelling at the trans-Golgi network. Nat Cell Biol *13*, 779-789.

Anderson, D.M., Maraskovsky, E., Billingsley, W.L., Dougall, W.C., Tometsko, M.E., Roux, E.R., Teepe, M.C., DuBose, R.F., Cosman, D., and Galibert, L. (1997). A homologue of the TNF receptor and its ligand enhance T-cell growth and dendritic-cell function. Nature *390*, 175-179.

Anton, I.M., Jones, G.E., Wandosell, F., Geha, R., and Ramesh, N. (2007). WASP-interacting protein (WIP): working in polymerisation and much more. Trends Cell Biol *17*, 555-562.

Arai, F., Miyamoto, T., Ohneda, O., Inada, T., Sudo, T., Brasel, K., Miyata, T., Anderson, D.M., and Suda, T. (1999). Commitment and differentiation of osteoclast precursor cells by the sequential expression of c-Fms and receptor activator of nuclear factor ŒJB (RANK) receptors. The Journal of experimental medicine *190*, 1741-1754.

Arber, S., Barbayannis, F.A., Hanser, H., Schneider, C., Stanyon, C.A., Bernard, O., and Caroni, P. (1998). Regulation of actin dynamics through phosphorylation of cofilin by LIM-kinase. Nature *393*, 805-809.

Arron, J.R., and Choi, Y. (2000). Bone versus immune system. Nature *408*, 535-536.

Ash, P., Loutit, J.F., and Townsend, K.M. (1980). Osteoclasts derived from haematopoietic stem cells. Nature *283*, 669-670.

Babb, S.G., Matsudaira, P., Sato, M., Correia, I., and Lim, S.S. (1997). Fimbrin in podosomes of monocyte-derived osteoclasts. Cell Motil Cytoskeleton *37*, 308-325.

Balemans, W., Van Wesenbeeck, L., and Van Hul, W. (2005). A clinical and molecular overview of the human osteopetroses. Calcif Tissue Int *77*, 263-274.

Banon-Rodriguez, I., Monypenny, J., Ragazzini, C., Franco, A., Calle, Y., Jones, G.E., and Anton, I.M. (2011). The cortactin-binding domain of WIP is essential for podosome formation and extracellular matrix degradation by murine dendritic cells. Eur J Cell Biol *90*, 213-223.

Barrow, A.D., Raynal, N., Andersen, T.L., Slatter, D.A., Bihan, D., Pugh, N., Cella, M., Kim, T., Rho, J., Negishi-Koga, T., Delaisse, J.M., Takayanagi, H., Lorenzo, J., Colonna, M., Farndale, R.W., Choi, Y., and Trowsdale, J. (2011). OSCAR is a collagen receptor that costimulates osteoclastogenesis in DAP12-deficient humans and mice. J Clin Invest *121*, 3505-3516.

Bartl, R. (2009). Osteoporosis : diagnosis, prevention, therapy. Springer: New York.

Bartl, R., and Frisch, B. (2004). Osteoporosis : diagnosis, prevention, therapy : a practical guide for all physicians--from pediatrics to geriatrics. Springer: Berlin ; New York.

Blangy, A., Touaitahuata, H., Cres, G., and Pawlak, G. (2012). Cofilin activation during podosome belt formation in osteoclasts. PLoS One *7*, e45909.

Boissy, P., Machuca, I., Pfaff, M., Ficheux, D., and Jurdic, P. (1998). Aggregation of mononucleated precursors triggers cell surface expression of alphavbeta3 integrin, essential to formation of osteoclast-like multinucleated cells. J Cell Sci *111 (Pt 17)*, 2563-2574.

Boyce, B.F. (2013). Advances in osteoclast biology reveal potential new drug targets and new roles for osteoclasts. Journal of Bone and Mineral Research *28*, 711-722.

Boyce, B.F., Rosenberg, E., de Papp, A.E., and Duong, L.T. (2012). The osteoclast, bone remodelling and treatment of metabolic bone disease. Eur J Clin Invest *42*, 1332-1341.

Brunner, M., Jurdic, P., Tuckerman, J.P., Block, M.R., and Bouvard, D. (2013). New insights into adhesion signaling in bone formation. Int Rev Cell Mol Biol *305*, 1-68.

Bucay, N., Sarosi, I., Dunstan, C.R., Morony, S., Tarpley, J., Capparelli, C., Scully, S., Tan, H.L., Xu, W., Lacey, D.L., Boyle, W.J., and Simonet, W.S. (1998). osteoprotegerin-deficient mice develop early onset osteoporosis and arterial calcification. Genes Dev *12*, 1260-1268.

Bucci, C., Thomsen, P., Nicoziani, P., McCarthy, J., and van Deurs, B. (2000). Rab7: a key to lysosome biogenesis. Mol Biol Cell *11*, 467-480.

Calderwood, D.A. (2004). Integrin activation. J Cell Sci *117*, 657-666.

Calle, Y., Burns, S., Thrasher, A.J., and Jones, G.E. (2006). The leukocyte podosome. Eur J Cell Biol *85*, 151-157.

Calle, Y., Chou, H.C., Thrasher, A.J., and Jones, G.E. (2004). Wiskott-Aldrich syndrome protein and the cytoskeletal dynamics of dendritic cells. J Pathol *204*, 460-469.

Chabadel, A., Banon-Rodriguez, I., Cluet, D., Rudkin, B.B., Wehrle-Haller, B., Genot, E., Jurdic, P., Anton, I.M., and Saltel, F. (2007). CD44 and beta3 integrin organize two functionally distinct actin-based domains in osteoclasts. Mol Biol Cell *18*, 4899-4910.

Chellaiah, M., Kizer, N., Silva, M., Alvarez, U., Kwiatkowski, D., and Hruska, K.A. (2000a). Gelsolin deficiency blocks podosome assembly and produces increased bone mass and strength. J Cell Biol *148*, 665-678.

Chellaiah, M.A., Biswas, R.S., Rittling, S.R., Denhardt, D.T., and Hruska, K.A. (2003). Rho-dependent Rho kinase activation increases CD44 surface expression and bone resorption in osteoclasts. J Biol Chem *278*, 29086-29097.

Chellaiah, M.A., Soga, N., Swanson, S., McAllister, S., Alvarez, U., Wang, D., Dowdy, S.F., and Hruska, K.A. (2000b). Rho-A is critical for osteoclast podosome organization, motility, and bone resorption. J Biol Chem *275*, 11993-12002.

Cougoule, C., Van Goethem, E., Le Cabec, V., Lafouresse, F., Dupre, L., Mehraj, V., Mege, J.L., Lastrucci, C., and Maridonneau-Parini, I. (2012). Blood leukocytes and macrophages of various phenotypes have distinct abilities to form podosomes and to migrate in 3D environments. Eur J Cell Biol *91*, 938-949.

Coury, F., Annels, N., Rivollier, A., Olsson, S., Santoro, A., Speziani, C., Azocar, O., Flacher, M., Djebali, S., Tebib, J., Brytting, M., Egeler, R.M., Rabourdin-Combe, C., Henter, J.I., Arico, M., and Delprat, C. (2008). Langerhans cell histiocytosis reveals a new IL-17A-dependent pathway of dendritic cell fusion. Nat Med *14*, 81-87.

Coxon, F.P., and Taylor, A. (2008a). Vesicular trafficking in osteoclasts, *19*, 424-433.

Coxon, F.P., and Taylor, A. (2008b). Vesicular trafficking in osteoclasts. Semin Cell Dev Biol *19*, 424-433.

Croke, M., Ross, F.P., Korhonen, M., Williams, D.A., Zou, W., and Teitelbaum, S.L. (2011). Rac deletion in osteoclasts causes severe osteopetrosis. J Cell Sci *124*, 3811-3821.

Crotti, T.N., Flannery, M., Walsh, N.C., Fleming, J.D., Goldring, S.R., and McHugh, K.P. (2006). NFATc1 regulation of the human beta3 integrin promoter in osteoclast differentiation. Gene *372*, 92-102.

Dai, X.M., Ryan, G.R., Hapel, A.J., Dominguez, M.G., Russell, R.G., Kapp, S., Sylvestre, V., and Stanley, E.R. (2002). Targeted disruption of the mouse colony-stimulating factor 1 receptor gene results in osteopetrosis, mononuclear phagocyte deficiency, increased primitive progenitor cell frequencies, and reproductive defects. Blood *99*, 111-120.

de la Fuente, M.A., Sasahara, Y., Calamito, M., Anton, I.M., Elkhal, A., Gallego, M.D., Suresh, K., Siminovitch, K., Ochs, H.D., Anderson, K.C., Rosen, F.S., Geha, R.S., and Ramesh, N. (2007). WIP is a chaperone for Wiskott-Aldrich syndrome protein (WASP). Proc Natl Acad Sci U S A *104*, 926-931.

DeKoter, R.P., and Singh, H. (2000). Regulation of B lymphocyte and macrophage development by graded expression of PU.1. Science *288*, 1439-1441.

Dempster, D.W., Lambing, C.L., Kostenuik, P.J., and Grauer, A. (2012). Role of RANK ligand and denosumab, a targeted RANK ligand inhibitor, in bone health and osteoporosis: a review of preclinical and clinical data. Clin Ther *34*, 521-536.

Despars, G., Pandruvada, S.N., Anginot, A., Domenget, C., Jurdic, P., and Mazzorana, M. (2013). DAP12 Overexpression Induces Osteopenia and Impaired Early Hematopoiesis. PLoS One *8*, e65297.

Destaing, O., Saltel, F., Geminard, J.C., Jurdic, P., and Bard, F. (2003). Podosomes display actin turnover and dynamic self-organization in osteoclasts expressing actin-green fluorescent protein. Mol Biol Cell *14*, 407-416.

Destaing, O., Saltel, F., Gilquin, B., Chabadel, A., Khochbin, S., Ory, S., and Jurdic, P. (2005). A novel Rho-mDia2-HDAC6 pathway controls podosome patterning through microtubule acetylation in osteoclasts. J Cell Sci *118*, 2901-2911.

Destaing, O., Sanjay, A., Itzstein, C., Horne, W.C., Toomre, D., De Camilli, P., and Baron, R. (2008). The tyrosine kinase activity of c-Src regulates actin dynamics and organization of podosomes in osteoclasts. Mol Biol Cell *19*, 394-404.

Dewhirst, F.E., Stashenko, P.P., Mole, J.E., and Tsurumachi, T. (1985). Purification and partial sequence of human osteoclast-activating factor: identity with interleukin 1 beta. J Immunol *135*, 2562-2568.

Dobbins, D.E., Joe, B., Hashiramoto, A., Salstrom, J.L., Dracheva, S., Ge, L., Wilder, R.L., and Remmers, E.F. (2002a). Localization of the mutation responsible for osteopetrosis in the op rat to a 1.5-cM genetic interval on rat chromosome 10: identification of positional candidate genes by radiation hybrid mapping. J Bone Miner Res *17*, 1761-1767.

Dobbins, D.E., Sood, R., Hashiramoto, A., Hansen, C.T., Wilder, R.L., and Remmers, E.F. (2002b). Mutation of macrophage colony stimulating factor (Csf1) causes osteopetrosis in the tl rat. Biochem Biophys Res Commun *294*, 1114-1120.

Dougall, W.C., Glaccum, M., Charrier, K., Rohrbach, K., Brasel, K., De Smedt, T., Daro, E., Smith, J., Tometsko, M.E., Maliszewski, C.R., Armstrong, A., Shen, V., Bain, S., Cosman, D., Anderson, D., Morrissey, P.J., Peschon, J.J., and Schuh, J. (1999). RANK is essential for osteoclast and lymph node development. Genes Dev *13*, 2412-2424.

Duong, L.T., Lakkakorpi, P., Nakamura, I., and Rodan, G.A. (2000). Integrins and signaling in osteoclast function. Matrix Biol *19*, 97-105.

Everts, V., Delaisse, J.M., Korper, W., Niehof, A., Vaes, G., and Beertsen, W. (1992). Degradation of collagen in the bone-resorbing compartment underlying the osteoclast involves both cysteine-proteinases and matrix metalloproteinases. J Cell Physiol *150*, 221-231.

Faccio, R., Grano, M., Colucci, S., Villa, A., Giannelli, G., Quaranta, V., and Zallone, A. (2002). Localization and possible role of two different alpha v beta 3 integrin conformations in resting and resorbing osteoclasts. Journal of cell science *115*, 2919-2929.

Faccio, R., Novack, D.V., Zallone, A., Ross, F.P., and Teitelbaum, S.L. (2003a). Dynamic changes in the osteoclast cytoskeleton in response to growth factors and cell attachment are controlled by beta3 integrin. J Cell Biol *162*, 499-509.

Faccio, R., Takeshita, S., Zallone, A., Ross, F.P., and Teitelbaum, S.L. (2003b). c-Fms and the alphavbeta3 integrin collaborate during osteoclast differentiation. J Clin Invest *111*, 749-758.

Faccio, R., Teitelbaum, S.L., Fujikawa, K., Chappel, J., Zallone, A., Tybulewicz, V.L., Ross, F.P., and Swat, W. (2005). Vav3 regulates osteoclast function and bone mass. Nat Med *11*, 284-290.

Feng, S., Deng, L., Chen, W., Shao, J., Xu, G., and Li, Y.P. (2009). Atp6v1c1 is an essential component of the osteoclast proton pump and in F-actin ring formation in osteoclasts. Biochem J *417*, 195-203.

Feng, Y., Press, B., and Wandinger-Ness, A. (1995). Rab 7: an important regulator of late endocytic membrane traffic. J Cell Biol *131*, 1435-1452.

Franzoso, G., Carlson, L., Xing, L., Poljak, L., Shores, E.W., Brown, K.D., Leonardi, A., Tran, T., Boyce, B.F., and Siebenlist, U. (1997). Requirement for NF-kappaB in osteoclast and B-cell development. Genes Dev *11*, 3482-3496.

Fuller, K., Wong, B., Fox, S., Choi, Y., and Chambers, T.J. (1998). TRANCE is necessary and sufficient for osteoblast-mediated activation of bone resorption in osteoclasts. J Exp Med *188*, 997-1001.

Gallois, A., Lachuer, J., Yvert, G., Wierinckx, A., Brunet, F., Rabourdin-Combe, C., Delprat, C., Jurdic, P., and Mazzorana, M. (2010). Genome-wide expression analyses establish dendritic cells as a new osteoclast precursor able to generate bone-resorbing cells more efficiently than monocytes. J Bone Miner Res *25*, 661-672.

Geddes, A.C. (1913). The Origin of the Osteoblast and of the Osteoclast. J Anat Physiol *47*, 159-176.

Geissmann, F. (2007). The origin of dendritic cells. Nat Immunol *8*, 558-560.

Gluckman, E., Esperou, H., Devergie, A., Traineau, R., Leverger, G., and Schaison, G. (1989). Pediatric bone marrow transplantation for leukemia and aplastic anemia. Report of 222 cases transplanted in a single center. Nouv Rev Fr Hematol *31*, 111-114.

Goodison, S., Urquidi, V., and Tarin, D. (1999). CD44 cell adhesion molecules. Mol Pathol *52*, 189-196.

Grigoriadis, A.E., Wang, Z.Q., Cecchini, M.G., Hofstetter, W., Felix, R., Fleisch, H.A., and Wagner, E.F. (1994). c-Fos: a key regulator of osteoclast-macrophage lineage determination and bone remodeling. Science *266*, 443-448.

Gruber, R., Pietschmann, P., and Peterlik, M. (2008). Introduction to Bone Development, Remodelling and Repair. In: Radiology of Osteoporosis, ed. S. Grampp: Springer Berlin Heidelberg, 1-23.

Guasch, R.M., Scambler, P., Jones, G.E., and Ridley, A.J. (1998). RhoE regulates actin cytoskeleton organization and cell migration. Mol Cell Biol *18*, 4761-4771.

Hall, A. (2012). Rho family GTPases. Biochem Soc Trans *40*, 1378-1382.

Hammarfjord, O., Falet, H., Gurniak, C., Hartwig, J.H., and Wallin, R.P. (2011). Gelsolin-independent podosome formation in dendritic cells. PLoS One *6*, e21615.

Hardy, L.R. (2012). Fluorescence recovery after photobleaching (FRAP) with a focus on F-actin. Curr Protoc Neurosci *Chapter 2*, Unit 2 17.

Harre, U., Georgess, D., Bang, H., Bozec, A., Axmann, R., Ossipova, E., Jakobsson, P.J., Baum, W., Nimmerjahn, F., Szarka, E., Sarmay, G., Krumbholz, G., Neumann, E., Toes, R., Scherer, H.U., Catrina, A.I.,

Klareskog, L., Jurdic, P., and Schett, G. (2012). Induction of osteoclastogenesis and bone loss by human autoantibodies against citrullinated vimentin. J Clin Invest *122*, 1791-1802.
Henriksen, K., Sorensen, M.G., Nielsen, R.H., Gram, J., Schaller, S., Dziegiel, M.H., Everts, V., Bollerslev, J., and Karsdal, M.A. (2006). Degradation of the organic phase of bone by osteoclasts: a secondary role for lysosomal acidification. J Bone Miner Res *21*, 58-66.
Hikita, A., Yana, I., Wakeyama, H., Nakamura, M., Kadono, Y., Oshima, Y., Nakamura, K., Seiki, M., and Tanaka, S. (2006). Negative regulation of osteoclastogenesis by ectodomain shedding of receptor activator of NF-kappaB ligand. J Biol Chem *281*, 36846-36855.
Hirvonen, M.J., Buki, K.G., Sun, Y., Mulari, M.T., Harkonen, P.L., and Vaananen, K.H. (2013). Novel interaction of Rab13 and Rab8 with endospanins. FEBS Open Bio *3*, 83-88.
Hodivala-Dilke, K.M., McHugh, K.P., Tsakiris, D.A., Rayburn, H., Crowley, D., Ullman-Cullere, M., Ross, F.P., Coller, B.S., Teitelbaum, S., and Hynes, R.O. (1999). Beta3-integrin-deficient mice are a model for Glanzmann thrombasthenia showing placental defects and reduced survival. J Clin Invest *103*, 229-238.
Hollberg, K., Marsell, R., Norgard, M., Larsson, T., Jonsson, K.B., and Andersson, G. (2008). Osteoclast polarization is not required for degradation of bone matrix in rachitic FGF23 transgenic mice. Bone *42*, 1111-1121.
Holmes, M.L., Carotta, S., Corcoran, L.M., and Nutt, S.L. (2006). Repression of Flt3 by Pax5 is crucial for B-cell lineage commitment. Genes Dev *20*, 933-938.
Horne, W.C., Neff, L., Chatterjee, D., Lomri, A., Levy, J.B., and Baron, R. (1992). Osteoclasts express high levels of pp60c-src in association with intracellular membranes. J Cell Biol *119*, 1003-1013.
Horowitz, M.C., and Lorenzo, J.A. (2007a). B lymphocytes and the skeleton. Ann N Y Acad Sci *1117*, 82-93.
Horowitz, M.C., and Lorenzo, J.A. (2007b). Immunologic regulation of bone development. Adv Exp Med Biol *602*, 47-56.
Horowitz, M.C., Xi, Y., Pflugh, D.L., Hesslein, D.G., Schatz, D.G., Lorenzo, J.A., and Bothwell, A.L. (2004). Pax5-deficient mice exhibit early onset osteopenia with increased osteoclast progenitors. J Immunol *173*, 6583-6591.
Horton, J.E., Raisz, L.G., Simmons, H.A., Oppenheim, J.J., and Mergenhagen, S.E. (1972). Bone resorbing activity in supernatant fluid from cultured human peripheral blood leukocytes. Science *177*, 793-795.
Hu, S., Biben, T., Wang, X., Jurdic, P., and Geminard, J.C. (2011a). Internal dynamics of actin structures involved in the cell motility and adhesion: Modeling of the podosomes at the molecular level. J Theor Biol *270*, 25-30.
Hu, S., Planus, E., Georgess, D., Place, C., Wang, X., Albiges-Rizo, C., Jurdic, P., and Geminard, J.C. (2011b). Podosome rings generate forces that drive saltatory osteoclast migration. Mol Biol Cell *22*, 3120-3126.
Hynes, R.O. (2002). Integrins: bidirectional, allosteric signaling machines. Cell *110*, 673-687.
Ikeda, F., Nishimura, R., Matsubara, T., Tanaka, S., Inoue, J., Reddy, S.V., Hata, K., Yamashita, K., Hiraga, T., Watanabe, T., Kukita, T., Yoshioka, K., Rao, A., and Yoneda, T. (2004). Critical roles of c-Jun signaling in regulation of NFAT family and RANKL-regulated osteoclast differentiation. J Clin Invest *114*, 475-484.
Inoue, M., Namba, N., Chappel, J., Teitelbaum, S.L., and Ross, F.P. (1998). Granulocyte macrophage-colony stimulating factor reciprocally regulates alphav-associated integrins on murine osteoclast precursors. Mol Endocrinol *12*, 1955-1962.
Ishii, M., Egen, J.G., Klauschen, F., Meier-Schellersheim, M., Saeki, Y., Vacher, J., Proia, R.L., and Germain, R.N. (2009). Sphingosine-1-phosphate mobilizes osteoclast precursors and regulates bone homeostasis. Nature *458*, 524-528.
Ito, M., Nakano, T., Erdodi, F., and Hartshorne, D.J. (2004). Myosin phosphatase: structure, regulation and function. Mol Cell Biochem *259*, 197-209.
Jacome-Galarza, C.E., Lee, S.K., Lorenzo, J.A., and Aguila, H.L. (2013). Identification, characterization, and isolation of a common progenitor for osteoclasts, macrophages, and dendritic cells from murine bone marrow and periphery. J Bone Miner Res *28*, 1203-1213.
Jockusch, B.M., and Rudiger, M. (1996). Crosstalk between cell adhesion molecules: vinculin as a paradigm for regulation by conformation. Trends Cell Biol *6*, 311-315.
Johnson, R.S., Spiegelman, B.M., and Papaioannou, V. (1992). Pleiotropic effects of a null mutation in the c-fos proto-oncogene. Cell *71*, 577-586.
Jordens, I., Fernandez-Borja, M., Marsman, M., Dusseljee, S., Janssen, L., Calafat, J., Janssen, H., Wubbolts, R., and Neefjes, J. (2001). The Rab7 effector protein RILP controls lysosomal transport by inducing the recruitment of dynein-dynactin motors. Curr Biol *11*, 1680-1685.
Jotereau, F.V., and Le Douarin, N.M. (1978). The development relationship between osteocytes and osteoclasts: a study using the quail-chick nuclear marker in endochondral ossification. Dev Biol *63*, 253-265.
Jurdic, P., Saltel, F., Chabadel, A., and Destaing, O. (2006). Podosome and sealing zone: specificity of the osteoclast model. Eur J Cell Biol *85*, 195-202.

Kahn, A.J., and Simmons, D.J. (1975). Investigation of cell lineage in bone using a chimaera of chick and quial embryonic tissue. Nature *258*, 325-327.
Kahn, A.J., Stewart, C.C., and Teitelbaum, S.L. (1978). Contact-mediated bone resorption by human monocytes in vitro. Science *199*, 988-990.
Kaverina, I., Stradal, T.E., and Gimona, M. (2003). Podosome formation in cultured A7r5 vascular smooth muscle cells requires Arp2/3-dependent de-novo actin polymerization at discrete microdomains. J Cell Sci *116*, 4915-4924.
Khurana, J.S. (2009). Bone pathology. Humana Press: Dordrecht ; New York.
Kim, G.S., Koh, J.M., Chang, J.S., Park, B.L., Kim, L.H., Park, E.K., Kim, S.Y., and Shin, H.D. (2005a). Association of the OSCAR promoter polymorphism with BMD in postmenopausal women. J Bone Miner Res *20*, 1342-1348.
Kim, M.S., Day, C.J., and Morrison, N.A. (2005b). MCP-1 is induced by receptor activator of nuclear factor-{kappa}B ligand, promotes human osteoclast fusion, and rescues granulocyte macrophage colony-stimulating factor suppression of osteoclast formation. J Biol Chem *280*, 16163-16169.
Kim, M.S., Day, C.J., Selinger, C.I., Magno, C.L., Stephens, S.R., and Morrison, N.A. (2006). MCP-1-induced human osteoclast-like cells are tartrate-resistant acid phosphatase, NFATc1, and calcitonin receptor-positive but require receptor activator of NFkappaB ligand for bone resorption. J Biol Chem *281*, 1274-1285.
Kim, N., Takami, M., Rho, J., Josien, R., and Choi, Y. (2002). A novel member of the leukocyte receptor complex regulates osteoclast differentiation. The Journal of experimental medicine *195*, 201-209.
Kinley, A.W., Weed, S.A., Weaver, A.M., Karginov, A.V., Bissonette, E., Cooper, J.A., and Parsons, J.T. (2003). Cortactin interacts with WIP in regulating Arp2/3 activation and membrane protrusion. Curr Biol *13*, 384-393.
Klein, R.M., and Aplin, A.E. (2009). Rnd3 regulation of the actin cytoskeleton promotes melanoma migration and invasive outgrowth in three dimensions. Cancer Res *69*, 2224-2233.
Kobayashi, K., Takahashi, N., Jimi, E., Udagawa, N., Takami, M., Kotake, S., Nakagawa, N., Kinosaki, M., Yamaguchi, K., Shima, N., Yasuda, H., Morinaga, T., Higashio, K., Martin, T.J., and Suda, T. (2000). Tumor necrosis factor alpha stimulates osteoclast differentiation by a mechanism independent of the ODF/RANKL-RANK interaction. J Exp Med *191*, 275-286.
Kodama, H., Yamasaki, A., Nose, M., Niida, S., Ohgame, Y., Abe, M., Kumegawa, M., and Suda, T. (1991). Congenital osteoclast deficiency in osteopetrotic (op/op) mice is cured by injections of macrophage colony-stimulating factor. J Exp Med *173*, 269-272.
Koga, T., Inui, M., Inoue, K., Kim, S., Suematsu, A., Kobayashi, E., Iwata, T., Ohnishi, H., Matozaki, T., Kodama, T., Taniguchi, T., Takayanagi, H., and Takai, T. (2004). Costimulatory signals mediated by the ITAM motif cooperate with RANKL for bone homeostasis. Nature *428*, 758-763.
Komander, D., Garg, R., Wan, P.T., Ridley, A.J., and Barford, D. (2008). Mechanism of multi-site phosphorylation from a ROCK-I:RhoE complex structure. EMBO J *27*, 3175-3185.
Komatsu, N., and Takayanagi, H. (2012a). Autoimmune arthritis: the interface between the immune system and joints. Adv Immunol *115*, 45-71.
Komatsu, N., and Takayanagi, H. (2012b). Inflammation and bone destruction in arthritis: synergistic activity of immune and mesenchymal cells in joints. Front Immunol *3*, 77.
Kong, Y.Y., Yoshida, H., Sarosi, I., Tan, H.L., Timms, E., Capparelli, C., Morony, S., Oliveira-dos-Santos, A.J., Van, G., Itie, A., Khoo, W., Wakeham, A., Dunstan, C.R., Lacey, D.L., Mak, T.W., Boyle, W.J., and Penninger, J.M. (1999). OPGL is a key regulator of osteoclastogenesis, lymphocyte development and lymph-node organogenesis. Nature *397*, 315-323.
Konig, A., Muhlbauer, R.C., and Fleisch, H. (1988). Tumor necrosis factor alpha and interleukin-1 stimulate bone resorption in vivo as measured by urinary [3H]tetracycline excretion from prelabeled mice. J Bone Miner Res *3*, 621-627.
Kotani, M., Kikuta, J., Klauschen, F., Chino, T., Kobayashi, Y., Yasuda, H., Tamai, K., Miyawaki, A., Kanagawa, O., Tomura, M., and Ishii, M. (2013). Systemic circulation and bone recruitment of osteoclast precursors tracked by using fluorescent imaging techniques. J Immunol *190*, 605-612.
Krzewski, K., Chen, X., Orange, J.S., and Strominger, J.L. (2006). Formation of a WIP-, WASp-, actin-, and myosin IIA-containing multiprotein complex in activated NK cells and its alteration by KIR inhibitory signaling. J Cell Biol *173*, 121-132.
Kuna, A.T. (2012). Mutated citrullinated vimentin antibodies in rheumatoid arthritis. Clin Chim Acta *413*, 66-73.
Kwan Tat, S., Padrines, M., Theoleyre, S., Heymann, D., and Fortun, Y. (2004). IL-6, RANKL, TNF-alpha/IL-1: interrelations in bone resorption pathophysiology. Cytokine Growth Factor Rev *15*, 49-60.
Labernadie, A., Thibault, C., Vieu, C., Maridonneau-Parini, I., and Charriere, G.M. (2010). Dynamics of podosome stiffness revealed by atomic force microscopy. Proc Natl Acad Sci U S A *107*, 21016-21021.

Lacey, D.L., Timms, E., Tan, H.L., Kelley, M.J., Dunstan, C.R., Burgess, T., Elliott, R., Colombero, A., Elliott, G., Scully, S., Hsu, H., Sullivan, J., Hawkins, N., Davy, E., Capparelli, C., Eli, A., Qian, Y.X., Kaufman, S., Sarosi, I., Shalhoub, V., Senaldi, G., Guo, J., Delaney, J., and Boyle, W.J. (1998). Osteoprotegerin ligand is a cytokine that regulates osteoclast differentiation and activation. Cell *93*, 165-176.

Lakkakorpi, J.T., and Rajaniemi, H.J. (1991). Application of the immunofluorescence technique and confocal laser scanning microscopy for studying the distribution of the luteinizing hormone/chorionic gonadotropin (LH/CG) receptor on rat luteal cells. J Histochem Cytochem *39*, 397-400.

Lane, N.E., Yao, W., Nakamura, M.C., Humphrey, M.B., Kimmel, D., Huang, X., Sheppard, D., Ross, F.P., and Teitelbaum, S.L. (2005). Mice lacking the integrin beta5 subunit have accelerated osteoclast maturation and increased activity in the estrogen-deficient state. J Bone Miner Res *20*, 58-66.

Lappalainen, P., and Drubin, D.G. (1997). Cofilin promotes rapid actin filament turnover in vivo. Nature *388*, 78-82.

Leah, E. (2012). Rheumatoid arthritis. Linking ACPA to bone loss in rheumatoid arthritis. Nat Rev Rheumatol *8*, 308.

Lee, S.H., Rho, J., Jeong, D., Sul, J.Y., Kim, T., Kim, N., Kang, J.S., Miyamoto, T., Suda, T., Lee, S.K., Pignolo, R.J., Koczon-Jaremko, B., Lorenzo, J., and Choi, Y. (2006). v-ATPase V0 subunit d2-deficient mice exhibit impaired osteoclast fusion and increased bone formation. Nat Med *12*, 1403-1409.

Li, P., Schwarz, E.M., O'Keefe, R.J., Ma, L., Boyce, B.F., and Xing, L. (2004). RANK signaling is not required for TNFalpha-mediated increase in CD11(hi) osteoclast precursors but is essential for mature osteoclast formation in TNFalpha-mediated inflammatory arthritis. J Bone Miner Res *19*, 207-213.

Linder, S. (2007). The matrix corroded: podosomes and invadopodia in extracellular matrix degradation. Trends in Cell Biology *17*, 107-117.

Linder, S., and Aepfelbacher, M. (2003). Podosomes: adhesion hot-spots of invasive cells. Trends in Cell Biology *13*, 376-385.

Linder, S., Hufner, K., Wintergerst, U., and Aepfelbacher, M. (2000). Microtubule-dependent formation of podosomal adhesion structures in primary human macrophages. J Cell Sci *113 Pt 23*, 4165-4176.

Linder, S., and Kopp, P. (2005). Podosomes at a glance. Journal of Cell Science *118*, 2079-2082.

Linder, S., Nelson, D., Weiss, M., and Aepfelbacher, M. (1999). Wiskott-Aldrich syndrome protein regulates podosomes in primary human macrophages. Proc Natl Acad Sci U S A *96*, 9648-9653.

Linder, S., Wiesner, C., and Himmel, M. (2011a). Degrading devices: invadosomes in proteolytic cell invasion. Annu Rev Cell Dev Biol *27*, 185-211.

Linder, S., Wiesner, C., and Himmel, M. (2011b). Degrading devices: invadosomes in proteolytic cell invasion. Annual review of cell and developmental biology *27*, 185-211.

Ljusberg, J., Wang, Y., Lang, P., Norgard, M., Dodds, R., Hultenby, K., Ek-Rylander, B., and Andersson, G. (2005). Proteolytic excision of a repressive loop domain in tartrate-resistant acid phosphatase by cathepsin K in osteoclasts. J Biol Chem *280*, 28370-28381.

Lomaga, M.A., Yeh, W.C., Sarosi, I., Duncan, G.S., Furlonger, C., Ho, A., Morony, S., Capparelli, C., Van, G., Kaufman, S., van der Heiden, A., Itie, A., Wakeham, A., Khoo, W., Sasaki, T., Cao, Z., Penninger, J.M., Paige, C.J., Lacey, D.L., Dunstan, C.R., Boyle, W.J., Goeddel, D.V., and Mak, T.W. (1999). TRAF6 deficiency results in osteopetrosis and defective interleukin-1, CD40, and LPS signaling. Genes Dev *13*, 1015-1024.

Lowell, C.A., and Soriano, P. (1996). Knockouts of Src-family kinases: stiff bones, wimpy T cells, and bad memories. Genes Dev *10*, 1845-1857.

Luchin, A., Purdom, G., Murphy, K., Clark, M.Y., Angel, N., Cassady, A.I., Hume, D.A., and Ostrowski, M.C. (2000). The microphthalmia transcription factor regulates expression of the tartrate-resistant acid phosphatase gene during terminal differentiation of osteoclasts. J Bone Miner Res *15*, 451-460.

Luxenburg, C., Addadi, L., and Geiger, B. (2006a). The molecular dynamics of osteoclast adhesions. European Journal of Cell Biology *85*, 203-211.

Luxenburg, C., Geblinger, D., Klein, E., Anderson, K., Hanein, D., Geiger, B., and Addadi, L. (2007). The architecture of the adhesive apparatus of cultured osteoclasts: from podosome formation to sealing zone assembly. PLoS One *2*, e179.

Luxenburg, C., Parsons, J.T., Addadi, L., and Geiger, B. (2006b). Involvement of the Src-cortactin pathway in podosome formation and turnover during polarization of cultured osteoclasts. Journal of Cell Science *119*, 4878-4888.

Luxenburg, C., Parsons, J.T., Addadi, L., and Geiger, B. (2006c). Involvement of the Src-cortactin pathway in podosome formation and turnover during polarization of cultured osteoclasts. J Cell Sci *119*, 4878-4888.

Luxenburg, C., Winograd-Katz, S., Addadi, L., and Geiger, B. (2012a). Involvement of actin polymerization in podosome dynamics. J Cell Sci.

Luxenburg, C., Winograd-Katz, S., Addadi, L., and Geiger, B. (2012b). Involvement of actin polymerization in podosome dynamics. Journal of Cell Science *125*, 1666-1672.

MacDonald, B.R., Mundy, G.R., Clark, S., Wang, E.A., Kuehl, T.J., Stanley, E.R., and Roodman, G.D. (1986). Effects of human recombinant CSF-GM and highly purified CSF-1 on the formation of multinucleated cells with osteoclast characteristics in long-term bone marrow cultures. J Bone Miner Res *1*, 227-233.

Maekawa, M., Ishizaki, T., Boku, S., Watanabe, N., Fujita, A., Iwamatsu, A., Obinata, T., Ohashi, K., Mizuno, K., and Narumiya, S. (1999). Signaling from Rho to the actin cytoskeleton through protein kinases ROCK and LIM-kinase. Science *285*, 895-898.

Mansky, K.C., Marfatia, K., Purdom, G.H., Luchin, A., Hume, D.A., and Ostrowski, M.C. (2002a). The microphthalmia transcription factor (MITF) contains two N-terminal domains required for transactivation of osteoclast target promoters and rescue of mi mutant osteoclasts. J Leukoc Biol *71*, 295-303.

Mansky, K.C., Sulzbacher, S., Purdom, G., Nelsen, L., Hume, D.A., Rehli, M., and Ostrowski, M.C. (2002b). The microphthalmia transcription factor and the related helix-loop-helix zipper factors TFE-3 and TFE-C collaborate to activate the tartrate-resistant acid phosphatase promoter. J Leukoc Biol *71*, 304-310.

Marchisio, P.C., Cirillo, D., Naldini, L., Primavera, M.V., Teti, A., and Zambonin-Zallone, A. (1984). Cell-substratum interaction of cultured avian osteoclasts is mediated by specific adhesion structures. J Cell Biol *99*, 1696-1705.

Marie, P.J., and Kassem, M. (2011). Osteoblasts in osteoporosis: past, emerging, and future anabolic targets. Eur J Endocrinol *165*, 1-10.

Martinez-Quiles, N., Ho, H.Y., Kirschner, M.W., Ramesh, N., and Geha, R.S. (2004). Erk/Src phosphorylation of cortactin acts as a switch on-switch off mechanism that controls its ability to activate N-WASP. Mol Cell Biol *24*, 5269-5280.

Matsumoto, M., Kogawa, M., Wada, S., Takayanagi, H., Tsujimoto, M., Katayama, S., Hisatake, K., and Nogi, Y. (2004). Essential role of p38 mitogen-activated protein kinase in cathepsin K gene expression during osteoclastogenesis through association of NFATc1 and PU.1. J Biol Chem *279*, 45969-45979.

Matsuo, K., Galson, D.L., Zhao, C., Peng, L., Laplace, C., Wang, K.Z., Bachler, M.A., Amano, H., Aburatani, H., Ishikawa, H., and Wagner, E.F. (2004). Nuclear factor of activated T-cells (NFAT) rescues osteoclastogenesis in precursors lacking c-Fos. J Biol Chem *279*, 26475-26480.

Matsuo, K., and Ray, N. (2004). Osteoclasts, mononuclear phagocytes, and c-Fos: new insight into osteoimmunology. Keio J Med *53*, 78-84.

Matsuzaki, K., Udagawa, N., Takahashi, N., Yamaguchi, K., Yasuda, H., Shima, N., Morinaga, T., Toyama, Y., Yabe, Y., Higashio, K., and Suda, T. (1998). Osteoclast differentiation factor (ODF) induces osteoclast-like cell formation in human peripheral blood mononuclear cell cultures. Biochem Biophys Res Commun *246*, 199-204.

McHugh, K.P., Hodivala-Dilke, K., Zheng, M.H., Namba, N., Lam, J., Novack, D., Feng, X., Ross, F.P., Hynes, R.O., and Teitelbaum, S.L. (2000). Mice lacking beta3 integrins are osteosclerotic because of dysfunctional osteoclasts. J Clin Invest *105*, 433-440.

McInnes, I.B., and Schett, G. (2011). The pathogenesis of rheumatoid arthritis. N Engl J Med *365*, 2205-2219.

Meddens, M.B., Rieger, B., Figdor, C.G., Cambi, A., and van den Dries, K. (2013). Automated podosome identification and characterization in fluorescence microscopy images. Microsc Microanal *19*, 180-189.

Mersich, A.T., Miller, M.R., Chkourko, H., and Blystone, S.D. (2010). The formin FRL1 (FMNL1) is an essential component of macrophage podosomes. Cytoskeleton (Hoboken) *67*, 573-585.

Mizuno, A., Amizuka, N., Irie, K., Murakami, A., Fujise, N., Kanno, T., Sato, Y., Nakagawa, N., Yasuda, H., Mochizuki, S., Gomibuchi, T., Yano, K., Shima, N., Washida, N., Tsuda, E., Morinaga, T., Higashio, K., and Ozawa, H. (1998). Severe osteoporosis in mice lacking osteoclastogenesis inhibitory factor/osteoprotegerin. Biochem Biophys Res Commun *247*, 610-615.

Mochizuki, A., Takami, M., Miyamoto, Y., Nakamaki, T., Tomoyasu, S., Kadono, Y., Tanaka, S., Inoue, T., and Kamijo, R. (2012). Cell Adhesion Signaling Regulates RANK Expression in Osteoclast Precursors. PLoS One *7*.

Mocholi, E., Ballester-Lurbe, B., Arque, G., Poch, E., Peris, B., Guerri, C., Dierssen, M., Guasch, R.M., Terrado, J., and Perez-Roger, I. (2011). RhoE deficiency produces postnatal lethality, profound motor deficits and neurodevelopmental delay in mice. PLoS One *6*, e19236.

Monypenny, J., Chou, H.C., Banon-Rodriguez, I., Thrasher, A.J., Anton, I.M., Jones, G.E., and Calle, Y. (2011). Role of WASP in cell polarity and podosome dynamics of myeloid cells. Eur J Cell Biol *90*, 198-204.

Moreau, V., Tatin, F., Varon, C., and Genot, E. (2003). Actin can reorganize into podosomes in aortic endothelial cells, a process controlled by Cdc42 and RhoA. Mol Cell Biol *23*, 6809-6822.

Mori, K., Berreur, M., Blanchard, F., Chevalier, C., Guisle-Marsollier, I., Masson, M., Redini, F., and Heymann, D. (2007). Receptor activator of nuclear factor-kappaB ligand (RANKL) directly modulates the gene expression profile of RANK-positive Saos-2 human osteosarcoma cells. Oncol Rep *18*, 1365-1371.

Motyckova, G., Weilbaecher, K.N., Horstmann, M., Rieman, D.J., Fisher, D.Z., and Fisher, D.E. (2001). Linking osteopetrosis and pycnodysostosis: regulation of cathepsin K expression by the microphthalmia transcription factor family. Proc Natl Acad Sci U S A *98*, 5798-5803.

Mulari, M., Vaaraniemi, J., and Vaananen, H.K. (2003a). Intracellular membrane trafficking in bone resorbing osteoclasts. Microsc Res Tech *61*, 496-503.
Mulari, M.T., Zhao, H., Lakkakorpi, P.T., and Vaananen, H.K. (2003b). Osteoclast ruffled border has distinct subdomains for secretion and degraded matrix uptake. Traffic *4*, 113-125.
Mundy, C.R., Altman, A.J., Gondek, M.D., and Bandelin, J.G. (1977). Direct resorption of bone by human monocytes. Science *196*, 1109-1111.
Mundy, G.R., Raisz, L.G., Cooper, R.A., Schechter, G.P., and Salmon, S.E. (1974). Evidence for the secretion of an osteoclast stimulating factor in myeloma. N Engl J Med *291*, 1041-1046.
Muto, A., Mizoguchi, T., Udagawa, N., Ito, S., Kawahara, I., Abiko, Y., Arai, A., Harada, S., Kobayashi, Y., Nakamichi, Y., Penninger, J.M., Noguchi, T., and Takahashi, N. (2011). Lineage-committed osteoclast precursors circulate in blood and settle down into bone. J Bone Miner Res *26*, 2978-2990.
Nakashima, T., and Takayanagi, H. (2011a). New regulation mechanisms of osteoclast differentiation. Ann N Y Acad Sci *1240*, E13-18.
Nakashima, T., and Takayanagi, H. (2011b). New regulation mechanisms of osteoclast differentiation. Ann N Y Acad Sci *1240*, E13-18.
Negi, S.S., and Olson, M.O. (2006). Effects of interphase and mitotic phosphorylation on the mobility and location of nucleolar protein B23. J Cell Sci *119*, 3676-3685.
Negishi-Koga, T., and Takayanagi, H. (2009). Ca2+-NFATc1 signaling is an essential axis of osteoclast differentiation. Immunol Rev *231*, 241-256.
Nesbitt, S., Nesbit, A., Helfrich, M., and Horton, M. (1993). Biochemical characterization of human osteoclast integrins. Osteoclasts express alpha v beta 3, alpha 2 beta 1, and alpha v beta 1 integrins. J Biol Chem *268*, 16737-16745.
Nishikawa, K., Nakashima, T., Hayashi, M., Fukunaga, T., Kato, S., Kodama, T., Takahashi, S., Calame, K., and Takayanagi, H. (2010). Blimp1-mediated repression of negative regulators is required for osteoclast differentiation. Proc Natl Acad Sci U S A *107*, 3117-3122.
Novack, D.V., and Faccio, R. (2011). Osteoclast motility: putting the brakes on bone resorption. Ageing Res Rev *10*, 54-61.
Nutt, S.L., Heavey, B., Rolink, A.G., and Busslinger, M. (1999). Commitment to the B-lymphoid lineage depends on the transcription factor Pax5. Nature *401*, 556-562.
O'Brien, C.A., Nakashima, T., and Takayanagi, H. (2013). Osteocyte control of osteoclastogenesis. Bone *54*, 258-263.
Oikawa, T., Oyama, M., Kozuka-Hata, H., Uehara, S., Udagawa, N., Saya, H., and Matsuo, K. (2012). Tks5-dependent formation of circumferential podosomes/invadopodia mediates cell-cell fusion. J Cell Biol *197*, 553-568.
Ojakian, G.K., Ratcliffe, D.R., and Schwimmer, R. (2001). Integrin regulation of cell-cell adhesion during epithelial tubule formation. J Cell Sci *114*, 941-952.
Okamoto, K., and Takayanagi, H. (2011a). Osteoclasts in arthritis and Th17 cell development. Int Immunopharmacol *11*, 543-548.
Okamoto, K., and Takayanagi, H. (2011b). Regulation of bone by the adaptive immune system in arthritis. Arthritis Res Ther *13*, 219.
Olsson Akefeldt, S., Maisse, C., Belot, A., Mazzorana, M., Salvatore, G., Bissay, N., Jurdic, P., Arico, M., Rabourdin-Combe, C., Henter, J.I., and Delprat, C. (2013). Chemoresistance of human monocyte-derived dendritic cells is regulated by IL-17A. PLoS One *8*, e56865.
Ory, S., Brazier, H., Pawlak, G., and Blangy, A. (2008a). Rho GTPases in osteoclasts: orchestrators of podosome arrangement. Eur J Cell Biol *87*, 469-477.
Ory, S., Munari-Silem, Y., Fort, P., and Jurdic, P. (2000). Rho and Rac exert antagonistic functions on spreading of macrophage-derived multinucleated cells and are not required for actin fiber formation. J Cell Sci *113 (Pt 7)*, 1177-1188.
Ory, S.p., Brazier, H.l.n., Pawlak, G.r., and Blangy, A. (2008b). Rho GTPases in osteoclasts: orchestrators of podosome arrangement. European journal of cell biology *87*, 469-477.
Pap, T., Claus, A., Ohtsu, S., Hummel, K.M., Schwartz, P., Drynda, S., Pap, G., Machner, A., Stein, B., George, M., Gay, R.E., Neumann, W., Gay, S., and Aicher, W.K. (2003). Osteoclast-independent bone resorption by fibroblast-like cells. Arthritis Res Ther *5*, R163-173.
Papagrigoriou, E., Gingras, A.R., Barsukov, I.L., Bate, N., Fillingham, I.J., Patel, B., Frank, R., Ziegler, W.H., Roberts, G.C., Critchley, D.R., and Emsley, J. (2004). Activation of a vinculin-binding site in the talin rod involves rearrangement of a five-helix bundle. EMBO J *23*, 2942-2951.
Paradise, R.K., Lauffenburger, D.A., and Van Vliet, K.J. (2011). Acidic extracellular pH promotes activation of integrin alpha(v)beta(3). PLoS One *6*, e15746.

Pettit, A.R., Ji, H., von Stechow, D., Muller, R., Goldring, S.R., Choi, Y., Benoist, C., and Gravallese, E.M. (2001). TRANCE/RANKL knockout mice are protected from bone erosion in a serum transfer model of arthritis. Am J Pathol *159*, 1689-1699.

Rao, H., Lu, G., Kajiya, H., Garcia-Palacios, V., Kurihara, N., Anderson, J., Patrene, K., Sheppard, D., Blair, H.C., Windle, J.J., Choi, S.J., and Roodman, G.D. (2006). Alpha9beta1: a novel osteoclast integrin that regulates osteoclast formation and function. J Bone Miner Res *21*, 1657-1665.

Razzouk, S., Lieberherr, M.l., and Cournot, G. (1999). Rac-GTPase, osteoclast cytoskeleton and bone resorption. European journal of cell biology *78*, 249-255.

Ressad, F., Didry, D., Xia, G.X., Hong, Y., Chua, N.H., Pantaloni, D., and Carlier, M.F. (1998). Kinetic analysis of the interaction of actin-depolymerizing factor (ADF)/cofilin with G- and F-actins. Comparison of plant and human ADFs and effect of phosphorylation. J Biol Chem *273*, 20894-20902.

Riento, K., Guasch, R.M., Garg, R., Jin, B., and Ridley, A.J. (2003). RhoE binds to ROCK I and inhibits downstream signaling. Mol Cell Biol *23*, 4219-4229.

Riento, K., Villalonga, P., Garg, R., and Ridley, A. (2005). Function and regulation of RhoE. Biochem Soc Trans *33*, 649-651.

Ritchlin, C.T., Haas-Smith, S.A., Li, P., Hicks, D.G., and Schwarz, E.M. (2003). Mechanisms of TNF-alpha- and RANKL-mediated osteoclastogenesis and bone resorption in psoriatic arthritis. J Clin Invest *111*, 821-831.

Rivollier, A., Mazzorana, M., Tebib, J., Piperno, M., Aitsiselmi, T., Rabourdin-Combe, C., Jurdic, P., and Servet-Delprat, C. (2004). Immature dendritic cell transdifferentiation into osteoclasts: a novel pathway sustained by the rheumatoid arthritis microenvironment. Blood *104*, 4029-4037.

Roodman, G.D. (1999). Cell biology of the osteoclast. Exp Hematol *27*, 1229-1241.

Ross, F.P. (2006). M-CSF, c-Fms, and signaling in osteoclasts and their precursors. Ann N Y Acad Sci *1068*, 110-116.

Sabokbar, A., Crawford, R., Murray, D.W., and Athanasou, N.A. (2000). Macrophage-osteoclast differentiation and bone resorption in osteoarthrotic subchondral acetabular cysts. Acta Orthop Scand *71*, 255-261.

Salo, J., Lehenkari, P., Mulari, M., Metsikko, K., and Vaananen, H.K. (1997). Removal of osteoclast bone resorption products by transcytosis. Science *276*, 270-273.

Salo, J., Metsikko, K., Palokangas, H., Lehenkari, P., and Vaananen, H.K. (1996). Bone-resorbing osteoclasts reveal a dynamic division of basal plasma membrane into two different domains. J Cell Sci *109 (Pt 2)*, 301-307.

Saltel, F., Chabadel, A., Bonnelye, E., and Jurdic, P. (2008). Actin cytoskeletal organisation in osteoclasts: a model to decipher transmigration and matrix degradation. Eur J Cell Biol *87*, 459-468.

Saltel, F., Chabadel, A., Zhao, Y., Lafage-Proust, M.H., Clezardin, P., Jurdic, P., and Bonnelye, E. (2006). Transmigration: a new property of mature multinucleated osteoclasts. J Bone Miner Res *21*, 1913-1923.

Saltel, F., Destaing, O., Bard, F., Eichert, D., and Jurdic, P. (2004). Apatite-mediated actin dynamics in resorbing osteoclasts. Mol Biol Cell *15*, 5231-5241.

Sanchez-Fernandez, M.A., Gallois, A., Riedl, T., Jurdic, P., and Hoflack, B. (2008). Osteoclasts control osteoblast chemotaxis via PDGF-BB/PDGF receptor beta signaling. PLoS One *3*, e3537.

Schett, G. (2012). Synovitis--an inflammation of joints destroying the bone. Swiss Med Wkly *142*, w13692.

Schett, G., and Gravallese, E. (2012). Bone erosion in rheumatoid arthritis: mechanisms, diagnosis and treatment. Nat Rev Rheumatol *8*, 656-664.

Schmidt, S., Nakchbandi, I., Ruppert, R., Kawelke, N., Hess, M.W., Pfaller, K., Jurdic, P., Fassler, R., and Moser, M. (2011). Kindlin-3-mediated signaling from multiple integrin classes is required for osteoclast-mediated bone resorption. J Cell Biol *192*, 883-897.

Servet-Delprat, C., Arnaud, S., Jurdic, P., Nataf, S., Grasset, M.F., Soulas, C., Domenget, C., Destaing, O., Rivollier, A., Perret, M., Dumontel, C., Hanau, D., Gilmore, G.L., Belin, M.F., Rabourdin-Combe, C., and Mouchiroud, G. (2002). Flt3+ macrophage precursors commit sequentially to osteoclasts, dendritic cells and microglia. BMC Immunol *3*, 15.

Shibutani, T., Iwanaga, H., Imai, K., Kitago, M., Doi, Y., and Iwayama, Y. (2000). Use of glass slides coated with apatite-collagen complexes for measurement of osteoclastic resorption activity. J Biomed Mater Res *50*, 153-159.

Simonet, W.S., Lacey, D.L., Dunstan, C.R., Kelley, M., Chang, M.S., Luthy, R., Nguyen, H.Q., Wooden, S., Bennett, L., Boone, T., Shimamoto, G., DeRose, M., Elliott, R., Colombero, A., Tan, H.L., Trail, G., Sullivan, J., Davy, E., Bucay, N., Renshaw-Gegg, L., Hughes, T.M., Hill, D., Pattison, W., Campbell, P., Sander, S., Van, G., Tarpley, J., Derby, P., Lee, R., and Boyle, W.J. (1997). Osteoprotegerin: a novel secreted protein involved in the regulation of bone density. Cell *89*, 309-319.

Soriano, P., Montgomery, C., Geske, R., and Bradley, A. (1991). Targeted disruption of the c-src proto-oncogene leads to osteopetrosis in mice. Cell *64*, 693-702.

Souabni, A., Cobaleda, C., Schebesta, M., and Busslinger, M. (2002). Pax5 promotes B lymphopoiesis and blocks T cell development by repressing Notch1. Immunity *17*, 781-793.

Southwick, F.S. (2000). Gelsolin and ADF/cofilin enhance the actin dynamics of motile cells. Proc Natl Acad Sci U S A *97*, 6936-6938.
Speziani, C., Rivollier, A., Gallois, A., Coury, F., Mazzorana, M., Azocar, O., Flacher, M., Bella, C., Tebib, J., Jurdic, P., Rabourdin-Combe, C., and Delprat, C. (2007). Murine dendritic cell transdifferentiation into osteoclasts is differentially regulated by innate and adaptive cytokines. Eur J Immunol *37*, 747-757.
Stenbeck, G. (2002). Formation and function of the ruffled border in osteoclasts. Semin Cell Dev Biol *13*, 285-292.
Steven, F. (1961). Starch gel electrophoresis of hen egg white, oviduct white, yolk, ova and serum proteins. Nature *192*, 972.
Susa, M., Luong-Nguyen, N.H., Cappellen, D., Zamurovic, N., and Gamse, R. (2004). Human primary osteoclasts: in vitro generation and applications as pharmacological and clinical assay. J Transl Med *2*, 6.
Tagaya, H., Kunisada, T., Yamazaki, H., Yamane, T., Tokuhisa, T., Wagner, E.F., Sudo, T., Shultz, L.D., and Hayashi, S.I. (2000). Intramedullary and extramedullary B lymphopoiesis in osteopetrotic mice. Blood *95*, 3363-3370.
Takagi, J., Petre, B.M., Walz, T., and Springer, T.A. (2002). Global conformational rearrangements in integrin extracellular domains in outside-in and inside-out signaling. Cell *110*, 599-511.
Takayanagi, H. (2007). The role of NFAT in osteoclast formation. Ann N Y Acad Sci *1116*, 227-237.
Takayanagi, H. (2009). Osteoimmunology and the effects of the immune system on bone. Nat Rev Rheumatol *5*, 667-676.
Takayanagi, H., Kim, S., Koga, T., Nishina, H., Isshiki, M., Yoshida, H., Saiura, A., Isobe, M., Yokochi, T., Inoue, J., Wagner, E.F., Mak, T.W., Kodama, T., and Taniguchi, T. (2002a). Induction and activation of the transcription factor NFATc1 (NFAT2) integrate RANKL signaling in terminal differentiation of osteoclasts. Dev Cell *3*, 889-901.
Takayanagi, H., Kim, S., Matsuo, K., Suzuki, H., Suzuki, T., Sato, K., Yokochi, T., Oda, H., Nakamura, K., Ida, N., Wagner, E.F., and Taniguchi, T. (2002b). RANKL maintains bone homeostasis through c-Fos-dependent induction of interferon-beta. Nature *416*, 744-749.
Takayanagi, H., Ogasawara, K., Hida, S., Chiba, T., Murata, S., Sato, K., Takaoka, A., Yokochi, T., Oda, H., Tanaka, K., Nakamura, K., and Taniguchi, T. (2000). T-cell-mediated regulation of osteoclastogenesis by signalling cross-talk between RANKL and IFN-gamma. Nature *408*, 600-605.
Tanaka, S., Takahashi, N., Udagawa, N., Tamura, T., Akatsu, T., Stanley, E.R., Kurokawa, T., and Suda, T. (1993). Macrophage colony-stimulating factor is indispensable for both proliferation and differentiation of osteoclast progenitors. J Clin Invest *91*, 257-263.
Teitelbaum, S.L. (2007). Osteoclasts: what do they do and how do they do it? Am J Pathol *170*, 427-435.
Tezuka, K., Takeshita, S., Hakeda, Y., Kumegawa, M., Kikuno, R., and Hashimoto-Gotoh, T. (1990). Isolation of mouse and human cDNA clones encoding a protein expressed specifically in osteoblasts and brain tissues. Biochem Biophys Res Commun *173*, 246-251.
Thomson, B.M., Mundy, G.R., and Chambers, T.J. (1987). Tumor necrosis factors alpha and beta induce osteoblastic cells to stimulate osteoclastic bone resorption. J Immunol *138*, 775-779.
Tondravi, M.M., McKercher, S.R., Anderson, K., Erdmann, J.M., Quiroz, M., Maki, R., and Teitelbaum, S.L. (1997). Osteopetrosis in mice lacking haematopoietic transcription factor PU.1. Nature *386*, 81-84.
Touaitahuata, H., Planus, E., Albiges-Rizo, C., Blangy, A., and Pawlak, G. (2013). Podosomes are dispensable for osteoclast differentiation and migration. Eur J Cell Biol *92*, 139-149.
Tsuji-Takechi, K., Negishi-Koga, T., Sumiya, E., Kukita, A., Kato, S., Maeda, T., Pandolfi, P.P., Moriyama, K., and Takayanagi, H. (2012). Stage-specific functions of leukemia/lymphoma-related factor (LRF) in the transcriptional control of osteoclast development. Proc Natl Acad Sci U S A *109*, 2561-2566.
Turner, C.E., Glenney, J.R., Jr., and Burridge, K. (1990). Paxillin: a new vinculin-binding protein present in focal adhesions. J Cell Biol *111*, 1059-1068.
Vaaraniemi, J., Halleen, J.M., Kaarlonen, K., Ylipahkala, H., Alatalo, S.L., Andersson, G., Kaija, H., Vihko, P., and Vaananen, H.K. (2004). Intracellular machinery for matrix degradation in bone-resorbing osteoclasts. J Bone Miner Res *19*, 1432-1440.
van den Dries, K., Meddens, M.B., de Keijzer, S., Shekhar, S., Subramaniam, V., Figdor, C.G., and Cambi, A. (2013a). Interplay between myosin IIA-mediated contractility and actin network integrity orchestrates podosome composition and oscillations. Nat Commun *4*, 1412.
van den Dries, K., Meddens, M.B.M., de Keijzer, S., Shekhar, S., Subramaniam, V., Figdor, C.G., and Cambi, A. (2013b). Interplay between myosin IIA-mediated contractility and actin network integrity orchestrates podosome composition and oscillations. Nature communications *4*.
van den Dries, K., Schwartz, S.L., Byars, J., Meddens, M.B., Bolomini-Vittori, M., Lidke, D.S., Figdor, C.G., Lidke, K.A., and Cambi, A. (2013c). Dual color super-resolution microscopy reveals nanoscale organization of mechanosensory podosomes. Mol Biol Cell.

Van Goethem, E., Guiet, R., Balor, S., Charriere, G.M., Poincloux, R., Labrousse, A., Maridonneau-Parini, I., and Le Cabec, V. (2011). Macrophage podosomes go 3D. Eur J Cell Biol *90*, 224-236.
Van Goethem, E., Poincloux, R., Gauffre, F., Maridonneau-Parini, I., and Le Cabec, V. (2010). Matrix architecture dictates three-dimensional migration modes of human macrophages: differential involvement of proteases and podosome-like structures. J Immunol *184*, 1049-1061.
Vega, F.M., and Ridley, A.J. (2008). Rho GTPases in cancer cell biology. FEBS Lett *582*, 2093-2101.
Vernejoul, M.-C.d., and Marie, P. (2008). Trait√© des maladies m√©taboliques osseuses de l'adulte. Flammarion m√©decine-sciences: Paris.
Verollet, C., Gallois, A., Dacquin, R., Lastrucci, C., Pandruvada, S.N., Ortega, N., Poincloux, R., Behar, A., Cougoule, C., Lowell, C., Al Saati, T., Jurdic, P., and Maridonneau-Parini, I. (2013). Hck contributes to bone homeostasis by controlling the recruitment of osteoclast precursors. FASEB J.
Vignery, A. (2005). [Macrophage fusion: are somatic and cancer cells possible partners?]. Med Sci (Paris) *21*, 1070-1075.
Vives, V., Laurin, M., Cres, G., Larrousse, P., Morichaud, Z., Noel, D., Cote, J.F., and Blangy, A. (2011a). The Rac1 exchange factor Dock5 is essential for bone resorption by osteoclasts. J Bone Miner Res *26*, 1099-1110.
Vives, V., Laurin, M.l., Cres, G., Larrousse, P., Morichaud, Z., Noel, D.l., C√¥t√©, J.-F.c., and Blangy, A. (2011b). The Rac1 exchange factor Dock5 is essential for bone resorption by osteoclasts. Journal of Bone and Mineral Research *26*, 1099-1110.
Walker, D.G. (1975). Bone resorption restored in osteopetrotic mice by transplants of normal bone marrow and spleen cells. Science *190*, 784-785.
Wang, Y., Lebowitz, D., Sun, C., Thang, H., Grynpas, M.D., and Glogauer, M. (2008). Identifying the relative contributions of Rac1 and Rac2 to osteoclastogenesis. J Bone Miner Res *23*, 260-270.
Wang, Z.Q., Ovitt, C., Grigoriadis, A.E., Mohle-Steinlein, U., Ruther, U., and Wagner, E.F. (1992). Bone and haematopoietic defects in mice lacking c-fos. Nature *360*, 741-745.
Wanger, M., Keiser, T., Neuhaus, J.M., and Wegner, A. (1985). The actin treadmill. Can J Biochem Cell Biol *63*, 414-421.
Wei, S., Kitaura, H., Zhou, P., Ross, F.P., and Teitelbaum, S.L. (2005). IL-1 mediates TNF-induced osteoclastogenesis. J Clin Invest *115*, 282-290.
Weir, E.C., Lowik, C.W., Paliwal, I., and Insogna, K.L. (1996). Colony stimulating factor-1 plays a role in osteoclast formation and function in bone resorption induced by parathyroid hormone and parathyroid hormone-related protein. J Bone Miner Res *11*, 1474-1481.
Weiss, A., Baumgartner, M., Radziwill, G., Dennler, J., and Moelling, K. (2007). c-Src is a PDZ interaction partner and substrate of the E3 ubiquitin ligase Ligand-of-Numb protein X1. FEBS Lett *581*, 5131-5136.
Weisswange, I., Newsome, T.P., Schleich, S., and Way, M. (2009). The rate of N-WASP exchange limits the extent of ARP2/3-complex-dependent actin-based motility. Nature *458*, 87-91.
Wiktor-Jedrzejczak, W., Bartocci, A., Ferrante, A.W., Jr., Ahmed-Ansari, A., Sell, K.W., Pollard, J.W., and Stanley, E.R. (1990). Total absence of colony-stimulating factor 1 in the macrophage-deficient osteopetrotic (op/op) mouse. Proc Natl Acad Sci U S A *87*, 4828-4832.
Winkler, J., Lunsdorf, H., and Jockusch, B.M. (1997). Energy-filtered electron microscopy reveals that talin is a highly flexible protein composed of a series of globular domains. Eur J Biochem *243*, 430-436.
Witten, P.E., and Huysseune, A. (2009). A comparative view on mechanisms and functions of skeletal remodelling in teleost fish, with special emphasis on osteoclasts and their function. Biol Rev Camb Philos Soc *84*, 315-346.
Wong, B.R., Rho, J., Arron, J., Robinson, E., Orlinick, J., Chao, M., Kalachikov, S., Cayani, E., Bartlett, F.S., 3rd, Frankel, W.N., Lee, S.Y., and Choi, Y. (1997). TRANCE is a novel ligand of the tumor necrosis factor receptor family that activates c-Jun N-terminal kinase in T cells. J Biol Chem *272*, 25190-25194.
Wu, H., and Parsons, J.T. (1993). Cortactin, an 80/85-kilodalton pp60src substrate, is a filamentous actin-binding protein enriched in the cell cortex. J Cell Biol *120*, 1417-1426.
Xing, L., Schwarz, E.M., and Boyce, B.F. (2005a). Osteoclast precursors, RANKL/RANK, and immunology. Immunol Rev *208*, 19-29.
Xing, L.P., Schwarz, E.M., and Boyce, B.F. (2005b). Osteoclast precursors, RANKL/RANK, and immunology. Immunological Reviews *208*, 19-29.
Xiong, J., Onal, M., Jilka, R.L., Weinstein, R.S., Manolagas, S.C., and O'Brien, C.A. (2011). Matrix-embedded cells control osteoclast formation. Nat Med *17*, 1235-1241.
Xiong, J.P., Stehle, T., Diefenbach, B., Zhang, R., Dunker, R., Scott, D.L., Joachimiak, A., Goodman, S.L., and Arnaout, M.A. (2001). Crystal structure of the extracellular segment of integrin alpha Vbeta3. Science *294*, 339-345.

Xiong, J.P., Stehle, T., Zhang, R., Joachimiak, A., Frech, M., Goodman, S.L., and Arnaout, M.A. (2002). Crystal structure of the extracellular segment of integrin alpha Vbeta3 in complex with an Arg-Gly-Asp ligand. Science *296*, 151-155.

Yadav, V.K., Oury, F., Tanaka, K.F., Thomas, T., Wang, Y., Cremers, S., Hen, R., Krust, A., Chambon, P., and Karsenty, G. (2011). Leptin-dependent serotonin control of appetite: temporal specificity, transcriptional regulation, and therapeutic implications. J Exp Med *208*, 41-52.

Yamashita, T., Yao, Z., Li, F., Zhang, Q., Badell, I.R., Schwarz, E.M., Takeshita, S., Wagner, E.F., Noda, M., Matsuo, K., Xing, L., and Boyce, B.F. (2007a). NF-kappaB p50 and p52 regulate receptor activator of NF-kappaB ligand (RANKL) and tumor necrosis factor-induced osteoclast precursor differentiation by activating c-Fos and NFATc1. J Biol Chem *282*, 18245-18253.

Yamashita, T., Yao, Z.Q., Li, F., Zhang, Q., Badell, I.R., Schwarz, E.M., Takeshita, S., Wagner, E.F., Noda, M., Matsuo, K., Xing, L.P., and Boyce, B.F. (2007b). NF-kappa B p50 and p52 regulate receptor activator of NF-kappa B ligand (RANKL) and tumor necrosis factor-induced osteoclast precursor differentiation by activating c-Fos and NFATc1. Journal of Biological Chemistry *282*, 18245-18253.

Yasuda, H., Shima, N., Nakagawa, N., Yamaguchi, K., Kinosaki, M., Mochizuki, S., Tomoyasu, A., Yano, K., Goto, M., Murakami, A., Tsuda, E., Morinaga, T., Higashio, K., Udagawa, N., Takahashi, N., and Suda, T. (1998). Osteoclast differentiation factor is a ligand for osteoprotegerin/osteoclastogenesis-inhibitory factor and is identical to TRANCE/RANKL. Proc Natl Acad Sci U S A *95*, 3597-3602.

Yavropoulou, M.P., and Yovos, J.G. (2008). Osteoclastogenesis--current knowledge and future perspectives. J Musculoskelet Neuronal Interact *8*, 204-216.

Yin, H.L., Albrecht, J.H., and Fattoum, A. (1981). Identification of gelsolin, a Ca2+-dependent regulatory protein of actin gel-sol transformation, and its intracellular distribution in a variety of cells and tissues. J Cell Biol *91*, 901-906.

Yoon, K.A., Cho, H.S., Shin, H.I., and Cho, J.Y. (2012). Differential regulation of CXCL5 by FGF2 in osteoblastic and endothelial niche cells supports hematopoietic stem cell migration. Stem Cells Dev *21*, 3391-3402.

Yoshida, H., Hayashi, S., Kunisada, T., Ogawa, M., Nishikawa, S., Okamura, H., Sudo, T., and Shultz, L.D. (1990). The murine mutation osteopetrosis is in the coding region of the macrophage colony stimulating factor gene. Nature *345*, 442-444.

Yu, X., Collin-Osdoby, P., and Osdoby, P. (2003). SDF-1 increases recruitment of osteoclast precursors by upregulation of matrix metalloproteinase-9 activity. Connect Tissue Res *44 Suppl 1*, 79-84.

Zaidi, M., Troen, B., Moonga, B.S., and Abe, E. (2001). Cathepsin K, osteoclastic resorption, and osteoporosis therapy. J Bone Miner Res *16*, 1747-1749.

Zallone, A.Z., Teti, A., Primavera, M.V., Naldini, L., and Marchisio, P.C. (1983). Osteoclasts and monocytes have similar cytoskeletal structures and adhesion property in vitro. J Anat *137 (Pt 1)*, 57-70.

Zhang, D., Udagawa, N., Nakamura, I., Murakami, H., Saito, S., Yamasaki, K., Shibasaki, Y., Morii, N., Narumiya, S., and Takahashi, N. (1995). The small GTP-binding protein, rho p21, is involved in bone resorption by regulating cytoskeletal organization in osteoclasts. Journal of cell science *108*, 2285-2292.

Zhao, B., and Ivashkiv, L.B. (2011). Negative regulation of osteoclastogenesis and bone resorption by cytokines and transcriptional repressors. Arthritis Res Ther *13*, 234.

Zhao, H., Liu, S., Huang, D., Xu, Q., Shuto, T., and Iwamoto, Y. (2006). The protective effects of incadronate on inflammation and joint destruction in established rat adjuvant arthritis. Rheumatol Int *26*, 732-740.

Zhao, H., and Vaananen, H.K. (2006). Pharmacological sequestration of intracellular cholesterol in late endosomes disrupts ruffled border formation in osteoclasts. J Bone Miner Res *21*, 456-465.

Zou, W., Izawa, T., Zhu, T., Chappel, J., Otero, K., Monkley, S.J., Critchley, D.R., Petrich, B.G., Morozov, A., and Ginsberg, M.H. (2013). Talin1 and Rap1 are Critical for Osteoclast Function. Molecular and cellular biology *33*, 830-844.

Zou, W., Kitaura, H., Reeve, J., Long, F., Tybulewicz, V.L., Shattil, S.J., Ginsberg, M.H., Ross, F.P., and Teitelbaum, S.L. (2007). Syk, c-Src, the alphavbeta3 integrin, and ITAM immunoreceptors, in concert, regulate osteoclastic bone resorption. J Cell Biol *176*, 877-888.

Zou, W., and Teitelbaum, S.L. (2010). Integrins, growth factors, and the osteoclast cytoskeleton. Ann N Y Acad Sci *1192*, 27-31.

Zukauskas, A., Merley, A., Li, D., Ang, L.H., Sciuto, T.E., Salman, S., Dvorak, A.M., Dvorak, H.F., and Jaminet, S.C. (2011). TM4SF1: a tetraspanin-like protein necessary for nanopodia formation and endothelial cell migration. Angiogenesis *14*, 345-354.

ANNEX PUBLICATION

Research article

Induction of osteoclastogenesis and bone loss by human autoantibodies against citrullinated vimentin

Ulrike Harre,[1] Dan Georgess,[2] Holger Bang,[3] Aline Bozec,[1] Roland Axmann,[1] Elena Ossipova,[4] Per-Johan Jakobsson,[4] Wolfgang Baum,[1] Falk Nimmerjahn,[5] Eszter Szarka,[6] Gabriella Sarmay,[6] Grit Krumbholz,[7] Elena Neumann,[7] Rene Toes,[8] Hans-Ulrich Scherer,[8] Anca Irinel Catrina,[3] Lars Klareskog,[3] Pierre Jurdic,[2] and Georg Schett[1]

[1]Department of Internal Medicine 3, University of Erlangen-Nuremberg, Erlangen, Germany. [2]Institut de Génomique Fonctionnelle de Lyon, Université de Lyon, and CNRS, Ecole Normale Superieure de Lyon, Lyon, France. [3]Orgentec Diagnostika, Mainz, Germany. [4]Rheumatology Unit, Department of Medicine, Karolinska Institute and Karolinska University Hospital, Stockholm, Sweden. [5]Department of Genetics, University of Erlangen-Nuremberg, Erlangen, Germany. [6]Department of Immunology, Eotvos Lorand University, Budapest, Hungary. [7]Department of Rheumatology, University of Giessen, Bad Nauheim, Germany. [8]Department of Rheumatology, Leiden University Medical Center, Leiden, Netherlands.

Autoimmunity is complicated by bone loss. In human rheumatoid arthritis (RA), the most severe inflammatory joint disease, autoantibodies against citrullinated proteins are among the strongest risk factors for bone destruction. We therefore hypothesized that these autoantibodies directly influence bone metabolism. Here, we found a strong and specific association between autoantibodies against citrullinated proteins and serum markers for osteoclast-mediated bone resorption in RA patients. Moreover, human osteoclasts expressed enzymes eliciting protein citrullination, and specific N-terminal citrullination of vimentin was induced during osteoclast differentiation. Affinity-purified human autoantibodies against mutated citrullinated vimentin (MCV) not only bound to osteoclast surfaces, but also led to robust induction of osteoclastogenesis and bone-resorptive activity. Adoptive transfer of purified human MCV autoantibodies into mice induced osteopenia and increased osteoclastogenesis. This effect was based on the inducible release of TNF-α from osteoclast precursors and the subsequent increase of osteoclast precursor cell numbers with enhanced expression of activation and growth factor receptors. Our data thus suggest that autoantibody formation in response to citrullinated vimentin directly induces bone loss, providing a link between the adaptive immune system and bone.

Introduction

RA affects about 1% of the population worldwide and is one of the most destructive diseases in humans (1, 2). Current concepts suggest that RA emerges by complex gene-environment interactions involving HLA and other genes, as well as in response to environmental factors (3, 4). Smoking, for instance, elicits cellular responses, such as posttranslational modification of proteins; among these, citrullination is considered a key stress response of cells to noxious stimuli. Citrullination is achieved by a group of enzymes called peptidylarginine deiminases (PADs), which metabolize the amino acid arginine into citrulline (5). Smoking induces citrullination of the bronchial epithelium. In addition, bacteria involved in periodontitis, such as *Porphyromonas gingivalis*, also strongly induce protein citrullination (3, 6). Interestingly, more than 70% of patients with RA show a breach in tolerance for citrullinated proteins eliciting an anti–citrullinated protein antibody (ACPA) response (7, 8). This ACPA response is highly specific for RA and not found in other forms of autoimmune disease. The formation of ACPAs is closely related to certain HLA genotypes, like the shared epitope and environmental factors (such as smoking). Interestingly, ACPAs emerge years before the onset of clinically overt RA, which suggests that autoimmunity precedes inflammation in RA (9).

Authorship note: Ulrike Harre and Dan Georgess contributed equally to this work.
Conflict of interest: Holger Bang is an employee of Orgentec Diagnostika.
Citation for this article: *J Clin Invest* doi:10.1172/JCI60975.

It has always been stunning how effectively RA destroys bone. If the inflammatory disease process is not treated early and effectively, then bone erosions emerge after a few months of disease and lead to the destruction of the entire joint (10). Moreover, osteoporosis emerges fast in RA and affects even patients with early disease, leading to an increased fracture risk later on. Inflammation appears to be a key risk factor for bone loss in RA. Surrogate markers for high inflammatory disease activity, such as high C-reactive protein levels, are predictive for local and systemic bone loss (11). The negative influence of inflammation on bone reflects the tight interactions between the immune system and the skeleton, which have recently lead to a new research field termed *osteoimmunology* (12). Apart from inflammatory disease burden, however, the strongest risk factor for bone loss is the presence of ACPAs. Several studies have shown that ACPAs are among the strongest predictors for bone-erosive disease in RA, strongly suggesting a direct link between autoantibody response in RA and the ability of the disease to elicit structural bone damage (13–16). We therefore hypothesized that the main autoantibody response in RA, namely that of ACPAs, directly influences bone homeostasis. As bone resorption is considered to be among the leading mechanisms of bone loss in RA, we studied whether ACPAs influence bone resorption.

Results

ACPAs are associated with increased bone resorption in patients with RA. Given that the presence of ACPAs in RA patients is associated with bone loss and our hypothesis that ACPAs themselves can precipitate bone loss by influencing bone metabolism, we first sought to

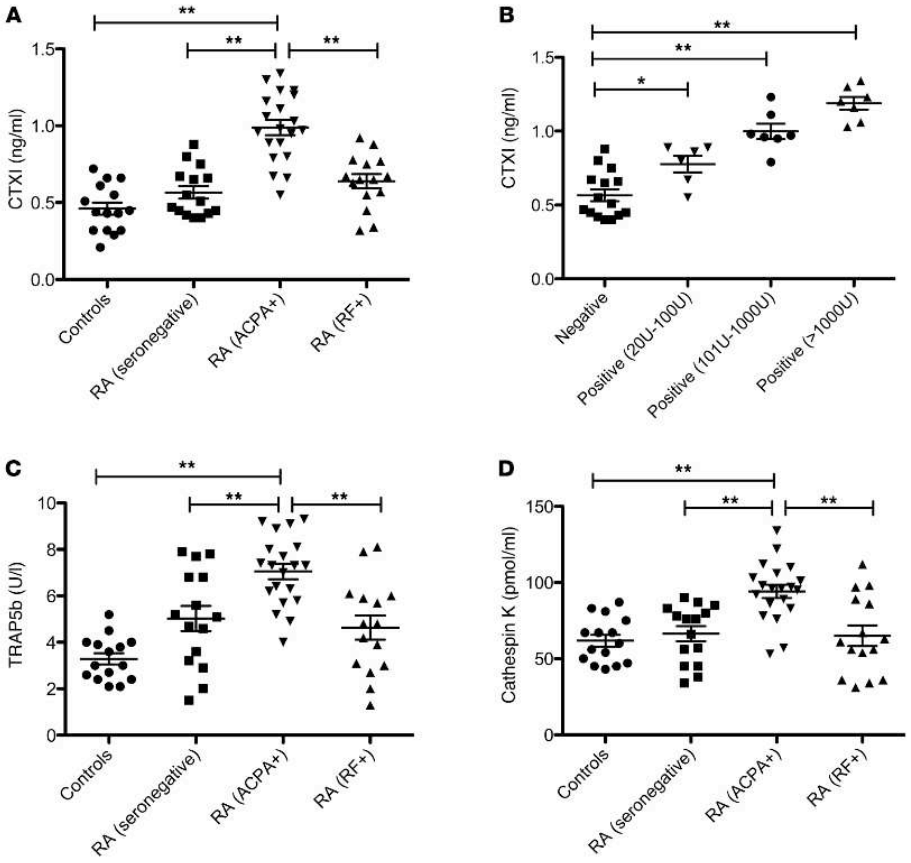

Figure 1
ACPAs are linked to high bone resorption in humans. Serum samples obtained from healthy controls as well as patients with RA without ACPAs or with positivity for rheumatoid factor (RF) or ACPAs were investigated for the bone resorption parameters CTXI (**A** and **B**), TRAP5b (**C**), and cathepsin K (**D**). In **B**, different ACPA responses are shown (expressed in units). $^{*}P < 0.05$; $^{**}P < 0.01$.

determine whether the presence of ACPAs in RA patients is linked to altered bone metabolism. We investigated serum samples from RA patients with ACPAs for markers of bone resorption and bone formation and compared the results with those of RA patients without ACPAs as well as normal controls. To minimize bias, we focused on newly diagnosed RA patients without concomitant treatment of glucocorticoids or other immunosuppressants. We also carefully matched the groups (ACPA-positive/rheumatoid factor–negative RA, ACPA-negative/rheumatoid factor–positive RA, ACPA-negative/rheumatoid factor–negative RA, and healthy controls) for age and sex as well as for disease activity and disease duration. When analyzing C-terminal cleavage products for collagen type I (CTXI) as a marker of bone resorption, we found significantly higher CTXI in ACPA-positive patients than in all other groups ($P < 0.01$; Figure 1A). The influence of ACPA on bone resorption in RA patients was even more evident when ACPA titers were correlated with CTXI levels. Even patients with low ACPA levels (<200 U/ml) had higher CTXI than did RA patients without ACPA (Figure 1B). Moreover, CTXI level was related to ACPA titer, as patients with modest and high ACPA levels showed a dose-dependent increase of bone resorption (Figure 1B). Similar results were observed with other markers of bone resorption, such as the serum level of the osteoclast-derived enzymes tartrate-resistant acid phosphatase 5b (TRAP5b) and cathepsin K: RA patients with ACPA showed significantly higher levels of these markers (Figure 1, C and D). In contrast, bone formation, which was measured by bone alkaline phosphatase, was the same among RA patients with or without ACPA, with levels tending toward lower than those of healthy controls. These data support the notion that the presence of ACPA is associated with bone loss in RA.

Isolation of ACPAs with specificity to mutated citrullinated vimentin from human RA patients. We consequently sought to determine the mechanism by which ACPAs are linked to enhanced bone resorption, hypothesizing that these autoantibodies directly stimulate the differentiation of bone-resorbing cells. To test this concept, we first had to exactly define the ACPA responses in human RA patients that are strongly linked to bone resorption. We therefore affinity-purified ACPAs from 3 individual RA patients with very high ACPA responses (>1,000 U) and high levels of bone resorp-

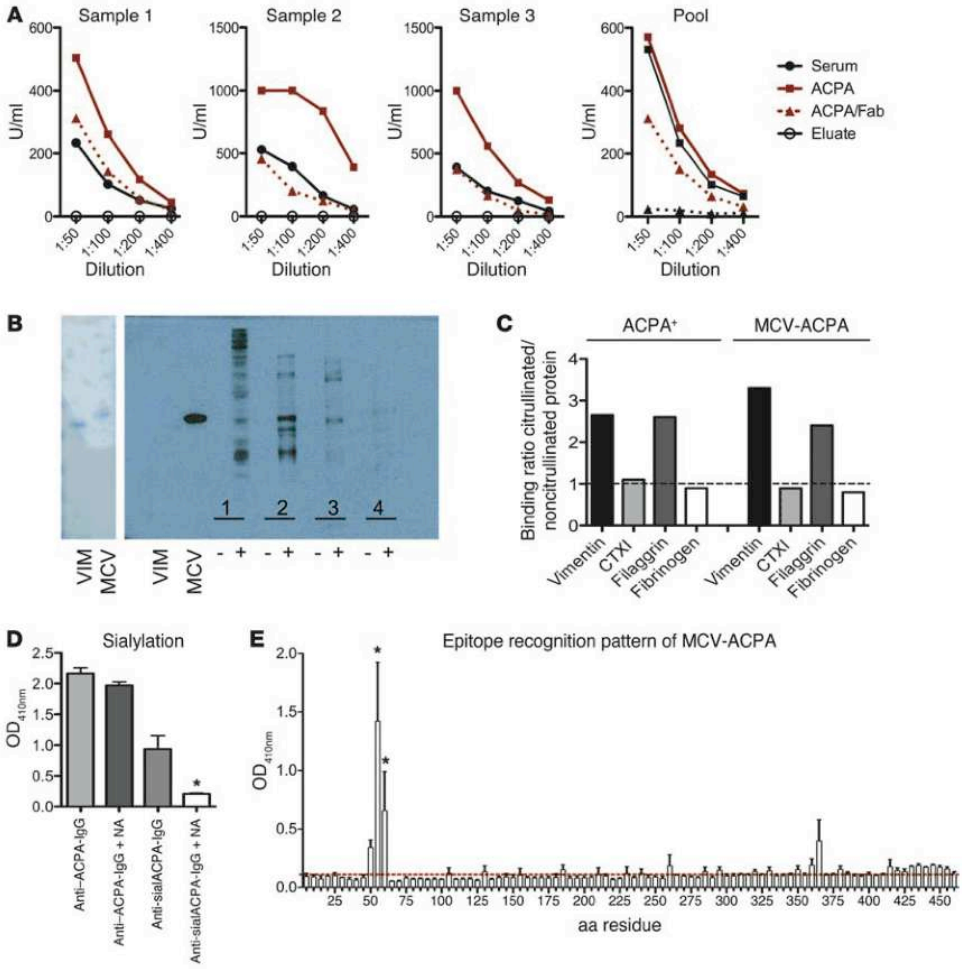

Figure 2

Isolation of ACPAs from human serum. (**A**) ACPA reactivity of the original serum from RA patients, purified ACPAs, the corresponding Fab fragment (ACPA/Fab), and the remaining eluated IgG fraction (eluate) for 3 individual serum samples as well as the pooled samples. Dotted curves in the graph of the pooled sample indicate detection with an Fc- specific antibody, with loss of reactivity of the Fab fraction confirming its purity. (**B**) Coomassie gel and Western blot of HeLa cells showing the binding of purified antibodies against vimentin (VIM), MCV, and cytosolic (1), membrane (2), nuclear (3) and actin-containing cytoskeletal (4) cell factions before (–) and after (+) treatment with PAD. (**C**) ELISA showing reactivity of ACPAs and MCV-ACPAs against noncitrullinated and citrullinated peptides of vimentin, fibrinogen, and CTXI. *y* axis shows the binding ratio with specificity to citrullinated peptides giving values higher than 1 (dotted line). (**D**) Sialylation of MCV-ACPAs was analyzed by assessing the S2 glycoform (anti-sial ACPA) by ELISA before and after neuraminidase (NA) treatment. (**E**) Epitope reaction pattern of MCV-ACPAs was analyzed by assessing binding to 25-mer peptides spanning the entire sequence of citrullinated vimentin. OD_{410nm}, OD at a wavelength of 410 nm. $^*P < 0.05$.

tion. We decided to isolate human ACPAs with specificity to mutated citrullinated vimentin (MCV), as these autoantibodies are highly specific for RA (17, 18), and vimentin is expressed by mononuclear cells and osteoclasts (19). By using a CNBr-sepharose column loaded with MCV, we were able to purify ACPAs and retain — and even enrich — their strong reactivity to MCV (Figure 2A). Moreover, we also cleaved the affinity-purified ACPAs with pepsin to receive F(ab′)2 fragments, which also retained high reactivity against MCV but lacked the Fc portion (Figure 2A).

Western blot analysis of the isolated affinity-purified human ACPAs against MCV (referred to herein as MCV-ACPAs) on naive and PAD-treated HeLa cells showed exclusive specificity to citrullinated vimentin, but not to noncitrullinated vimentin, after PAD treatment (Figure 2B). When analyzing binding to citrullinated and noncitrullinated protein extracts from different subcellular compartments, we observed that MCV-ACPAs particularly bound to the membrane fraction and, to a lesser extent, to the nuclear and cytosolic fractions, but exhibited virtually no binding to the

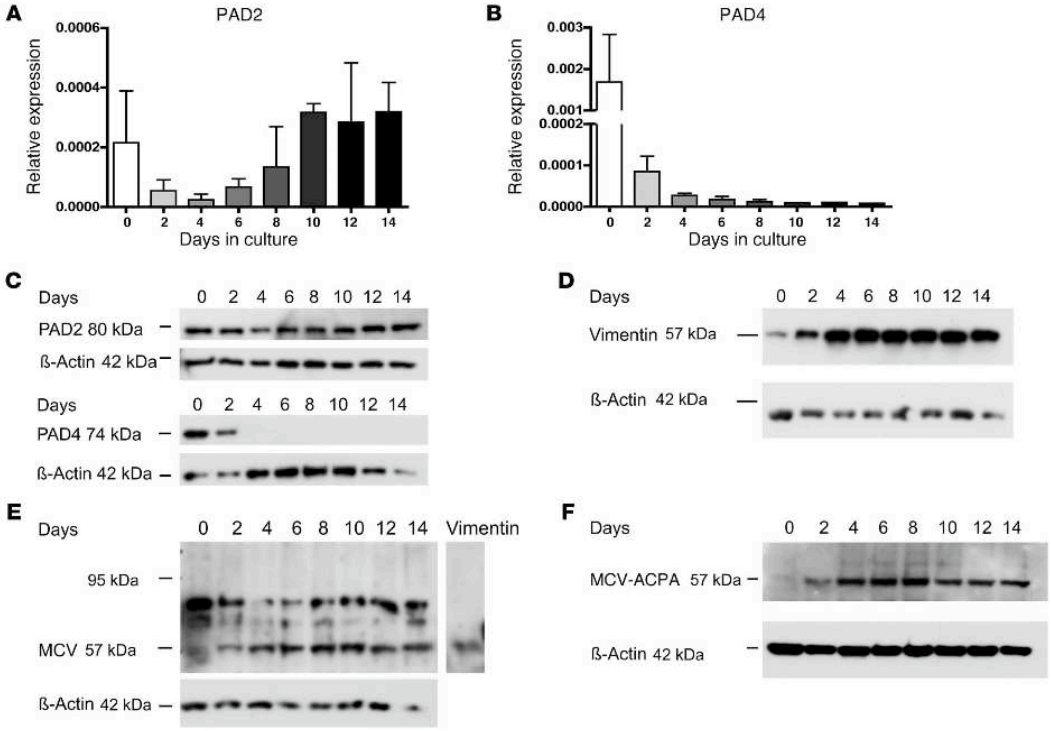

Figure 3

Expression of PAD enzyme and citrullinated vimentin in osteoclasts. (**A** and **B**) Real-time PCR for PAD2 (**A**) and PAD4 (**B**) of human osteoclast precursor cells stimulated with MCSF and RANKL to achieve osteoclast differentiation. (**C**) Western blotting showing protein expression of PAD4 and PAD2 at various stages of osteoclast differentiation. (**D**) Western blotting showing protein expression of vimentin at various stages of osteoclast differentiation (**E** and **F**) Western blotting showing MCV expression using a chicken antibody against citrullinated vimentin (**E**; recombinant vimentin used as positive control) and MCV-ACPAs (**F**). For control purposes, staining for β-actin was performed. Representative blots from 3 independent experiments are shown.

actin-containing cytoskeletal compartment (Figure 2B). Moreover, MCV-ACPAs not only showed specificity to peptides from citrullinated vimentin, in contrast to peptides from noncitrullinated vimentin, but also did not recognize citrullinated peptides from other proteins, like CTXI and fibrinogen (Figure 2C) as well as GFAP and neurofascin (data not shown). The cross-reaction of MCV-ACPAs was only observed with citrullinated peptides of the epithelial protein fillagrin.

Analysis of the presence of sugar moieties by enzyme-linked lectin assay showed glycosylation of MCV-ACPAs, which was sensitive to neuraminidase digestion (Figure 2D). Analysis of the epitope recognition pattern of isolated MCV-ACPAs by testing binding to a peptide library spanning the entire citrullinated vimentin protein revealed a dominant N-terminal epitope at amino acid position 56–77 (Figure 2E).

Osteoclasts express enzymes involved in citrullination and show citrullination of vimentin. We next validated the expression of the target of MCV-ACPA in the osteoclast lineage. Citrullination of proteins depends on the presence of the enzyme PAD, which metabolizes arginine into citrullin. Among the different PAD enzymes, only PAD2 and PAD4 were expressed in the monocyte lineage and were also found in osteoclast precursor cells at the mRNA and protein levels (Figure 3, A–C). Whereas PAD4 expression decreased with further differentiation of osteoclast precursors into osteoclasts, PAD2 expression increased during this process (Figure 3C). Furthermore, vimentin expression increased during osteoclast differentiation (Figure 3D). When using a commercially available antibody against citrullinated vimentin or MCV-ACPAs, we observed that expression of citrullinated vimentin also increased during osteoclast differentiation (Figure 3, E and F), which suggests that the target for MCV-ACPAs is indeed inducibly expressed in the osteoclast lineage. These data suggested strong binding of MCV-ACPAs to cells of the osteoclast lineage, particularly to cells in more advanced osteoclastogenic differentiation state with increased citrullination of vimentin.

Finally, these data were validated by performing mass spectrometry of citrullinated proteins from various differentiation stages (days 0, 2, 5, 8, 10, and 14) of osteoclast lineage cells. Only 3 proteins (vimentin, actin, and α-2-HS-glycoprotein) showed consistent citrullination during the process of osteoclast differentiation; of these, vimentin was the only one specifically citrullinated at more advanced differentiation stages (i.e., after day 5). Moreover, the

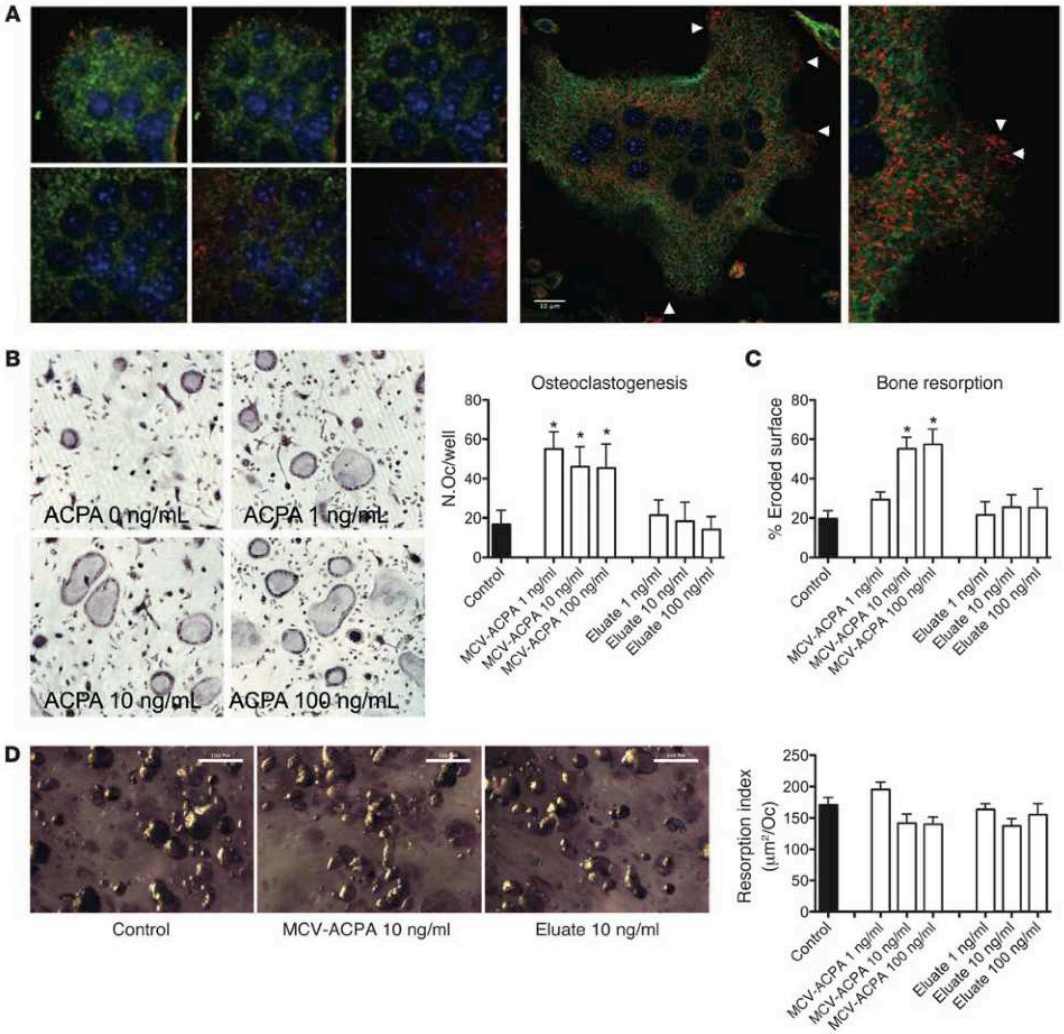

Figure 4
MCV-ACPAs stimulate osteoclastogenesis. (**A**) Laser scanning microscopy of 2-mm osteoclast sections showing binding of MCV-ACPAs. Left: green, MCV-ACPA staining for citrullinated vimentin; red, phalloidin staining for actin; blue, DAPI staining for the nucleus. Right: green, vimentin staining; red, MCV-ACPA staining for citrullinated vimentin; blue, DAPI staining for the nucleus. Arrowheads indicate surface staining for citrullinated vimentin. (**B**) Osteoclastogenesis ($n = 3$) induced by 10 ng/ml MCSF, 1 ng/ml RANKL, and different concentrations of MCV-ACPAs and of IgG fractions deprived of ACPAs (eluate) in the presence of MCSF and RANKL. N.Oc, number of osteoclasts. (**C**) Resorption pit assay ($n = 3$) with different concentrations of MCV-ACPAs and of IgG fractions deprived of ACPA. (**D**) Assessment of resorption index ($n = 3$) by transposing a defined number of osteoclasts on bone slices and measuring the resorption pit size per single osteoclast. Control indicates no antibody addition. Original magnification, ×20 (**A**); ×100 (**A**, enlarged view); ×10 (**B** and **D**). Scale bars: 100 μm. $^*P < 0.05$.

citrullinated peptide sequence of vimentin detected by mass spectrometry (KVELQELNDXFANYIDKV$_{[0]}$; citrullin denoted by X) was colocalized with the citrullinated epitope in the N-terminal part of vimentin recognized by the ACPA.

MCV-ACPAs induce osteoclastogenesis and bone resorption. Based on our clinical observations and the experimental evidence for vimentin citrullination in osteoclasts, we hypothesized that ACPAs can directly stimulate osteoclast-mediated bone resorption. We therefore sought to determine whether ACPAs can trigger osteoclastogenesis, testing the ability of ACPA-containing serum and MCV-ACPAs to stimulate osteoclastogenesis. Using laser scanning microscopy, we found the plasma membrane and cytoplasm of osteoclasts to be stained by MCV-ACPAs (Figure 4A), indicative of citrullinated vimentin expression. Expression of citrullinated

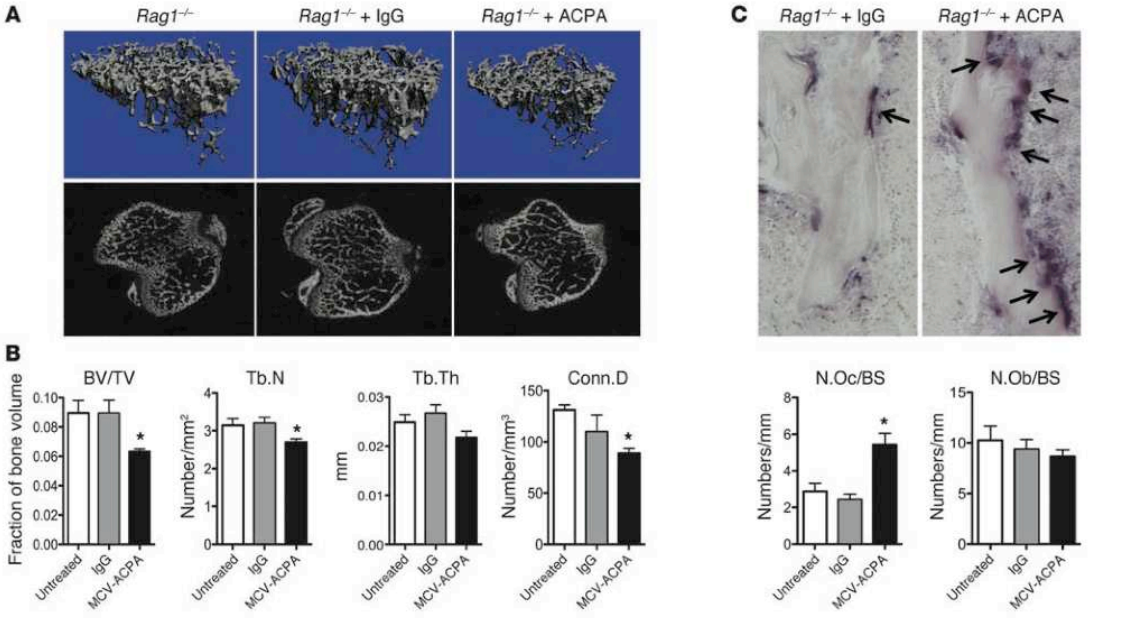

Figure 5
MCV-ACPAs induce bone loss in vivo. (**A**) 3-dimensional (top) and 2-dimensional (bottom) μCT images of the tibial metaphysis of *Rag1*$^{-/-}$ mice that were left untreated or treated with control IgG or MCV-ACPAs. (**B**) Structural parameters of the tibial bone (n = 5 per group), including the ratio of bone volume to total volume (BV/TV), trabecular number (Tb.N), trabecular thickness (Tb.Th), and connectivity density (Conn.D). (**C**) Microphotographs (original magnification, ×400) of tibial bones of *Rag1*$^{-/-}$ mice treated with either IgG or MCV-ACPAs, stained for osteoclasts (purple stain and arrows) by histochemical detection of TRAP. Histomorphometric quantification of osteoclast number and osteoblast number (N.Ob) on the tibial bone surface (BS) is also shown. *P < 0.05.

vimentin was not colocalized to the actin cytoskeleton, nor, interestingly, to noncitrullinated vimentin. Importantly, when performing osteoclast differentiation assays with MCSF and RANKL, we observed that addition of ACPA-containing serum (data not shown) or MCV-ACPAs increased the formation of osteoclasts (Figure 4B). In contrast, RA serum without ACPAs, as well as IgG (isolated from ACPA-positive serum samples) deprived of MCV-ACPAs, did not stimulate MCSF/RANKL-mediated osteoclastogenesis. Furthermore, osteoclast differentiation was enhanced by ACPAs, since TRAP-positive mononuclear cells appeared earlier in ACPA-challenged osteoclast cultures (data not shown).

When assessing bone resorption, we found a dose-dependent increase of resorption pits in the presence of ACPA-containing serum as well as MCV-ACPAs (Figure 4C), which suggests that ACPAs induce bone resorption. These findings were consistent with the use of MCV-ACPA or a Fab fragment of this antibody, excluding osteoclastogenesis stimulation and bone resorption by a solely Fc-mediated effect. Moreover, when noncitrullinated vimentin was used as an autoantigen for antibody isolation, only low amounts of antibodies could be isolated, which (a) did not recognize citrullinated vimentin and (b) did not induce osteoclastogenesis (data not shown). Furthermore, we assessed the resorption capacity of individual osteoclasts after differentiating and transposing them on bovine bone slices. These experiments showed that ACPAs did not enhance the resorptive potential of individual osteoclasts (as measured by resorption pit size of individual osteoclasts; Figure 4D), which suggests that enhancement of overall bone resorption by ACPAs is based on enhanced differentiation and, consequently, increased numbers of osteoclasts.

MCV-ACPAs induce systemic bone loss and osteoclast formation in vivo. We next tested whether ACPAs can also induce bone loss in vivo. We challenged lymphocyte-deficient *Rag1*$^{-/-}$ mice with MCV-ACPAs and control IgG, then analyzed bone structure after 4 weeks by micro-CT (μCT). Analysis of bone volume relative to total volume at the tibial metaphysis showed significant reduction of trabecular bone with MCV-ACPAs compared with control IgG (Figure 5, A and B). Bone loss was based on reduced trabecular number and, consequently, lower connectivity density of trabecular bone, whereas trabecular thickness was not changed (Figure 5B). In addition, histomorphometry of trabecular bone showed a significant increase in osteoclast number along the metaphysis of ACPA-treated mice (Figure 5C), which supports the in vitro assay data and suggests that enhanced bone loss in conjunction with MCV-ACPAs is based on enhanced osteoclastogenesis and bone resorption.

Enhanced TNF production and augmentation of the osteoclast precursor cell pool as the mechanism of bone loss by MCV-ACPAs. To further elucidate the mechanism by which MCV-ACPAs induce bone loss in vivo, we examined systemic bone resorption and bone formation parameters. In accordance with the observed increase in osteoclasts in mice exposed to ACPAs, we found an increase in CTXI, a common measure of bone-resorptive activity, in the serum of ACPA-

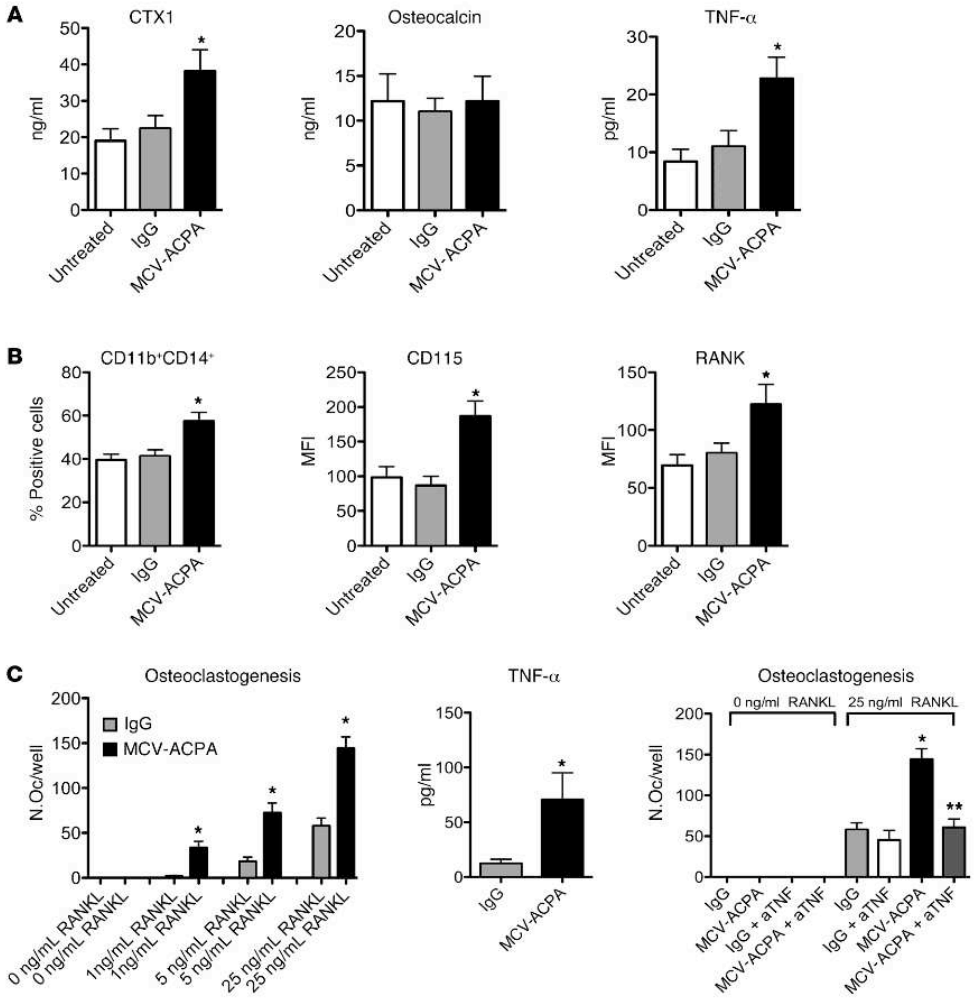

Figure 6
Bone loss elicited by MCV-ACPAs is induced by TNF-mediated increase of osteoclast precursor trafficking and differentiation. (**A**) Serum levels ($n = 5$ per group) of CTXI, osteocalcin, and TNF-α in *Rag1*$^{-/-}$ mice that were left untreated or treated with control IgG or MCV-ACPAs. (**B**) FACS analysis ($n = 5$ per group) of spleen cells for the number of CD11b^{+}CD14^{+} cells (osteoclast precursors) and their expression of CD115 and RANK. (**C**) Osteoclastogenesis assay ($n = 3$ per group) of spleen cells from *Rag1*$^{-/-}$ mice treated with control IgG or MCV-ACPAs with various concentrations of RANKL. TNF-α release and osteoclastogenesis assays ($n = 3$ per group) from spleen cells of wild-type mice treated with control IgG or MCV-ACPAs are also shown. aTNF, blockade of TNF-α by 100 ng/ml etanercept. *$P < 0.05$.

challenged mice. In contrast, serum levels of osteocalcin, a marker of bone formation, were not affected (Figure 6A). Interestingly, we also found an increase in systemic levels of TNF-α in mice exposed to ACPAs (Figure 6A), although we did not find signs of arthritis, induction of which may depend on a specific susceptible genetic background, as reported previously (20). TNF-α, however, is also a major inducer of osteoclastogenesis by enhancing differentiation of osteoclasts and by trafficking of osteoclast precursors (21, 22).

Indeed, when assessing the spleens of ACPA-challenged mice, we found a significant increase of CD11b^{+}CD14^{+} osteoclast precursors (Figure 6B), which has been previously shown as an effect of TNF-α on cells of the osteoclast lineage (22). Moreover, the cells expressed higher surface levels of the MSCF receptor CD115 (also known as c-Fms) and the RANKL receptor RANK, making them more susceptible to further differentiation into mature osteoclasts (Figure 6B). Accordingly, spleen cells from ACPA-challenged mice showed overall higher osteoclastogenic potential by being more sensitive to stimulation by small amounts of RANKL, as well as allowing differentiation of higher numbers of osteoclasts (Figure 6C). These in vivo results were confirmed by further in vitro obser-

vations: exposure to MCV-ACPAs elicited TNF-α release from spleen cells of untreated wild-type mice and enhanced osteoclastogenesis in the presence of MCSF and RANKL, an effect that was blocked by TNF-α inhibition (Figure 6C).

Discussion

The present study provides a link between immune system and bone. We showed that autoantibodies against citrullinated vimentin (i.e., MCV-ACPAs), which are specifically found in patients with RA, directly led to osteoclast differentiation and bone resorption in vitro and in vivo. RA is one of the most common autoimmune diseases, affecting 1% of the worldwide population, and a major trigger for local and systemic bone loss, resulting in joint destruction and increased fracture risk. More than two-thirds of patients with RA develop immune responses against citrullinated proteins, which is highly specific for RA (3). Despite being known for many years, it has been always unclear why these autoantibodies are associated with a more severe disease course, in particular more destructive joint disease. Although the direct link we have demonstrated between autoantibodies and bone loss may not be the only explanation for the more severe disease course of ACPA-positive patients (yet-unidentified differences in the gestalt of inflammation between ACPA-positive and -negative patients cannot be ruled out completely), these data provide an attractive concept of how the breakdown of immune tolerance can damage our skeletal system.

Current concepts suggest a finely balanced interplay between the immune system and bone. These concepts have been driven by clinical observation of bone destruction in RA and other inflammatory diseases. Activation of the innate immune system and production of proinflammatory cytokines, in particular TNF, triggers bone loss by inducing the expression of RANKL, a key osteoclastogenic molecule (21). Moreover, activation of the adaptive immune system, in particular T cell activation, also supports bone destruction. T cell activation, particularly that of the proinflammatory TH17 subset, fosters the expression of RANKL and induces osteoclastogenesis (23). These processes also explain why autoimmune inflammatory diseases such as RA are linked to bone loss.

Although not all RA patients experience bone destruction, others face rapid bone loss and destruction of the joints leading to crippling and functional loss. The clinical heterogeneity of RA with respect to joint damage suggests that there are additional factors that determine bone destruction in patients with arthritis. In fact, the strongest risk factor is the presence of ACPAs. Despite this strong clinical association, the role of autoantibodies on bone has so far been largely neglected. The potential principle that autoantibodies modify bone has been shown in rare cases of autoantibodies against the decoy receptor of RANKL, osteoprotegerin, which caused bone loss in patents with celiac diseases (24). However, so far none of the classical (i.e., frequently observed) autoantibodies has been mechanistically linked to bone loss.

Our study directly links ACPA, a common autoantibody prevalent in RA patients worldwide, to bone loss. ACPA binding to citrullinated vimentin enhanced the differentiation of osteoclast precursors into mature bone resorbing cells in vitro and in vivo. As a consequence, ACPAs enhanced bone resorption in vitro and in vivo and elicited bone loss in vivo by increasing osteoclast differentiation. Interestingly, the mechanism by which ACPAs trigger bone loss involved TNF-α, the pivotal cytokine in the pathogenesis of RA: MCV-ACPAs induced production of TNF-α by osteoclast precursors, extending previous observations that ACPAs can directly affect cells of the monocyte/macrophage lineage (25–28). For bone, TNF-α is highly important, as it not only facilitates the trafficking of osteoclast precursors from the bone marrow to the lymphoid organs, but also renders them more susceptible to further differentiation into osteoclasts by inducing the receptors of key differentiation factors for osteoclasts, such as MSCF and RANKL. The net effect of ACPAs is thus a TNF-mediated induction of osteoclastogenesis and bone resorption. Although vimentin affects osteoblast differentiation (29), we could not detect relevant citrullination of vimentin in osteoblasts, and ACPAs also did not affect osteoblast differentiation and bone formation in vitro. We conclude that ACPAs, which are known to emerge years ahead of the clinical onset of RA (30), not only increase susceptibility to RA development, but also appear to disturb bone balance by making individuals more prone to bone resorption. This concept also serves to explain why RA patients already show low bone mass at the onset of disease (31) and why bone damage in RA patients with ACPAs is far higher compared with those without ACPAs.

The observation that osteoclasts contained large amounts of citrullinated vimentin also sheds light on the role of posttranslational modifications, in particular citrullination, on the differentiation of cells of the monocyte lineage. Previous studies have shown that PAD2 and PAD4 are the predominant isoforms expressed in monocytes (32). We observed here that osteoclast precursors shared a similar PAD expression pattern, with PAD2 and PAD4 as the dominant PAD isoforms. In contrast, cells of the osteoclast lineage did not express PAD1 and PAD3. This expression pattern of PADs in osteoclasts was in fact similar to the one found in the inflamed synovial tissue of RA patients (33, 34). Furthermore, during the process of osteoclast differentiation, the PAD expression pattern of cells shifted from PAD4 to PAD2. This observation suggests that PAD2 is the major contributor to protein citrullination in osteoclasts. Interestingly, previous studies have shown that monocyte differentiation into macrophages also induces a shift from PAD4 to PAD2 expression, similar to what we found in osteoclasts (32, 35). In contrast, PAD4 has been recently shown to function as an antimicrobial component forming extracellular traps (36). These data indicate that PAD expression and the citrullination pattern of proteins may differ among the various leukocytes subsets and allow for different functional properties of the individual subsets.

Remarkably, calcium has been shown to be a key inducer of PAD, and the calcium-rich environment to which osteoclasts are exposed may foster PAD expression and protein citrullination (37). Indeed, a strong increase in the citrullination of vimentin was observed during osteoclast differentiation, and citrullination occurred at the same region of citrullinated vimentin, which is recognized by the human autoantibody. Vimentin, in fact, has been identified as an important component of the adhesion zone of the osteoclast (38), and it remains to be determined whether its citrullination affects cell function and/or survival. Macrophages, for instance, can secrete vimentin, which facilitates bacterial killing and oxidation product synthesis (39).

In summary, our data showed a disease-relevant link among autoantibody formation, autoimmune disease, and bone loss in humans, which we believe to be novel. Autoantibodies against citrullinated vimentin bind to cells of the osteoclast lineage, foster their differentiation into bone resorbing cells, and promote bone loss. Our data extended current concepts on the interactions of immune system, inflammation, and bone by directly linking ACPA, a key autoantibody in human inflammatory disease, with

bone loss, leading to joint destruction and functional decline in arthritis. Thus, our findings suggest a link between autoimmunity and the skeleton in human disease.

Methods

Purification of MCV-ACPAs. Samples of serum with very high ACPA response (>1,000 IU/ml) were obtained from 3 RA patients presenting at the Department of Medicine 3 of the University Clinic of Erlangen. ACPA activity was detected with a commercially available ELISA for detection of antibodies against citrullinated vimentin (Orgentec Diagnostika).

Recombinant MCV was conjugated to CNBr-sepharose (GE Healthcare) (1 mg protein/ml equilibrated sepharose) according to the manufacturer's instructions and stored at 4°C in PBS with 0.1% BSA. Prior to affinity purification of ACPAs, IgG was purified by affinity chromatography on a protein A column (GE Healthcare). Eluted IgG fractions were immediately neutralized with 1:10 volume of 1 M Tris-buffer (pH 8.0) and dialyzed against PBS (pH 7.2). Each purified IgG fraction was applied to a separate citrullinated vimentin affinity column (1 ml matrix per serum sample) and incubated for 2 hours at 4°C, rotating end over end. The column was washed with 0.5 M NaCl with 0.05% Tween 20 in PBS (pH 7.2), and the unbound fraction was collected. The bound anti-MCV antibodies (i.e., MCV-ACPAs) were eluted with 3.5 M $MgCl_2$ (pH 7.5). The high salt buffer of the purified IgG fractions was exchanged against PBS using a desalting column (Zebra Spin; Pierce). MCV-ACPA concentration was increased by ultrafiltration on a Vivaspin 30 K unit (Millipore). The content of the MCV-ACPAs was verified with ELISA for measuring MCV autoantibodies (Orgentec Diagnostika). Additionally, the purification of the MCV-ACPAs and the successful cleavage with immobilized pepsin was verified with SDS-PAGE electrophoresis and staining with Coomassie blue.

Generation of Fab fragments. Immobilized pepsin allows efficient generation of F(ab′)2 fragments from IgG. Pepsin is a nonspecific endopeptidase that is active only at acidic pH and irreversibly denatured at neutral or alkaline pH. Immobilized pepsin is advantageous because the digestion can be immediately stopped by simply removing the gel from the IgG. Digestion by pepsin normally produces a F(ab′)2 fragment and numerous small peptides of the Fc portion. The buffer of the MCV-ACPAs was exchanged against digestion buffer (0.1 M sodium acetate; pH 4.5) with Zebra spin column. 1 ml of this prepared IgG solution was added to a tube containing 100 μl equilibrated Immobilized Pepsin (catalog no. 20343; Pierce) and incubated in a thermomixer for 4 hours with constant mixing at 600 rpm at 37°C. To separate digested protein from the Immobilized Pepsin, the solution was centrifuged at 1,000 *g* for 5 minutes. The supernatant-containing digested protein was decanted into a new tube, and Protein A Columns (Pierce) were used to separate undigested IgG from F(ab′)2 fragments. To remove small Fc fragments, the eluted fractions were dialyzed and concentrated with ultrafiltration units (50K MWCO).

Analysis of antibody sialylation. Enzyme-linked lectin–specific ACPA assay (sialACPA ELISA) was used to analyze ACPA sialylation. Neuraminidase treatment was done to cleave selectively sialic acid–containing carbohydrates on the autoantibodies. Sialic acid release was induced by digestion at 25°C for 2 hours with 50 mU neuraminidase cloned from *Clostridium perfringens* and overexpressed in *E. coli* (NEB) in 200 μl of 50 μM sodium citrate (pH 6.0).

Synthesis of MCV peptides. Previously published sequences of MCV (17) were used as a template to synthesize overlapping 17-mer peptides, in accordance with Fmoc-chemistry at the Peptide Specialty of Perbio Mimotopes (Perbio Science Deutschland GmbH). Each peptide had a 12–amino acid residue overlap with the neighboring peptide. The synthesis through the MCV amino acid sequence resulted in 91 peptides with the general formula Biotin-SGSG-PEPTIDE-Amide. The N-terminal extension of the peptides (Biotin-SGSG) was designed for defined flexibility and to incorporate an affinity tag. Each arginine-containing peptide was synthesized as the citrulline residue variant. Crude fractions after peptide synthesis were purified using high-performance liquid chromatography. Quality and purity of the peptide was assessed by mass spectrometry and analytical high-performance liquid chromatography according to the manufacture's instructions (Perbio Science Deutschland GmbH).

Epitope characterization by peptide ELISA. Microtiter plates (Maxisorb) were precoated with 1 μg/ml streptavidin (Perbio Science Deutschland GmbH) in PBS (pH 7.6). After incubation for 2 hours at 25°C, plates were blocked with 1% BSA in PBS for 30 minutes at room temperature. Theses plates were used for binding of the biotinylated peptides/antigens. The biotinylated 17-mer peptides at a concentration of 0.5 μg/ml were also diluted in PBS (pH 7.6) and incubated overnight at 4°C (100 μl/well). In addition to the 91 peptides, biotinylated recombinant MCV, protein A, and rheumatoid factor antigen were used as internal control antigens in the available 5 cavities of a 96-well microtiter plate. Coating and blocking was done as described for peptides. Possible excesses of peptides/antigens were eliminated by washing the cavities with 200 μl/well 0.1% Tween 20 in PBS. Finally, flicking and slapping removed any residual solution. The assay was performed in accordance with the general protocol for the Orgentec ELISA system. In brief, the serum samples were diluted 1:101 in sample buffer (PBS containing BSA and Tween), added to the wells, and then incubated for 30 minutes (100 μl/well). After 3 washing steps (300 μl/well), horseradish peroxidase–conjugated anti-human IgG (Dianova) was added and incubated for 30 minutes (100 μl/well). Visualization was done by incubation with 3,3′,5,5′-tetra-methyl benzidine substrate for 15 minutes (100 μl/well), and the reaction was terminated by adding 50 μl stop solution (0.5 mol/l H_2SO_4) to each well. Finally, absorbance at 450 nm was determined using an ELISA reader (Rainbow Reader; Tecan). All steps were carried out at room temperature. Background OD was obtained by adding each serum to a well without protein. A positive serum was defined by an OD value more than twice that of background OD (40). Each serum sample was tested in duplicate and to further define the assay characteristics.

Reactivity to citrullinated and noncitrullinated peptides. Citrullin- and respective arginine-containing peptides (denoted by bold X and R, respectively) of vimentin (normal, SAVRA**R**SSVPGVRK; citrullinated, SAVRA**X**SSVPGVRK), fillagrin (normal, SHQEST**R**G**R**S**R**GRSGRSGS; citrullinated, SHQEST**X**G**X**S**X**GRSGRSGS), and collagen (normal, A**R**GLTG**R**PGDAK; citrullinated, A**X**GLTG**X**PGDAK) as well as fibrinogen-derived peptides (normal, RPAPPPISGGGY**R**A**R**; citrullinated, RPAPPPISGGGY**X**A**X**) were synthesized by solid-phase peptide synthesis (FMOC strategy) in the Department of Peptide Chemistry of Eötvös Loránd University (Budapest, Hungary). Biotinylated peptides were bound to NeutrAvidin-precoated (5 μg/ml) plates. After adding biotinylated peptides (1 μg/ml), the wells were blocked (40 mM Tris-HCl, 150 mM NaCl, 0.1% Tween, 0.5% BSA), sera samples were added (1:400 or 1:100), and then plates were incubated for 1 hour at 37°C. After washing, rabbit anti-human IgG conjugated to horseradish peroxidase was added at 1:2,000 dilution for 1 hour at 37°C. The signal was developed by tetramethylbenzidin (10 mg/ml, diluted in 0.1 M acetate buffer [pH 5.5] and 30% H_2O_2) for about 5 minutes at room temperature. The reaction was stopped by 4N H_2SO_4. Absorbance was measured at 450 nm (correction wavelength set at 620 nm) using a Labsystems Multiskan MS spectrophotometer. To analyze our results, an OD ratio (OD of citrullin-containing peptide minus OD of arginine-containing peptide) was calculated and compared between various groups (Kruskal-Wallis test).

Mass spectrometry of citrullinated proteins in osteoclast lineage cells. Cell pellets (1×10^6 cells each) were suspended in 400 μl lysis buffer containing 0.1% *Rapi*Gest in 50 mM ammonium bicarbonate and protease inhibitor cocktail (Complete Mini; Roche Diagnostics). The homogenate was sonicated using

a probe tip sonicator (power 50%; Bandelin Sonopuls, Buch & Holm) 3 times for 20 seconds on ice. The homogenate was centrifuged at 9,000 *g* at 4°C for 5 minutes, and the pellet was discarded. Prepacked PD SpinTrap columns (GE Healthcare) were used for desalting and buffer exchange against 50 mM ammonium bicarbonate. The protein concentration was measured using a NanoDrop spectrophotometer (Thermo Scientific). 100 μg protein from each cell sample was reduced in 200 mM dithiothreitol at 56°C for 30 minutes followed by alkylation by 1M indoleacetic acid for 1 hour at room temperature in darkness. Endoproteinase Lys-C sequencing grade (Roche Diagnostics GmbH) was added at 1:50 enzyme/substrate, and samples were incubated at 37°C overnight. After digestion, the samples were transferred to a Pall Nanosep centrifugal device with Omega membrane MWCO 10 kDa (Pall Corp.). Peptides were cleaned up by ZipTip pipette tips containing C_{18} media (Millipore) and dried using speed-vac prior to mass spectrometry analysis.

Samples were resuspended in 0.1% formic acid and 1 μg of each was injected onto a Waters NanoAquity UPLC equipped with a nanoAquity 5-μm TRAP C18 180-μm i.d. × 20-mm trapping column and a 1.7-μm BEH130 C18 75-μm i.d. × 150-mm reversed-phase analytical column. The mobile phase consisted of (a) 0.1% formic acid in water and (b) 0.1% formic acid in acetonitrile. The peptides were separated using a gradient of 3%–40% of the latter for the first 90 minutes, then 40%–90% of the latter again for the following 8 minutes. The peptides were analyzed using a Waters Q-Tof Premier mass spectrometer operated in data-dependent mode with 4 components, each acquired for 0.9 s/spectra, 1–3 spectra/peptide. High mass accuracy was achieved by lock-spray using Glu-1-Fibrinopeptide. The raw data were processed using Mascot Distller version 2.4.0 into .mgf files.

Peptide and protein identification was performed using X!Tandem open source software. The searches were performed against the human SwissProt database, with Lys-C specificity and semi-style cleavage allowed. Mass deviations for precursor ions and for fragment ions were set to 20 ppm and 0.5 Da, respectively. Carbamidomethylation was chosen as a fixed modification, while citrullination (R), deamidation (N, Q), and oxidation (M) were set as variable modifications. Only proteins with expectation value $\log_e$ below –3 were considered as a positive match.

Osteoclast cultures and resorption tests. Peripheral blood mononuclear cells (PBMCs) were isolated from 10 ml EDTA-blood of healthy donors using a Ficoll gradient (Lyphoflot; BioRad) and incubated in 48-well plates (7.5×10^5 cells/well) in α-MEM with 1% PenStrep (both Gibco, Invitrogen). After 3 hours, cells were washed for monocyte enrichment and cultivated for 14 days in α-MEM supplemented with 10% heat-inactivated fetal BSA (Biochrom AG), 1% penicillin/streptomycin (Gibco, Invitrogen), 10 ng/ml MCSF, and submaximal concentrations of 1 ng/ml RANKL (both Peprotech). Every 3 days, medium was replaced with fresh medium. Various concentrations of ACPA-positive serum or MCV-ACPAs were added as indicated. Osteoclast differentiation was evaluated by staining cells for TRAP using a Leukocyte Acid Phosphatase Kit (Sigma-Aldrich) according to the manufacturer's instructions. For global bone resorption, the same protocol was performed on bovine bone slides, and resorption pit area was assessed. For assessment of bone resorption per single osteoclast (resorption index), osteoclasts were detached from plastic plates using acutase (A6964; Sigma-Aldrich) and replated on bone slices after 4 days of culture. After 48 hours, osteoclasts were scraped from the slices using cotton buds, and slices were stained for 30 seconds in a 1% toluidin solution. Acquisition of images was done on a widefield microscope with side illumination, which identified resorption pits by their dark color and 1-sided shining ("dawn on the valley" effect).

Immunofluorescence. Osteoclasts were fixed with 4% PFA (pH 7.2) in PBS for 10 minutes at 37°C. Fixed samples were then washed 3 times in PBS and permeabilized for 10 minutes with 0.2% Triton X-100 in PBS. Next, samples were preblocked for 10 minutes with a solution of 2% BSA, 0.1% Triton X-100, and 0.1% azide in PBS. All remaining washing steps and antibody dilutions were done using this solution. Samples were incubated with 1:50 dilution of MCV-ACPA, Alexa Fluor 488 mouse anti-human vimentin antibody, or Alexa Fluor 488 phalloidin (all Sigma-Aldrich). For detection of bound MCV-ACPA, either Alexa Fluor 488– or Alexa Fluor 647–conjugated anti-human IgG antibody was used. Cells were then incubated with DAPI (10 μg/ml) and mounted with FluorSave reagent (Calbiochem). Fluorescence images were acquired with a Zeiss spinning disk confocal microscope.

Immunoblotting. PBMCs (7.5×10^5 cells/well) were cultivated in 48-well plates with MCSF, RANKL and TGF-β for 14 days as indicated above. Cells were lysed in Laemmli buffer (BioRad) either directly after the isolation or after various times of culture. Proteins were separated by electrophoresis in 10% sodium dodecyl sulfate–polyacrylamide gels and blotted onto polyvinylidene difluoride membranes (Millipore). After blocking with 5% dry milk prepared in PBS containing 0.1% Tween 20, the membranes were subjected to immunoblotting. Antibodies used were as follows: rabbit anti–β-actin antibody (Sigma-Aldrich), chicken anti–citrullinated vimentin antibody, purified human MCV autoantibody (i.e., MCV-ACPAs), rabbit anti-PAD2 antibody, rabbit anti-PAD4 antibody, mouse anti-vimentin antibody (all Abcam). Detection was done by respective peroxidase-conjugated antibodies (all Promega) and chemoluminescence reagent (ECL; Thermo Scientific).

Quantitative real-time PCR analysis. PBMCs (7.5×10^5 cells/well) were cultivated in 48-well plates with MCSF, RANKL, and TGF-β for 14 days. Directly after the isolation or after various times of culture, total RNA was extracted using peqGOLD TriFast (Peqlab) according to the manufacturer's instructions. RNA was transcribed into cDNA using an oligo(dT) primer and MuLV reverse transcriptase (Roche). Quantitative real-time PCR was performed using SYBR Green I-dTTP (Eurogentec) using the following primer pairs: β_2-microglobulin (β_2-MG) forward, GATGAGTATGCCTGCCGTGTG; β_2-MG reverse, CAATCCAAATGCGGCATCT; PAD2 forward, AGCTCTACCATGTGGTCAAGT; PAD2 reverse, GGTGTCCGTGAAGATGGGAG; PAD4 forward, CCGGCAAAGTGAAGCCAAC; PAD4 reverse, CTCAGGGTCATCAGCGACA. Each sample was analyzed in duplicate and normalized to the level of β_2-MG.

Serum parameters. In human serum samples, we measured CTXI using a commercial kit (Immundiagnostic Systems) based on ELISA. TRAP5b (Quidel) and cathepsin K (Biomedica) were also measured by ELISA. ACPAs were measured by commercial ELISA (Phadia/Thermofisher Scientific), rheumatoid factor by nephelometry (Beckmann Coulter). In murine serum samples, CTXI (Ratlaps; Nordic Bioscience), osteoclacin (Quidel), and TNF-α (R&D) were measured by commercial ELISAs.

μCT. 10 female *Rag1*$^{-/-}$ mice were injected i.p. with 50 μg lipopolysaccharide and with 500 μg normal human IgG, 500 μg MCV-ACPAs, or PBS. After 4 weeks, mice were sacrificed. The right tibia was prepared and stored in 70% ethanol for μCT analysis (41). μCT analyses were done with a commercially available desktop μCT (μCT35; SCANCO Medical AG) (42). The following acquisition parameters were used: voltage, 40 kV; X-ray current, 250 μA; exposure time, 5,000 ms/projection for 720 projections; matrix, 1024 × 1024; voxel size in reconstructed image, 9 μm. Images were analyzed using a plugin programmed for Amira 4.1.2 (Mercury) for histomorphometric parameters at the metaphyses of the proximal tibiae: ratio of bone volume to total volume, trabecular number, and trabecular thickness (41).

Mouse histology. Mice were treated as described above, and the left tibia was used for histology Bones were fixed overnight in 4% formalin and decalcified in EDTA (Sigma-Aldrich) until they were pliable. Serial paraffin sections (2 μm) were stained for TRAP for osteoclast detection. All analyses were performed using a microscope (Nikon) equipped with a digital camera and an image analysis system for performing histomorphometry (Osteomeasure; OsteoMetrics).

FACS and murine osteoclast assays. For FACS staining, 1×10^6 murine spleen cells were washed with 1 ml PBS containing 0.1% BSA resuspended in 100 μl FACS buffer and incubated with saturating amounts of PE-Cy7–, FITC-, biotin-, or PE-labeled antibodies against CD11b, CD14 (both BD Bioscience), CD115 (c-Fms, MCSF receptor; Biolegends), and RANK (CD265; Abcam) for 30 minutes at 4°C in the dark. Cells were also stained with isotype control antibody. A FACSCanto Flow Cytometer (BD Bioscience) was used for analysis. For osteoclast assays, bone marrow was isolated by flushing femoral bones with complete αDMEM. Osteoclast precursors were then isolated from bone marrow–derived cell suspensions using CD11b microbeads (Miltenyi Biotec) according to the manufacturer's instructions. The purity of isolated monocytes was assessed by flow cytometry analysis using FITC-labeled antibodies against CD11b (Miltenyi Biotec). $CD11b^+$ monocytes were plated in 96-well plates (2.5×10^5 cells/well) or 48-well plates (5×10^5 cells/well) in αMEM supplemented with 10% fetal calf serum, 30 ng/ml M-CSF, and various doses (0, 1, 5, or 25 ng/ml) of RANKL (all R&D Systems). To examine the contribution of ACPAs to osteoclast development, MCV-ACPAs (10 ng/ml) were added to the cultures. Medium was changed after 72 hours. To examine the contribution of TNF-α blocking, experiments with 100 ng/ml etanercept, a TNF receptor 2–Fc fusion protein that also inhibits murine TNF-α, were performed. Osteoclast differentiation was evaluated by staining cells for TRAP using a Leukocyte Acid Phosphatase Kit (Sigma-Aldrich) according to the manufacturer's instructions.

Statistics. For comparison of multiple groups, 1-way ANOVA with Bonferroni correction was used in case values showed Gaussian distribution. In the absence of Gaussian distribution, the Kruskal-Wallis test with Dunn's correction was performed. A *P* value less than 0.05 was considered significant.

Study approval. Studies in animals and humans were reviewed and approved by the ethics committee of the University Clinic of Erlangen. All subjects provided informed consent prior to their participation in the study.

Acknowledgments

We thank Fruzsina Babos and Anna Magyar (HAS-ELTE Research Group of Peptide Chemistry, Eötvös Loránd University, Budapest, Hungary) for peptide synthesis, as well as Marlène Gallet (Institut de Génomique Fonctionnelle de Lyon, Lyon, France) for valuable input on the bone resorption assay. This study was supported by the Deutsche Forschungsgemeinschaft (FG 661/TP4 and SPP1468-IMMUNOBONE), the Bundesministerium für Bildung und Forschung (BMBF; project ANCYLOSS), the MASTERSWITCH project of the European Union, the IMI-funded project BTCure, and Agence de Recherche contra le Cancer (ARC). G. Sarmay and E. Szarka are supported by the Hungarian National Development Agency and OTKA (CK80689). U. Harre is a member of the Graduiertenkolleg 1660. D. Georgess is an Early Scientific Researcher recipient from a Marie Curie action (T3Net project). The authors acknowledge the contribution of the PLATIM platform of UMS344/US8 Biosciences.

Received for publication September 12, 2011, and accepted in revised form March 7, 2012.

Address correspondence to: Georg Schett, Department of Internal Medicine 3, Rheumatology and Immunology, University of Erlangen-Nuremberg, Krankenhausstrasse 12, Erlangen D-91054, Germany. Phone: 49.9131.85.33363; Fax: 49.9131.85.34770; E-mail: georg.schett@uk-erlangen.de.

1. Firestein GS. Evolving concepts of rheumatoid arthritis. *Nature*. 2003;423(6937):356–361.
2. McInnes IB, Schett G. Cytokines in the pathogenesis of rheumatoid arthritis. *Nat Rev Immunol*. 2007;7(6):429–442.
3. Klareskog L, et al. A new model for an etiology of rheumatoid arthritis: smoking may trigger HLA-DR (shared epitope)-restricted immune reactions to autoantigens modified by citrullination. *Arthritis Rheum*. 2006;54(1):38–46.
4. Mahdi H, et al. Specific interaction between genotype, smoking and autoimmunity to citrullinated alpha-enolase in the etiology of rheumatoid arthritis. *Nat Genet*. 2009;41(12):1319–1324.
5. Vossenaar ER, Zendman AJ, van Venrooij WJ, Pruijn GJ. PAD, a growing family of citrullinating enzymes: genes, features and involvement in disease. *Bioessays*. 2003;25(11):1106–1118.
6. Wegner N, et al. Peptidylarginine deiminase from Porphyromonas gingivalis citrullinates human fibrinogen and α-enolase: implications for autoimmunity in rheumatoid arthritis. *Arthritis Rheum*. 2010;62(9):2662–2672.
7. Vincent C, de Keyser F, Masson-Bessiere C, Sebbag M, Veys E, Serre G. Anti-perinuclear factor compared with the so called "antikeratin" antibodies and antibodies to human epidermis filaggrin, in the diagnosis of arthritides. *Ann Rheum Dis*. 1999;58(1):42–48.
8. De Rycke L, et al. Rheumatoid factor and anticitrullinated protein antibodies in rheumatoid arthritis: diagnostic value, associations with radiological progression rate, and extra-articular manifestations. *Ann Rheum Dis*. 2004;63(12):1587–1593.
9. van der Woude D, et al. Epitope spreading of the anti-citrullinated protein antibody response occurs before disease onset and is associated with the disease course of early arthritis. *Ann Rheum Dis*. 2010;69(8):1554–1561.
10. Schett G, Teitelbaum SL. Osteoclasts and arthritis. *J Bone Miner Res*. 2009;24(7):1142–1146.
11. Schett G, et al. High-sensitivity C-reactive protein and risk of nontraumatic fractures in the Bruneck study. *Arch Intern Med*. 2006;166(22):2495–2501.
12. Takayanagi H. Osteoimmunology: shared mechanisms and crosstalk between the immune and bone systems. *Nat Rev Immunol*. 2007;7(4):292–304.
13. van Gaalen FA, et al. Autoantibodies to cyclic citrullinated peptides predict progression to rheumatoid arthritis in patients with undifferentiated arthritis: a prospective cohort study. *Arthritis Rheum*. 2004;50(3):709–715.
14. Syversen SW, et al. Prediction of radiographic progression in rheumatoid arthritis and the role of antibodies against mutated citrullinated vimentin: results from a 10-year prospective study. *Ann Rheum Dis*. 2010;69(2):345–351.
15. van der Linden MP, et al. Value of anti-modified citrullinated vimentin and third-generation anti-cyclic citrullinated peptide compared with second-generation anti-cyclic citrullinated peptide and rheumatoid factor in predicting disease outcome in undifferentiated arthritis and rheumatoid arthritis. *Arthritis Rheum*. 2009;60(8):2232–2241.
16. Raza K, Mathsson L, Buckley CD, Filer A, Rönnelid J. Anti-modified citrullinated vimentin (MCV) antibodies in patients with very early synovitis. *Ann Rheum Dis*. 2010;69(3):627–628.
17. Bang H, et al. Mutation and citrullination modifies vimentin to a novel autoantigen for rheumatoid arthritis. *Arthritis Rheum*. 2007;56(8):2503–2511.
18. Mathsson L, et al. Antibodies against citrullinated vimentin in rheumatoid arthritis: higher sensitivity and extended prognostic value concerning future radiographic progression as compared with antibodies against cyclic citrullinated peptides. *Arthritis Rheum*. 2008;58(1):36–45.
19. Dellagi K, Vainchenker W, Vinci G, Paulin D, Brouet JC. Alteration of vimentin intermediate filament expression during differentiation of human hemopoietic cells. *EMBO J*. 1983;2(9):1509–1514.
20. Kuhn KA, et al. Antibodies against citrullinated proteins enhance tissue injury in experimental autoimmune arthritis. *J Clin Invest*. 2006;116(4):961–973.
21. Lam J, Takeshita S, Barker JE, Kanagawa O, Ross FP, Teitelbaum SL. TNF-alpha induces osteoclastogenesis by direct stimulation of macrophages exposed to permissive levels of RANK ligand. *J Clin Invest*. 2000;106(12):1481–1488.
22. Li P, et al. RANK signaling is not required for TNF-mediated increase in CD11(hi) osteoclast precursors but is essential for mature osteoclast formation in TNFalpha-mediated inflammatory arthritis. *J Bone Miner Res*. 2004;19(2):207–213.
23. Sato K, et al. Th17 functions as an osteoclastogenic helper T cell subset that links T cell activation and bone destruction. *J Exp Med*. 2006; 203(12):2673–2682.
24. Riches PL, McRorie E, Fraser WD, Determann C, van't Hof R, Ralston SH. Osteoporosis associated with neutralizing autoantibodies against osteoprotegerin. *N Engl J Med*. 2009;361(15):1459–1465.
25. Clavel C, et al. Induction of macrophage secretion of tumor necrosis factor alpha through Fcgamma receptor IIa engagement by rheumatoid arthritis-specific autoantibodies to citrullinated proteins complexed with fibrinogen. *Arthritis Rheum*. 2008;58(3):678–688.
26. Laurent L, et al. Fc{gamma} receptor profile of monocytes and macrophages from rheumatoid arthritis patients and their response to immune complexes formed with autoantibodies to citrullinated proteins. *Ann Rheum Dis*. 2011;70(6):1052–1059.
27. Lu MC, Lai NS, Yu HC, Huang HB, Hsieh SC, Yu CL. Anti-citrullinated protein antibodies bind surface-expressed citrullinated Grp78 on monocyte/macrophages and stimulate tumor necrosis factor alpha

production. *Arthritis Rheum*. 2010;62(5):1213–1223.
28. Sokolove J, Zhao X, Chandra PE, Robinson WH. Immune complexes containing citrullinated fibrinogen costimulate macrophages via Toll-like receptor 4 and Fcγ receptor. *Arthritis Rheum*. 2011;63(1):53–62.
29. Lian N, Wang W, Li L, Elefteriou F, Yang X. Vimentin inhibits ATF4-mediated osteocalcin transcription and osteoblast differentiation. *J Biol Chem*. 2009;284(44):30518–30525.
30. Guler-Yuksel M, et al. Changes in hand and generalised bone mineral density in patients with recent-onset rheumatoid arthritis. *Ann Rheum Dis*. 2009;68(3):330–336.
31. Rantapää-Dahlqvist S, et al. Antibodies against cyclic citrullinated peptide and IgA rheumatoid factor predict the development of rheumatoid arthritis. *Arthritis Rheum*. 2003;48(10):2741–2749.
32. Vossenaar ER, et al. Expression and activity of citrullinating peptidylarginine deiminase enzymes in monocytes and macrophages. *Ann Rheum Dis*. 2004;63(4):373–381.
33. Foulquier C, et al. Peptidyl arginine deiminase type 2 (PAD-2) and PAD-4 but not PAD-1, PAD-3, and PAD-6 are expressed in rheumatoid arthritis synovium in close association with tissue inflammation. *Arthritis Rheum*. 2007;56(11):3541–3553.
34. Chang X, et al. Localization of peptidylarginine deiminase 4 (PADI4) and citrullinated protein in synovial tissue of rheumatoid arthritis. *Rheumatology (Oxford)*. 2005;44(1):40–50.
35. Hojo-Nakashima I, Sato R, Nakashima K, Hagiwara T, Yamada M. Dynamic expression of peptidylarginine deiminase 2 in human monocytic leukaemia THP-1 cells during macrophage differentiation. *J Biochem*. 2009;146(4):471–479.
36. Li P, Li M, Lindberg MR, Kennett MJ, Xiong N, Wang Y. PAD4 is essential for antibacterial innate immunity mediated by neutrophil extracellular traps. *J Exp Med*. 2010;207(9):1853–1862.
37. Arita K, Hashimoto H, Shimizu T, Nakashima K, Yamada M, Sato M. Structural basis for Ca(2+)-induced activation of human PAD4. *Nat Struct Mol Biol*. 2004;11(8):777–783
38. Marchisio PC, Cirillo D, Naldini L, Primavera MV, Teti A, Zambonin-Zallone A. Cell-substratum interaction of cultured avian osteoclasts is mediated by specific adhesion structures. *J Cell Biol*. 1984;99(5):1696–1705.
39. Mor-Vaknin N, Punturieri A, Sitwala K, Markovitz DM. Vimentin is secreted by activated macrophages. *Nat Cell Biol*. 2003;5(1):59–63.
40. Auger I, Balandraud N, Rak J, Lambert N, Martin M, Roudier J. New autoantigens in rheumatoid arthritis (RA): screening 8268 protein arrays with sera from patients with RA. *Ann Rheum Dis*. 2009;68(4):591–594.
41. Bouxsein ML, Boyd SK, Christiansen BA, Guldberg RE, Jepsen KJ, Müller R. Guidelines for assessment of bone microstructure in rodents using micro-computed tomography. *J Bone Miner Res*. 2010;25(7):1468–1486.
42. Hildebrand T, Laib A, Muller R, Dequeker J, Ruegsegger P. Direct three-dimensional morphometric analysis of human cancellous bone: microstructural data from spine, femur, iliac crest, and calcaneus. *J Bone Miner Res*. 1999;14(7):1167–1174.